

## University of Southampton Research Repository ePrints Soton

Copyright © and Moral Rights for this thesis are retained by the author and/or other copyright owners. A copy can be downloaded for personal non-commercial research or study, without prior permission or charge. This thesis cannot be reproduced or quoted extensively from without first obtaining permission in writing from the copyright holder/s. The content must not be changed in any way or sold commercially in any format or medium without the formal permission of the copyright holders.

When referring to this work, full bibliographic details including the author, title, awarding institution and date of the thesis must be given e.g.

AUTHOR (year of submission) "Full thesis title", University of Southampton, name of the University School or Department, PhD Thesis, pagination

**UNIVERSITY OF SOUTHAMPTON**

FACULTY OF ENGINEERING AND THE ENVIRONMENT

**Tissue regeneration in porous structures for bone engineering  
applications**

by

**Jonathan Knychala**

Thesis for the degree of Doctor of Philosophy

November 2013



**UNIVERSITY OF SOUTHAMPTON**

FACULTY OF ENGINEERING AND THE ENVIRONMENT

Thesis for the degree of Doctor of Philosophy

**Tissue regeneration in porous structures for bone engineering applications**

by Jonathan Knychala

**ABSTRACT**

Scaffold design for bone regeneration is currently widely investigated as pore architecture can dramatically impact tissue formation in porous biomaterials used in regenerative medicine. A wide variety of 3D structures is used for this purpose, which has become even more important given the geometric freedom offered by emerging rapid prototyping techniques. Therefore, optimal design of pore architecture to maximize tissue formation and ingrowth is required. Tissue formation is frequently assessed in certain established scaffold structures, produced mainly as the end result of a particular fabrication process and its limitations. However, instead, scaffold architecture design should be based on the knowledge of how tissue actually forms in porous structures in the first place.

Tissue formation within porous structures can be dependent on several parameters, such as cell generated forces, cell division, cytoskeleton and extracellular matrix arrangement. Tissue differentiation is also an important aspect as once cells commit to a lineage, the proliferation could decrease. These aspects have been extensively shown to be modulated biochemically. However, the impact of different 3D structures is still largely unclear. Therefore, in this thesis, it is aimed to characterise 3D tissue formation within different structures. For this purpose, an *in vitro* system with well-defined open pore slots of 1 cm length, 1 mm thickness and varying width (hundreds of micrometres) was used to characterise tissue growth solely as a function of pore geometry. This system provided a 3D environment for neo-tissue formation while minimizing nutrient limitations associated with full 3D constructs.

This thesis is the outcome of three studies. The first was focused on tissue formation kinetics in four different pore widths of 200, 300, 400 and 500  $\mu\text{m}$ . For this purpose, a unique system made of calcium phosphate cement with open pores was designed and fabricated. Several types of microscopy were used such as optical microscopy, time-lapse microscopy, epi-fluorescence microscopy and confocal microscopy. Results demonstrated that the material was biocompatible with Human Bone Marrow Stromal Cells and that tissue formation was strongly influenced by pore geometry. Both velocity of tissue invasion and area of tissue formed increased as pores became narrower. This was associated with distinct patterns of actin cytoskeleton organisation depending on pore width, indicating the role of active cell generated forces.

The second study is a more detailed characterisation of the type of tissue regenerated and its organisation. The neo-tissue was seen to display an osteoid-like collagen matrix. The main elements constituting a tissue i.e. cells, actin cytoskeleton and collagen matrix were imaged and their organisation was quantified with various image analysis methods. Results showed a significantly higher alignment with the longitudinal pore axis in the 200  $\mu\text{m}$  compared to the 500  $\mu\text{m}$  pores for all the tissue components analysed. By relating tissue orientation with its expansion rate, the results suggested that increased tissue alignment could be an important factor enhancing tissue formation.

In the third study, tissue differentiation was assessed as a function of pore size. Expression of intermediate and late bone markers was assessed, Alkaline Phosphatase and Osteopontin respectively. Results showed that both markers were expressed, indicating that the neo-tissue regenerated reached late state of differentiation and is prepared for mineralization. The expression of these markers was semi-quantitatively evaluated. ALP expression was expressed increasingly as tissue “age” increased. A gradient was observed with increasing staining intensity towards the starting point of tissue formation. Thus, the results revealed presence of distinct zones in which cells are in different states associated with various functions (proliferation or differentiation). Additionally, the expression of Osteopontin assessed semi quantitatively did not show any notable differences between pore widths. However, the results obtained displayed high variability between replicates. Therefore, it was only concluded that neo-tissue formed in both structures was able to express early (second study, chapter 4), intermediate and late osteogenic markers, although no significant differences were found between the different pore widths. This demonstrated that the tissue regenerated had committed to the osteogenic pathway, with the potential for full differentiation into mineralized tissue, which needs to be confirmed in future studies.

Overall, the results presented in this thesis provide evidence for the hypothesis that pore geometry affects tissue growth capacity by modulating tissue organisation. Key factors governing tissue formation in vitro were elucidated, highlighting the importance of the interplay between cell division, cell mechanics, cytoskeleton dynamics, tissue spatial organisation, matrix deposition and differentiation in relation to porous structure.

# Contents

<b>ABSTRACT</b> .....	<b>i</b>
<b>Contents</b> .....	<b>iii</b>
<b>List of tables</b> .....	<b>ix</b>
<b>List of figures</b> .....	<b>xi</b>
<b>Definitions and Abbreviations</b> .....	<b>xxii</b>
<b>List of Symbols</b> .....	<b>xxii</b>
<b>DECLARATION OF AUTHORSHIP</b> .....	<b>xxiii</b>
<b>Acknowledgements</b> .....	<b>xxv</b>
<b>Chapter 1 Introduction</b> .....	<b>1</b>
1.1 Background.....	1
1.2 Objectives and Scope .....	4
1.2.1 Objectives.....	4
1.2.2 Scope.....	5
1.3 Layout of the Thesis.....	5
<b>Chapter 2 Literature Review</b> .....	<b>7</b>
2.1 Bone tissue .....	7
2.1.1 The cells of bone tissue.....	7
2.1.1.1 Osteoblasts .....	7
2.1.1.2 Osteocytes.....	9
2.1.1.3 Osteoclasts.....	9
2.1.2 Osteoid.....	9
2.1.2.1 Collagen .....	9
2.1.2.2 Non Collagenic proteins .....	10
2.2 Biological components for bone tissue engineering .....	11
2.2.1 Bone Marrow Cells .....	11
2.3 Materials used for porous implants fabrication .....	12
2.3.1 Collagen Matrices .....	13
2.3.2 Synthetic Polymers.....	13
2.3.3 Calcium Phosphates.....	14

2.4 Porous Scaffolds.....	16
2.4.1 Interconnectivity.....	17
2.4.2 Pore Geometry & Pore Size.....	18
2.4.2.1 Influence of pore size on tissue growth in vitro .....	18
2.4.2.2 Influence of pore size on tissue growth <i>in vivo</i> .....	20
2.4.3 Pore Geometry .....	21
2.4.3.1 Pore Geometry & Tissue Organisation .....	21
2.4.3.2 Pore Geometry, Cell Generated Forces and Tissue Formation.....	22
2.5 Cell mechanics & Tissue Development.....	23
2.5.1 Actin: Molecular Aspects.....	23
2.5.2 Actin Cytoskeleton & Cell Surface Receptor in Tissue Formation: Integrins & Focal Adhesions .....	24
2.5.3 The Cytoskeleton and Cell Surface Receptors in Tissue Formation: Role of Cadherins.....	25
2.5.3.1 Structure of a Cadherin mediated Cell-Cell Adhesion .....	25
2.5.3.2 Cell-Cell Adhesion Dynamics.....	26
2.5.3.3 Cell Adhesion Bonding Force.....	27
2.5.4 Cell contraction mediated by Actin-Myosin association.....	27
2.5.5 Actin in Cell Adhesion & Migration .....	29
2.5.6 Actin in Cell division.....	29
2.5.7 Effect of internal tension on cellular behaviour.....	30
2.5.7.1 Proliferation.....	30
2.5.7.2 Differentiation .....	31
2.5.8 Stem Cell to Osteoblasts differentiation: Internal Tension Kinetics.....	32
2.5.9 Contractile Potential of Musculoskeletal Tissue .....	35
2.5.10 Contractile Behaviour & Substrate Stiffness.....	36
2.5.11 Morphogenesis & Mechanical Forces .....	37
2.5.11.1 Cell Division During Organ Formation.....	38
2.5.11.2 Cell Rearrangement & Intercalation.....	39
2.5.12 Forces Involved in Cell Intercalation & Localisation.....	41

2.6	Summary of the Literature Review .....	43
2.7	Research Questions.....	45
<b>Chapter 3 Pore Geometry Regulates Human Bone Marrow</b>		
	<b>Cells Tissue Formation .....</b>	<b>47</b>
3.1	Material and Methods .....	48
3.1.1	Scaffold Fabrication & Preparation .....	48
3.1.1.1	Mould Production.....	48
3.1.1.2	Preparation of $\alpha$ -TCP powder and cement production .....	49
3.1.1.3	Preparation of the microstructures .....	49
3.1.1.4	Scaffold Conditioning.....	50
3.1.2	Scanning Electron Microscopy .....	50
3.1.3	Cell Culture & Scaffold Seeding .....	50
3.1.4	Optical Inverted Microscopy .....	51
3.1.5	Laser Confocal Microscopy .....	52
3.1.6	Time Lapse Microscopy.....	53
3.1.7	Overall summary of samples used & experiments performed.....	53
3.2	Results.....	54
3.2.1	Material Characteristics.....	54
3.2.2	Biocompatibility & Cell Attachment.....	55
3.2.3	Growth Kinetics in Pores of Different Widths .....	56
3.2.4	Actin Network Imaging.....	59
3.2.5	Time Lapse & EdU .....	60
3.2.6	3D Tissue Reconstruction .....	63
3.3	Discussion .....	64
3.3.1	Curvature driven growth.....	64
3.3.2	Tissue formation mechanisms.....	66
3.3.3	Tissue thickening and expansion along z-axis.....	68
3.3.4	Actin organisation .....	70
3.4	Summary.....	71
<b>Chapter 4 Ingrowth Enhancement Due to Pore-Induced</b>		
	<b>Tissue Orientation .....</b>	<b>73</b>
4.1	Material and Methods .....	74
4.1.1	Scaffold Fabrication & Preparation .....	74

4.1.2 Human Bone Marrow Cells Isolation, Expansion and Seeding .....	74
4.1.3 Optical Inverted Microscopy.....	75
4.1.4 Laser Confocal Microscopy.....	76
4.1.5 Cell counting .....	77
4.1.6 Tissue Volume Estimation.....	77
4.1.7 Tissue Orientation Measurements.....	78
4.1.7.1 Cell Orientation Measurements .....	78
4.1.7.2 Fibre Orientation Measurements.....	79
4.1.8 Overall recap of samples used & purposes.....	81
4.2 Results.....	82
4.2.1 Kinetics .....	82
4.2.2 Cell number.....	84
4.2.3 Percentage of EdU positive stained cells .....	85
4.2.4 Neo- tissue volume.....	85
4.2.5 Tissue Imaging.....	86
4.2.6 Cell Orientation Distribution.....	88
4.2.7 Spatial Tissue Organisation.....	89
4.2.8 Cell division orientation.....	91
4.2.9 Osteogenic Lineage Commitment .....	94
4.3 Discussion.....	95
4.3.1 Tissue quantification.....	95
4.3.2 Tissue Constraints & Actin Patterns .....	96
4.3.3 Actin organisation and tension on cell number .....	97
4.3.4 Extracellular Matrix Orientation.....	99
4.3.5 Cell Division Orientation.....	100
4.4 Summary .....	102
<b>Chapter 5 Tissue Differentiation .....</b>	<b>103</b>
5.1 Material and Methods .....	103
5.1.1 Cell isolation, Scaffold fabrication & Tissue growth kinetics.....	103
5.1.2 Alkaline Phosphatase Assay .....	103
5.1.3 Laser confocal Microscopy .....	104
5.1.4 Semi quantitative assessment of ALP intermediate bone marker expression.....	104

5.1.5	Semi quantitative assessment of Osteopontin late bone marker expression .....	106
5.2	Results.....	108
5.2.1	Kinetics .....	108
5.2.2	Tissue Imaging – Intermediate & Late Markers Staining .....	109
5.2.2.1	Alkaline Phosphatase .....	109
5.2.2.2	Osteopontin.....	109
	110	
5.2.3	Osteogenic Lineage Commitment Assessment.....	114
5.2.3.1	Differentiation over time – ALP .....	114
5.2.3.2	Semi-quantitative analysis – Osteopontin .....	119
5.3	Discussion .....	120
5.3.1	Alkaline Phosphatase .....	120
5.3.2	Osteopontin.....	122
5.3.3	Potential implications of internal tension.....	124
5.3.4	Summary .....	124
	<b>Chapter 6 Discussion and Conclusion .....</b>	<b>125</b>
6.1	Summary of the thesis outcomes.....	125
6.2	Experimental Limitations and Optimisation.....	130
6.2.1	Limitations.....	130
6.2.2	Advantages.....	132
6.3	Open questions and future work.....	132
6.3.1	Tissue formation in different media conditions .....	133
6.3.2	Internal tension and cell division modulation with drugs.....	134
6.3.3	Molecular biology.....	136
6.3.4	Tissue behaviour under mechanical loading.....	136
6.3.5	Computational Modelling.....	137
6.3.6	Summary of future work.....	137
6.3.7	Open questions .....	138
6.4	Epilogue .....	139
	<b>Appendices.....</b>	<b>140</b>
	<b>Appendix 1 – Supplementary materials.....</b>	<b>141</b>
	<b>Appendix 2 – ALP staining analysis: Proof of concept .....</b>	<b>142</b>

Appendix 3 – Publications.....	143
<b>List of References / Bibliography.....</b>	<b>144</b>
<b>Notes .....</b>	<b>155</b>

## List of tables

Table 4-1 Overall summary of samples used & experiments performed.....	81
Table 4-2: Area of newly formed tissue in the different pore sizes.....	84
Table 5-1 Slope values of linear fit of Red staining intensity curves in 200 $\mu\text{m}$ pores .....	118
Table 5-2 Slope values of linear fit of Red staining intensity curves in 500 $\mu\text{m}$ pores .....	118
Table 5-3 Percentage of the total area occupied by Osteopontin for each replicates .....	119
Table 6-1: Outcomes .....	129



# List of figures <sup>1</sup>

Fig. 2-1 Temporal expression of genes reflecting osteoblastic differentiation for cells in culture. Expression of Histone 4 (H4) and Collagen I (Col I) occur during proliferative phase. During matrix maturation, specific genes for bone markers are expressed i.e Alkaline Phosphatase (ALP) and Osteopontin (OP). During the mineralization phase, Osteocalcin (OC) gene is expressed. Drawing from Hollinger et al. 2004 ..... 8

Fig. 2-2 Collagen fibres formation and intermolecular cross-link process (Fratzl 2008). ..... 10

Fig. 2-3 Radiographs obtained before, immediately and months after porous HA implantation for bone defect treatment. (Top) 41 years old female patient treated for unsuccessful tibiae lengthening attempt. (Bottom) 16 years old female patient treated for bone loss after trauma. Both of the cases are 4cm defects. (a, d) Pre surgery, arrow shows the bone defect. (b, e) Immediately after surgery, arrow shows the porous implant. (c) 18 months and (f) 8 months after surgery. Adapted from Quarto et al. 2001 (Quarto et al. 2001) ..... 16

Fig. 2-4 Examples of various porous architecture in scaffolds for bone engineering. Picture from *royalsocietypublishing.org* ..... 17

Fig. 2-5 Organization of a focal adhesion and its linkage to the actin cytoskeleton (Mitra et al., 2005) ..... 24

---

<sup>1</sup> For reproduction of copyrighted material, i.e. figures and tables, permission has been obtained from the legal owner via the Copyright Clearance Centre (<http://www.copyright.com/>)

Fig. 2-6 Cadherin-Actin connection mediated by intracellular proteins (Mege et al., 2006).....	26
Fig. 2-7 Cell-Cell interactions dynamics involving Cadherins and the Actin-cytoskeleton (Mege et al. 2006) .....	27
Fig. 2-8 ATP-dependent molecular mechanism of act myosin contraction ( <i>themedicalbiochemistrypage.Org</i> ) .....	28
Fig. 2-9 Actin cytoskeleton rearrangement during human amniotic fluid-derived stem cells hAFSCs osteodifferentiation in 2D: (a) – (d), actin cytoskeleton after osteodifferentiation 0, 7, 14, 21 days, respectively. Within 21 days of the induction of osteogenic differentiation, more and thicker stress fibres are replaced with a thinner actin filament meshwork typical for mature osteoblasts. Scale bar, 20 µm. From Chen, Xiao et al 2010. ....	34
Fig. 2-10 Qualitative schematic, summarizing the potential role of internal tension during osteogenic-differentiation. ....	34
Fig. 2-11 Random(top) and oriented (bottom) cell division.....	38
Fig. 2-12 Cell intercalation.....	39
Fig. 2-13 Cell intercalation in Drosophila. Cell contacts in the type 1 configuration (red dashed line in a and d) progress towards the type 2 (yellow dashed line in b and d) and then to the type 3 configuration (green dashed line in c and d) (Bertet et al. 2004).....	40
Fig. 2-14 Myosin II staining during Germ-Band Elongation in Drosophila (Rauzzi et al. 2008).....	41
Fig. 2-15 Myosin involvement in T1 transition phase of cell intercalation (Rauzzi et al.).....	42
Fig. 3-1 Construct fabrication. (a) Female mould used for production of male moulds. (b) Male mould obtained .....	48

Fig. 3-2 (a) Schematic of the construct used for the study. (b) TCP scaffolds obtained, pore slot width: 600, 500, 400, 300, and 200  $\mu\text{m}$  from left to right..... 50

Fig. 3-3 Example, measurement of the pore spanning distance by cells in a 200  $\mu\text{m}$  pore at day 3..... 52

Fig. 3-4 (left) Scanning Electron Microscopy (SEM) pictures of the surface of TCP cements displaying micro structures. (right) Scanning Electron Microscopy (SEM) pictures of the surface of TCP cements displaying nano structures..... 54

Fig. 3-5 HBMSC attachment and viability on TCP cement 14 h following seeding (calcein-AM)..... 55

Fig. 3-6 Initial steps of pore spanning by cell-formed tissue. (a) Cells (white arrows) attach to the convex wall (red arrows) of the pore extremity, (b) as well as in the middle of the slot. (c) Pore spanning by cells attached to the walls started from the curved end of the pore. .... 56

Fig. 3-7 Optical microscopy showing the tissue growing suspended in the open pore slots. Bottom: day 3. Top: day 7. Pore width 200, 300, 400, 500  $\mu\text{m}$  from left to right. Scale bar: 100  $\mu\text{m}$ ..... 57

Fig. 3-8 Effect of pore size on tissue growth kinetics (a) Comparison of growth curves for the different pore widths (n=3). (b) Growth speed obtained by linear fitting of the grow curves for the different pore sizes. R-Square values for 200, 300, 400 and 500  $\mu\text{m}$  pores were 0.93, 0.99, 0.97, and 0.99 respectively. '\*' indicates statistically different results (p<0.05, one-way analysis of variance (ANOVA) with post-hoc Tukey HSD test (Error bars represent standard deviation). 58

Fig. 3-9 Projected Tissue Area of newly formed tissue after 18 days for the different pore widths..... 58

Fig. 3-10 Effect of pore width on actin network organisation: Laser scanning confocal microscopy. Tissue within constructs labelled with Alexa Fluor 568-Phalloidin for F-actin cellular cytoskeleton (scale bar = 100µm). Pictures displaying the actin network at the front of migration (a-d) and in the bulk of the tissue formed (e-h) in different pore sizes: 200 µm (a, e); 300 µm (b, f); 400 µm (c, g); 500 µm (d, h).....59

Fig. 3-11 Results showing the location of cell division and DNA production. (a-c) Cell division at the front, as indicated by arrows. Intervals between pictures: 20 min. (d, e) EdU labelled cells reflecting DNA production at the front of migration (d) and in the bulk, approximately 1 mm away from the front of migration (e) in a 200 µm pore ..... 61

Fig. 3-12 (a-c) Cell contraction. Example of a leading cell shortening, indicated by '\*'. Lines indicate the extent the tissue is stretched due to cell generated stresses. Intervals between pictures: 1h40. The original video is provided as a supplementary material. For comparison an additional video shows this phenomena occurring in a 500 µm pore. (d) Schematic representation of forces exerted by aligned cells at the tissue front on the underlying tissue, which could drive tissue expansion, increasing with curvature..... 62

Fig. 3-13 (a) Example of a 3D reconstruction of the actin network in a 400 µm pore (70 µm z-stack, pore walls were indicated manually for illustrative purposes only). (b) Perpendicular cross section along the y- z plane showing the thin cell layer at the immediate front. (c) Longitudinal cross section along (x-z) plane showing tissue thickening away from the front of migration. (d-f) Examples of longitudinal cross sections showing EdU stained cell orientation in sections parallel to the (x-z) plane..... 63

Fig. 3-14 Digitalised curvature curves according to pore widths ..... 65

Fig. 3-15 (a-top) Mathematical modelling results, showing the shape of the tissue front during steady growth progression for a 500  $\mu\text{m}$  wide pore (Model courtesy Dr C. Catt, Southampton). The arrows indicate the local speed and direction of growth. High growth is associated with high curvature. (a-bottom) Predicted position of the progressing front shown at day 1, 5, 9, 13 and 17 (500  $\mu\text{m}$  pore, all units in mm). (b-e) Predictive mathematical modelling of growth as function of curvature versus experimental results. The model was fitted to the 300  $\mu\text{m}$  pore and then applied to the other configurations using the same growth parameter  $\lambda$ , showing good overall correspondence..... 66

Fig. 3-3-16 (a) Laser scanning confocal microscopy picture representing pore closure corresponding to the concept of a contracting "purse string". Tissue was stained for actin (Alexa Phalloidin 568) and nuclei (Hoescht) (b-d) Pore closure final steps (40 mins intervals) ..... 67

Fig. 3-17 Scherk type surface potentially representing the front of migration (http://page.mi.fu-berlin.de/sfroehli/minimal\_pstricks.php.html) ..... 69

Fig. 3-18 Schematic of potential mechanism of cell division in the xz plane leading to an increase in tissue thickness..... 70

Fig. 4-1 Human Bone Marrow Cells isolation process. (1) Fresh pieces of trabecular bone containing bone marrow. (2) Bone pieces after cell extraction. (3) Solution obtained after processing the bone pieces. (4) Bone marrow cells freshly seeded in T150 flasks..... 75

Fig. 4-2 Cell nuclei recognition with Cell Profiler ..... 77

Fig. 4-3 Tissue orientation analysis. (a) Schematic showing how tissue was divided into 5 zones. (b) Schematic explaining the meaning of the orientation measurements. .... 78

Fig. 4-4 Orientation J plugins applied for fibre orientation assessment in 200 & 500  $\mu\text{m}$  pores. Dotted lines represent the five zones the tissue was split into and the ellipses represent the average orientation of the fibres within the zone. In this figure, actin fibres are shown..... 80

Fig. 4-5 Experiment 1 (14 days): Effect of pore size on tissue growth kinetics (a) Comparison of growth curves for the different pore widths over 14 days ( $n=3$ ). (b) Growth speed obtained by linear fitting of the grow curves for the different pore sizes. Statistical analysis was performed using analysis of variance (one-way ANOVA) followed by post-Tukey test in Origin Lab software ( $p < 0.05$ ). Bars and error bars represent mean values and standard deviation respectively ( $n=3$ ). .. 83

Fig. 4-6 Experiment 2 (30 days): Effect of pore size on tissue growth kinetics (a) Comparison of growth curves for the different pore widths over 30 days ( $n=3$ ). (b) Growth speed obtained by linear fitting of the grow curves for the different pore sizes. Statistical analysis was performed using analysis of variance (one-way ANOVA) followed by post-Tukey test in Origin Lab software ( $p < 0.05$ ). Bars and error bars represent mean values and standard deviation respectively ( $n=3$ ).... 83

Fig. 4-7 Number of cells counted in each condition after 30 days of growth ( $n=3$ )..... 84

Fig. 4-8 Experiment 2: Percentage of EdU positive cells in each condition ( $n=3$ )..... 85

Fig. 4-9 Experiment 2. Volume occupied by neo-tissue formed within the pore for each condition after 30 days ( $n=3$ )..... 86

Fig. 4-10 Confocal microscopy images of the tissue components. (a, b) Cell nuclei stained with Hoescht dye in 200  $\mu\text{m}$  pore (a) and 500  $\mu\text{m}$  pore (b). (c, d) Actin cytoskeleton stained with Alexa Fluor 568-Phalloidin in 200  $\mu\text{m}$  pore (c) and 500  $\mu\text{m}$  pores (d). (e, f) Collagen I

matrix stained with primary antibody anti-Collagen from rabbit and Alexa Fluor 488 anti-Rabbit in 200 $\mu\text{m}$ pore (e) and 500 $\mu\text{m}$ pore (f). Primary antibody was omitted for negative control. (Scale bar = 50 $\mu\text{m}$ ) .....	87
Fig. 4-11 Cell orientation distribution in 200 $\mu\text{m}$ pore and 500 $\mu\text{m}$ pore. (n=6 per conditions).....	88
Fig. 4-12 Measurements of average nuclei orientation in the 5 zones across the pore width in (black) 200 $\mu\text{m}$ pore and (blue) 500 $\mu\text{m}$ pore (n=6).....	89
Fig. 4-13 Measurements of average actin fibre orientation in the 5 zones across the pore width in (a) 200 $\mu\text{m}$ pore and (b) 500 $\mu\text{m}$ pore (n=5) .....	90
Fig. 4-14 Measurements of average collagen fibre orientation in the 5 zones across the pore width in (a) 200 $\mu\text{m}$ pore and (b) 500 $\mu\text{m}$ pore (n=5).....	90
Fig. 4-15 EdU labelled cells reflecting DNA production in 200 $\mu\text{m}$ pore (a) and 500 $\mu\text{m}$ pore (b) .....	91
Fig. 4-16 Dividing cells orientation distribution in 200 $\mu\text{m}$ pore and 500 $\mu\text{m}$ pore (n=3 per condition). .....	92
Fig. 4-17 Measurements of Nuclei orientation of dividing cells after 30 days in the 5 zones across the pore width in (black) 200 $\mu\text{m}$ pore and (orange) 500 $\mu\text{m}$ pore (n=3) .....	93
Fig. 4-18 Measurements of cell nuclei orientation after 30 days in the 5 zones across the pore width in (black) 200 $\mu\text{m}$ pore and (blue) 500 $\mu\text{m}$ pore (n=3) .....	93
Fig. 4-19 Alkaline Phosphatase (ALP) staining in 200 $\mu\text{m}$ (a) and 500 $\mu\text{m}$ (b) pores at day 28. Pink colour shows positive staining for ALP reflecting osteogenic lineage commitment .....	94

Fig. 4-20 Actin remodelling during tissue formation. Tissue scale: Illustration of tension changes and mechanical equilibrium recovery via actin remodelling during new cell apparition (Red parts). Cellular Scale: Illustration of actin remodelling around cellular boundaries during cell contraction. Subsequently, actin distribution is evened after stabilization. Drawing from (Heisenberg et al. 2013).....98

Fig. 4-21 Cell division cycle phases.  $G_1$  phase ensures that DNA synthesis can take place. During S Phase, DNA replication occurs.  $G_2$  phase ensures that mitosis can take place. During phase M, two daughter cells appear.....99

Fig. 4-22 (a, b) Cell division within the zone investigated for tissue orientation. Time Lapse results showing cells dividing along longitudinal axis in 200  $\mu\text{m}$  pore (a) and 500  $\mu\text{m}$  pore (b). Schematic for proposed mechanism of the contribution of the orientation of cell division in tissue growth in 200  $\mu\text{m}$  pore (c) and 500  $\mu\text{m}$  pore (d). Cell division orientation in the same direction as the one imposed by the confinement of the structure enhances tissue ingrowth (Scale bar = 50  $\mu\text{m}$  unless indicated otherwise) ..... 101

Fig. 5-1 An example of image reconstruction using ImageJ. (a) The original picture (RGB) is split in three colours: Red (R), Green (G) and Blue (B). (b) Isolation of the colour of interest, different ALP red stain intensity measures  $I_{RS}$ , as represented by grey-scale pixels, Red - Blue (left) and Red - Green (right)..... 105

Fig. 5-2 Schematic explaining how the grey scale values representing red intensity along longitudinal axis of pore are obtained. Subsequently, these values were plotted as a function of their location on the longitudinal axis in section 5.2.3.1. .... 106

Fig. 5-3 Osteopontin (red) area analysis using thresholding & masking method..... 107

Fig. 5-4 Tissue growth kinetics monitored over 30 days on 3 different replicates in a 200  $\mu\text{m}$  pore for F63<sub>1</sub> ..... 108

Fig. 5-5 Tissue growth kinetics monitored over 30 days on 3 different replicates in a 500  $\mu\text{m}$  pore for F63<sub>1</sub> ..... 108

Fig. 5-6 Tissue in 200  $\mu\text{m}$  pore, replicate 1. (a) ALP staining at day 30. (b) Nuclei stained with Hoescht (blue) & Osteopontin stained with Alexa Fluor 564 at day 30. (c) Kinetics over 30 days for replicate 1 110

Fig. 5-7 Tissue in 200  $\mu\text{m}$  pore, replicate 2. (a) ALP staining at day 30. (b) Nuclei stained with Hoescht (blue) & Osteopontin stained with Alexa Fluor 564 at day 30. (c) Kinetics over 30 days for replicate 2 111

Fig. 5-8 Tissue in 200  $\mu\text{m}$  pore, replicate 3. (a) ALP staining at day 30. (b) Nuclei stained with Hoescht (blue) & Osteopontin stained with Alexa Fluor 564 at day 30. (c) Kinetics over 30 days for replicate 3 112

Fig. 5-9 Tissue in 500  $\mu\text{m}$  pore, Replicate 1. (a) ALP staining at day 30. (b) Nuclei stained with Hoescht (blue) & Osteopontin stained with Alexa Fluor 564 at day 30. (c) Kinetics over 30 days for replicate 1 113

Fig. 5-10 Tissue in 500  $\mu\text{m}$  pore, Replicate 2. (a) ALP staining at day 30. (b) Nuclei stained with Hoescht (blue) & Osteopontin stained with Alexa Fluor 564 at day 30. (c) Kinetics over 30 days for replicate 2 113

Fig. 5-11 Tissue in 500  $\mu\text{m}$  pore, replicate 3. (a) ALP staining at day 30. (b) Nuclei stained with Hoescht (blue) & Osteopontin stained with Alexa Fluor 564 at day 30. (c) Kinetics over 30 days for replicate 3 114

Fig. 5-12 Replicate.1, 200  $\mu\text{m}$ . Red intensity as a function of tissue location along longitudinal pore axis. Red – Blue (Blue) & Red – Green (Green) curves are plotted in order to isolate the signal on a grey scale. The labels on the top x axis correspond to the day at which tissue spanned the distance corresponding to the bottom x-axis ..... 115

Fig. 5-13 Replicate.2, 200  $\mu\text{m}$ . Red intensity as a function of tissue location along longitudinal pore axis. Red – Blue (Blue) & Red – Green (Green) curves are plotted in order to isolate the signal on a grey scale. The labels on the top x axis correspond to the day at which tissue spanned the distance corresponding to the bottom x-axis ..... 115

Fig. 5-14 Replicate.3, 200  $\mu\text{m}$ . Red intensity as a function of tissue location along longitudinal pore axis. Red – Blue (Blue) & Red – Green (Green) curves are plotted in order to isolate the signal on a grey scale. The labels on the top x axis correspond to the day at which tissue spanned the distance corresponding to the bottom x-axis. .... 116

Fig. 5-15 Replicate.1, 500  $\mu\text{m}$ . Red intensity as a function of tissue location along longitudinal pore axis. Red – Blue (Blue) & Red – Green (Green) curves are plotted in order to isolate the signal on a grey scale. The labels on the top x axis correspond to the day at which tissue spanned the distance corresponding to the bottom x-axis ..... 116

Fig. 5-16 Replicate.2, 500  $\mu\text{m}$ . Red intensity as a function of tissue location along longitudinal pore axis. Red – Blue (Blue) & Red – Green (Green) curves are plotted in order to isolate the signal on a grey scale. The labels on the top x axis correspond to the day at which tissue spanned the distance corresponding to the bottom x-axis ..... 117

Fig. 5-17 Replicate.3, 500  $\mu\text{m}$ . Red intensity as a function of tissue location along longitudinal pore axis. Red – Blue (Blue) & Red – Green (Green) curves are plotted in order to isolate the signal on a grey scale. The labels on the top x axis correspond to the day at which tissue spanned the distance corresponding to the bottom x-axis ..... 117

Fig. 5-18 Measurement of the percentage of total tissue area covered by Osteopontin stain.....	120
Fig. 5-19 Schematic of endochondral ossification process showing the different zones and progressive differentiation along the bone long axis.....	122
Fig. 6-1 Proposed zones with allocated behaviour throughout the tissue.....	128
Fig. 6-2 Schematic of an optimized device with less surface available for 2D growth .....	131
Fig. 6-3 Tissue growth monitoring over 12 days in basal and osteogenic media. (Left) Pore spanning monitored over 12 days. (Right) Tissue growth velocity in each conditions obtained by linear fitting.....	133
Fig. 6-4 Pore spanning rate under the influence of actin fibres formation inhibitor. From 0 to 24h, the media was Y27632 free. From 24h-48h, the media was containing 10 $\mu$ M Y27632. From 48h-72h, the media was containing 100 $\mu$ M Y27632.....	134
Fig. 6-5 Mechanical loading device fitting on top of a 6 well culture plate (left). Schematic picture of a scaffold mechanically loaded by two loading units (right).....	137

# Definitions and Abbreviations

2D	Two Dimensional
3D	Three Dimensional
ALP	Alkaline Phosphatase
BCP	Biphasic Calcium Phosphate
BMP	Bone Morphogenic Protein
BSA	Bovine Serum Albumin
BSP	Bone Sialoprotein
DNA	DeoxyriboNucleic Acid
ECM	Extra Cellular Matrix
EDTA	Ethylenediaminetetraacetic Acid
EdU	5-ethynyl-2'-deoxyuridine
FBS	Foetal Bovine Serum
FCS	Foetal Calf Serum
HA	Hydroxyapatite
HAP	Hydroxyapatite
HBMC	Human Bone Marrow Cells
HBMSC	Human Bone Marrow Stromal Cells
MEM	Minimum Essential Medium
MSC	Mesenchymal Stem Cells
NRK	Normal Rat Kidney
OPN	Osteopontin
PBS	Phosphate Buffer Saline
P	Passage
PHBV	(poly-3-hydroxy butyrate- co-valerate)
polyHIPE	Porous polymers of High Internal Phase Emulsion
PTA	Projected Tissue Area
ROI	Region Of Interest
SEM	Scanning Electron Microscopy
STD	Standard Deviation
TCP	Tri-Calcium Phosphate

## List of Symbols

### Statistics

$p$   $p$ -value probability

# DECLARATION OF AUTHORSHIP

I, Jonathan Knychala declare that the thesis entitled “TISSUE REGENERATION IN POROUS STRUCTURES FOR BONE ENGINEERING APPLICATIONS” and the work presented in the thesis are both my own, and have been generated by me as the result of my own original research. I confirm that:

- this work was done wholly while in candidature for a research degree at this University;
- where any part of this thesis has previously been submitted for a degree or any other qualification at this University or any other institution, this has been clearly stated;
- where I have consulted the published work of others, this is always clearly attributed;
- where I have quoted from the work of others, the source is always given. With the exception of such quotations, this thesis is entirely my own work;
- I have acknowledged all main sources of help;
- where the thesis is based on work done by myself jointly with others, I have made clear exactly what was done by others and what I have contributed myself;
- Parts of this work have been published as: Knychala J., Bouropoulos N., Catt C.J, Katsamenis O.L., Please C.P. and Sengers B.G. 2013. "Pore geometry regulates early stage Human Bone Marrow Cell tissue formation and organisation". Annals of Biomedical Engineering, May 2013, Vol 41, issue 5, pages 917-930

Signed: .....

Date:.....



# Acknowledgements

My most sincere thanks are due to:

My principal supervisor, Dr. Bram G. Sengers, for offering me the opportunity of doing a PhD at the University of Southampton and supervising me.

Orestis Katsamenis for his help establishing a durable collaboration with Pr. Nikos Bouropoulos who kindly provided the material and produced the samples for me. Without them, the project would have not been.

Special thanks to Bone & Joint group for allowing me to use their facilities. Especially Kate Murawski-White for training me with cell isolation and always being happy to help with everything I asked. Dr Rahul Tare & Dr Janos Kanczler for advising me.

A very special thank goes to Dr Hans Schuppe, who tragically died from a heart attack in February 2013. A man with an incredible kindness and an endless patience. May his soul rest in peace.

A thank to the bioengineering office & lab mates for the nice working atmosphere, Lorenzo, Dario, Federico, Orestis, Dyan, Natalya, Hatice, Margareth, Siwei, Yu-Hin, Amir, Maria

I would also like to acknowledge the Faculty of Engineering and the Environment of the University of Southampton for the financial support of this project.

I would like to address a very special thanks to Lavinia, thanks for always being there for me and supporting me during all of it.

Thanks Seb & Marco for your friendship and your help when I needed it.

Thank you to the Alma people Joey, Danny, Marta & Ernst, Shioban for their joy!

Un hommage à mes amis de Cergy que je n'oublie pas, Furet, Pipit, Delo, Monss, Frero, Mendy, Burrhus, Asmah, Bidoch, Bambi, Gejor, Minous, Jojos, Odas, Geupch

Un clin d'œil à Olivier Gallet, vous qui m'avez « lancé » à l'international.

Chciałem mocno podziękować moja rodzinę w Polsce, o która nigdy nie zapomniałem, Włodek, Babcia i Beata. Serdecznie was pozdrawiam.

Mon plus grand merci va à toi, ma mère, celle grâce à qui j'existe et je suis ce que je suis aujourd'hui, toi qui m'a tout donné et dévoué ta vie pour moi. Sans toi et ta force, rien de tout cela ne serait arrivé. Merci pour ton éducation, ton soutien éternel et ton amour. De la part de ton fils qui t'aime du fond du cœur, c'est à toi que va toute ma reconnaissance. Merci d'être ma mère..





*to my mother Bojena, Dziadek, Nino, Danek and Binou*





# **Chapter 1**

## **Introduction**

### **1.1 Background**

Bone fractures and bone diseases affect a large number of people, especially elderly populations. This can result in bone defects with variable sizes. Complete bone regeneration is possible as long as the defect is small enough. However, for critical size defects that do not heal naturally, a support material or scaffold is required for neo-tissue formation. Bone grafting is the most common mean used to fill a defect that bone cannot heal by itself. This consists of inserting new bone or bone substitutes to replace missing bone into spaces around a broken bone or bone defects.

Bone defects emanate generally from direct bone fracture as well as diseases such as osteoporosis or bone tumours removals. The most common use of bone grafts are for repairing complex fractures in broken bones that have not healed, and for supplementing bone stock after osteoporotic fracture, or tumour removal, but also for maxillo-facial reconstruction, dental implants, as well as joint and spinal fusion to prevent movement and alleviate pain.

Bone grafting represented a market estimated at more than €1.45 billion in 2010 and is predicted to reach a value of €2.5 billion in 2017 (Gunnam 2011). In more detail, the American, European and rest of the world market represented 1 billion, 400 million and 50 million respectively. Therefore, the great expansion of the bone graft market generates a highly lucrative business for manufacturers and a worthwhile as well as challenging field of investigation for tissue engineering research. Indeed, bone graft

market development is boosted by an increasing amount of orthopaedic procedures in which the use of bone graft substitutes is used to augment the native bone stock. In addition, the population older than 65 is growing by 2% every year, a noticeably faster rate compared to the overall growth rate of the population. Therefore, the older population is expected to grow more rapidly than other age categories. Consequently, the increase of elderly population across the world is an additional significant driver for the bone graft substitute market.

There are different types of bone grafts available. First, autologous graft which is basically bone harvested from the patient's own body, often from the iliac crest. Autologous grafts are considered as the "gold standard graft" because of the decreased risks of immune rejection by the body. The second type frequently used are allografts, which are usually cadaveric human bones obtained from a bone bank where people agreed to give their bone for healthcare purposes. Worldwide, 2.2 million orthopaedic interventions per year involve autografts or allografts (Giannoudis et al. 2005; Sundelacruz et al. 2009). On the other hand, synthetic bone grafts made of biocompatible materials usage is globally on rise. Indeed, 18-20% of the orthopaedics procedures involve the use of bone grafts (Gunnam 2011). The most popular category of those materials is made of calcium-phosphate in different forms, which are recognized for their biocompatibility and their similar properties to bone mineral matrix.

Essential characteristics for bone grafts are osteoconductivity, which means that the architecture promotes bone tissue formation and ingrowth, and osteoinductivity, which is the ability to stimulate osteoprogenitors to differentiate into osteoblasts (Hollinger et al. 2004). A bone graft material displaying both osteoconductivity and osteoinductivity will serve as a scaffold for newly differentiated as well as existing osteoblasts and also promote their proliferation, which should lead to a quicker integration of the implant.

Nevertheless, there are still recurrent issues encountered using autografts or allografts such as limited supply of bone grafts, donor site morbidity, graft versus host diseases, infection transmission and graft failure (Dawson et al. 2008; Sundelacruz et al. 2009). To overcome these problems, regenerative medicine or tissue engineering strategies for bone reconstruction are critically focused on the combination of stem/progenitor cells with porous biomaterials or scaffolds. Porous constructs seeded

with autologous progenitor cells, e.g. extracted from the bone marrow, could address some of the main issues associated with the current use of autologous or allogenic bone grafts (Hollinger et al. 2004). The main advantage of using stem cells is that they are provided by the patients, thus avoiding all risks of rejection by the body. Furthermore, cell expansion *in vitro* of these cells is possible which avoids a massive biopsy which is often painful for the patient (Iliac crest, chin). The success of such tissue regeneration approaches is, however, determined to a large extent by the interaction between the cells and the porous biomaterial scaffold, which should be osteoconductive and ideally osteoinductive. In the end, this should lead to achieving the aim of restoring tissue functionality by regenerating new tissue, either *in vitro* or *in vivo*.

Many scaffold parameters play a critical role in optimal tissue formation and ingrowth, such as chemical composition, physical surface characteristics (micro and nano roughness) and 3D architecture. Interconnectivity (Lu et al. 1999; Melchels et al. 2010), porosity and pore geometry (Zeltinger et al. 2001; Pamula et al. 2008) are among the main factors influencing 3D growth. Although some general trends have been established, the effects of pore geometry on tissue formation and differentiation *in vitro*, remain altogether controversial. Moreover, comparing the results of different studies is compounded by the wide variety in scaffold architecture ranging from completely random to highly structured and thus ‘pore size’ alone is insufficient to describe the 3D pore geometry (Hollister et al. 2002; Moroni et al. 2006; Yang et al. 2008).

The 3D environment provided by the pore geometry guides the spatial arrangement of cells and hence governs tissue organization, proliferation and differentiation, as demonstrated in targeted studies investigating pores of different shape and aspect ratio (Engelmayr et al. 2006; Rumpler et al. 2007). Thus while it has been demonstrated that pore architecture is highly important in modulating tissue formation, accurate quantification of tissue growth remains an issue. In addition, how to achieve optimal tissue formation, colonization and ultimately functionality is still largely unclear. Therefore, a more profound understanding of tissue formation in well-defined porous structure is required in order to achieve optimal scaffold design.

## 1.2 Objectives and Scope

The overall aim of the project is to investigate how initial tissue formation occurs *in vitro* in a 3D environment in order to improve macro-porous scaffold design. However, parameters accounting *in vivo* for implantation e.g. blood flow, mechanical constraint on host site will not be simulated in the experiments. The research will be achieved using human bone marrow stromal cells growing in a precisely defined porous structure made of calcium phosphate cements in static conditions.

### 1.2.1 Objectives

- To determine the factors responsible for different patterns of growth to understand the basic mechanisms of tissue formation in porous biomaterials.
- To determine whether variations in 3D structure lead to different tissue formation pattern (kinetics & amount).
- To determine why tissue would grow differently in varying structures.
- To determine the location of tissue proliferation and the possible existence of regions where cell division would happen preferably.
- To determine how tissue would differentiate and whether one structure is more favourable for osteogenic lineage commitment.
- To determine criteria for optimizes structures, leading to improved tissue formation, in order to inform better porous scaffold design.

Thus, in this work it was investigated whether variations in 3D structure led to different tissue formation pattern in terms of growth velocity and amount of tissue formed. The question why tissue has different orientations and why tissue would grow differently in varying structures was also addressed. To explain the results we particularly focused on the potential role of mechanical forces generated during tissue formation. An important point investigated was the location of tissue proliferation and the possible existence of regions where cell division would happen preferentially because of mechanical conditions which would be more suitable than others for tissue formation. Our results showed that specific structures (i.e. pore slots of different width) promoted growth more than others. The results also provided insights in how a specific structure affects tissue organization. The potential role of cell generated mechanical forces in cellular

orientation and multi-cellular rearrangement was also investigated, which will need to be confirmed directly in future studies.

### **1.2.2 Scope**

A full understanding of the dynamics of *in vitro* tissue formation in 3D has not been achieved to date, while this knowledge is clearly of crucial importance for regenerative medicine purposes. The common approach to regenerate tissue in porous constructs is, first to produce a scaffold with a given architecture, largely prescribed by the fabrication technique, and then to assess how this structure performs in terms of tissue formation and organisation. This is usually achieved using histological methods and by investigating the overall cellular response (cell quantity, expression level of markers, cytotoxicity). However, it has never been satisfactorily explained why the tissue would organize in one preferential way as opposed to another on the micro level, or why there is more tissue formed in a certain case. Using such previous approaches, no particular structure has emerged to be generally accepted as the optimal 3D environment for tissue regeneration. Therefore, the rationale for the current studies is that scaffold architecture needs to be designed from the start, based on the actual knowledge of how precisely tissue forms *in vitro*, which is the missing link that this work is focused on.

## **1.3 Layout of the Thesis**

This thesis is structured in several parts. First, a literature review section in which the relevant topics related to the work done in this thesis are detailed. Second, an experimental section composed of three studies. In the first experimental study, the development of the device used for investigating tissue formation is detailed. Initially, several materials were considered as potential candidates, however, TCP cement was chosen as it is an established biocompatible material for bone regeneration and can be easily moulded. Subsequently, biocompatibility with human bone marrow stromal cells was confirmed. Therefore, porous TCP devices were fabricated and tissue formation was investigated. The first experimental part (Chapter 3) provided evidence for a tissue growth mechanism involving cell division, associated with differences in tissue formation within various pore structures. Further results revealed different cytoskeletal organisation depending on pore structure and indicated the potential role of cell

mechanics in this process. Furthermore, initial results showed that tissue organisation might impact tissue formation. Thus, in the second experimental part (Chapter 4), the detailed tissue organisation, as well as the amount of tissue formed, was quantified precisely, demonstrating clear differences in orientation which can potentially explain further the observed growth patterns. In the third experimental study (Chapter 5), tissue differentiation was investigated in order to comprehend how osteogenic differentiation progresses during cell invasion and whether this could potentially affect a trade-off between promoting ingrowth and differentiation. Eventually, a brief discussion summarizing the results of these three related individual studies has been included. In addition, improvements for the actual device used, limitations and advantages are discussed, as well as outstanding questions and opportunities for future work.



## **Chapter 2**

### **Literature Review**

In this chapter, several relevant aspects for bone tissue engineering will be reviewed. First, the organic composition of bone will be described such as proteins and cells and their respective role. Next, the components of bone engineering will be summarized including the cells potentially used as well as the materials for implants manufacturing. Additionally, porous scaffolds structure will be discussed especially the effect of pore geometry and size on tissue formation within these structures. Eventually, the role of internal stress generated by cells on tissue behaviour will be discussed.

#### **2.1 Bone tissue**

Bone is a complex tissue formed by distinct parts. Bone anatomy will not be discussed here as the main focus of this study is tissue formation *in vitro*. Bone is a tissue formed of blood vessels, cells and a matrix compounding an organic part (Osteoid) and a mineral part.

##### **2.1.1 The cells of bone tissue**

Bone tissue is formed of 3 types of cells: Osteoblasts, Osteocytes and Osteoclasts. Osteoblasts are the cells forming bone, therefore, their role will be emphasised in this section.

###### **2.1.1.1 Osteoblasts**

Osteoblasts are the cells responsible for bone formation i.e. they synthesize osteoid which is composed mainly of Collagen I and other non-collagenic proteins (Marieb 2010). The role of these proteins will be detailed in the next section. Furthermore,

osteoblasts also release vesicles containing several components required for tissue mineralization such as enzymes and minerals ( $\text{Ca}^{2+}$ ,  $\text{PO}_4^-$ ) (Dean et al. 1994). Osteoblasts are mononuclear cells arising from pluripotent progenitors located in the periosteum and bone marrow which can also differentiate into various cell types such as adipocytes, myocytes and chondrocytes (Aubin 2001). Once the commitment into osteoblastic lineage of pluripotent progenitor is triggered, they undergo three developmental stages: proliferation, matrix maturation, and mineralization. Collagen I secretion peak occurs during the proliferation phase. Alkaline phosphatase activity peaks during the early matrix maturation, whereas the Osteopontin and Osteocalcin secretion peaks take place during the late matrix maturation and early matrix mineralization phase (Lian et al. 1998) (Fig. 2-1).

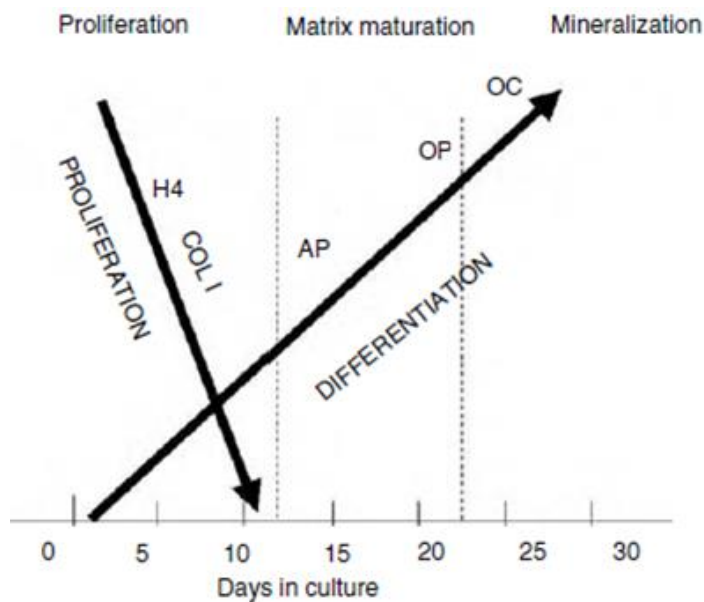


Fig. 2-1 Temporal expression of genes reflecting osteoblastic differentiation for cells in culture. Expression of Histone 4 (H4) and Collagen I (Col I) occur during proliferative phase. During matrix maturation, specific genes for bone markers are expressed i.e Alkaline Phosphatase (ALP) and Osteopontin (OP). During the mineralization phase, Osteocalcin (OC) gene is expressed. Drawing from Hollinger et al. 2004

Knowledge about the expression of these genes is important for bone engineering purposes. Indeed, by investigating the expression of these markers, assessment of tissue differentiation in various conditions *in vitro* is possible.

### **2.1.1.2 Osteocytes**

Osteocytes are osteoblasts which have become entrapped within the matrix they have produced. Osteoblast transformation into an osteocyte is the terminal step in osteoblast differentiation. *In vivo*, they represent the majority of the cells present in bone, up to 90% of the cell population (Parfitt 1977). Nevertheless, osteocyte isolation as well as culture *in vitro* is difficult, therefore, they are the least studied type of cells of bone tissue. However, osteoblasts were seen to differentiate into a type of cell displaying the same morphological aspect as osteocytes when they are embedded within a three-dimensional collagen gel, which was not observed when cells were grown in traditional culture plates. Therefore, three-dimensional environment seem to be required for complete osteoblast differentiation into osteocytes (Karsdal et al. 2002).

### **2.1.1.3 Osteoclasts**

Bone tissue undergoes constant remodelling. During this process, osteoblasts are the cells producing bone, as mentioned earlier. On the other hand, osteoclasts are the cells responsible for bone resorption. They are multinuclear cells developing long extensions similar to dendritic cells which penetrate the established matrix. Osteoclasts regulate bone resorption by rendering the local environment acidic via protons release. Therefore, osteoclast action is essential for bone turnover and metabolism. In case of an unbalanced production-resorption ratio, several pathologies can appear such as Osteoporosis in the case of higher resorption or osteosarcoma in the case bone over production.

## **2.1.2 Osteoid**

### **2.1.2.1 Collagen**

Collagen is the principal component of the osteoid, it represents 90% of the proteins present in the organic matrix of bone. Collagen is an assembly of 3 monomers forming a triple helix which is stabilized by hydroxylated proline molecules. Once released in the extracellular matrix, collagen molecules form larger structure by forming cross links leading to the formation of a dense fibrillar network (Fig. 2-2).

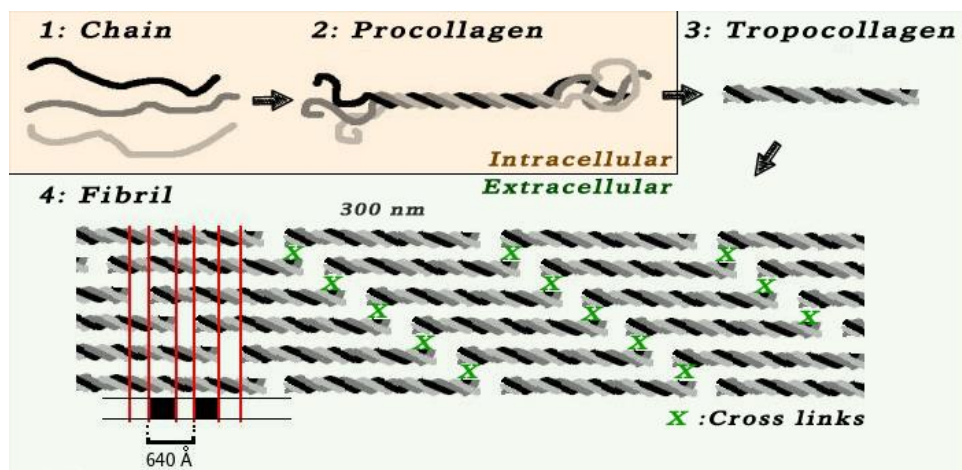


Fig. 2-2 Collagen fibres formation and intermolecular cross-link process (Fratzl 2008).

*In vivo*, bone is made of units called osteons. Osteons are built of sub-units called lamellae which are concentrically assembled around a canal (Haversian canal). Here we will not go into detail regarding bone anatomy, however, mentioning the organisation of lamellae is important to introduce the notion of a highly organised sub-unit. A single lamella is made of collagen fibres aligned parallel to each other. Indeed, in each lamella the collagen network displays a distinct orientation. Therefore, collagen matrix orientation appears as a crucial factor *in vivo*. Thus, being able to control Collagen organisation for bone regeneration purposes is an aspect which should be taken in account. For a long time, the main function of collagen was believed to be structural only, i.e. it would serve solely to maintain tissue architecture and provide mechanical strength in tension. However, Collagen I also serves as a backbone for bone mineral deposition. Indeed, calcium phosphate crystals are deposited parallel to their long axis along collagen fibres. Therefore, collagen is also required for tissue calcification (Hollinger et al. 2004)

### 2.1.2.2 Non Collagenic proteins

Non collagenic proteins represent 5-10 % of the osteoid, these proteins seem to have a crucial role during the matrix mineralization process. However, their involvement seems to be dependent on intrinsic parameters such as degree of phosphorylation, glycosylation and sulfation. In order to assess late osteogenic lineage commitment, the most commonly investigated non-collagenic proteins are Bone Sialoproteins (BSPs). One of the most studied BSPs is Osteopontin, known also as BSP-1 (Hollinger et al. 2004). Bone SialoProteins account for ~ 15% of the non collagenic protein pool.

---

## 2.2 Biological components for bone tissue engineering

### 2.2.1 Bone Marrow Cells

Bone marrow is the flexible tissue found within bone cavities. Osteogenic precursor cells can be found in the bone marrow. Several studies showed the relevance of Bone Marrow Cells for enhanced osseous defects repairs. According to the literature, Connolly & Shindell (Connolly et al. 1986) were the first to introduce the concept of using autologous bone marrow to heal bone defects. For this purpose, bone marrow was injected into tibial non-unions sites. After 6 months post-injection, the procedure showed union by observing radiographs. Additionally, after removal of bone tumours from eight patients, bone marrow injection induced union in seven cases (Healey et al. 1990; Garg et al. 1993). Based on these findings, combining bone marrow with porous implants was the next logical step. Using bone marrow to functionalize porous implants introduces several necessary components such as blood cells, growth factors, proteins and most importantly osteoprogenitors. For example, in the case of defect treatment in the metaphysis of sheep tibiae, porous implants impregnated with bone marrow demonstrated improved osteointegration over implants impregnated with venous blood 12 weeks after surgery (Stoll et al. 2004 & Becker et al. al 2006). Although these procedures were seen to be successful, osteoprogenitors, or skeletal stem cells, represent a low percentage of the whole bone marrow cells population. Indeed, one cell out of fifty thousand nucleated cells is capable of osteoblastic differentiation in the case of young patients and one out of two millions in the elderly population (Werntz et al. 1996). Therefore, prior to association with porous scaffolds, osteoprogenitors should be expanded *in vitro*. This concept has been initialized in a study carried by Bruder et al. where prior combination with porous scaffold, osteoprogenitors were expanded under specific culture conditions (Bruder et al. 1998). Bone marrow is commonly obtained from patients undergoing hip replacements (Tare et al. 2012) or other surgical procedures permitting access to bone cavities.

Several types of cells can be found in the bone marrow such as blood stem cells (haematopoietic stem cells) and a variety of different types of cells belonging to a group commonly called “mesenchymal” cells or otherwise “unselected bone marrow stromal cells”. These cells can be isolated *in vitro* by their capacity to adhere to a plastic surface.

The plastic adherent cell population is not homogeneous. In reality, they constitute a pool of stromal precursor cells composed of multi-, pluri-, bi- and uni-potential progenitors. Additionally, other cell types can adhere to a plastic surface such as endothelial, smooth muscle, and macrophage cells and, therefore, increase the variability of cell types in the mesenchymal cells. However, these “contaminating cells” eventually disappear after continuous expansion *ex vivo*. Thus, unselected bone marrow stromal cells constitute a relevant cellular population to be combined with porous scaffolds for *in vitro* investigation or *in vivo* implantation as their number is quite high and easily isolable.

Furthermore, among the unselected bone marrow cells, a particular type of cells which have become popular for bone engineering exists. The terminology for these cells can be ambiguous, the most common names are: “Bone Marrow Stromal Stem Cells” or “Mesenchymal Stem Cells” or “Skeletal Stem Cells” as the bone marrow derived varieties show mainly a skeletal predisposition. Their particularity lies in the fact that these cells are undifferentiated progenitors which can commit into different types of tissues such as muscle, fat, cartilage and bone (Bruder et al. 1998). Moreover, they represent only a tiny fraction of the cells present in bone marrow i.e. 0.001-0.01% (Pittenger et al. 1999). Therefore, specific techniques have been developed to isolate such cells for bone tissue engineering purposes (Zhu et al. 2012). These cells express particular markers enabling distinction between “unselected bone marrow stromal” and “skeletal stem cells”. One of the most popular antigens for identification of “Skeletal stem cells” is STRO-1. STRO-1<sup>+</sup> cells are usually isolated using specific antibodies and magnetic cell sorting techniques (Dennis et al. 2001; Gothard et al. 2011).

### **2.3 Materials used for porous implants fabrication**

Porous scaffolds are generally used as a carrier to supply the site of interest with cells and growth factors. Several requirements are essential for any potential scaffold material, such as the ability to support bone ingrowth and differentiation and the capacity of resorption *in vivo* while neo-bone is formed. Various materials have been investigated regarding their potential application in bone engineering.

### 2.3.1 Collagen Matrices

As detailed earlier, collagen is the major protein present in bone tissue and has been considered as a relevant material use for bone engineering purposes. Indeed, collagen is used as a scaffold *in vivo* and provides the organic bone matrix and also establishes bounds with mineral crystals as well as with Osteopontin. For instance, collagen gels combined with bone marrow cells were used successfully to heal diaphysal defects. Moreover, this healing was enhanced compared to a case using cancellous bone graft (Laffargue et al. 1999). Nonetheless, Collagen matrices display poor mechanical properties as in gels. However, this problem can be overcome by mixing collagen with other polymers, doping it with ions present in the apatite layer i.e.  $\text{Ca}^{2+}$ ,  $\text{Mg}^{2+}$  and  $\text{PO}_4^{3-}$  or using freeze drying techniques.

### 2.3.2 Synthetic Polymers

Synthetic polymers appear as an advantageous alternative for bone engineering purposes due to their good biocompatibility and the absence of the risk of disease transmission. Furthermore, the practical aspects of synthetic polymers include their availability and ease of manipulation for the fabrication of complex 3D structures. Additionally, synthetic polymers can be shaped precisely to fill defects with particular geometry (Oreffo et al. 1999).

Popular synthetic polymers used are saturated poly- $\alpha$ -hydroxyesters. This includes PolyLactic Acid (PLA), PolyGlycolic Acid (PGA) and PolyLactic-co-Glycolic Acid (PLGA). These polymers present relevant characteristics such as their degradability. Ester groups can be hydrolysed at a low rate and this process can be catalysed in presence of acidic elements. Hydrolysis of these polymers results in an acidic environment and the body is then able to remove the monomeric components of Lactic and Glycolic acids that are left (Rezwan et al. 2006). Furthermore, the mechanical properties of these polymers can easily be adjusted for load-bearing applications by creating “blends”. However, because of the bulk erosion these polymers undergo, the probability of scaffold failure cannot be neglected. Also, strong inflammatory reactions can emanate from the acid released during de-esterification of these polymers (Bergsma et al. 1993; Martin et al. 1996).

Nevertheless, several studies reported success in the use of such synthetic polymers for bone engineering purposes. For example, PGA scaffolds containing periosteum-derived cells were seen to promote neo-bone formation and eventually bridge a defect of 9 mm in rat femurs after 12 weeks (Puelacher et al. 1996). In addition, PLGA seeded with periosteum, chondrocytes and tenocytes has been used to recreate a finger joint in a mice. 20 weeks after subcutaneous implantation, phalanges with appropriate shape and size were formed (Isogai et al. 1999). Furthermore, an isoform of PLA (PLLA) was used in the form of a porous membrane to cover 1 cm diaphyseal defects in New Zealand White rabbits. The results showed cortical bone regeneration without any noticeable side effects (Meinig et al. 1996). On the other hand, there is a critical defect size above which synthetic polymers applied solely are not able to induce complete healing. Indeed, to treat defects of 4 cm in sheep, a combination of PLLA and cancellous bone graft was required to successfully bridge the defect (Gugala et al. 1999).

### **2.3.3 Calcium Phosphates**

Calcium Phosphates are certainly the most popular material used for bone engineering purposes. The main characteristic of these materials is their similar chemical composition to the mineral component of the bone matrix in mammals (Lowenstam et al. 1989; Weiner et al. 1998; Dorozhkin 2007). Moreover, calcium phosphates display very good biocompatibility, no cytotoxicity and are not recognized as foreign material by the body, therefore, generating minimal inflammation (Best et al. 2008). Consequently, when implanted, calcium Phosphates create strong bonds with the host tissue site (Osteointegration) (Legeros et al. 1993; Ong et al. 2000).

However, the fact that Calcium Phosphates are brittle materials with a low fatigue resistance constitutes a major limitation for load-bearing applications (Hench 1991; Cao et al. 1996; Dorozhkin 2010). Therefore, due to this disadvantage, biomedical use of calcium phosphates mainly consists of non-load bearing implants and filling bone defects in oral and orthopaedic surgery, as well as coatings for dental implants and metallic prostheses. Nevertheless, to counter the brittleness of calcium phosphates, reinforcements with metals or polymers can be achieved (Dorozhkin 2009). Logically, poor mechanical resistance is amplified as porosity is increased. This is an important

issue, because the minimal scaffold pore size for bone engineering is commonly agreed to be higher than 100  $\mu\text{m}$  to allow for bone ingrowth as well as vascularization (Carotenuto et al. 1999; Gauthier et al. 1999; Hing et al. 1999).

In terms of chemistry, the majority of calcium phosphates are based on Hydroxyapatite (HA),  $\alpha$ -Tricalcium Phosphate ( $\alpha$ -TCP),  $\beta$ -Tricalcium Phosphate ( $\beta$ -TCP). Also, mixtures of HA &  $\alpha$ -TCP or HA +  $\beta$ -TCP can be used in materials called biphasic calcium phosphates (BCP) (Dorozhkin 2010). Regarding the preparation of Calcium Phosphates, an important factor is the Calcium/Phosphate ratio. Indeed, materials with Ca/P ratio lower than 1 are not suitable for biomedical applications due to their high solubility and acidity.

Despite of serious mechanical limitations, calcium phosphates are found in numerous forms including powders, particles, granules, dense blocks, porous scaffolds, injectable formulations, self-setting cements and implant coatings (Best et al. 2008). Several studies reported successful outcomes using Calcium Phosphate for the treatment of bone defects. For instance, calcium phosphate loaded with Mesenchymal Stem Cells was used to treat large bone defects in canine femurs. After four months, woven and lamellar bone ingrowth was noticed in the implants (Bruder et al. 1998). Furthermore, positive results were obtained for long bone defects in humans. Indeed, defects up to 7 cm were effectively treated with macroporous HA ceramics. Two months postoperatively, regenerated bone tissue spanned the implants, which showed good osteointegration at the interface between the implants and the host tissue (Quarto et al. 2001) (Fig. 2-3).



Fig. 2-3 Radiographs obtained before, immediately and months after porous HA implantation for bone defect treatment. (Top) 41 years old female patient treated for unsuccessful tibiae lengthening attempt. (Bottom) 16 years old female patient treated for bone loss after trauma. Both of the cases are 4cm defects. (a, d) Pre surgery, arrow shows the bone defect. (b, e) Immediately after surgery, arrow shows the porous implant. (c) 18 months and (f) 8 months after surgery. Adapted from Quarto et al. 2001 (Quarto et al. 2001)

## 2.4 Porous Scaffolds

Scaffolds for bone tissue engineering are generally porous structures which can have a wide variety in architecture (Fig. 2-4). Tissue formation and ingrowth within scaffolds is governed by a large number of parameters, which include the surface chemical composition (Ducheyne et al. 1999; Sabetrasekh et al. 2010), surface topography i.e. micro and nano roughness. (Deligianni et al. 2001; Lossdörfer et al. 2004; Lamolle et al. 2009; Mathur et al. 2012). These parameters mainly govern 2D growth, namely, cell spreading over the surface of the scaffold. Once 2D confluence is reached, the subsequent step is actual 3D tissue formation. This implies filling of the voids within the construct. 3D tissue formation is governed by structural factors, especially 3D architecture. For instance, interconnections between pores and tortuosity regulate ingrowth and nutrient transport to the centre of the scaffold (Lu et al. 1999; Melchels et al. 2010). Additionally, scaffold porosity, surface to volume ratio, pore size (Zeltinger et

al. 2001; Pamula et al. 2008) and pore geometry (Karageorgiou et al. 2005; Sundelacruz et al. 2009) are the main parameters controlling 3D tissue formation. In this chapter, we review how pore size, pore geometry and interconnectivity influence tissue formation in porous structures.

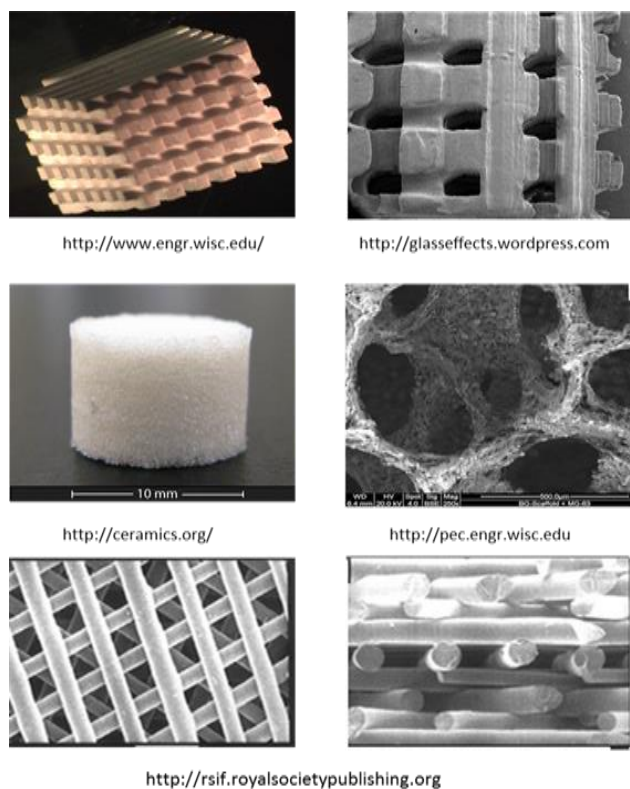


Fig. 2-4 Examples of various porous architecture in scaffolds for bone engineering. Picture from *royalsocietypublishing.org*

### 2.4.1 Interconnectivity

Interconnectivity is a key determinant factor of tissue formation within the scaffold. Connections between pores have been shown to influence nutrient transport (Martys et al. 1994) as well as cell migration (Moore et al. 2004). The main parameter investigated is how the size of these interconnections affects tissue growth. Pore interconnections of 50-100  $\mu\text{m}$  are recommended. For instance, the size of the interconnections has been found to be a critical parameter in porous titanium scaffolds. Narrow interconnections prevented tissue growth and the threshold for interconnection size allowing tissue ingrowth was reported to be around 50 $\mu\text{m}$  (Otsuki et al. 2006). Below this value, tissue displayed a poorly differentiated aspect, which means low levels of mineralization (Otsuki et al. 2006). In another example, HAp porous scaffolds were fabricated with a

mean pore size of 300  $\mu\text{m}$ , which is often cited as the optimal pore size for bone ingrowth. Interconnections were mainly about 200  $\mu\text{m}$  and bone ingrowth was enhanced by a better bone ingrowth within the scaffold. However, when the size of the interconnections was decreased to less than 50  $\mu\text{m}$ , bone ingrowth throughout the scaffold was dramatically reduced (Jones et al. 2007). These data suggest that despite an optimal pore size, if the interconnectivity of the network is not taken into account, bone ingrowth might be prevented. A study by Lu et al. supported that interconnection size should be at least 50  $\mu\text{m}$  in order to allow mineralized bone ingrowth, as interconnections of 20  $\mu\text{m}$  led to chondroid tissue formation (Lu et al. 1999). Thus, pore interconnection size is seen to affect scaffold colonization by cells and also the mechanism by which bone tissue is formed. In the case of interconnections below 50  $\mu\text{m}$ , endochondral ossification might occur as chondroid tissue formation is observed.

## **2.4.2 Pore Geometry & Pore Size**

Pore geometries can be defined in different ways, e.g. in porous biomaterials with mainly round pore shapes, the size can be defined as the diameter of the largest sphere that can be contained in the pore (Jones et al. 2009). In general, due to variation, pore size can only be defined as a range or distribution. In porous biomaterials made of fibres, the definition is different. The minimum gap between two adjacent filaments (inter-fibre space) was used to define void size by Yang et al. (Yang et al. 2008). In the following paragraphs, several studies into the effect of pore size are listed. These studies, however, all have the limitation that scaffold pore size represents an average, with a wide variation. Also, pore interconnectivity is not fixed. Therefore, the ability to design and fabricate scaffolds with fixed architectures and pore sizes is required for a better understanding of the influence of scaffold architecture on bone regeneration.

### **2.4.2.1 Influence of pore size on tissue growth in vitro**

Despite numerous studies the effect of pore size on tissue growth in vitro is still unclear, as different trends have been reported regarding the dependency of colonization on pore size. A study with scaffolds containing pores ranging from 50 to 300  $\mu\text{m}$  revealed an equivalent growth in all pores with MC3T3 – E1 cells (Itoh et al. 2004). The main trend reported in numerous studies is that tissue growth would increase relative to the size of pores (Karageorgiou et al. 2005). This trend is supported by the fact that generally

bigger pores provide better nutrient transport and a better oxygen supply. However, some results from other studies show a different trend, as outlined below.

*Evidence of growth and osteogenic potential increasing with pore size*

Polymers scaffolds made of polyHIPE (porous polymers made of High Internal Phase Emulsion) with pores of 40, 60 and 100  $\mu\text{m}$  revealed a slight difference for proliferation of osteoblasts, however, the rate of cell penetration within the scaffold was significantly higher in 100 $\mu\text{m}$  pores after 35 days (Akay et al. 2004). On PHBV (poly-3-hydroxy butyrate-co-valerate) polymers it was observed that in scaffolds with pores of 300-500  $\mu\text{m}$ , stromal osteoblasts isolated from rat marrow displayed a better proliferation than for pores in the range of 75-300 $\mu\text{m}$  after 29 days (Kose et al. 2003). In scaffolds made of PLG (a degradable copolymer of L-lactide and glycolide) with pores of 40, 200 and 600  $\mu\text{m}$ , MG63 cultured for 7 days displayed a well spread morphology, good penetration (around 30% of the total thickness of the scaffold) and greater proliferation in the scaffolds when pores were above 200  $\mu\text{m}$ , with an optimal rate for pores of 600  $\mu\text{m}$  (Pamula et al. 2008). In a different study using similar materials and pore sizes, rat bone marrow stromal cells revealed a lower rate of proliferation (Ishaug-Riley et al. 1998). Indeed, MG63, a cell line well adapted to in vitro growth, showed greater and faster colonization compared to primary cell lines. Thus the type of cells used might influence the capacity of migration. Ceramic scaffolds made of hydroxyapatite with aligned channels reflected the same trend of greater growth with increasing pore size (Frosch et al. 2004; Rose et al. 2004). Analysis of cell penetration into the aligned channels revealed that cell coverage increased with increasing channel diameter. Cells cover 22% and 38% of the pore surface when pores have a diameter of 170 and 420  $\mu\text{m}$  respectively. Cell penetration from outside into the channel of the 421  $\mu\text{m}$  diameter channel was significantly greater than that observed within the 170  $\mu\text{m}$  channel (Rose et al. 2004).

*Absence of correlation between growth/osteogenesis and pore size*

Frosch et al. have grown human osteoblasts in titanium drilled channel with diameters ranging from 300 to 1000  $\mu\text{m}$ . The highest osteogenic potential was found in the channels with a diameter of 600  $\mu\text{m}$  and the highest cell number in the 300  $\mu\text{m}$ . (Frosch et al. 2004) Indeed, the highest cell density and amount of DNA was found in the channels with a diameter of 300  $\mu\text{m}$ . On the other hand, after 20 days the highest

amount of osteocalcin RNA, highest percentage of mineralized tissue (11%) after 40 days appeared in the 600  $\mu\text{m}$  channel (Frosch et al. 2002; Frosch et al. 2004). Eventually, the network of extracellular matrix proteins and osteoblasts began to form an osteon-like structure (Frosch et al. 2002). Therefore, the improved amount of new tissue formed is not related to a higher number of cells due to a higher surface area available in the 600  $\mu\text{m}$  channel. Furthermore the channel diameter did not influence collagen I production (Frosch et al. 2004), which is secreted during the proliferation phase of primary osteoblasts (Hollinger 2004). Thus in this study, the increasing pore size had the effect of improving differentiation instead of proliferation, in contrast to the conclusions from the studies listed in the previous paragraph. Nevertheless, it has also been shown that in smaller channels bone tissue is not directly formed, instead it undergoes a process similar to endochondral ossification. In other words, the tissue goes first through a step of chondrogenesis and only afterwards it differentiates into bone tissue (Karageorgiou et al. 2005), while larger pores favoured direct osteogenesis (Sundelacruz et al. 2009). This mechanism reflects the physiological mechanism of bone formation in early stages of life (Marieb 2010).

### **2.4.2.2 Influence of pore size on tissue growth *in vivo***

The work of Hulbert et al was pioneering in the field of pore size effects in porous implants *in vivo*. In calcium aluminate porous scaffolds, it was shown that pore size affected tissue growth inside the material. Porous ceramics implanted *in vivo*, with pores ranging from 10 to 75  $\mu\text{m}$  revealed only connective fibrous tissue growth. Between 75-100  $\mu\text{m}$  osteoid is produced, however, the tissue is unable to mineralize. The threshold in pore size that allowed growth of mineralized tissue was reported to be around 100  $\mu\text{m}$  (Hulbert et al. 1970). Further studies determined that the ideal pore size for *in vivo* implantations is slightly higher. Above this threshold, the effect of pore sizes ranging from 100 to 600  $\mu\text{m}$  has been investigated in porous hydroxyapatite in the presence of BMP-2. ALP activity, amount of osteocalcin and new bone formation were optimal for pore sizes of 300-400  $\mu\text{m}$  and only above this size capillaries are formed (Tsuruga et al. 1997; Kuboki et al. 2001; Karageorgiou et al. 2005). The same trend as *in vitro* is observed, i.e. that smaller pores promote chondrogenic tissue formation (Karageorgiou et al. 2005; Sundelacruz et al. 2009). A very promising study has been realized by Petite et al, using scaffolds made of coral preloaded with bone marrow stromal cells, with a

---

mean pore size of 250  $\mu\text{m}$ . In sheep metatarsus, bone defects ranging from 6 to 25 mm were successfully healed. Complete filling of the defect was observed after 16 weeks, with new bone formation with a tubular pattern (Petite et al. 2000). The newly formed bone displayed a normal bone macrostructure, with a well-differentiated marrow cavity and cortices and was well vascularized. The coral had almost completely disappeared after four months. This study shows that pore size can be lowered down to 250  $\mu\text{m}$  for successful use. Furthermore, a nitinol scaffold (made of Nickel and Titanium) with different pore sizes (ranging from 180 to 350  $\mu\text{m}$ ) placed in cranial defects in rabbits revealed no difference in bone ingrowth related to pore size (Ayers et al. 1999; Karageorgiou et al. 2005). As the thickness of the implant was in the same order of magnitude as the pores, the authors of this study suggested the existence of a minimum implants thickness to pore size ratio to observe the effect of different pore sizes on bone ingrowth. Therefore, the studies summarized in this paragraph demonstrate the fact the pore dimension for positive outcomes after implantations *in vivo* is fairly broad i.e. several hundred microns. Nevertheless, the pore size providing the fastest and densest regeneration still has to be determined. Furthermore, the ideal pore size may also vary as a function of pore geometry.

### **2.4.3 Pore Geometry**

#### **2.4.3.1 Pore Geometry & Tissue Organisation**

Several studies illustrate that the ability of cells to colonize a void is strongly dependent on pore geometry. Within a range of pore sizes, the maximum void that cells were able to completely fill had a maximum inter-fibre space of only 273  $\mu\text{m}$  in 3D fibre deposited scaffolds (Wang et al. 2005), whereas the maximum size that cells were capable to fill in round drilled channels was 600  $\mu\text{m}$  in diameter (Frosch et al. 2004). Consequently, the capacity of cells to fill a void is dependent on pore architecture. Furthermore, tissue filling voids within scaffolds can display distinct differences in 3D organisation according to the specific porous architecture of the structure. In 3D fibre deposited scaffolds with a mean pore size of 262  $\mu\text{m}$ , ECM fibres together with cells were arranged in a way to surround the polymeric fibres. In contrast, ECM fibres were reported to be randomly organised in scaffolds with round interconnected pores having a similar mean diameter of 255  $\mu\text{m}$  (Wang et al. 2010). Additionally, tissue formed in a scaffold with rectangular open pores displayed cells and collagen fibres oriented along

the longitudinal pore axis (Engelmayr et al. 2006). Therefore, the organisation of tissue formed by cells is likely to depend on the structure provided by the scaffold. It is clear from the above that pore architecture can affect tissue capacity to span a void as well as its spatial organisation. However, the relationship between the two remains to be explored, i.e. whether differences in tissue organisation could directly affect the potential of tissue to grow and expand within porous scaffolds.

#### **2.4.3.2 Pore Geometry, Cell Generated Forces and Tissue Formation**

Pore shape affects the pattern of tissue growth. In cellular monolayer studies investigating 2D growth patterns on adhesive patches of different shape, proliferation, at early stages is primarily confined to the edges and corners of the adhesive patch (Nelson et al. 2005). Furthermore, proliferation rate is found to be higher in corners. Additionally, the degree of curvature has an effect on tissue growth. In a 3D study different pore shapes with increasing curvature were used, such as hexagonal, square and triangular shapes. The thickness of the tissue grown in the corners increased relative to the curvature (Rumpler et al. 2008). On the other hand tissue formation (Quantified in terms of Projected Tissue Area (PTA)) is greater on faces with decreased curvature. When plotting the location of proliferation in 2D, this appeared to occur nonetheless around edges and corners while cells in the centre displayed a low rate of proliferation (Nelson et al. 2005). A model revealed that a contractile sheet of cells exerts higher traction forces around edges and corners with peaks at corners. The distribution of traction forces exerted matched with the distribution of proliferation foci. Cells generate traction force on a substrate by contraction of the actin-myosin cytoskeleton (Reilly et al. 2010) and it has been shown that modulation of the internal tension influences proliferation patterns (Nelson et al. 2005). Pore geometry may influence tissue growth through generating different patterns of internal tension probed by surface receptors and transmitted throughout a cellular network via cell-cell interaction. Nevertheless, it is still required to determine systematically how pore size and shape affect tissue growth and differentiation through the generation of internal tension.

## 2.5 Cell mechanics & Tissue Development

The cellular skeleton or cytoskeleton is composed of microtubules, intermediate fibres and actin fibres. The actin network is the most active element under constant remodelling and able to generate mechanical forces. Actin participates in many crucial cellular processes requiring mechanical input such as cell contraction, adhesion, migration and division. Furthermore, the implication of actin in these cellular processes is often coupled with important trans-membranous receptors i.e. integrins & cadherins. These cellular receptors are associated through a physical linkage to actin cytoskeleton and mediate the interactions between the cell and its environment, such as neighbouring cell, extracellular matrix or artificial substrates. In the following paragraphs, actin structure and these receptors will be described. Next, the coupled action of actin and these receptors will be briefly illustrated in several cellular processes mentioned above.

### 2.5.1 Actin: Molecular Aspects

Individual subunits of actin microfilaments are known as globular actin (G-actin), a globular protein of 42-kDa found in all eukaryotic cells. G-actin subunits assemble into long filamentous polymers called F-actin. F-actin filaments can rearrange into microfilaments by interacting together and forming a double helix structure. Microfilaments measure approximately 7 nm in diameter with a loop of the helix repeating every 37 nm. These filaments form the main part of the contractile apparatus in cells. The F-actin microfilaments can be cross-linked to form bigger structures called actin bundles or actin fibres. Actin fibres can contract by sliding along each other thanks to acto-myosin interactions. Actin fibres are stabilized by small molecules called Actin Binding Proteins (ABP). In contractile fibres, the actin-bundling protein  $\alpha$ -actinin separates each thin filament by approximately 35 nm. This increase in distance allows thick filaments to fit in between and interact, enabling deformation or contraction.

## 2.5.2 Actin Cytoskeleton & Cell Surface Receptor in Tissue Formation: Integrins & Focal Adhesions

Integrins are trans-membraneous receptors mediating the attachment between a cell and its environment. Integrins transmit information to the inner cellular apparatus regarding chemical composition and mechanical properties of the extracellular matrix or the substrate they are attached to. Thus, integrins are implicated in cell signalling, cell adhesion, cell motility and mechanical forces transmission. They form the major mechanoresponsive ECM adhesion sites and are also called focal adhesions or focal contacts (Bershadsky et al. 2003). These receptors link the extracellular matrix to the actin cytoskeleton. This trans-membrane interaction is mediated by a network of adapter or anchor proteins (more than 50 known to date) that form a submembrane plaque. Integrins are linked to this submembrane plaque by their cytoplasmic subunits. Most known proteins that form this submembrane plaque are vinculin, talin, actinin, paxillin and tensin which can directly link with the actin filaments (Fig. 2-5) (Mitra et al. 2005). Indeed, the link between integrins and actin is an “eternal love affair” as described by Brakebusch et al.

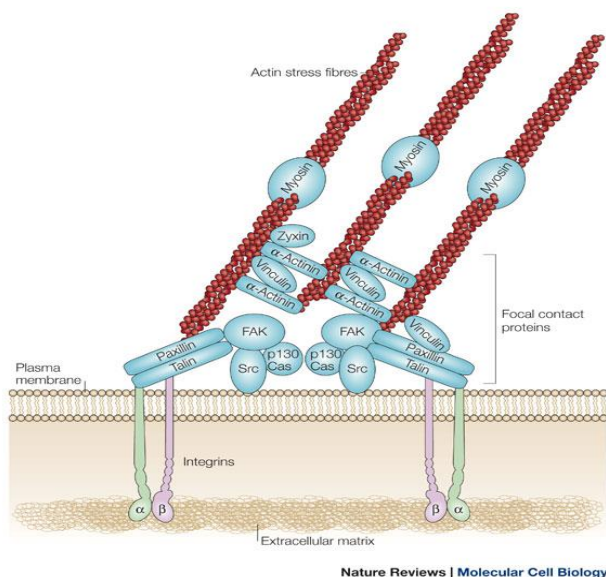


Fig. 2-5 Organization of a focal adhesion and its linkage to the actin cytoskeleton (Mitra et al., 2005)

Traction forces generated by contraction of the actomyosin network are applied to the surrounding ECM through integrins, which are linked to the actin network via focal adhesions. Indeed, if actomyosin contraction is prevented, focal adhesions disassemble and traction forces are not exerted on the matrix anymore in the following seconds (Balaban et al. 2001). Recent measurements of adhesion-mediated forces by seeding smooth muscle cells on substrates with micro-needles also revealed that the forces exerted ( $4.8 \text{ nN}/\mu\text{m}^2$ ) at these adhesion sites increase with focal adhesion size (considering a focal adhesion defined as an adhesion site larger than  $1\mu\text{m}^2$ ). Interestingly, it was observed that adhesions smaller than  $1 \mu\text{m}^2$  generated large forces that do not correlate to the adhesion site size. In general, different cell types produce different traction forces and develop matrix adhesions of varying sizes. Therefore, it is most surprising that the forces per unit of the adhesion area (stress) exerted by different cell types appear to be very similar. The capacity to exert tensile (pulling) forces is not dependent on cell type. It is more likely that the environment, rather than cell type, is the main determinant which dictates whether a cell will exert tension.

### **2.5.3 The Cytoskeleton and Cell Surface Receptors in Tissue Formation: Role of Cadherins**

#### **2.5.3.1 Structure of a Cadherin mediated Cell-Cell Adhesion**

Calcium-dependent cell adhesion, mediated by cadherins, is the main adhesion mode providing strong cell-cell interaction. The cytoskeleton has been shown to regulate cadherin-mediated adherents-type intercellular junctions and hence regulates the mode of cell-cell communication in various developmental and pathological contexts. The intracellular domain of cadherin, which is connected to other proteins such as catenins, is essential for efficient cell aggregation. This complex formed by the cadherin intracellular domain, catenin and several other proteins is inherently linked to actin filaments (Fig. 2-6). An important aspect is how the cytoskeleton-dependent assembly of cadherins and catenins under the cellular membrane contributes to cell contact formation.

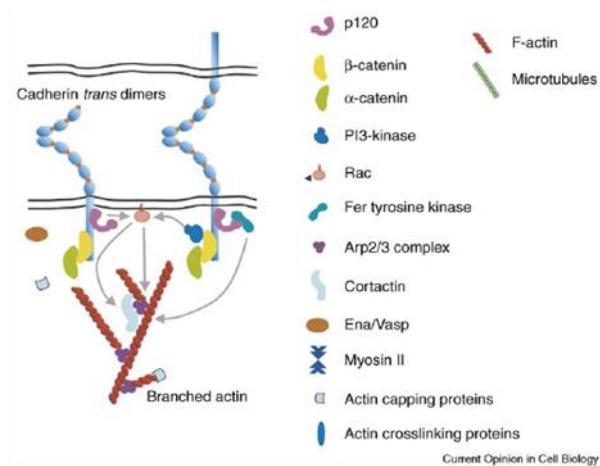


Fig. 2-6 Cadherin-Actin connection mediated by intracellular proteins (Mege et al., 2006)

### 2.5.3.2 Cell-Cell Adhesion Dynamics

To establish cellular contacts, fast and highly dynamic interactions between cadherin receptors are required. First, cadherin receptors diffuse freely throughout the cell membrane prior commitment into contacts. Secondly, cadherins form aggregates and their movement become restricted when engaged in cell-cell adhesion. The determinant parameters are the availability of cadherin receptors at the cell membrane, their mobility, and the ability of their intracellular and extracellular domains to form protein-protein bonds. When cells make contact, driven either by the mechanical pressure of their environment or by an active migration process, the most obvious response is the induction of lamellipodial extension (Gavard et al. 2004). The initial engagement of a few cadherins may be the most important event for maintaining the high membrane remodelling and actin dynamics necessary for the enhanced lamellipodial protrusion and the associated cell contact extension (Fig. 2-7)(Mege et al. 2006). The branching and polymerization of actin may provide the driving force that pushes the membranes of adjacent cells over each other. Alternatively, another type of actin polymerization generating unbranched long filaments may also be involved in contact extension via the formation of filopodia, frequently observed at cell-cell contacts. However, recent studies clearly show that in older cadherin contacts, cadherins are recruited in highly patterned protein complex tightly anchored to actin cables, named cadherin adhesions or macroclusters.

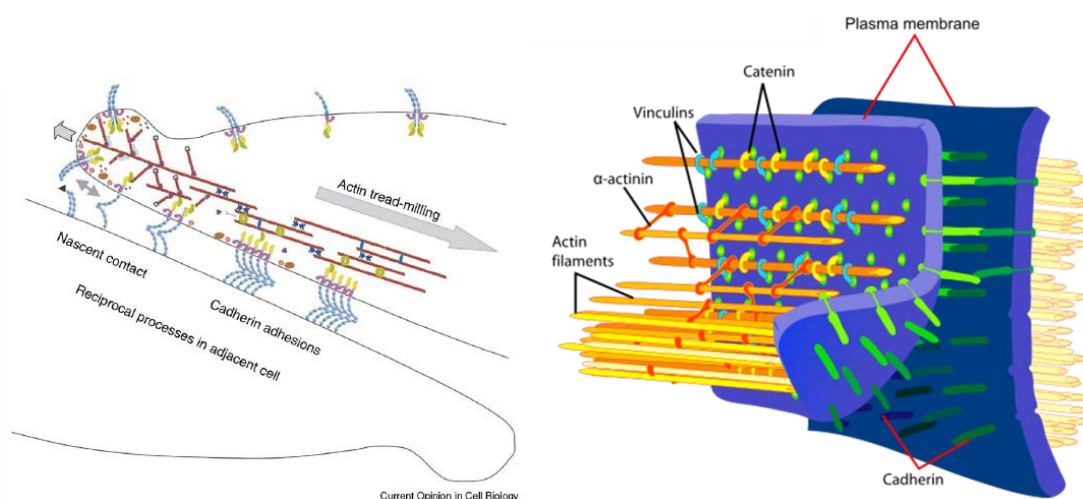


Fig. 2-7 Cell-Cell interactions dynamics involving Cadherins and the Actin-cytoskeleton (Mege et al. 2006)

### 2.5.3.3 Cell Adhesion Bonding Force

A single adhesion bond displays a half-life in the range of seconds (Leckband et al. 2006) but in a cellular context, adhesive bonds based on type E, N or 11 cadherins exhibited half-lives in the range of ten minutes or more (Kiener et al. 2006; Thoumine et al. 2006). The order of magnitude of the force associated with a single bond is piconewtons (Leckband et al. 2006) whereas measurements of cell separations showed values in the tens of nano-Newtons (Chu et al. 2004; Chu et al. 2006). Cell adhesion maturation and bonding forces are dependent on several factors such as cadherin subtype, density and signalling protein activities controlling actin polymerisation. Indeed, the strength of the contact becomes higher with time and is actin-cytoskeleton-dependent (Chu et al. 2004). Besides, cadherin is linked to actin via small scaffolding proteins such as catenin for example (Mege et al. 2006). The remodelling of this linkage complex involving actin cytoskeleton is believed to play a crucial role in cell adhesion bonding force.

### 2.5.4 Cell contraction mediated by Actin-Myosin association

Actin fibres can exert a contractile stress by sliding over each other via the coupling of actin with myosin (Fig. 2-8) (Marieb 2010). Therefore, this phenomenon induces cell contraction. At the beginning of the process the myosin head contains bound ADP and inorganic phosphate (Pi) and has a weak affinity for actin (1). Once the myosin head attaches properly on an actin filament, phosphate is released. The release of phosphate

strengthens the binding of the myosin head to the actin fibre and also triggers the force generating power stroke that moves the actin filament (2-3). ADP then dissociates and ATP binds the myosin head causing its detachment from the actin filament (3-4-5). On the detached head ATP is hydrolysed which allows the myosin head to go back to its initial state (5-6). The myosin head stores the energy released by the ATP hydrolysis and then the cycle can take place again. The actin filament does not slide back after being released by the motor head because there are many other myosin molecules attached to it holding it under tension. The contraction of the actin-network generates an internal cellular stress. This results in the shortening, or contraction, of the actin-myosin bundle (but not the actin filament itself).

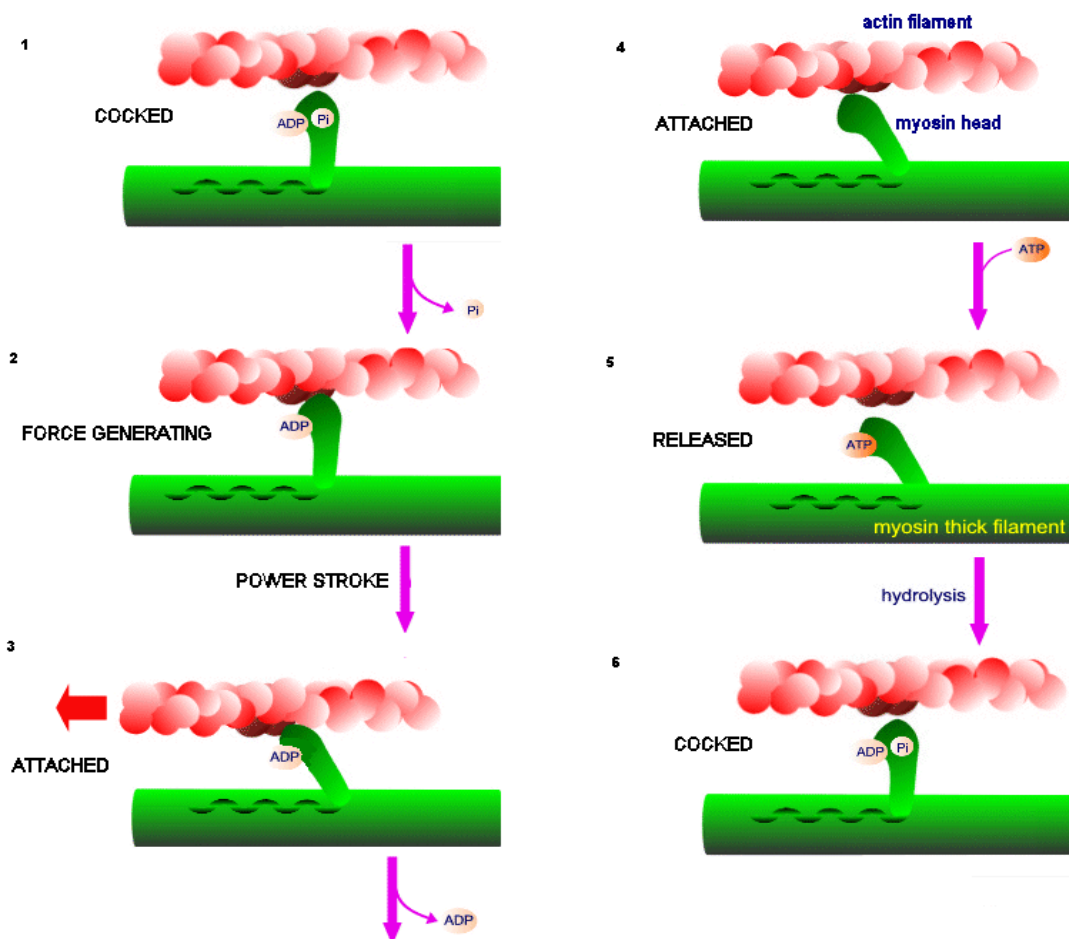


Fig. 2-8 ATP-dependent molecular mechanism of act-myosin contraction (*themedicalbiochemistrypage.Org*)

---

### **2.5.5 Actin in Cell Adhesion & Migration**

As described briefly in paragraph 2.5.2, cell adhesion to a substrate is mediated via integrins surface receptors. Also, recent data suggest that actin is involved in cell adhesion formation. Indeed, actin polymerisation near the membrane induce integrins clustering, a phenomena prevented upon actin polymerization disruption (Galbraith et al.2007). Therefore, actin polymerisation at the adhesion site seems to be essential for focal contact formation. Cellular adhesions consist in a temporary supramolecular assembly of several actin binding proteins (described in paragraph 2.5.2), therefore, adhesion form and deform relatively quickly. This is due to the fact that a cell can switch from a static to a mobile state depending on the signals received from the extracellular environment. Therefore, in reaction to these signals, cell adhesions and, therefore, cell migration is driven by actin cytoskeleton (Wehrle-Haller et al. 2003).

At the leading edge of migrating cells, integrins bind the ECM, recruit the actin cytoskeleton and initiate local reorganization of the actin network i.e. polymerisation, promoting different types of membrane protrusion such as filipodia and lamellipodia (Brakebusch et al. 2003). The continuous addition of monomers on actin fibres connected to focal contacts generate pushing forces on the plasma membrane and lead to protrusion extension at the leading edge of migrating cells (Borisy et al. 2000). On the other hand, at the rear of the cell, integrins are disconnected from ECM and actin cytoskeleton and are reused at the front of the cell for new adhesion formation (Ballestrem et al. 2001; Laukaitis et al. 2001)

### **2.5.6 Actin in Cell division**

Actin has been shown to be implicated in cell division using chemical drugs modulating actin filaments in the cells. Indeed, mitosis in primary cells was seen to be delayed using drugs preventing actin polymerisation (Gachet et al 2001, Lee and Song, 2007). Conversely, stimulation of actin polymerization results in an increased apparition of multinucleated cells (Moulding et al. 2007). These results suggest that intact actin cytoskeleton is required for efficient cell division. Disruption of actin prevented the activation of proteins permitting cell progression through early cell cycle step (Reshetnikova et al. 2000). Furthermore, actin implication in the final step of cell division i.e. the mitosis has recently been proved. Indeed, actin disruption prevents

mitotic spindle assembly as well as chromosomes separation (Uzbekov et al. 2002). Additionally, upon myosin II activity blockage, spindle assembly is also blocked (Rosenblatt et al. 2004), therefore, this suggests that preserved actin cytoskeleton is necessary for final step of cell division and that contractile potential of the latter is requested. Further evidences for a tight link between actin cytoskeleton and mitotic spindle were brought by studies showing actin presence within the mitotic apparatus and attachment to astral microtubules (Woolner et al. 2008, Wuhr et al. 2008). The connections between actin fibres and the tips of astral microtubules are likely to be the source of the pulling forces requested to position and orientate the spindle (Kunda et al. 2009) Moreover, integrins have been showed to be necessary for correct spindle orientation (Toyoshima et al. 2007). Integrins and the astral microtubules would serve as anchorage points for actin fibres, determining the global axis along which pulling forces for spindle orientation and separation would be exerted.

## **2.5.7 Effect of internal tension on cellular behaviour**

### **2.5.7.1 Proliferation**

Cells can exert an internal tension following the mechanism described earlier in paragraph 2.5.4, which increases with the stiffness of the substrate they are seeded on (Kong et al. 2005). Therefore, seeding cells on materials with different stiffness is an elegant way to investigate the effect of the level of internal tension on cellular behaviour. It was seen that pre-osteoblasts cells, seeded on stiff matrix, were exerting higher traction forces resulting in a higher proliferation rate (Kong et al. 2005). Internal stress can also affect proliferation of endothelial and epithelial cells in monolayers. Indeed, when internal cellular tension is increased or decreased with drugs modulating acto-myosin contraction, the proliferation rate scales with the level of internal tension (Nelson et al. 2005). This internal cellular stress can be propagated from cell to cell via cadherin-cadherin interactions, thus generating a stress field at a multicellular scale (Nelson et al. 2005). Therefore it is hypothesized that increased internal stress is likely to activate proliferation pathways and provide mechanical forces for cell mitosis.

---

### 2.5.7.2 Differentiation

The level of internal tension in undifferentiated stem cells participates to lineage commitment. Increased internal tension via Rho A pathway stimulation results in an osteogenic commitment of human mesenchymal stem cells (HMSCs) regardless of their shape (McBeath et al. 2004). Usually, a stem cell with a round shape undergoes adipogenic commitment, while a spread and flattened stem cell commits to the osteogenic lineage. In other words, the findings of McBeath et al. show that the effect of the level of internal tension dominates over the influence of cell shape on cell lineage fate. Furthermore, the level of internal stress exerted by undifferentiated stem cells direct their lineage commitment. A study emphasized this fact by measuring numerical values of internal stress. HMSCs committing to the osteogenic lineage exerted traction forces of 66.3 nN on average, peaking at 110 nN, whereas cells becoming adipocytes exerted forces of 23.6 nN on average, reaching up to 40 nN (Ruiz et al. 2008). Supporting results showed that MSCs grown on polymer gels mimicking the ECM stiffness of a certain type of tissue displayed a similar morphology and behaviour as the cell type typically present in that tissue (Engler et al. 2006). MSCs seeded on a stiff matrix and hence generating high internal stress (Kong et al. 2005), display an osteoblasts-like shape and produce early osteogenic markers such as the transcription factor CBF alpha as well as Collagen I (Engler et al. 2006). The trend observed in 2D (Engler et al. 2006) was found to be the same in a 3D environment. MSCs cells cultured in 3D in a thixotropic gel committed to different lineages according to the stiffness of the gel and hence the level of internal tension generated. The highest expression of osteogenic transcription factors (Runx2, Osteocalcin) was obtained for stiffer gels inducing higher internal stress (Pek et al. 2010).

Taking into account these data and the mechano-sensing mechanism suggested by Reilly (Reilly et al. 2010), which states that a higher internal tension is generated by actomyosin contraction on stiffer substrates, it can be assumed that the commitment to the osteogenic lineage of MSCs is triggered by generating a high internal tension pattern in response to a stiff substrate. Actin is constantly remodelled and hence the intensity of the stress varies over time. In the next paragraph, it is hypothesised that the internal tension level would change during the different phases of cell differentiation.

## **2.5.8 Stem Cell to Osteoblasts differentiation: Internal Tension Kinetics**

### *Cell adhesion and internal tension threshold reach*

Stem cells anchorage to a surface is mediated by forming focal adhesions which are linked to the actin cytoskeleton. After cell attachment, actin filaments synthesis (actin polymerization) is upregulated leading to formation of actin bundles (Fig. 2-9). Thus, before osteogenic differentiation occurs, the thickness of the actin fibres increase and hence the level of internal tension is raised (Fig. 2-10). This increase in internal tension results in an increased cell stiffness reflected by a higher compressive modulus (Chen et al. 2010). During this phase a high proliferative state is maintained and the internal tension increases further until reaching a certain threshold. This step could correspond to the time needed by the cell to reach internal tension equilibrium depending on the surface they adhere to.

The maximal tension corresponding to the threshold appears to involve two steps i.e. formation of super mature focal adhesion (suFAs) and the recruitment of  $\alpha$  Smooth Muscle Actin (SMA) in actin fibres. It was shown that the forces generated by the actin network on an adhesion site, defined as an area larger than  $1 \mu\text{m}^2$ , are correlated with the size of a focal adhesion (FA) (Tan et al. 2003). FA with sizes ranging from  $4$  to  $12 \mu\text{m}^2$  were undergoing forces of on average respectively  $20 \text{ nN}$  and  $60 \text{ nN}$ , which gives an approximate stress of  $5 \text{ nN}/\mu\text{m}^2$  (Balaban et al. 2001; Tan et al. 2003). The recruitment of  $\alpha$ -SMA in actin fibres can raise the stress applied to up to  $12 \text{ nN}/\mu\text{m}^2$  and occurs when focal adhesions become superFAs i.e. FA with a size larger than  $8 \mu\text{m}^2$  (Goffin et al. 2006). Recruitment of  $\alpha$ -SMA to pre-existing stress fibres requires a critical tension that is only generated upon formation of superFAs. Collectively, these results strongly suggest that the FA size limits the maximum tension developed in stress fibres and  $\alpha$ -SMA recruitment. Therefore, it is hypothesized that superFAs formation and SMA recruitment correspond to the moment where the internal stress is maximal and triggers differentiation.

---

*Differentiation onset*

Once cells reach a maximum tension threshold, commitment to the osteoblastic lineage is triggered. This appears to be linked to the fact that internal tension drops (Fig. 2-10), reflected by the appearance of actin fibres with a decreased thickness after day 7 (Fig. 2-9) (Chen et al. 2010). At that time, cells enter the early differentiation stage (pre-osteoblast) and consistently start to produce early bone markers, such as Cbf-alpha activity upregulation and Collagen I secretion (osteoid secretion), but are still able to proliferate (Hollinger 2004). This step could be assumed to correspond to the transition stage from stem cell to pre-osteoblast.

*Intermediate Differentiation*

After 2 weeks, once a substantial amount of osteoid has been produced, cells become confined in a compliant matrix (Raisz 1999). Therefore, the stress generated by cells continues to decrease. This could also be supported by the observation made Chen et al. where actin bundles become thinner at day 14 (Chen et al. 2010). Lowering internal stress is likely to induce further differentiation. Decreased internal stress associated with differentiation progression is supported by the fact that osteoblasts exert 6 times lower traction forces on a compliant substrate and undergo a differentiation process with a 4 times greater secretion of osteocalcin and a 20 times higher mineralization rate (Kong et al. 2005).

*Late Differentiation*

The softened environment then induces full differentiation into osteoblasts (Kong et al. 2005; Keogh et al. 2010). This occurs after 2-3 weeks when the secretion of late differentiation markers such as osteopontin and osteocalcin occurs and finally mineralization takes place and confers tissue rigidity characteristic of bone tissue (Raisz 1999; Hollinger 2004). A softer matrix may fail to provide stable anchoring sites for cell receptors, limiting focal contact formation and the generation of traction forces. Subsequently, cells are not stimulated to enter the cell cycle, but instead differentiate and increase bone tissue specific function.

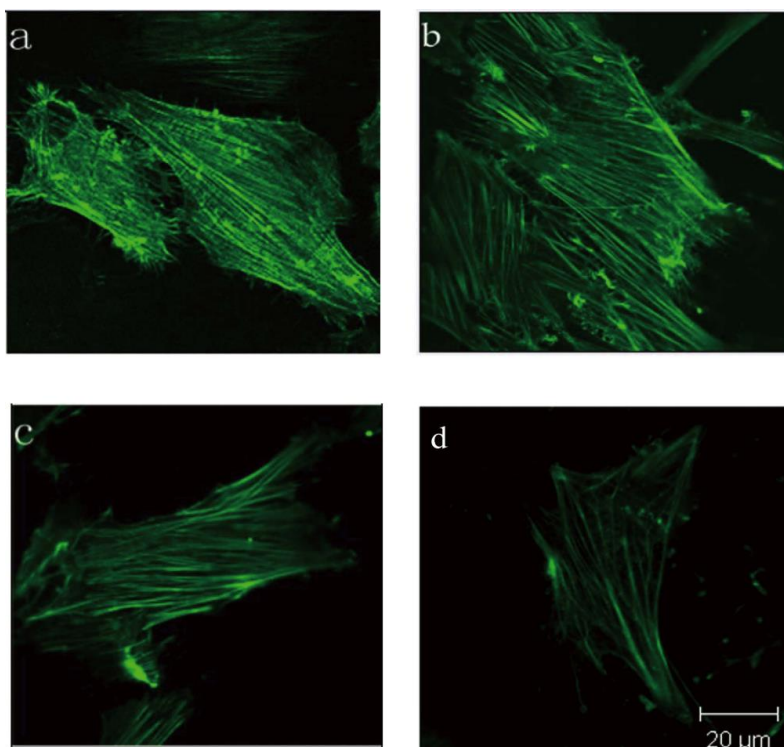


Fig. 2-9 Actin cytoskeleton rearrangement during human amniotic fluid-derived stem cells hAFSCs osteodifferentiation in 2D: (a) – (d), actin cytoskeleton after osteodifferentiation 0, 7, 14, 21 days, respectively. Within 21 days of the induction of osteogenic differentiation, more and thicker stress fibres are replaced with a thinner actin filament meshwork typical for mature osteoblasts. Scale bar, 20  $\mu\text{m}$ . From Chen, Xiao et al 2010.

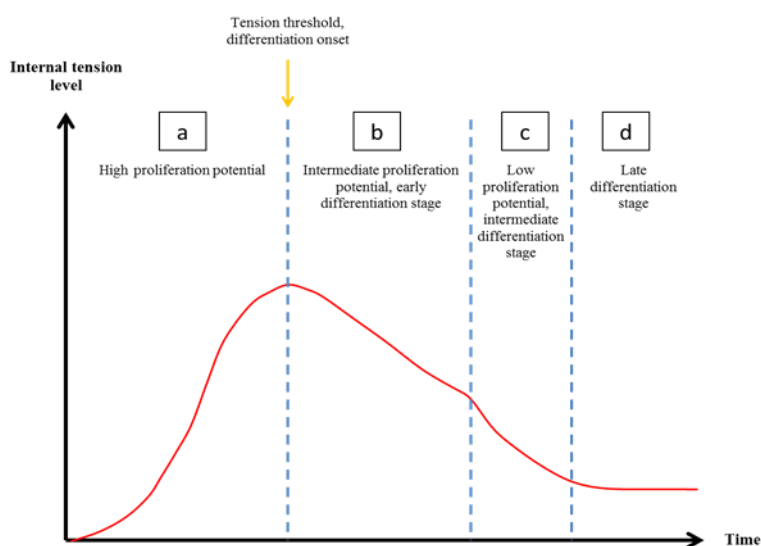


Fig. 2-10 Qualitative schematic, summarizing the potential role of internal tension during osteogenic-differentiation.

---

### 2.5.9 Contractile Potential of Musculoskeletal Tissue

In the past, fibroblasts and muscle cells were thought to be the only cells able to display a contractile behaviour. Smooth muscle cells were involved in blood vessels contraction (Davis et al. 1992; Crotty 1999) and dermal fibroblasts displayed a contractile behaviour in the case of wound healing to facilitate wound closure (Gabbiani et al. 1971). In pathological conditions these cells are involved in contraction (Gabbiani 1998) which can lead to dysfunction such as scar formation. Cells capable of contractile behaviour were termed “myofibroblasts” as they had characteristics of both fibroblasts and smooth muscle cells. Several researchers proposed that myofibroblasts could be identified by the fact that they contain SMA, one of the six isoforms of actin.

SMA belongs to a group of four isoforms related to contractile behaviour, the three others are  $\gamma$ -smooth muscle actin,  $\alpha$ -skeletal muscle actin, and  $\alpha$ -cardiac muscle actin. Two other isoforms;  $\beta$  and  $\gamma$  cytoplasmic actins are present in most cells and are involved in maintaining cell shape and promoting migration (Herman 1993). Nevertheless the presence of these contractile actin isoforms does not prove that the cell is contracting in any case, it only shows a potential for contractile behaviour. The presence of SMA has been revealed in chondrocytes (Zaleskas et al. 2004), in an osteoblast cell line (Menard et al. 2000) and in animal bone marrow stromal cells and has been shown to be incorporated in actin fibres (Cai et al. 2001).

The most promising cells, bone marrow stromal cells, used in work involving tissue regeneration *in vitro* in porous structure are capable of contractile behaviour. Therefore, particular attention should be paid to how the process of tissue contraction could be involved in tissue formation *in vitro*. Contractile behaviour of tissue has been shown to be involved in several processes such as proliferation and differentiation of different cell types, but the role and the implication of tissue contraction in the dynamics of tissue formation *in vitro* has not been properly investigated.

The contractile behaviour of cells has to be considered for tissue regeneration *in vitro* in porous material as it can lead to scaffold deformation. Moreover, the contractile behaviour of these cells could impact the performance of porous matrices employed for tissue engineering (Huang et al. 2012). Therefore the material used for regenerative purpose must be able to bear tissue contraction without undergoing a deformation that

could affect tissue formation. Indeed, tissue formed by MC3T3 osteoblasts like cells displayed a contractile behaviour in three dimensional matrices. Once seeded, GAG-Collagen matrices pores shrank to approximately 65 % of their original size by 4 weeks, whereas pores of non-seeded matrices shrank to only 80% of their original size (Menard et al. 2000). From the second to the fourth week, a decrease in DNA content was noted, which could be due to a reduction in diffusion of nutrients because of the shrinking of the pores (Menard et al. 2000). This point raises the question of the importance of the stiffness of the material that should be used for bone engineering.

### **2.5.10 Contractile Behaviour & Substrate Stiffness**

While probing their local environment, cells are able to generate different levels of internal tension level according to the stiffness of their surrounding matrix (Reilly et al. 2010). Increased matrix rigidity has been shown to induce stronger bounds between integrins and cytoskeleton and thus allows higher traction forces to be applied to the substrate through adhesion sites(Choquet et al. 1997). The ability to generate increasing levels of tension depending on the stiffness of the matrix is regulated by myosin motor protein mediated contraction of the actin network (Reilly et al. 2010). Besides, we already discussed the effect of tension on cell proliferation and differentiation above in paragraph 2.5.7. Thus the effect of material stiffness is important with respect to the modulation of internal tension and implant behaviour.

A number of recent studies revealed that substrate stiffness (elastic modulus ranging from 0.5 to 1.4 kPa) can affect the contractile behaviour and the maturation of osteoblasts in 3D. Stiffer Collagen-GAG matrices seeded with osteoblasts were resistant to cellular contraction and thus kept their original architecture. Therefore an improved diffusion of nutrients and oxygen throughout the scaffold occurred, which allowed a 2 times greater cell number. On the other hand, more compliant scaffolds underwent a deformation resulting in a pore size contraction of 70% after 6 weeks. However, after the same amount of time, compliant scaffolds supported a higher level of osteogenic maturation displaying greater expression of late stage bone formation markers such as osteopontin and osteocalcin and a higher mineralization rate (Keogh et al. 2010). The fact that cells respond to substrate stiffness by increasing internal tension seems to occur in 3D when the tissue is suspended, which is a configuration that is highly likely to

occur during the filling of a pore void by the newly forming tissue. In an elegant study, NIH 3T3 cells, a fibroblastic cell line, were embedded within a collagen matrix to form a micro-tissue, tethered to flexible cantilevers and demonstrated to generate a tension. This tension increased proportionally to the number of cells. (Legant et al. 2009). Furthermore, the micro-tissue was tethered to cantilevers with different stiffness and generated a higher tissue tension when tethered to more rigid cantilevers (Legant et al. 2009). When tethered to cantilevers with a spring constant of  $0.098 \mu\text{N}/\mu\text{m}$ , cells generated 14 nN/cell. On the other hand, when the spring constant is  $0.397 \mu\text{N}/\mu\text{m}$  cells generated 24 nN/cell (Legant et al. 2009). These results prove the ability of cells to modulate the level of internal tension according to the stiffness of the substrate in a suspended configuration. In that case the tissue was oriented along an axis between the two anchorage points axis did not expand.

Contractile behaviour of tissue in a suspended configuration allowing tissue expansion and how this leads to new tissue formation, is a crucial question. This is an important point as this configuration is very likely to happen during tissue formation within porous implants. Taking into account how tension is modulated according to material stiffness and the effect of tension on cell proliferation and differentiation, it seems that a hard material is more appropriate for bone tissue engineering. Indeed, as a stiff material induces a higher internal tension leading to osteogenic commitment, a stiff substrate is required for this purpose. Besides their recognized biocompatibility, high tolerance by the body and stiffness (which could enhance osteogenic differentiation by increasing the internal tension), Calcium-Phosphate based materials appear to be a highly relevant material for *in vitro* bone tissue regeneration purposes.

### **2.5.11 Morphogenesis & Mechanical Forces**

In this section, it will be reviewed how cellular phenomena such as cell division, cell rearrangement and cell force generation can contribute to tissue development. Note that a considerable amount of information discussed in the following paragraph uses *Drosophila* models. *Drosophila* is a relevant and practical model for studying morphogenesis as organ development occurs much quicker than in human models. Additionally, its small size is a non-negligible advantage as it allows monitoring of entire organ formation. Therefore, the phenomena observed using *drosophila* model might not reflect fully human morphogenesis, however, similitudes can provide useful

data in order to understand how these processes take place in human models. Additionally, similar mechanisms as observed during morphogenesis should take place during tissue formation *in vitro*. Therefore, knowledge of organ formation dynamics *in vivo* is essential to understand tissue regeneration *in vitro*.

### 2.5.11.1 Cell Division During Organ Formation

Morphogenesis can be closely related to how tissue develops *in vitro* as both phenomena involve multi-cellular dynamics and organization. *In vitro*, tissue formation begins with only a few cells involved (i.e. 4 to 10 cells). A few days later there is a massive increase in cell number, which is under physiological control as long as there is no limitation in nutrient supply. *In vitro* the control of tissue expansion and size is intrinsic to the physical environment, which is provided by the scaffold. Tissue proliferation and the increase in tissue mass imply several cellular mechanisms such as either random or oriented cell division.

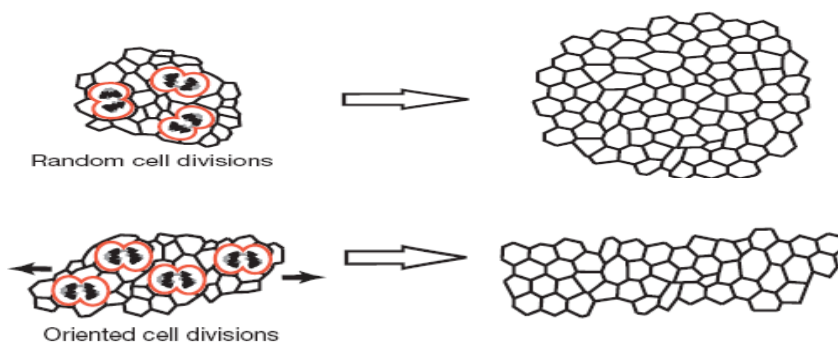


Fig. 2-11 Random(top) and oriented (bottom) cell division

Tissue proliferation and the increase in tissue mass are driven by continuous cell divisions (Fig. 2-11 outlined in red). Furthermore, the way cell division occurs can affect organ shape. For example, in *Drosophila* the thorax shows an isodiametric morphology, and the tissue grows as a circle expanding at a constant rate. Accordingly, no preferential orientation of the planar axes of cell divisions was found (Baena-Lopez et al. 2005). On the other hand, in the wing where a precise shape is required, cell division was strongly oriented. The majority of the cells divide along the proximal-distal axis of the wing blade. In contrast, in the wing margin, cells divide nearly parallel to the dorsal-ventral axis. Interestingly, the orientation of post-mitotic daughter cells conserves the positions determined by the angle of the oriented cell division (OCD). Furthermore, the orientation of the first cell division tends to be maintained in

subsequent division as it was observed that 57% of clones of four cells form straight lines of one cell width (Baena-Lopez et al. 2005). The fact that cell division orientation regulates tissue development *in vivo* raises the need to investigate whether a particular structure could modulate cell division orientation and affect tissue formation *in vitro*. The cell nucleus undergoes cleavage thanks to mitotic forces generated by microtubules (Li et al. 1995). Moreover, microtubules are connected to actin fibres and while contracting, the latter exert pulling forces on the nucleus indirectly (Maniotis et al. 1997). Therefore, forces exerted by actin fibres and their direction are likely to determine the axis along which the nucleus will divide. Thus, the actin fibres could orient cell division. Therefore, cell division and its orientation might be partially controlled by actin organisation and the mechanical forces generated by cells.

### 2.5.11.2 Cell Rearrangement & Intercalation

Cell rearrangements such as intercalation drive tissue elongation and affect organ shape, whereby cells change position by remodelling their adhesive contacts. During intercalation, cells lose contacts with anterior and posterior neighbours and gain new contacts along the perpendicular axis (Fig. 2-12). This is illustrated in Fig. 2-12 where the red interfaces shrink and new horizontal interfaces (blue) are formed, producing an exchange in cell neighbours (Lecuit et al. 2007).

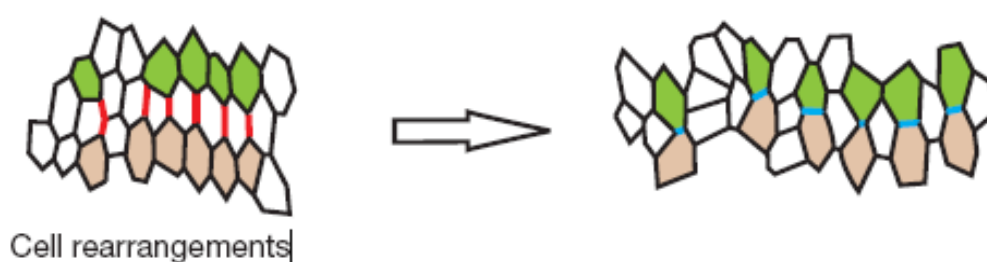


Fig. 2-12 Cell intercalation.

This phenomenon explaining tissue shape change has been studied in detail in *Drosophila* embryo during germ-band elongation (GBE). For instance, at the onset of GBE, a packed hexagonal array is formed by the epithelial cells. Subsequently, once the group of cells has completed the intercalation mechanism, it is elongated about 50% along the Anterior/Posterior (A/P) axis, and correspondingly shortens along the Dorsal/Ventral (D/V) axis (Bertet et al. 2004). Such mechanisms contribute strongly to

tissue formation besides participating in tissue elongation and shaping. The mechanism is highly detailed in the next paragraph.

Focusing on the four cells with white dots, it is observed that their boundaries are either parallel to the dorsal-ventral (D/V) axis (referred as type 1 in Fig. 2-13d) or at  $60^\circ$  to it (Fig. 2-13a). When the elongation begins, characteristic tetrads are formed by four cells around type 1 junctions (Fig. 2-13 a, d, red). In this type 1 configuration, cells are in contact along the antero-posterior (A/P) axis but dorsal and ventral cells have only their bottom and top corner in contact with each other, respectively. As GBE proceeds, the  $60^\circ$  junctions keep their orientation and average length ( $4 \mu\text{m}$ ). In contrast, type 1 junctions undergo a shrinking step (average time 10 min), which leads to a configuration where the four cells of the tetrad now share equal contacts (type 2; Fig. 2-13 b, d). The consequence of the shrinking step is the apparition of new junctions of type 3. Now, the remodelled junctions are perpendicular to the old type 1 junction, resulting in effective intercalation of the cells that were dorsal and ventral (Fig. 2-13 c, d).

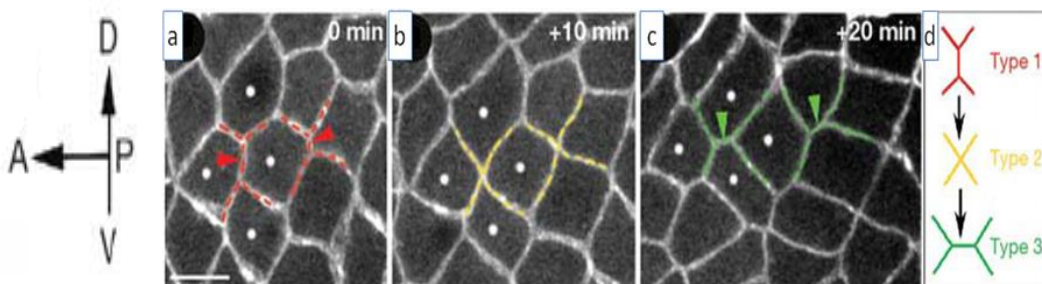


Fig. 2-13 Cell intercalation in *Drosophila*. Cell contacts in the type 1 configuration (red dashed line in a and d) progress towards the type 2 (yellow dashed line in b and d) and then to the type 3 configuration (green dashed line in c and d) (Bertet et al. 2004)

This pattern of junction remodelling highlights the fact that a cell is able to control each of its boundaries separately and modulate their behaviour independently (shrinkage or extension). Epithelial cells are a relevant model to study these phenomena as they display a strongly organized structure. Using these models is an easy way of showing the existence of such phenomena in cells. It is very likely to happen in other cell types far less structured, where it would be much more complicated to reveal these phenomena. Epithelial junctions in *Drosophila* and other organisms consist of a core E-cadherin/b-catenin/acatenin complex (the adherents junctions)(Knust et al. 2002; Lecuit

et al. 2002; Nelson 2003), whose recruitment at the membrane is stabilized by a crosslinking network of actin filaments (Adams et al. 1998). Thus cadherins and the actin network are likely to be the main elements mediating cell rearrangements.

### 2.5.12 Forces Involved in Cell Intercalation & Localisation

External forces, such as a pulling force from posterior cells or a compressive force from dorsal and/or ventral cells, could cause oriented remodelling of cell junctions in the *Drosophila* model. However, the remodelling of junctions is not driven by external forces on the tissue, but depends on local forces at cell boundaries. It was shown that forces controlling intercalation are inherent to the intercalating regions, raising the possibility that local generators of force, controlled by myosin II, may act directly at cell junctions, as myosin II is enriched in shrinking regions (Fig. 2-14)

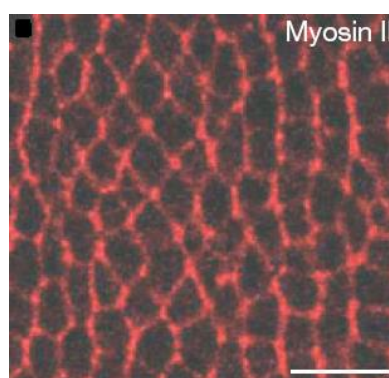


Fig. 2-14 Myosin II staining during Germ-Band Elongation in *Drosophila* (Rauzzi et al. 2008).

The tension generated by myosin II accumulation at cell boundaries reduces cell-cell adhesions by pulling together the boundaries oriented along the D/V axis (Fig. 2-15). This results in minimization of the perimeter occupied by the cell area enhancing cell intercalations. On the other hand tension is decreased by the expansion of cell contacts on the A/P axis (Rauzi et al. 2008). Actin filament configurations are susceptible to deformation by contractile forces generated by bipolar myosin filaments (predominantly myosin II) (Landsverk et al. 2005), which act especially on actin networks attached to membranes. Thus, the role of actin network coupled to myosin is strongly believed to orchestrate cellular rearrangement such as intercalation.

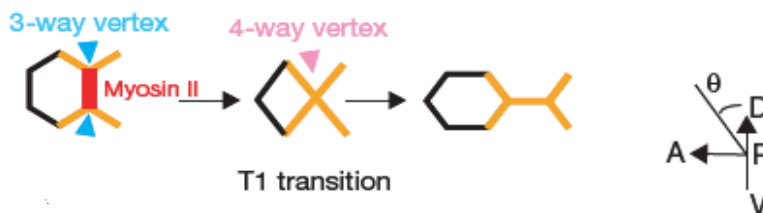


Fig. 2-15 Myosin involvement in T1 transition phase of cell intercalation (Rauzzi et al.)

Furthermore, it has been demonstrated that subcellular anisotropies in cortical tension controlled by myosin II are sufficient to drive a tissue out of equilibrium and force its mechanical evolution towards equilibrium by a succession of local relaxations. In other word, junction remodelling directionality is imposed by anisotropic cortical tension nearly perpendicular to the elongations axis (Rauzi et al. 2008). In addition, an experimentally validated model by Rauzzi et al. predicts tissue elongation abnormalities in case of unbalanced tension.

Clearly, cell division and orientation, as well as cell rearrangement such as intercalation, are among the main phenomena governing tissue formation and are controlled by mechanical forces and cell-cell adhesions remodelling.

---

## 2.6 Summary of the Literature Review

Initially, the essential requirements for bone tissue engineering were described, starting with relevant cell types, their potential, availability and clinical applicability. Next, the properties of the wide variety of materials relevant for bone engineering and their performance in surgical procedures were reviewed. The choice of the material for studying bone tissue formation *in vitro* is dependent on the fulfilment of basic factors such as biocompatibility and the ability to support osteogenic lineage commitment. Furthermore, in the case of particular 3D architectures required, the choice is influenced by ease of processing and fabrication capability.

Factors influencing porous scaffolds architecture were discussed with a focus on pore size and geometry. Despite contradictory findings, pore size affects tissue growth in porous structures. Varying pore sizes generate different patterns in terms of tissue formation and differentiation. However, it has never been explained why and how. There is definitely an obvious and logical effect on proliferation due the surface area available for cell attachment and spreading. Initially, cells are attached and form a 2D monolayer on the surface of the pores. 2D growth is mainly influenced by the substrate characteristics, such as chemical composition and surface roughness. However, 3D growth is poorly understood, particularly the influence of pore size. The process to fill a pore interstice (the void part of the pore) involves 3D growth, Therefore, it is likely that according to pore size, tissue could display different mechanisms of colonization. It was also discussed that pore geometry can affect the spatial rearrangement of the tissue. Therefore, whether a specific spatial tissue configuration, induced by certain pore geometry, could preferentially enhance tissue formation needs to be understood. In most of the porous scaffolds used for investigating the effect of architecture, the heterogeneity of pore size is considerable. This heterogeneity prevents researchers to extract precise data on the influence of pore size. Therefore, there is a tremendous need to define systematically how pore size affects growth in appropriate and reproducible structures. The first step would be to define the ideal growth in a single pore.

Next, the fact that internal tension is involved in different aspects of tissue development was discussed. The importance of the effect of cytoskeletal tension on cellular behaviour, proliferation and differentiation has been reviewed. The fact that musculoskeletal cells are capable of contractile behaviour was established, as well as

the fact that cytoskeletal tension has a potential role in osteogenic tissue formation in porous scaffolds. Furthermore the level of tension can be influenced by environmental factors, i.e. the effect of the stiffness of the surrounding ECM or the stiffness of the substrate that cells are seeded on was mentioned. However, importantly, the behaviour of the actin network has never been studied as a function of pore size in porous biomaterials. Physically and mechanically, cell shape and motility are governed by the cytoskeleton. Therefore, it is crucial to investigate in which manner cells organize their cytoskeleton as a function of pore size during pore colonization. Studies on 2D patterns have indicated the importance of the interactions between geometric shape, proliferation, internal tension and cytoskeletal dynamics. However, in 3D, the behaviour of the actin network and its tension as a function of pore size and shape in porous biomaterials is poorly understood. *In vivo*, cellular events such as division and rearrangement as well as shape and motility are directed by cellular forces involving acto-myosin contraction. Therefore, actin cytoskeleton rearrangement under influence of cell generated forces requires further understanding. This would reveal how cells organize their cytoskeleton as a function of pore size, geometry and shape during scaffold colonization and tissue formation.

## 2.7 Research Questions

It was pointed out that 3D architecture affects tissue formation in porous scaffolds, however, the differences observed cannot be systematically fully explained. Visual monitoring of how tissue colonizes a pore could improve understanding of such process. Therefore, investigating whether tissue uses different mechanisms to colonize a pore depending on 3D environment could eventually explain changing growth patterns in 3D scaffolds *in vitro*.

Furthermore, actin has been seen to impact on several cellular processes such as adhesion, migration, division. In addition, actin might be involved in signal transduction by modulating the level of tension. Actin has a role in contractile behaviour and also contributes to morphogenesis *in vivo* in *Drosophila* models by regulating multi-cellular rearrangements and cell division. However, actin behaviour and its potential implication has not been investigated in the situation of tissue formation in a 3D porous structure *in vitro*.

Regenerated tissue in 3D scaffold can display distinct organisations depending on pore architecture. Nevertheless, the systematic effect of varying 3D structure on tissue organisation has not been investigated extensively. Furthermore, it has not been determined whether a particular spatial arrangement, induced by a given structure, could enhance tissue development in 3D scaffolds.

Answering these questions could provide information about the relationships between tissue formation, organisation, actin and pore geometry. Information about basic mechanism of tissue development in 3D porous structures, would therefore provide valuable information for porous architecture design in 3D scaffolds for bone engineering purposes.



## Chapter 3

# Pore Geometry Regulates Human Bone Marrow Cells Tissue Formation

The study presented in this chapter is based on an article published in the Annals of Biomedical Engineering (ABME), vol 41, issue 5, 2013. Preliminary results obtained were presented in the Annual Meeting of the Scandinavian Society for Biomaterials Annual, May 2012, Sweden and published as an extended abstract in the European Journal of Cells & Materials (eCM), vol 23, supplement 5, 2012

3D tissue development *in vitro* over time in porous structures is rarely investigated and visually monitored. Therefore, the mechanisms of 3D tissue development are poorly understood. In this study, we propose to investigate tissue formation in a 3D configuration using an original system made of calcium phosphate cements seeded with Human Bone Marrow Cells.

An open pore system was adopted, consisting of long rectangular pores (slots) with varying width, made of calcium phosphate bone cement. These were kept raised above the bottom in a well plate to provide a 3D environment for tissue to grow unconstrained, suspended in the pore slots. This system presents several advantages over full 3D construct. It allowed for easy monitoring of tissue formation over time using optical microscopy and minimized nutrient supply restrictions. Therefore, the objective of this study was to determine systematically how pore geometry affects tissue formation and to identify the role of cellular and actin organisation during this process. It was hypothesized that the variation in pore width would lead to differences in tissue growth and morphology. In particular, this may be related to the level of curvature at the front of migration, which has been implicated in tissue formation. In addition, it was

hypothesised that differences in growth as a function of pore width could be related to variations in actin network organisation. Throughout the text the term ‘tissue’ or ‘neo-tissue’ is used to indicate the initial collective of cells filling up the pores, however it is important to note that a mature tissue structure will only arise after extracellular matrix formation and remodelling at a later stage.

### 3.1 Material and Methods

#### 3.1.1 Scaffold Fabrication & Preparation

Initially, several materials were considered as potential candidates such as TiO<sub>2</sub>, PDMS, PCL, Gelatine/Collagen Gels, TCP cements. Material was chosen according to its biocompatibility and more importantly, ease of use for device fabrication. The final choice was TCP cements for its very good established biocompatibility and its particular intrinsic characteristics. Initial TCP exist in powder form, which turns into a paste when mixed with an aqueous solution. Consequently, TCP in its slurry form can be readily used for mould casting. In addition, production does not require any sintering as it can settle and harden by itself.

##### 3.1.1.1 Mould Production

A two piece female mould made of PMMA (Fig. 3-1a) was used to produce male moulds (Fig. 3-1b) made of Silastic® M RTV Silicone Rubber in order to produce the experimental device.

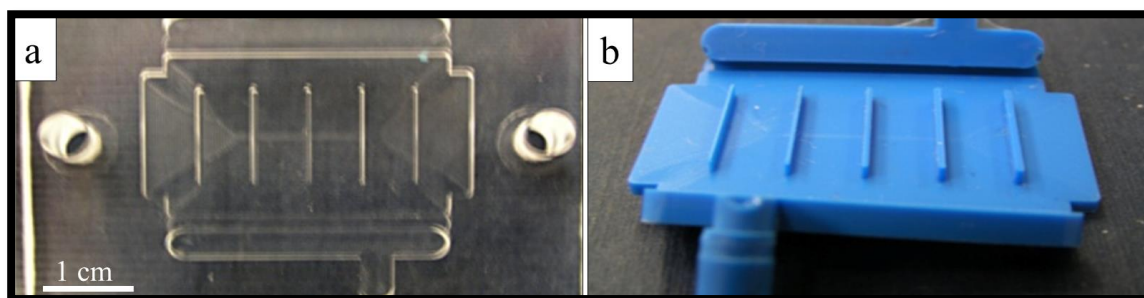


Fig. 3-1 Construct fabrication. (a) Female mould used for production of male moulds. (b) Male mould obtained

The female mould was designed to contain wells ranging from 200 to 600  $\mu\text{m}$  in width, 1 cm in length and 1 mm in depth. To generate male moulds, the rubber was poured through an inlet leading to the well and a vacuum was applied at the outlet to prevent air bubble formation. Subsequently, the rubber was left to polymerize and solidify at room temperature. When the rubber was solid the upper part of the female mould was removed and the rubber male mould was peeled off. The male mould appears as a rectangle of rubber with dimension 3 cm  $\times$  1 cm and 5 perpendicular standing teeth of 200; 300; 400; 500 and 600  $\mu\text{m}$  in width, 1 cm in length and 1 mm in height. Gaps in the corners were designed to allow generation of 1 mm high legs in the final structure in order to keep the pore slots raised above the bottom of the culture dish (Fig. 3-2a).

### 3.1.1.2 Preparation of $\alpha$ -TCP powder and cement production

Preparation of alpha-tricalcium phosphate ( $\alpha$ -TCP) powder was carried out using a solid state reaction between calcium carbonate ( $\text{CaCO}_3$ ) and calcium pyrophosphate ( $\text{Ca}_2\text{P}_2\text{O}_7$ ) as previously described with minor modifications (Andriotis et al. 2010). For the preparation of  $\alpha$ -TCP powder, equimolar quantities of calcium carbonate and calcium pyrophosphate were mixed under magnetic stirring in an ethanol suspension. Next, the mixture was dried at 80  $^\circ\text{C}$ , placed in a furnace at 1300  $^\circ\text{C}$  for 12 h and rapidly quenched on a metallic surface. The resulting material was crushed in an agate mortar and placed in a ball mill (Pulverisette 5, Fritsch, Germany). Ball milling was performed at 500 rpm using 1 cm diameter agate spheres for 5 cycles of 20 min. Milled powder was mixed with 4.0 % w/v disodium hydrogen phosphate ( $\text{Na}_2\text{HPO}_4$ ) solution at liquid (mL)/powder (g) ratio of 0.32 and homogenized by a spatula on a plastic slab for 1 min to produce a paste.

### 3.1.1.3 Preparation of the microstructures

The paste obtained was spread carefully on male moulds leaving the top of the teeth uncovered to allow for production of open pores. Specimens were kept humidified for 12 h and then placed in 60 ml of Ringer solution for 7 days to harden at 37  $^\circ\text{C}$ . Afterwards, male moulds were peeled off gently to avoid breaking the sample. An example of a final construct obtained is shown in Fig. 3-2

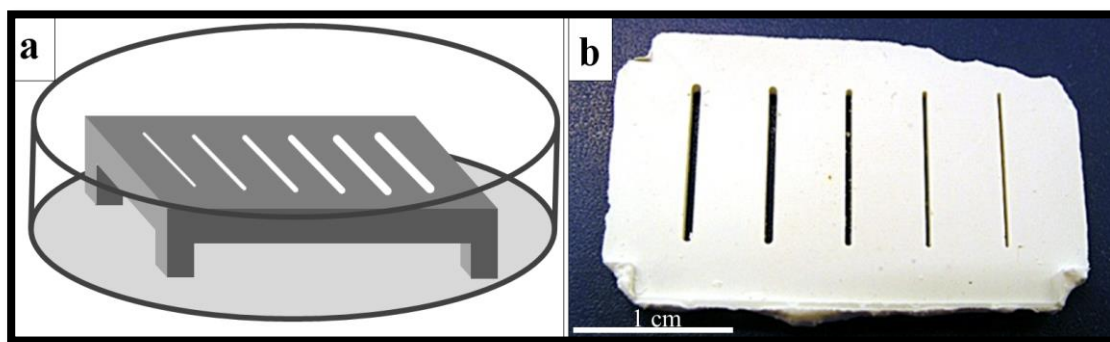


Fig. 3-2 (a) Schematic of the construct used for the study. (b) TCP scaffolds obtained, pore slot width: 600, 500, 400, 300, and 200  $\mu\text{m}$  from left to right.

#### 3.1.1.4 Scaffold Conditioning

Samples were sterilized by autoclave, kept for 1 h at a plateau of 123 °C. Prior to cell seeding samples were incubated in  $\alpha$ -MEM media supplemented with FCS to allow protein deposition on the material surface for enhanced cellular attachment. Media was changed repeatedly until its colour reached a stable state. Samples were rinsed with PBS three times prior to cell seeding.

#### 3.1.2 Scanning Electron Microscopy

Microstructure and surface morphology of the specimens were evaluated by Scanning Electron Microscopy (SEM; Zeiss SUPRA 35VP). Samples were attached to aluminium stubs using a double side adhesive carbon tape and gold coated prior to the examination.

#### 3.1.3 Cell Culture & Scaffold Seeding

Human Bone Marrow Stromal Cells (HBMSC) were extracted from bone marrow collected during a routine hip replacement from 80 and 87 year old male patients. Tissue samples were obtained from haematologically normal patients undergoing routine total hip replacement surgery, with approval from the Southampton Hospital Ethics Committee and appropriate patient consent. HBMSC were isolated from the marrow using plastic adherence and frozen down after routine cell culture at passage 0 (P0), using our standard protocols (Tare et al. 2008). HBMSCs were cultured up to passage 3 prior to the experiment. Briefly, cells were defrosted and seeded in a single T25 cell culture flask. Upon reaching 90% confluence, the flask was split and re-seeded in two T75 flasks (Canted neck, Corning). When 90% confluence was reached each T75

---

was split again in four new T75s. HBMSCs were cultured in  $\alpha$ -MEM medium (Sigma-Aldrich, UK) with 2.2 g/mL of sodium bicarbonate. Media was supplemented with 10 % Foetal Bovine Serum (FBS) (Sigma) and 1 % Penicillin-Streptomycin solution x100 (Sigma). A total number of 6 T75 flasks of HBMSCs at 90 % confluence were used for the experiment. Cells were incubated with collagenase for 45 mins and trypsinised with an EDTA-Trypsin (Sigma) solution 10 % in phosphate buffer saline (PBS) solution. Cells were resuspended in 18 mL of culture media to yield a seeding suspension of approximately  $1.6 \times 10^5$  cells/mL. Cell concentration was determined using a haemocytometer (Marienfield, Germany). Scaffolds were seeded in 6 well plates (Costar, Corning) with 6 mL of cell seeding suspension. The plate was put on an orbital shaker at 30 rpm inside an incubator operating at 37 °C and 5 % CO<sub>2</sub> for 14h. Following seeding, scaffolds were incubated at 37 °C and 5 % CO<sub>2</sub> in static conditions for up to 7 weeks. Scaffolds were washed 2 times with PBS prior to each media change. Culture media was changed daily during the entire study.

### 3.1.4 Optical Inverted Microscopy

Cell seeding and attachment, as well as the biocompatibility of the TCP cement were confirmed using a live/dead kit staining on a separate sample (Cellstain double staining kit, Sigma; calcein-AM (emission: 515 nm) for live and propidium iodide (emission: 617 nm) for dead cells respectively). In order to monitor and quantify tissue growth precisely, 3 replicates for each pore width were imaged every 24 h using an inverted optical bright-field microscope (IX71, *Olympus Corporation*, Tokyo, Japan) equipped with a high resolution 1392×1040 pixels CCD camera (QICAM Fast 1394, *QImaging*, Surrey, Canada). The same 3 replicate samples per pore width were used throughout the duration of the study. All samples were monitored at the same time and the distance spanned by the tissue was measured every day. At each time point, the mean amount of tissue formed for each of the different pore widths was calculated by averaging the values obtained for the 3 replicates. Growth did not start at the same time in every pore slot thus the first time point was set as the day when growth within the pore space became visible. Growth was first quantified using a 10× magnification objective. When the amount of tissue formed was too high to be imaged at 10× magnification, 4× magnification was used. The amount of tissue formed was measured using Image-J

software. The distance measured was set as the distance between the pore extremity and the middle of the front of migration of the tissue formed (Fig. 3-3).

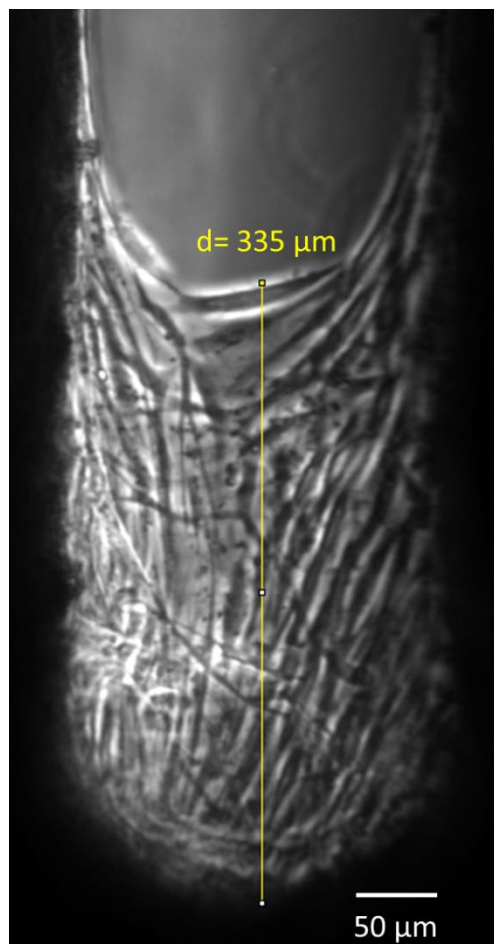


Fig. 3-3 Example, measurement of the pore spanning distance by cells in a 200 μm pore at day 3

### 3.1.5 Laser Confocal Microscopy

An EdU-Click kit (Invitrogen) was used to detect proliferating cells within the constructs (separate samples were used for this experiment). After allowing cells to span the pores within the constructs for 10 days in samples dedicated for proliferation detection, cells were incubated for 48 hours with medium containing EdU. Prior to staining, samples were washed 3 times in PBS and fixed in paraformaldehyde-PBS 4 % (w/v) and permeabilized with Triton-X 0.5 % for 15 min. Samples were incubated for 30 min in the cocktail reagent to allow for EdU detection. The cocktail reagent forms a complex with the EdU that has been incorporated in the DNA and this complex was stained with an Alexa-Fluor 488 probe. To evaluate actin network organisation patterns in pore slots of different width, samples were labelled for F-actin. Prior to staining,

samples were washed 3 times in PBS and fixed in paraformaldehyde-PBS 4 % (w/v) overnight. Samples were washed 3 times in PBS, 3 times in PBS-Tween 0.1 % (v/v) for permeabilization and then incubated in 1 % BSA (Sigma)-PBS (w/v) for 30 min. For actin staining, samples were incubated in Alexa-Fluor 568-Phalloidin (1/75 dilution (v/v)); Molecular probes, Invitrogen). After labelling, samples were washed 3 times in 1 % BSA-PBS and then 3 times in PBS, stored in PBS and imaged immediately. Samples were imaged using a laser confocal microscope (Leica TCS SP2, Germany). Z-axis image acquisition was performed using a 20× water-dipping objective (Leica, HCX APO L 20×/0.50 W U-V-I). Individual images planes were acquired in bi-directional scanning mode at 1 μm z-axis intervals with a resolution of 1024×1024 pixels for actin imaging.

### 3.1.6 Time Lapse Microscopy

HBMCs seeded constructs were cultured for 14 days prior to time-lapse experiments, under routine cell culture conditions, as described above. Pictures were taken every 20 minutes for 48 h, using a Zeiss Axiovert 200 inverted microscope, equipped with an Axiocam MRm monochrome camera and an incubator chamber. Samples were kept at 37 °C 5 % CO<sub>2</sub> in a humidified atmosphere during time-lapse recording.

### 3.1.7 Overall summary of samples used & experiments performed

	Kinetics	Actin	EdU	Time Lapse
M 80	Monitored for 18 days	Imaged on d <sub>18</sub>		
M 87	Cultured for 10 days or 14 days		EdU added on d <sub>10</sub> Imaged on d <sub>12</sub>	Recorded during 48h

## 3.2 Results

### 3.2.1 Material Characteristics

Hardened calcium phosphate cement displayed a characteristic multi-scale structure, consisting of spheroids with a typical dimension of 1-5  $\mu\text{m}$  (Fig. 3-4 left). At higher magnification, characteristic needle-like structure of calcium deficient hydroxyapatite formed after the hydrolysis of the initial  $\alpha$ -TCP during setting appears on the spheroids surface (Fig. 3-4 right). A micro-porosity is also visible with pores displaying a size of approximately 1  $\mu\text{m}$ . Both micro and nano-roughness are believed to enhance cell attachment and osteoconductivity (Bowers et al. 1992; Lincks et al. 1998; Lohmann et al. 2000; Dalby et al. 2007)

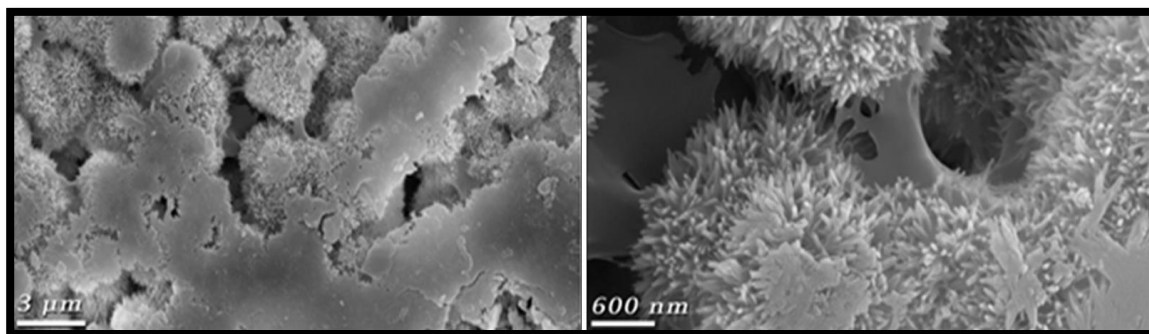


Fig. 3-4 (left) Scanning Electron Microscopy (SEM) pictures of the surface of TCP cements displaying micro structures. (right) Scanning Electron Microscopy (SEM) pictures of the surface of TCP cements displaying nano structures.

### 3.2.2 Biocompatibility & Cell Attachment

Calcein-AM staining revealed that HBMSCs readily attached to the TCP cements, spread out and displayed a spindle like morphology with long extensions indicating the good biocompatibility and favourable surface characteristics of the TCP cement (Fig. 3-5).

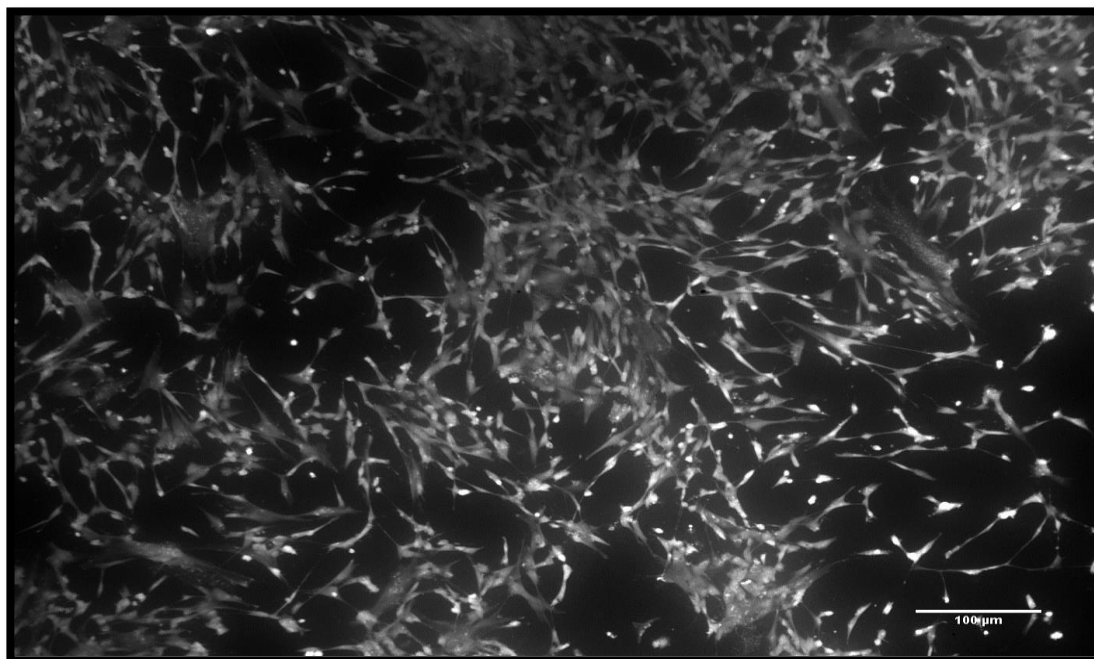


Fig. 3-5 HBMSC attachment and viability on TCP cement 14 h following seeding (calcein-AM).

At the density used, considered as low in this case, cells attach to the pore walls (Fig. 3-6a, b). Once cells reached 2D confluence on the walls, they start to span the interstice within the pore (Fig. 3-6c). At low density, cells do not form clusters in suspension. Therefore, when scaffolds are seeded, cells attach uniformly on the surface available. However, at high density, cells tend to form clusters which lodge in the middle of the pore. This is an unwanted phenomenon as tissue in this configuration is not suitable for monitoring growth and generally does not have high viability.

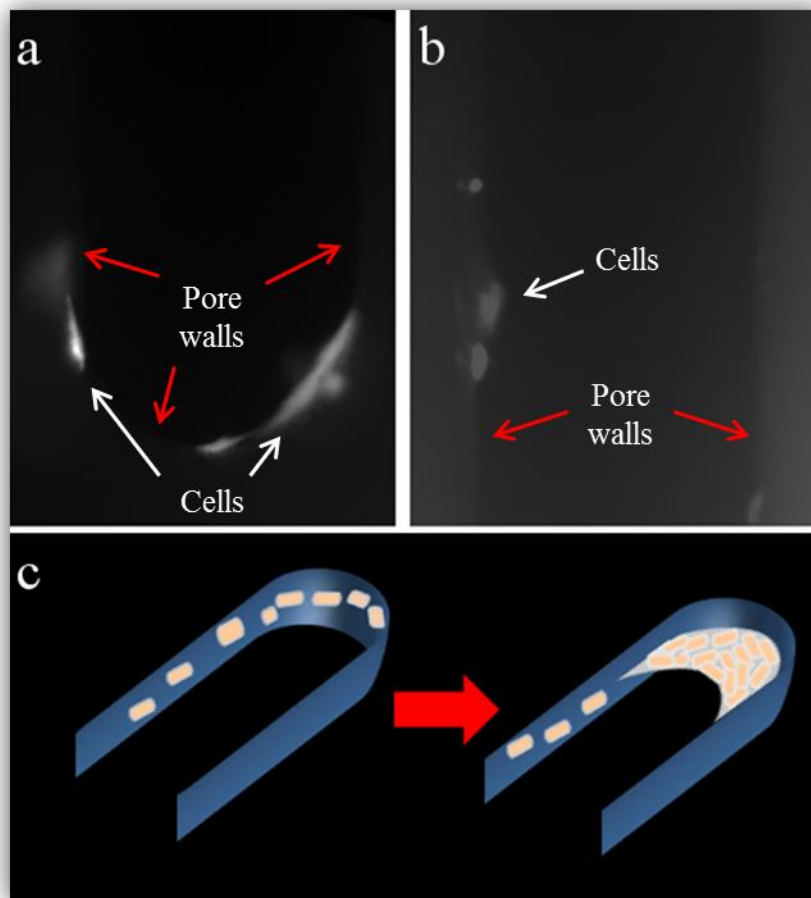


Fig. 3-6 Initial steps of pore spanning by cell-formed tissue. (a) Cells (white arrows) attach to the convex wall (red arrows) of the pore extremity, (b) as well as in the middle of the slot. (c) Pore spanning by cells attached to the walls started from the curved end of the pore.

### 3.2.3 Growth Kinetics in Pores of Different Widths

Optical microscopy showed that the newly formed tissue was anchored to pore walls and started growing from the curved end of the pore slot (Fig. 3-7), while cells covering the flat inside walls of the pore slot did not form any tissue. Note that because the structures were raised on legs, tissue grew suspended in 3D without any contact with the bottom of the culture dish for the whole duration of the study. Tissue progressively filled the pores inwards (Fig. 3-7 bottom to top) displaying a concave front of migration.

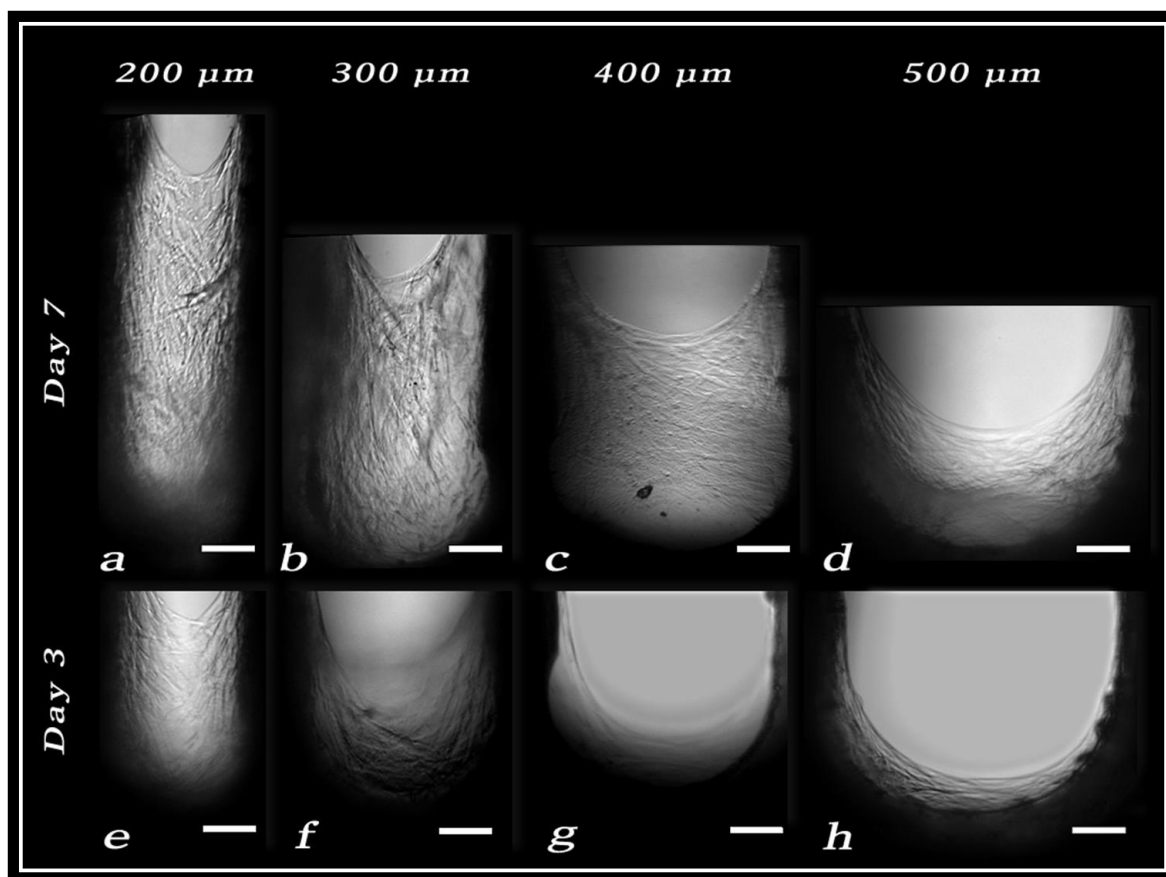


Fig. 3-7 Optical microscopy showing the tissue growing suspended in the open pore slots. Bottom: day 3. Top: day 7. Pore width 200, 300, 400, 500 μm from left to right. Scale bar: 100 μm

Tissue growth was characterised with 3 replicates for each pore width and was monitored daily during 18 days (Fig. 3-8a). Results for the 600 μm pores were omitted as not enough replicates were obtained. Overall growth progressed at an approximately constant rate for all pore widths (Fig. 3-8a). Looking in more detail, for 200 μm and 400 μm the average growth rate seemed to increase and decrease, respectively (Fig. 3-8a), which was due to an acceleration or deceleration in one or two of the replicate samples. Differences in growth progression depending on pore width became apparent by day 10 (Fig. 3-8a). The maximum distance reached by the tissue after 18 days increased as pore size decreased: i.e. 200, 300, 400 and 500 μm reached an average distance of (average ± standard deviation)  $3.17 \pm 1.04$ ,  $1.65 \pm 0.32$ ,  $1.20 \pm 0.18$  and  $0.54 \pm 0.20$  mm respectively (Fig. 3-8a). Mean growth velocity over 18 days was calculated by linear least-squares fitting of the migration distance as a function of time (Fig. 3-8b). Averaged growth velocities determined for the 200; 300; 400; 500 μm pores were 175; 97; 58 and 32 μm/day respectively.

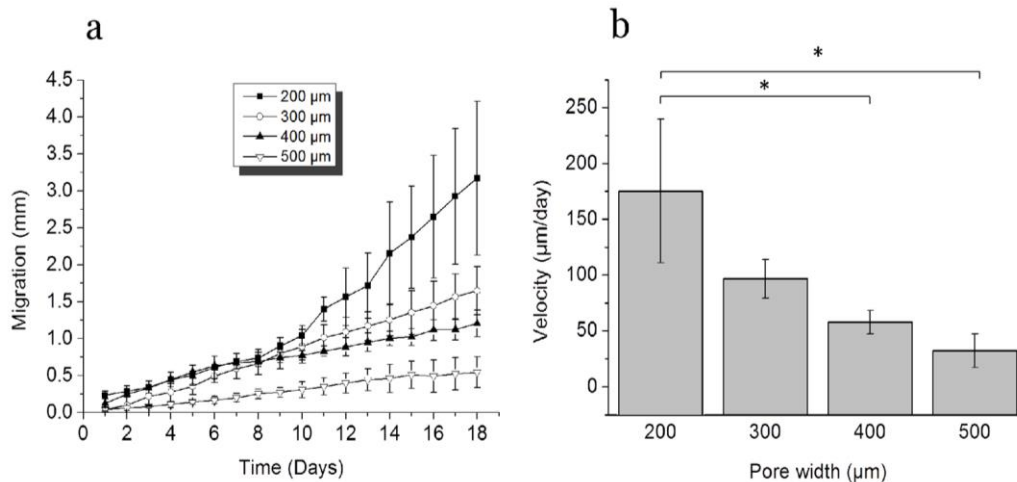


Fig. 3-8 Effect of pore size on tissue growth kinetics (a) Comparison of growth curves for the different pore widths (n=3). (b) Growth speed obtained by linear fitting of the grow curves for the different pore sizes. R-Square values for 200, 300, 400 and 500 μm pores were 0.93, 0.99, 0.97, and 0.99 respectively. ‘\*’ indicates statistically different results (p<0.05, one-way analysis of variance (ANOVA) with post-hoc Tukey HSD test (Error bars represent standard deviation).

Thus, growth speed increased substantially as pore size decreased. Furthermore, the total area of tissue formed, calculated as the product of pore width and average distance reached, decreased markedly as pore width increased (Fig. 3-9). The curved zone at the front was not included in the calculation of the tissue area as it represents a percentage error of 0.2%. Therefore, tissue was assumed to be rectangular for area calculation.

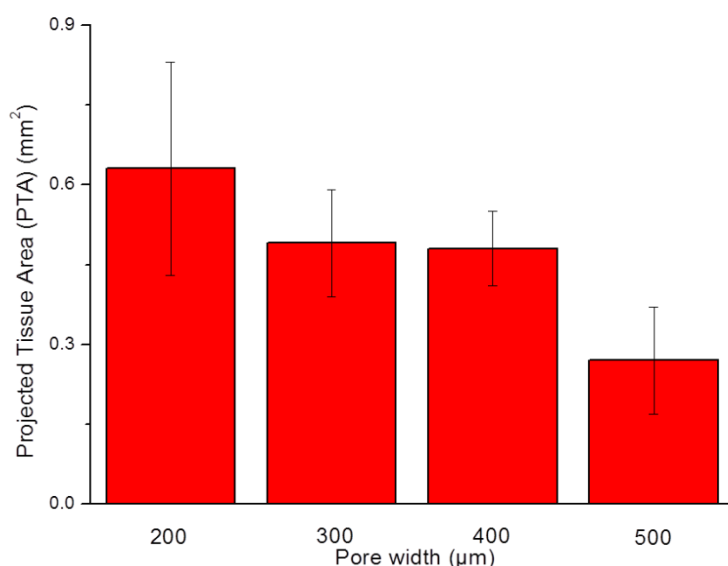


Fig. 3-9 Projected Tissue Area of newly formed tissue after 18 days for the different pore widths

### 3.2.4 Actin Network Imaging

For each pore width, the front of migration displayed a similar concave shape (Fig. 3-10a-d). Interestingly, the level of curvature at the migration front increased as pore width decreased.

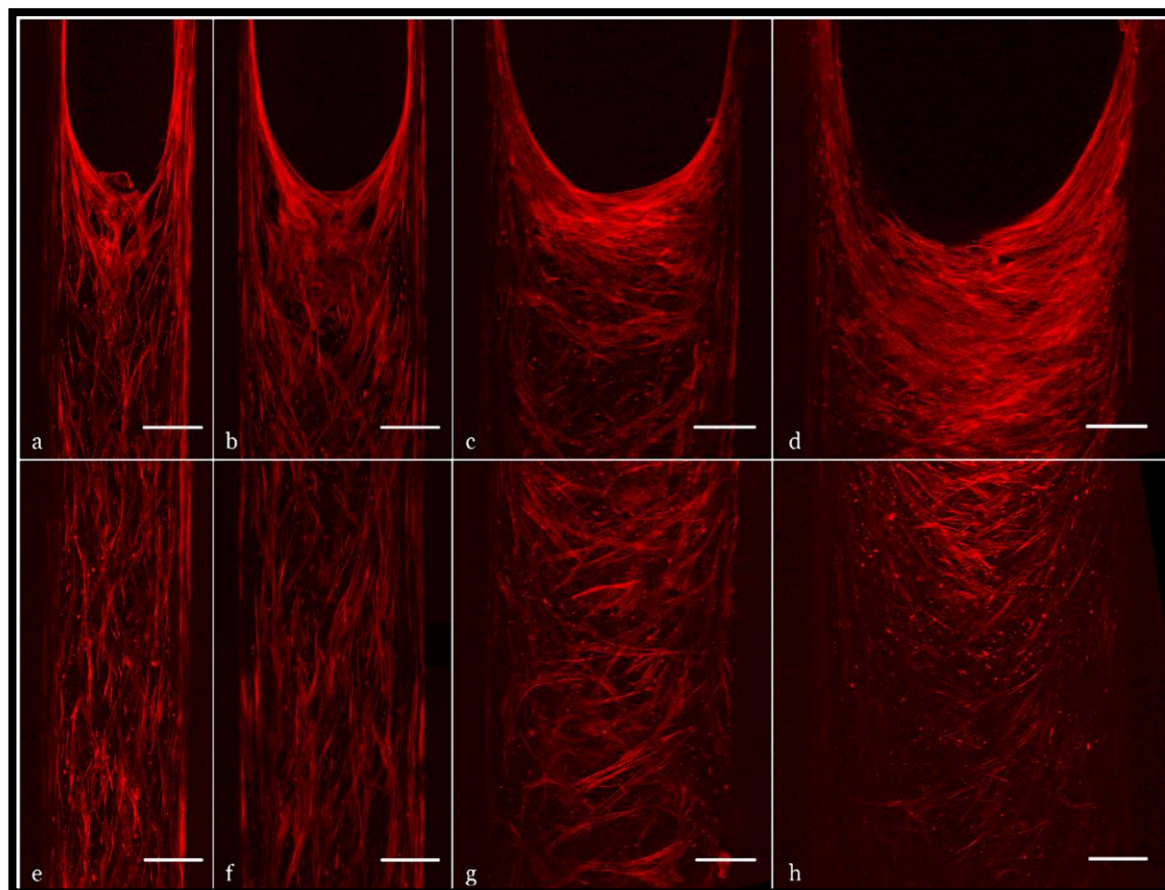


Fig. 3-10 Effect of pore width on actin network organisation: Laser scanning confocal microscopy. Tissue within constructs labelled with Alexa Fluor 568-Phalloidin for F-actin cellular cytoskeleton (scale bar = 100 $\mu$ m). Pictures displaying the actin network at the front of migration (a-d) and in the bulk of the tissue formed (e-h) in different pore sizes: 200  $\mu$ m (a, e); 300  $\mu$ m (b, f); 400  $\mu$ m (c, g); 500  $\mu$ m (d, h)

The migration front in pores of 200 and 300  $\mu$ m wide was characterised by the presence of thick actin fibres close to the pore wall, either oriented parallel or forming a low angle with the longitudinal axis of the pore (Fig. 3-10a, b). At the bottom of the concave shape actin fibres were much thinner but still oriented towards the migration direction. On the other hand, in pores of 400 and 500  $\mu$ m a completely different pattern was displayed. The actin fibres close to pore wall were much thinner and formed a much broader angle with the longitudinal axis than in the smaller pores. Thick actin fibres

were located at the bottom of the concave shape and oriented perpendicularly to the longitudinal axis (Fig. 3-10c, d). Away from the front in the bulk of the tissue, the organisation of the actin network also varies considerably depending on pore width (Fig. 3-10e-h). For pores of 200 and 300  $\mu\text{m}$  the pattern is quite similar. Fibres are mainly oriented along the longitudinal pore axis and a distinct cross-over pattern of fibres is also apparent (Fig. 3-10e, f). In the 400 and 500  $\mu\text{m}$  pore, the actin network is thinner and organised in a more random pattern, with fibres mainly oriented perpendicularly to the pore axis (Fig. 3-10g, h).

### **3.2.5 Time Lapse & EdU**

Time lapse results demonstrated extensive cell motility and cell division while cells spanned the pore space (S1-S2). An example of the cell division process at the front of migration is shown (Fig. 3-11a-c). First, a single cell is indicated which is about to divide (Fig. 3-11a). Second, the formation of two daughter cells along the longitudinal axis could be clearly distinguished (Fig. 3-11b). Third, after the division process was complete, the two daughter cells were completely separated (Fig. 3-11c). EdU results confirmed the time-lapse results, showing cell division right at the front of migration. In addition, cell proliferation occurred within a finite zone of up to approximately 300  $\mu\text{m}$  behind the front of migration (Fig. 3-11d). However, when moving further away from the front, only sporadic EdU incorporation occurred (Fig. 3-11e), indicating only minor division in the bulk zone. In addition, the time-lapse results demonstrated the contribution of cell contraction to the pore spanning process (Fig. 3-12). For instance, the cell marked with the white asterisk (Fig. 3-12a-c) was seen to contract up to half its original size while the tissue is dragged forward. The yellow dotted lines indicate the distance spanned by the tissue during cell contraction.

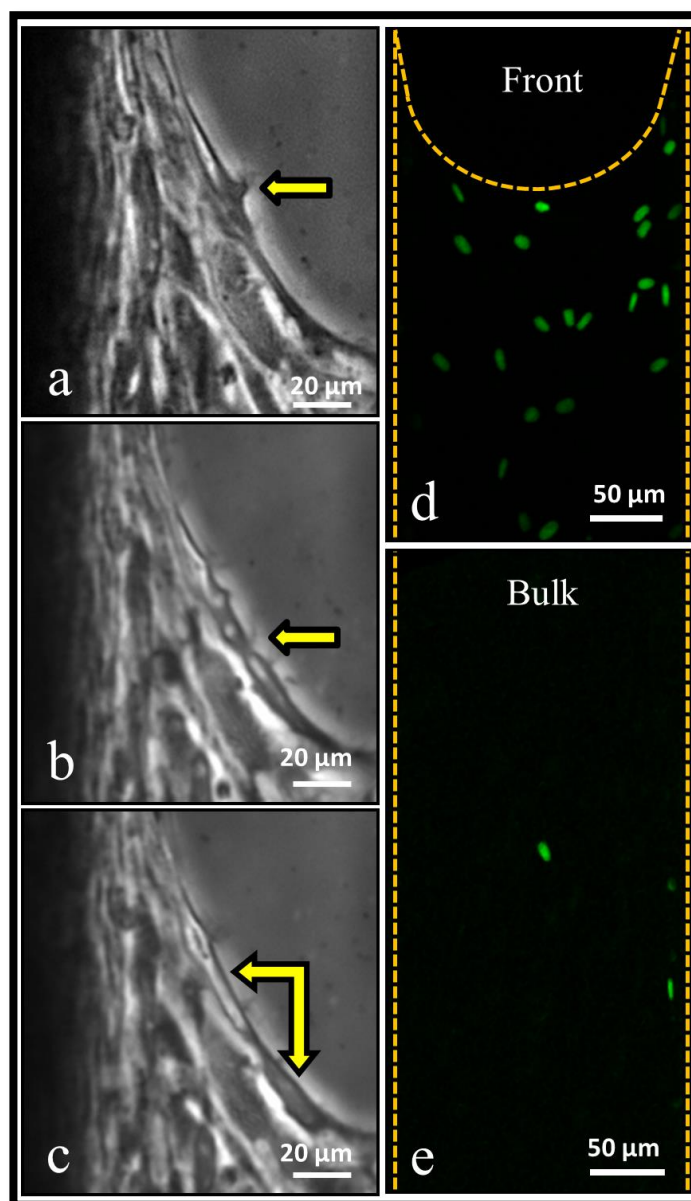


Fig. 3-11 Results showing the location of cell division and DNA production. (a-c) Cell division at the front, as indicated by arrows. Intervals between pictures: 20 min. (d, e) EdU labelled cells reflecting DNA production at the front of migration (d) and in the bulk, approximately 1 mm away from the front of migration (e) in a 200  $\mu\text{m}$  pore

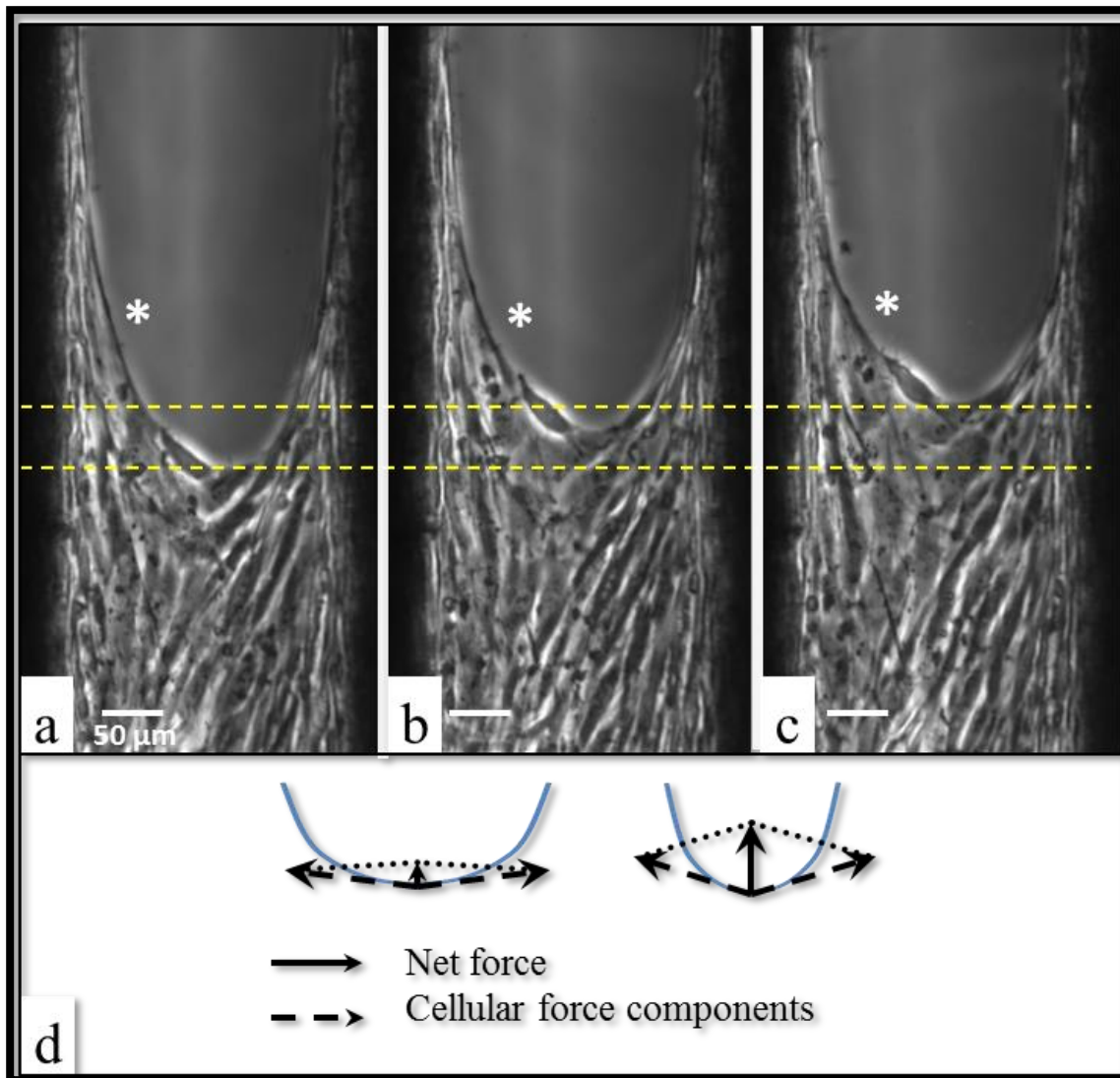


Fig. 3-12 (a-c) Cell contraction. Example of a leading cell shortening, indicated by '\*'. Lines indicate the extent the tissue is stretched due to cell generated stresses. Intervals between pictures: 1h40. The original video is provided as a supplementary material. For comparison an additional video shows this phenomena occurring in a 500 μm pore. (d) Schematic representation of forces exerted by aligned cells at the tissue front on the underlying tissue, which could drive tissue expansion, increasing with curvature.

### 3.2.6 3D Tissue Reconstruction

An example of a 3D reconstruction of the actin network for the 400  $\mu\text{m}$  pore is shown (Fig. 3-13). Perpendicular and longitudinal cross sections are shown (Fig. 3-13b, c). It can be observed that the cell layer is relatively thin at the immediate migration front, but rapidly increased in thickness moving away from the front (Fig. 3-13c) as well as closer towards the wall of the pore (Fig. 3-13b), with strong actin staining on the tissue surface.

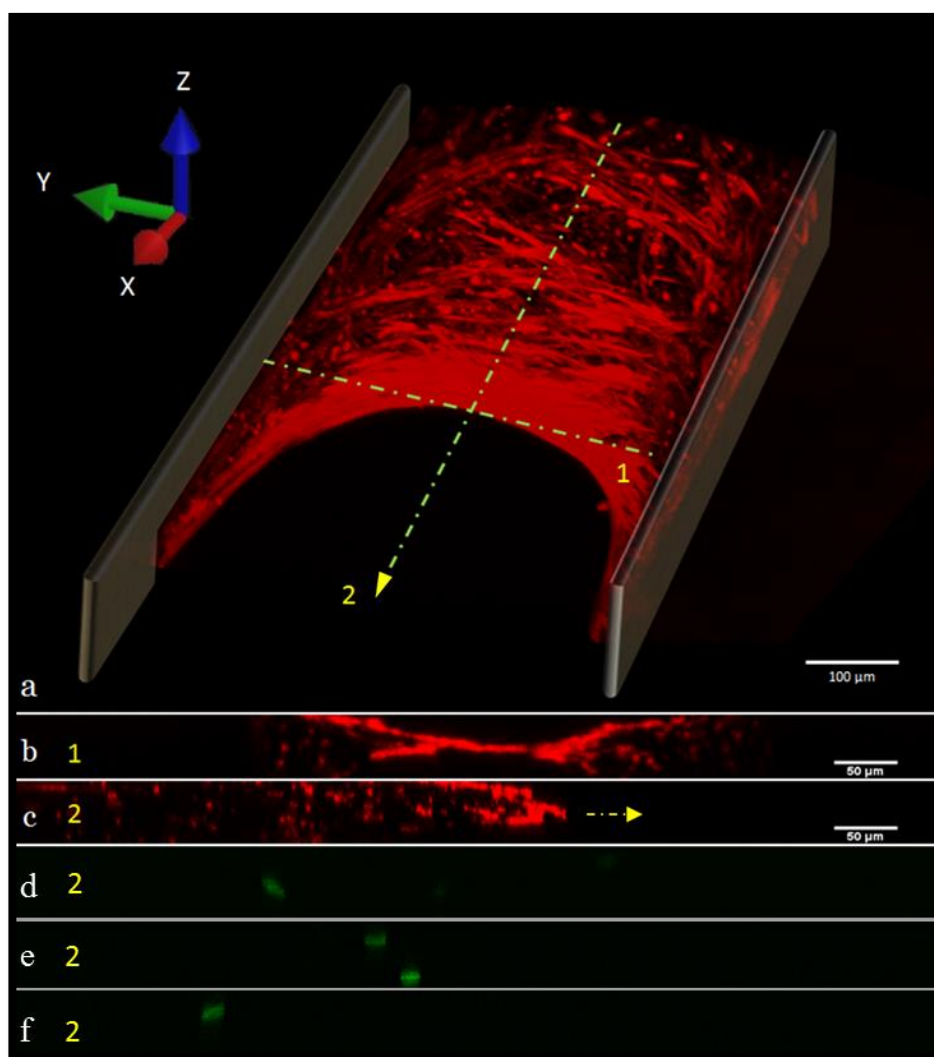


Fig. 3-13 (a) Example of a 3D reconstruction of the actin network in a 400  $\mu\text{m}$  pore (70  $\mu\text{m}$  z-stack, pore walls were indicated manually for illustrative purposes only). (b) Perpendicular cross section along the y- z plane showing the thin cell layer at the immediate front. (c) Longitudinal cross section along (x-z) plane showing tissue thickening away from the front of migration. (d-f) Examples of longitudinal cross sections showing EdU stained cell orientation in sections parallel to the (x-z) plane.

### 3.3 Discussion

We demonstrated that the pore width dramatically affected neo-tissue formation *in vitro*, both in terms of growth velocity and total area of tissue formed, using a well-defined experimental system. The results clearly showed that the highest pore spanning occurred in the narrowest pore and that tissue growth decreased significantly as pore width increased.

The curvature at the growth front varied according to pore width. Comparing these observations with the growth kinetics, it strongly suggested that the level of curvature had an important effect on neo-tissue formation.

It has been reported that cell/tissue geometry and internal cell generated tension interact to determine cell proliferation (Nelson et al. 2005; Li et al. 2009; Nelson 2009). Based on this evidence we investigated actin organization as the principle contractile element in the cell, to further elucidate the potential mechanisms driving growth at the front. The results revealed strongly aligned thick fibres at the front which have been previously associated with high tension and proliferation.

#### 3.3.1 Curvature driven growth

Tissue does not readily form from monolayers and essentially requires a 3D structure for many cell types. This was confirmed in our present study where cells initially covered the inside of the pore as a monolayer, but only started to fill the void of the pore as the migration front provided the necessary curved geometry allowing the cells to span the pore space.

Previously it has been shown that growth in 3D structures of different geometry followed a curvature-driven mechanism (Rumpler et al. 2008). The lowest initial tissue growth was observed in corners of hexagonal pore channels, increased in corners of square channels and was the highest in corners of triangular channels, that is, in the order of increasing curvature. However, this effect of pore shape disappeared in later stages, as the tissue filling the channel formed a circular front. From this point onwards the front of migration accelerated as this circle became smaller and curvature increased, while tissue area increased linearly over time.

In contrast, our structures allowed the tissue to preserve the same level of curvature for the whole duration of the study. This enabled us to accurately quantify growth kinetics and correlate growth with the effect of curvature. It was observed that narrower pores resulted in a higher level of curvature (Fig. 3-14), which was associated with sustained increased growth over the whole experiment.

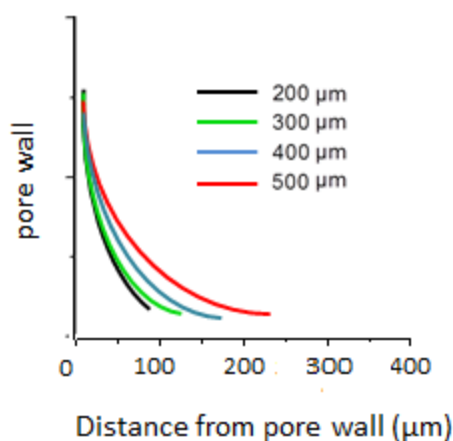


Fig. 3-14 Digitalised curvature curves according to pore widths

Comparison of the experimental results with a simple mathematical model appeared to provide additional support for curvature-driven growth. Dr. Chris Catt, School of Mathematics, University of Southampton developed a simple model based on the concept of curvature-driven growth as proposed by Rumpler et al <sup>35</sup>. This simple model successfully predicted both linear growth as well as the shape of the migration front observed in the experiments (Fig. 3-15a). Importantly, overall model predictions were shown to scale well across the different pore widths, providing further evidence that curvature played a critical role in tissue formation (Fig. 3-15b).

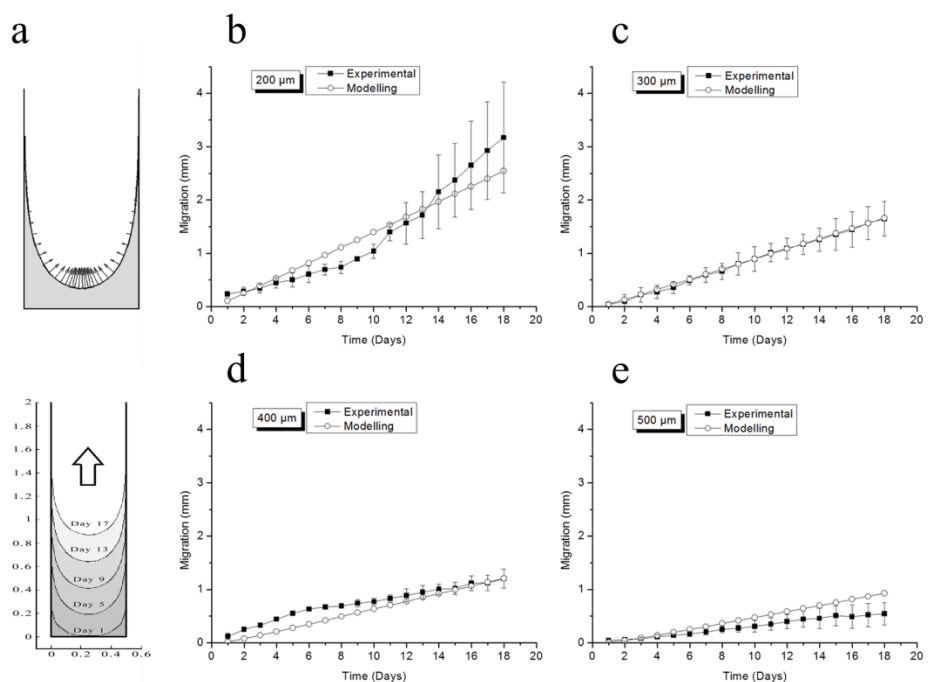


Fig. 3-15 (a-top) Mathematical modelling results, showing the shape of the tissue front during steady growth progression for a 500  $\mu\text{m}$  wide pore (Model courtesy Dr C. Catt, Southampton). The arrows indicate the local speed and direction of growth. High growth is associated with high curvature. (a-bottom) Predicted position of the progressing front shown at day 1, 5, 9, 13 and 17 (500  $\mu\text{m}$  pore, all units in mm). (b-e) Predictive mathematical modelling of growth as function of curvature versus experimental results. The model was fitted to the 300  $\mu\text{m}$  pore and then applied to the other configurations using the same growth parameter  $\lambda$ , showing good overall correspondence

### 3.3.2 Tissue formation mechanisms

While the current model could represent the overall patterns of growth observed, it is important to emphasize that it does not provide direct evidence for the underlying biological mechanisms. Thus, the precise underlying mechanisms responsible for curvature driven growth are still to be elucidated. Actin fibres determine cell contraction and traction forces (Tan et al. 2003) via coupling with myosin. Thick aligned actin fibres were observed at the migration front (Fig. 3-10) reflecting a zone of high tension (Aratyn-Schaus et al. 2010). It was previously demonstrated that zones of high tension were co-located with proliferation (Nelson et al. 2005), suggesting that the front of migration is a highly proliferative zone. Indeed the time-lapse results clearly confirmed cell division at the front (Fig. 3-11a-c), although additional division events were also apparent further away from the immediate front. Furthermore, the EdU incorporation results confirmed that cell proliferation did not occur only right at the front, but rather

took place in a finite zone, extending not more than a few hundreds  $\mu\text{m}$  from the front (Fig. 3-11d). Indeed, EdU results showed that cells further than a few hundreds  $\mu\text{m}$  away from the front did not produce DNA (Fig. 3-11e).

It has been noted previously, that growth driven by contraction of aligned actin corresponds to the concept of a contracting ‘purse string’ effecting closure in wound healing (Murray 2003; Rumpler et al. 2008). In our experiments, patterns similar to this concept appeared where actin fibres were aligned at the edges of the “wound” (Fig. 3-3-16).

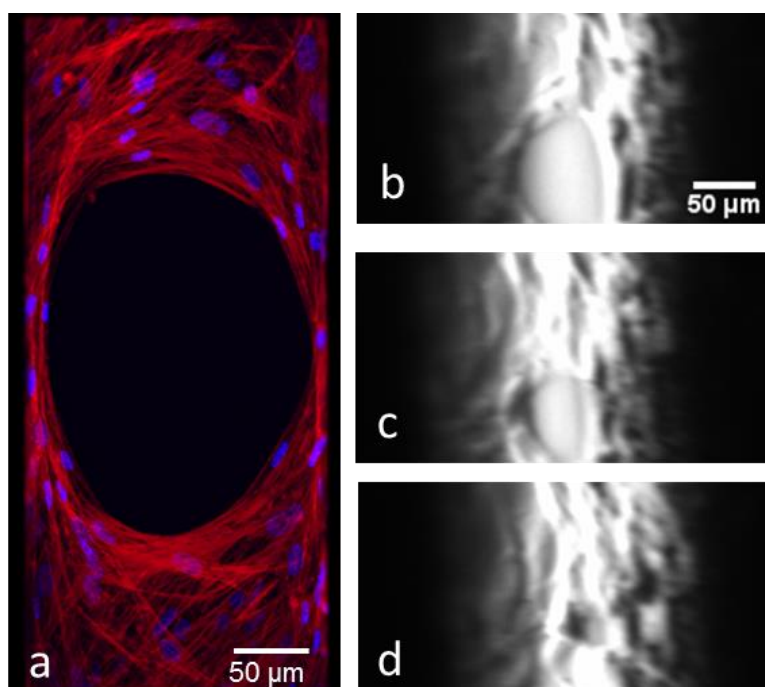


Fig. 3-3-16 (a) Laser scanning confocal microscopy picture representing pore closure corresponding to the concept of a contracting “purse string”. Tissue was stained for actin (Alexa Phalloidin 568) and nuclei (Hoescht) (b-d) Pore closure final steps (40 mins intervals)

Due to curvature, the tension generated by the aligned actin fibres at the curved front effectively exerts a tensile (stretching) stress on the underlying tissue, which could drive tissue growth forward. This is supported by the time lapse results in (Fig. 3-12a-c) showing tissue stretching as a result of cell contraction at the front (Original videos are provided as supplementary materials S3-S4 for 200  $\mu\text{m}$  and 500  $\mu\text{m}$ , as described in Appendix 1). The variation in tissue growth for different pore sizes could then be explained by a mechanism based on mechanical forces. As described in the schematic (Fig. 3-12d) and seen from the actin orientation at the front (Fig. 3-10a-d), the cellular

force components form a narrower angle with the longitudinal axis as curvature increases. Thus, the resulting net force exerted on the underlying tissue would increase as curvature does. This would correspond to higher tissue stress and increased growth for smaller pore widths as observed in the experiment.

In addition, cell migration could contribute to tissue growth, both directly and indirectly. It is well established that cellular internal stress generation, migration, spreading, and proliferation are intricately linked (Peyton et al. 2007; Li et al. 2009; Buxboim et al. 2010; Han et al. 2011; Nathan et al. 2011). The forces exerted by migrating cells (Galbraith et al. 1997) at the front can be transmitted to the neighbouring tissue via cell-cell junctions mediated by cadherins (Mege et al. 2006) and could contribute to dragging the tissue forward. Furthermore, stress fibre alignment can lead to stress anisotropy which could promote directed migration. For example in 2D multi-cellular configurations cells have been shown to migrate along the principle stress directions, sustaining minimal intercellular shear stress (Tambe et al.). Recently, Bidan et al. have proposed a “chord” model to explain the effect of curvature on tissue growth (Bidan et al. 2012). Cells spreading out on a concave surface and tensioning will span the pore void, flattening out the initial curvature. This can also be observed in Fig. 3-11a-c where straight tensioned cells can be seen to span the curved front, although our EDU results indicated that cell growth did not occur just at the immediate front, but rather in a finite zone (Fig. 3-11d, e)

Altogether our results suggest that initial tissue formation in a 3D environment is a highly dynamic process, involving a continuous cycle of migration, intracellular forces generation and proliferation, as apparent from time lapse videos (S1-S4). Nonetheless, eventually it is envisioned that cells will reach a mechanical equilibrium and become stabilized by extracellular matrix formation to form a mature tissue.

### **3.3.3 Tissue thickening and expansion along z-axis**

3D reconstruction revealed that tissue displays a convex appearance along the y-plane and a concave shape in the xz-plane, thus the 3D structure of the front of migration can be compared to a Scherk type surface (Fig. 3-17).

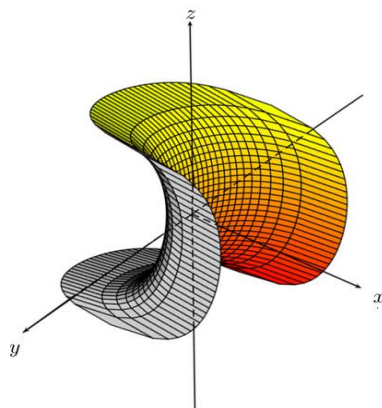


Fig. 3-17 Scherk type surface potentially representing the front of migration ([http://page.mi.fu-berlin.de/sfroehli/minimal\\_pstricks.php.html](http://page.mi.fu-berlin.de/sfroehli/minimal_pstricks.php.html))

Furthermore, it was seen that tissue thickness increased along the x-axis (Fig. 3-13b, c ). The tissue reaches a thickness of several tens of microns, thus the tissue is formed of several cell layers. Therefore, tissue expands along the z-axis as well. This is likely due to the fact that cell can divide either within the horizontal xy plane or by forming a fairly low angle with it, in the plane formed by the x and z axis (Fig. 3-13d-f).

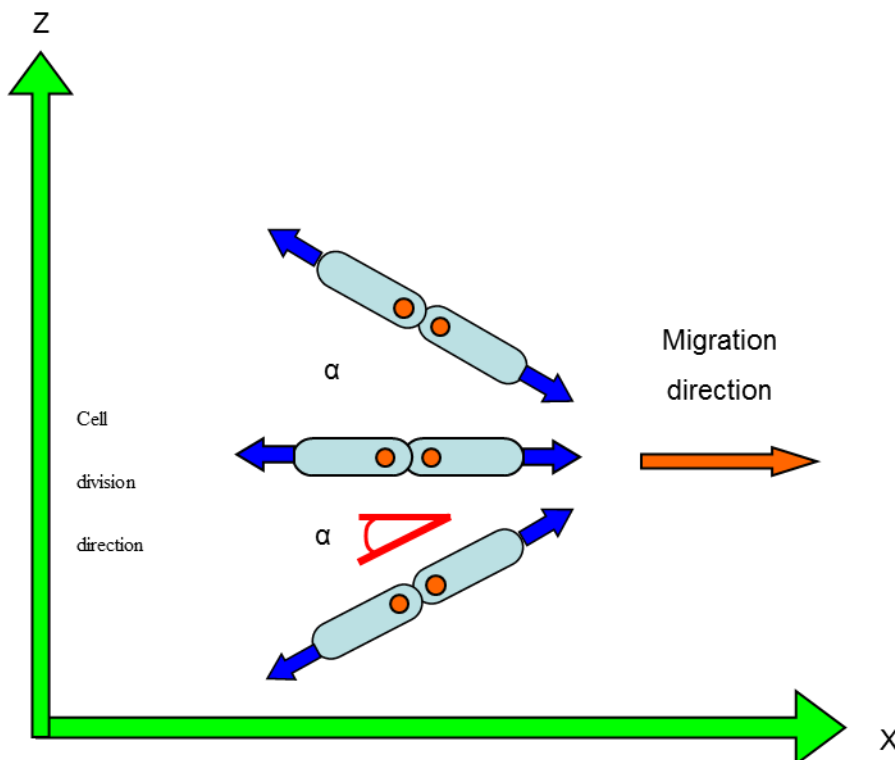


Fig. 3-18 Schematic of potential mechanism of cell division in the xz plane leading to an increase in tissue thickness

This type of oriented cell division pattern has been seen in *Drosophila* morphogenesis where the axis of cell division forms an angle  $\alpha$  of approximately 55 degrees with the proximo-distal axis to increase the thickness of the wing (Baena-Lopez et al. 2005). A similar mechanism may be applicable here, as the time lapse showed that cells were disappearing from the focal plane. This showed that cells move within the tissue along the vertical z-axis. A cell can migrate “inside” the tissue, and move along the z plane by sliding along neighbouring cells. Constant remodelling of cadherins mediated cell-cell contacts (described in paragraph 2.5.3.2, Chapter 2) coupled to actin polymerization providing the forces pushing the membranes of adjacent cells over each other could explain such process. Also, cell movement among surrounding cells could display similarities with the intercalation phenomena observed in *Drosophila* (described in paragraphs 2.5.3.12 & 2.5.3.13, Chapter 2). Thus, besides migration, cells can also divide and undergo mitosis along the vertical z axis i.e. two daughter cells can appear at different position on the vertical z axis (Fig. 3-13d, f; Fig. 3-18) leading to tissue thickening.

### **3.3.4 Actin organisation**

Additional effects of anisotropy can be seen in our results by considering the actin organisation in the bulk away from the migration front. Actin displayed a highly distinct orientation, i.e. more longitudinally for narrow and more perpendicularly for wide pores respectively. These oriented fibres could represent ‘remnants’ of previous migration fronts (Fig. 3-10), with their orientation determined by curvature. However, orientation could also arise from cytoskeletal remodelling and the stiffness experienced by the cell while attempting to reach tensional homeostasis (Peyton et al. 2007). Thus actin orientation would reflect the direction that enables the cell to exert tension, and may represent the net effect of the perpendicular resistance provided by the walls of the pore and the longitudinal stress exerted by the pulling of the curved front, depending on pore size. Understanding how actin organisation arises during growth is important as initial cell and actin orientation can serve as a template for subsequent tissue formation and

collagen fibre organisation, which determines eventual mechanical functionality (Wang et al. 2003; Engelmayr et al. 2006).

### **3.4 Summary**

In summary, in this study we have clearly demonstrated the relationships between pore width, initial tissue growth and curvature reflected by different actin organisation. We characterized growth solely as a function of pore geometry, proving that faster cell invasion occurred in narrower pores where the front curvature was the highest. Additionally, we showed that tissue formation resulted from a combination of cellular phenomena such as cell motility, cell contraction and cell division.

Regarding cell contraction, we proposed a mechanism whereby the effect of actin mediated cell generated forces would depend on pore width. Due to the higher curvature in the case of a narrow pore, higher tensile forces would be exerted on the underlying tissue which would contribute to an increased rate of tissue expansion.

With respect to cell division, this was seen to take place at the immediate front as well as within a finite zone extending up to a few hundred microns from the front. Furthermore, this zone was associated with different actin fibre orientation according to pore width.

Cell division occurs in a zone where the actin network organisation is affected by pore width. Therefore, it appears to be necessary to investigate whether differences in tissue orientation and cell division could potentially be one of the factors contributing to the tissue's capacity to expand. Furthermore, in this study, the amount of tissue formed has been quantified based on the concept of projected tissue area. Therefore, although it was clearly shown that invasion rate was strongly dependent on pore width, further quantification of the number of cells would be required to confirm that a higher absolute amount of tissue is formed per pore.



## Chapter 4

# Ingrowth Enhancement Due to Pore-Induced Tissue Orientation

The study presented in this chapter led to the writing of an article submitted for possible publication. Preliminary results obtained were presented at the Tissue Engineering & Regenerative Medicine International Society (TERMIS) World Congress, September 2012 and published as an extended abstract in the Journal of Tissue Engineering & Regenerative Medicine, (JTERM)

In the previous chapter, actin imaging results indicated the importance of tissue organisation and the capacity of pore geometry to modulate the organisation of the actin cytoskeleton. Furthermore, cell proliferation was seen to take place within a finite zone starting from the front of migration and extending up to a few hundred microns towards the rear. Therefore it was decided to further investigate tissue organisation as well as cell division in this zone

The aim of this study was to determine the tissue formation ability of Human Bone Marrow Stromal Cells, and to relate this to tissue organisation. For this purpose, in a first experiment, tissue formation was monitored during 14 days and time points taken every second day. 1 cm long open pores were used, with different widths of 200  $\mu\text{m}$  and 500  $\mu\text{m}$ , based on our previously established *in vitro* system. Projected tissue area was calculated after 14 days of monitoring. Next, F-actin and Collagen I were imaged to assess and quantify in detail the spatial organisation of the actin and collagen network. In addition, the cell nuclei orientation was also measured in the two different

structures. A second experiment was done in similar conditions to the first one, except that tissue formation was monitored for 30 days. Projected tissue area (PTA) was calculated after 30 days of monitoring and the number of cells present in each pore was calculated after 30 days. Additionally, the volume of the tissue regenerated was estimated after 30 days as well as the orientation of dividing cells in order to establish whether cell division orientation could impact tissue expansion. Combining all this data provided insight in how different physical structures are capable of modulating cell orientation, cell division orientation, actin network organisation and matrix anisotropy. Also, tissue differentiation into the osteogenic lineage was qualitatively assessed. Most importantly, this study showed that the capacity of tissue to form in different structures is highly dependent on tissue organisation which impacts on cell division orientation.

## **4.1 Material and Methods**

### **4.1.1 Scaffold Fabrication & Preparation**

Scaffolds were produced as in our previous study (Knychala et al. 2013). Briefly,  $\alpha$ -TCP slurry was cast on *Silastic*® M RTV Silicone Rubber male moulds and left for hardening during approximately 2 weeks at 37 °C in Ringer solution. Next, the silicone moulds were carefully peeled off to obtain hardened pieces of  $\alpha$ -TCP cement turned into Hydroxyapatite. Only two pore sizes i.e. 200  $\mu$ m or 500  $\mu$ m were used for the experiments presented in this chapter. Prior cell seeding, samples were treated as described in paragraph 3.1.1.4

### **4.1.2 Human Bone Marrow Cells Isolation, Expansion and Seeding**

Human Bone Marrow Stromal Cells (HBMSC) were extracted from bone marrow collected during routine hip replacement from 4 patients (64 to 95 years old, 2 male and 2 female). Tissue samples were obtained from haematologically normal patients undergoing routine total hip replacement surgery, with approval from the Southampton Hospital Ethics Committee and appropriate patient consent. HBMSC were isolated from the marrow using plastic adherence using our standard protocols (Tare et al. 2008) and seeded in T150 cell culture flasks (Fig. 4-1). HBMSCs were cultured in  $\alpha$ -MEM medium (Sigma-Aldrich, UK) with 2.2 g/mL of sodium bicarbonate. The media was

supplemented with 10% Foetal Bovine Serum (FBS) (Sigma) and 1% Penicillin-Streptomycin solution x100 (Sigma). Cells were expanded at a 1:4 ratio and were cultured until passage 1. From this point onwards, cells were treated and seeded as described in the previous chapter in paragraph 3.1.3. Following seeding, scaffolds were incubated at 37 °C and 5% CO<sub>2</sub> in static conditions for up to 4 weeks. The scaffolds were washed with PBS prior to each media change. Culture media was changed 3 to 4 times a week during the entire study.

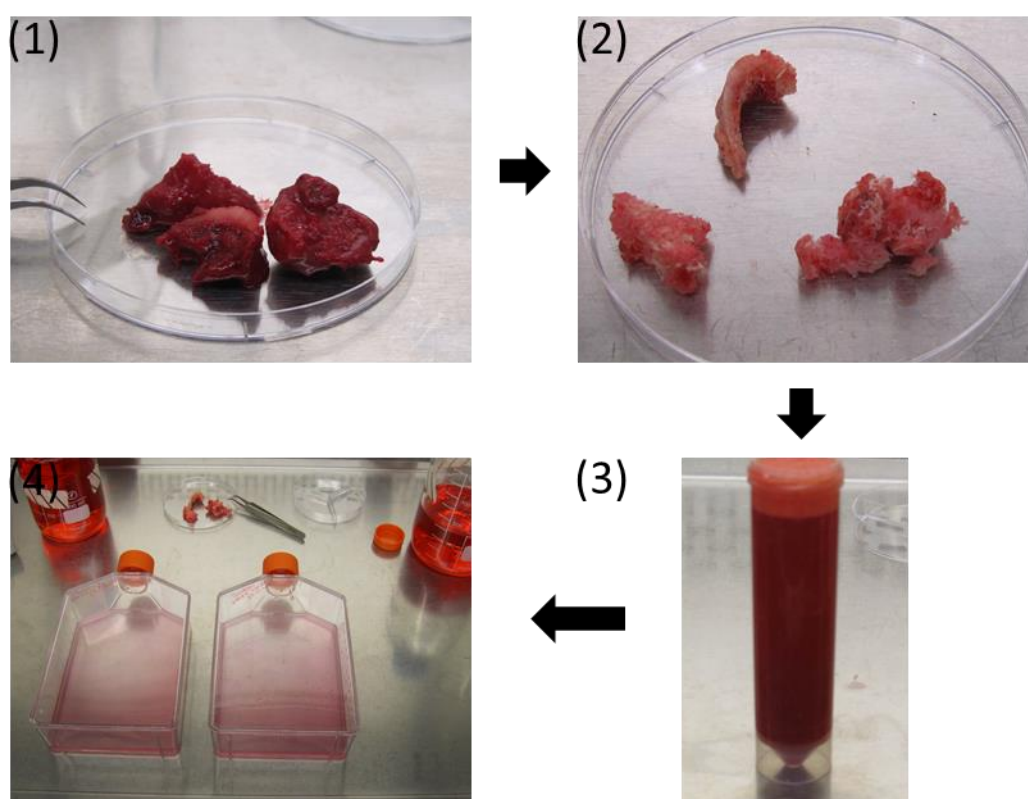


Fig. 4-1 Human Bone Marrow Cells isolation process. (1) Fresh pieces of trabecular bone containing bone marrow. (2) Bone pieces after cell extraction. (3) Solution obtained after processing the bone pieces. (4) Bone marrow cells freshly seeded in T150 flasks.

### 4.1.3 Optical Inverted Microscopy

In order to monitor and quantify tissue growth precisely, samples were imaged every 48h using a Zeiss Axiovert 200 inverted microscope, equipped with an AxioCam MRm monochrome camera. Growth did not start at the same time in every pore slot, thus the first time point was set as the day when growth within the pore space became visible.

The same replicates per condition were monitored and micrographs were taken every 2 days over 14 days (n=3) in the first experiment and over 30 days for the second experiment. Growth was first quantified using a 10× magnification objective. When the amount of tissue formed was too high to be imaged at 10× magnification, 4× magnification was used. The amount of tissue formed was measured using ImageJ software. The distance measured was set as the distance between the pore extremity and the middle of the front of migration of the tissue formed. Values reported represent mean ± std. Additional time lapse video of tissue formation was obtained using the same microscope system fitted with an incubator chamber providing normal cell culture conditions (Humidified, 37°C, 5% CO<sub>2</sub>).

### 4.1.4 Laser Confocal Microscopy

Prior to staining, all samples were washed 3 times in PBS and fixed in paraformaldehyde-PBS 4 % (w/v) for 20 min at room temperature. Next, samples were washed 3 times in PBS, incubated 20 min in PBS-Triton 0.5% (v/v) for permeabilization and then incubated in 1% BSA (Sigma)-PBS (w/v) for 30 min to block unspecific binding, followed by labelling for the different tissue components. For actin staining, samples were treated as described in 3.1.5. For Collagen I staining, samples were rinsed 3 times in PBS, incubated 30 min in PBS-BSA 1% and incubated with a primary antibody anti-Collagen I raised in rabbit (Abcam, 1/100) overnight at 4° C. Secondly, samples were rinsed 3 times in PBS and 3 times in PBS-BSA 1% and incubated overnight at 4° C with secondary antibody Alexa 488 anti-rabbit. Negative controls were done following the same procedure, but with the primary antibody (Anti-Collagen) omitted. Cell Nuclei were labelled using Hoescht stain for 30 mins. (1/1000 dilution (v/v) in PBS, Molecular probes, Invitrogen). For EdU staining, please refer to chapter 3, paragraph 3.1.5. Eventually, after labelling samples were rinsed 3 times in PBS and imaged immediately or within 1-3 days. Samples were imaged using a laser confocal microscope (Leica TCS SP2, Germany). Z-axis image acquisition was performed using a 20× water-dipping objective (Leica, HCX APO L 20×/0.50 W U-V-I). Individual images planes were acquired in bi-directional scanning mode at 1 µm z-axis intervals with a resolution of 1024×1024.

### 4.1.5 Cell counting

Cell-Profiler software was used. Nuclei recognition of cells stained with Hoescht stain (1/1000 dilution (v/v) in PBS, Molecular probes, Invitrogen) was done using automated object identification (minimum diameter of 7.2  $\mu\text{m}$  and a maximum of 36  $\mu\text{m}$ ) The “Robust Background per Object” threshold was used as it was providing the best object recognition (Fig. 4-2). The rate of recognition is estimated to be over 90% accuracy. Subsequently, the software provides the number of objects recognized. For this purpose, cell nuclei have been imaged and counted throughout the whole tissue formed after 30 days.

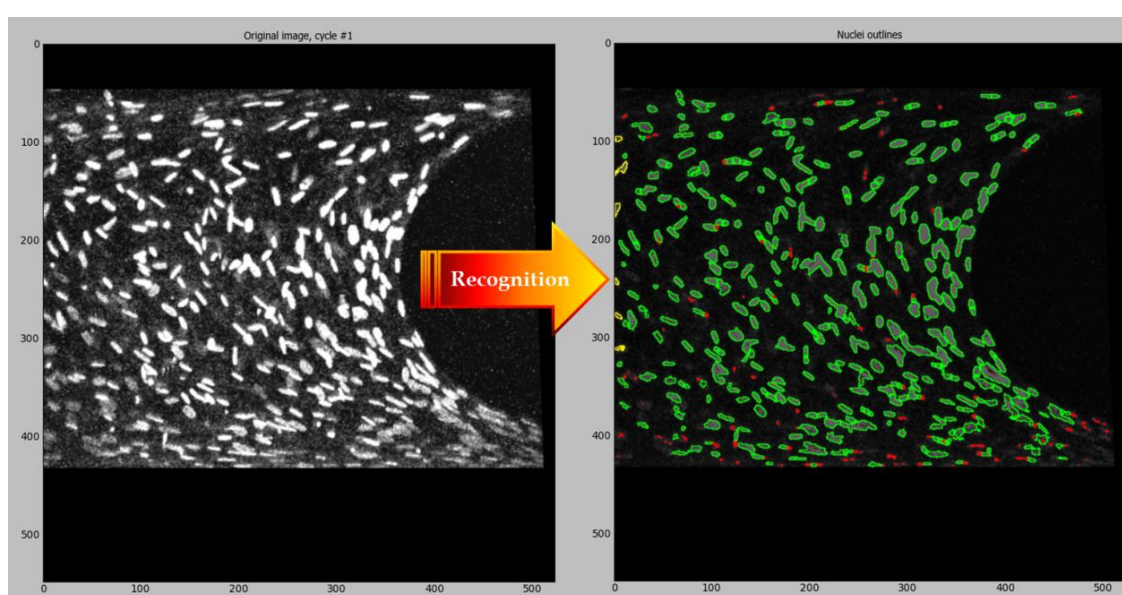


Fig. 4-2 Cell nuclei recognition with Cell Profiler

### 4.1.6 Tissue Volume Estimation

The volume of the new tissue formed within the structures was estimated using projected tissue area and data from confocal microscopy imaging. During confocal imaging along the z-axis (vertical axis), a stack of pictures was obtained during cell nuclei imaging. The thickness of the stack was calculated using the z resolution provided by the imaging software (Leica confocal software ©), then it was multiplied by the projected tissue area in order to obtain a final estimation of the volume occupied by the regenerated tissue.

### 4.1.7 Tissue Orientation Measurements

The pictures were divided in 5 Regions of Interest (ROI) or zones located right behind the front of migration (Fig. 4-3). Each ROI had a length of 360  $\mu\text{m}$  and a width corresponding to 20% of the pore width ( $\sim 40 \mu\text{m}$  for 200  $\mu\text{m}$  pores and 100  $\mu\text{m}$  for 500  $\mu\text{m}$  pores respectively). Next, the orientation of Cell Nuclei, Actin and Collagen I fibres was measured in each zone. Subsequently, a comparison was carried out between the corresponding zones of the two different pore sizes used

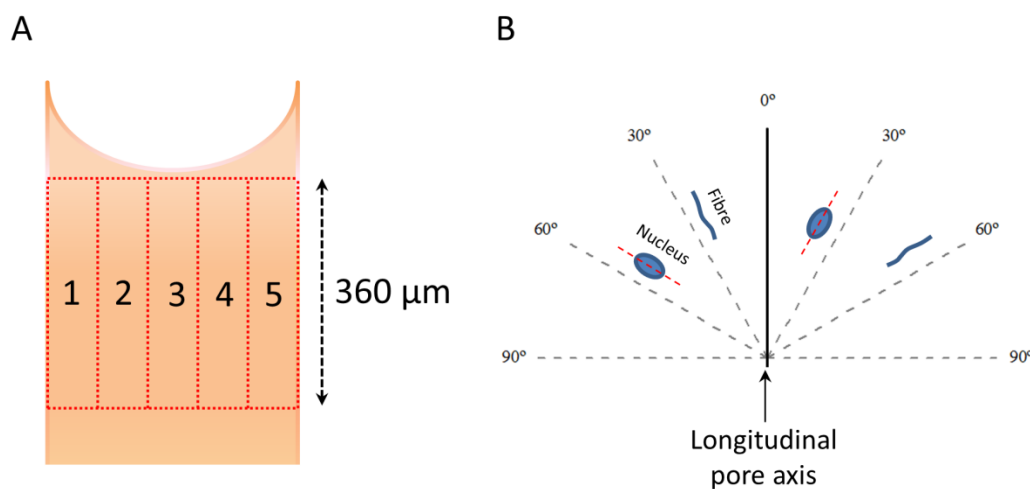


Fig. 4-3 Tissue orientation analysis. (a) Schematic showing how tissue was divided into 5 zones. (b) Schematic explaining the meaning of the orientation measurements.

#### 4.1.7.1 Cell Orientation Measurements

In order to measure cell orientation in the regenerated tissue, the initial step performed is the same as for the cell count, which is object recognition in Cell-profiler. Next, for each single nucleus recognised (Fig. 4-2), the software Cell-profiler provided values of orientation along the main pore axis (Fig. 4-3) using the module “Measure Object Size Shape”. The orientation is characterised as the angle between the pore axis and the major axis of the ellipse fitted around the nucleus. The values found ranged from  $-90^\circ$  to  $90^\circ$ , therefore, absolute values of the angles were used for clarity and consistency. To obtain a representative distribution of the orientation, the number of cells was normalized and the values were plotted in 5 bins of  $18^\circ$  starting from  $0^\circ$  to  $90^\circ$ . Four replicates were used for each pore width ( $n=6$ ), and statistics were calculated using

---

analysis of variance (one-way ANOVA) followed by post-Tukey test in Origin Lab software.

#### **4.1.7.2 Fibre Orientation Measurements**

The Actin and Collagen fibre organisation was characterized in ImageJ using the plugin OrientationJ implemented in the software (Fig. 4-4), which has been used in previous studies for similar purposes (Pathak et al. 2012; Rezakhaniha et al. 2012). Two parameters were measured for each zone, the orientation and the coherency. The orientation is given in degrees and reflects the fibre/ROI orientation with respect to the longitudinal pore axis. Coherency varies between 0, indicating isotropic distribution, to 1, indicating perfectly aligned structures. These two measurements were taken into account as coherency strengthens the orientation measurement by indicating the uniformity of fibre direction. Measurements of these two parameters were taken for all ROIs on different replicates (n=5 for Actin, n=5 for Collagen) and subsequently averaged for ROIs having the same location across pore width. Statistics were calculated using analysis of variance (one-way ANOVA) followed by post-Tukey test in Origin Lab software.

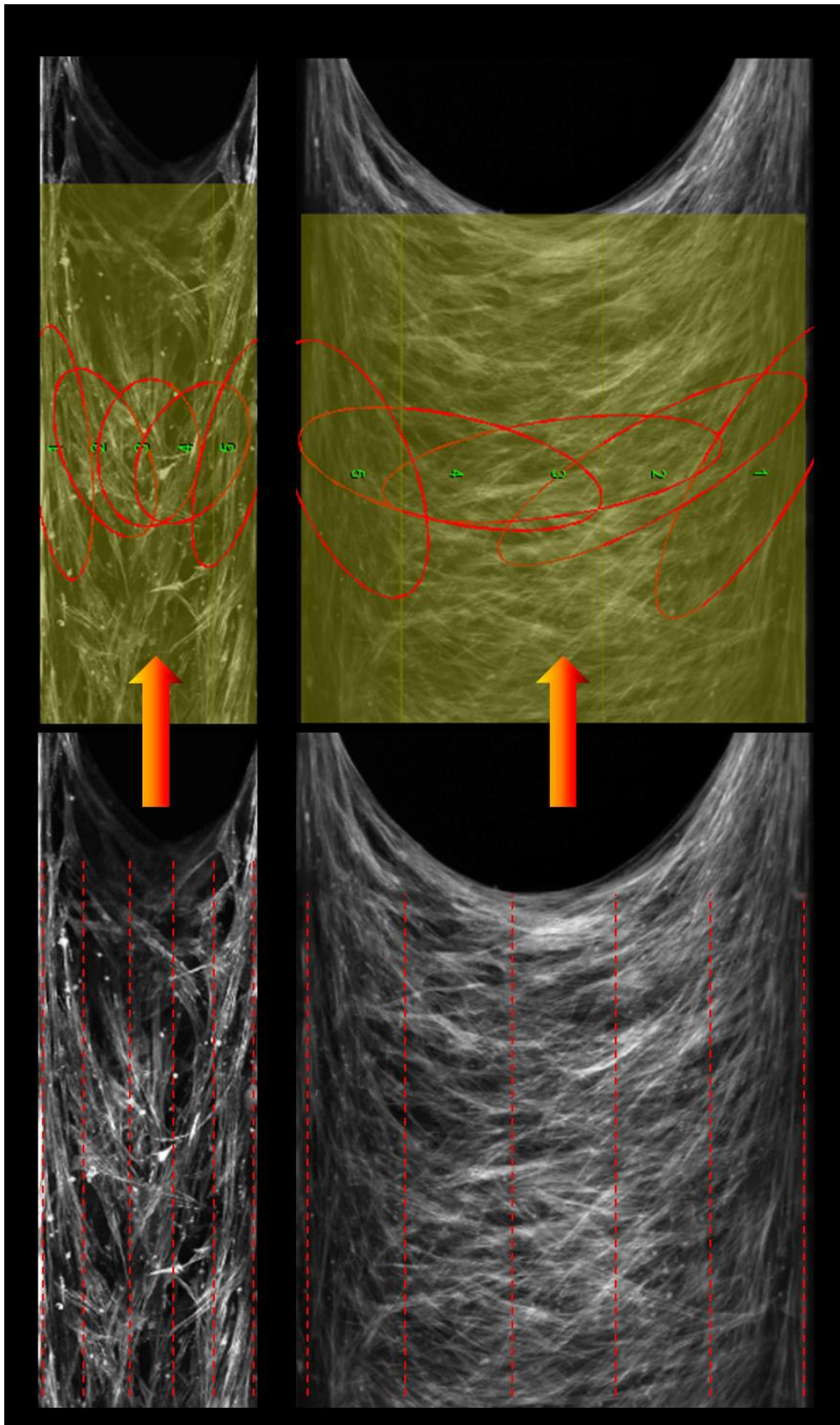


Fig. 4-4 Orientation J plugins applied for fibre orientation assessment in 200 & 500  $\mu\text{m}$  pores. Dotted lines represent the five zones the tissue was split into and the ellipses represent the average orientation of the fibres within the zone. In this figure, actin fibres are shown

#### 4.1.8 Overall recap of samples used & purposes

Table 4-1 Overall summary of samples used &amp; experiments performed.

	<b>Kinetics</b>	<b>Cells</b>	<b>EdU</b>	<b>Actin</b>	<b>Collagen</b>
F 63 <sub>1</sub>	Monitored for 30 days	Imaged & Cell number quantified (n=3)	/	/	/
F 63 <sub>2</sub>	Cultured for 30 days	Imaged & Orientation quantified (n=3)	Imaged & Orientation quantified (n=3)	/	/
F95	Monitored for 14 days	Imaged & Orientation quantified (n=3)	/	/	/
F84	Cultured for 14 days	Imaged & Orientation quantified (n=3)	/	Imaged & Orientation quantified (n=3)	Imaged & Orientation quantified (n=3)
M87	Cultured for 14 days	/	/	Imaged & Orientation quantified (n=2)	Imaged & Orientation quantified (n=2)

## 4.2 Results

### 4.2.1 Kinetics

After seeding the cells onto the constructs, tissue started to form at the pore extremity and filled the slots from there onwards as described in Fig. 3-6 in Chapter 3. Tissue grew suspended within the pore slot, being anchored to the pore walls, but free from below and above (Fig. 3-7). Tissue formation was monitored for a total number of 14 days (experiment 1) and 30 days (experiment 2). It was seen that tissue filled the 200  $\mu\text{m}$  pores more rapidly than the 500  $\mu\text{m}$  ones. Tissue was quantified based on the concept of projected tissue area (PTA), introduced previously (Rumpler et al. 2007; Bidan et al. 2012), in our study we measured the longitudinal distance spanned by the newly formed tissue in the open pores and subsequently PTA. In the first experiment, at day 14, tissue spanned a longitudinal distance of on average  $1.18 \pm 0.2$  mm in the 200  $\mu\text{m}$  pores (Fig. 4-5a), corresponding to a PTA of  $0.25 \pm 0.02$  mm<sup>2</sup> (Table 4-2). In the 500  $\mu\text{m}$  pores it spanned only  $0.35 \pm 0.09$  mm (Fig. 4-5a), corresponding to a PTA of  $0.17 \pm 0.04$  mm<sup>2</sup> (Table 4-2). Moreover, growth velocity over 14 days in 200  $\mu\text{m}$  and 500  $\mu\text{m}$  pores was 88  $\mu\text{m}/\text{day}$  and 25  $\mu\text{m}/\text{day}$  respectively (Fig. 4-5b). In the second experiment, tissue spanned a longitudinal distance of on average  $3.77 \pm 0.8$  mm in the 200  $\mu\text{m}$  pores (Fig. 4-6a), corresponding to a PTA of  $0.76 \pm 0.17$  mm<sup>2</sup> (Table 4-2). In the 500  $\mu\text{m}$  pore, it spanned only  $0.92 \pm 0.18$  mm (Fig. 4-6a), corresponding to a PTA of  $0.46 \pm 0.09$  mm<sup>2</sup> (Table 4-2). Similarly, the average growth velocity over 30 days in 200  $\mu\text{m}$  and 500  $\mu\text{m}$  pores was 124  $\mu\text{m}/\text{day}$  and 33  $\mu\text{m}/\text{day}$  respectively (Fig. 4-6b). The differences in spanning rates within same pore size were due to the fact that cells were obtained from different donors. However, the differences of growth rates between the two different pore sizes were maintained, accordingly to the previous findings from Chapter 3. The growth occurred linearly in both experiments over 14 days and 30 days of monitoring. Therefore, the velocity was measured by linear regression fitting for the 3 replicates separately and then averaged for each condition.

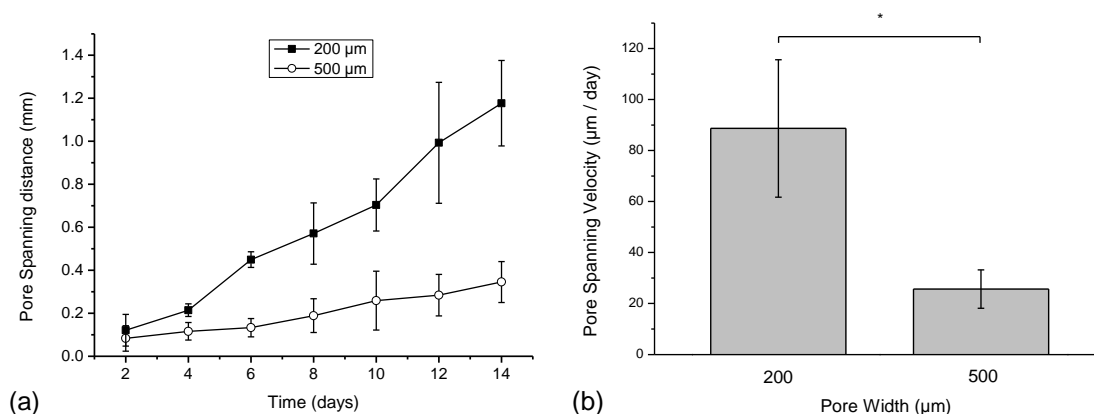


Fig. 4-5 Experiment 1 (14 days): Effect of pore size on tissue growth kinetics (a) Comparison of growth curves for the different pore widths over 14 days (n=3). (b) Growth speed obtained by linear fitting of the grow curves for the different pore sizes. Statistical analysis was performed using analysis of variance (one-way ANOVA) followed by post-Tukey test in Origin Lab software ( $p < 0.05$ ). Bars and error bars represent mean values and standard deviation respectively (n=3).

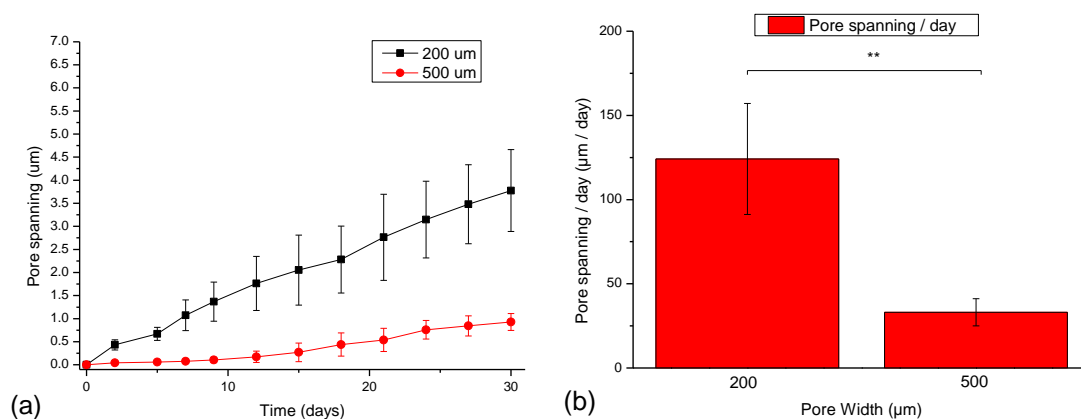


Fig. 4-6 Experiment 2 (30 days): Effect of pore size on tissue growth kinetics (a) Comparison of growth curves for the different pore widths over 30 days (n=3). (b) Growth speed obtained by linear fitting of the grow curves for the different pore sizes. Statistical analysis was performed using analysis of variance (one-way ANOVA) followed by post-Tukey test in Origin Lab software ( $p < 0.05$ ). Bars and error bars represent mean values and standard deviation respectively (n=3)

Table 4-2: Area of newly formed tissue in the different pore sizes

Pore Size	Projected Tissue area (mm <sup>2</sup> )	
	F 95 (after 14 days)	F 63 (after 30 days)
200 μm	0.25±0.02	0.76±0.17
500 μm	0.17±0.04	0.46±0.09

### 4.2.2 Cell number

After 30 days, the total number of cells found in the 200 μm pore was greater than in the 500 μm pore. The tissue formed in 200 μm contained 1119 ±101 cells and 408±35 cells in the 500 μm pores (Fig. 4-7).

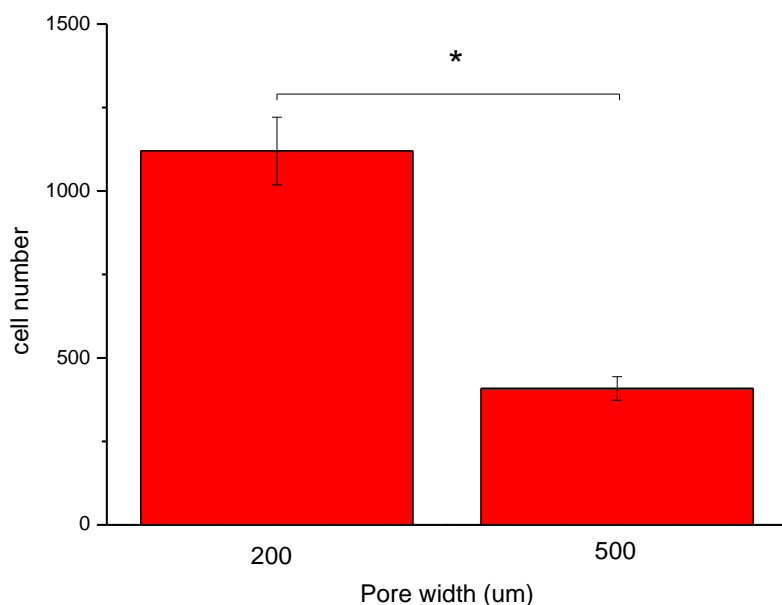


Fig. 4-7 Number of cells counted in each condition after 30 days of growth (n=3)

### 4.2.3 Percentage of EdU positive stained cells

After 30 days, the percentage of positive EdU stained cells in a zone extending up to 300  $\mu\text{m}$  behind the front of migration was calculated. The percentage of positive EdU stained cells was found to be higher in 500  $\mu\text{m}$ . The number of positive EdU stained cells was  $19\% \pm 3\%$  in 200  $\mu\text{m}$  and  $33\% \pm 7\%$  (Fig. 4-8). Statistically differences were found at  $p < 0.05$ .

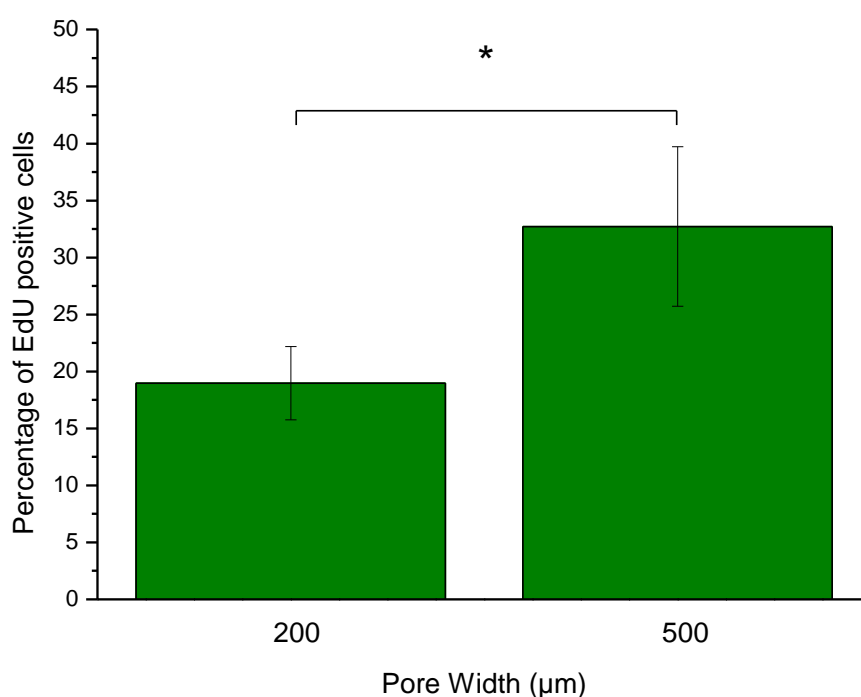


Fig. 4-8 Experiment 2: Percentage of EdU positive cells in each condition (n=3)

### 4.2.4 Neo- tissue volume

After 30 days, the volume occupied by the tissue regenerated within the constructs was approximately  $10 \times 10^7 \mu\text{m}^3 \pm 3 \times 10^7 \mu\text{m}^3$  in 200  $\mu\text{m}$  and  $8 \times 10^7 \mu\text{m}^3 \pm 3.7 \times 10^7 \mu\text{m}^3$  in 500  $\mu\text{m}$  pores (Fig. 4-9). However, no statistical differences were found between the two conditions due to high variability. The variability is likely to be related to the low accuracy of the measurements which will be discussed in section 4.3.

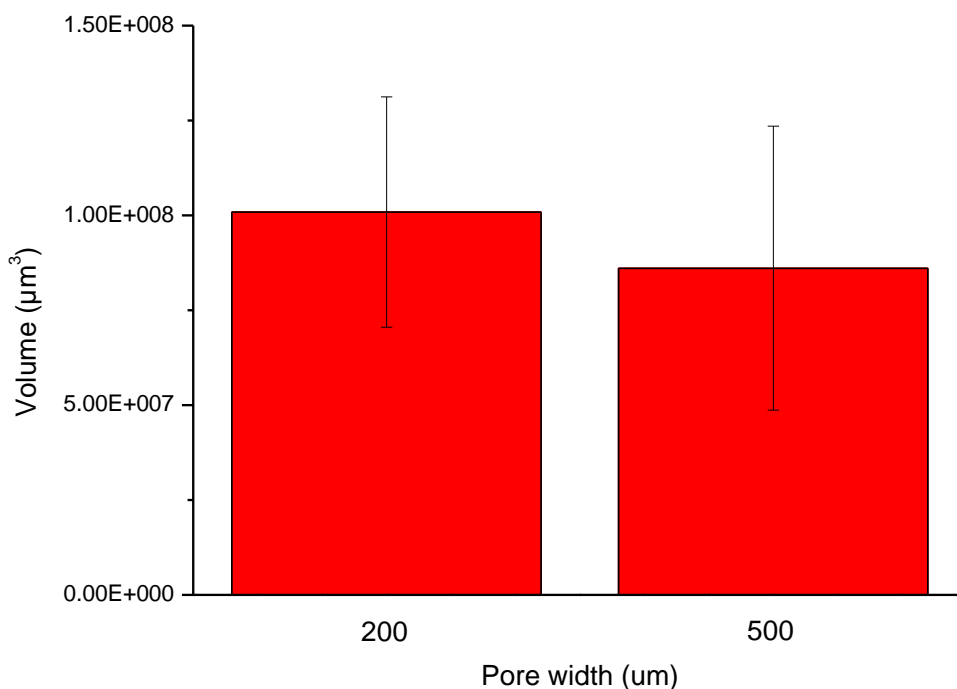


Fig. 4-9 Experiment 2. Volume occupied by neo-tissue formed within the pore for each condition after 30 days (n=3)

#### 4.2.5 Tissue Imaging

To determine tissue organisation, the tissue was stained for 3 main components, i.e. cell nuclei, actin and collagen. Cell nuclei labelling showed a uniform cell distribution throughout the tissue in both pore width conditions (Fig. 4-10a, b). Additionally, cell nuclei had an ellipsoid shape reflecting a preferred orientation. Furthermore, a dense actin network and collagenous matrix were seen to be formed for both pore widths. It was observed that both of these fibrillar networks displayed a similar pattern for the same pore width. However, this pattern was markedly different when comparing the two different pore widths (Fig. 4-10c-f). Pore width did not appear to affect the formation of a collagenous matrix in itself, but did affect its organisation.

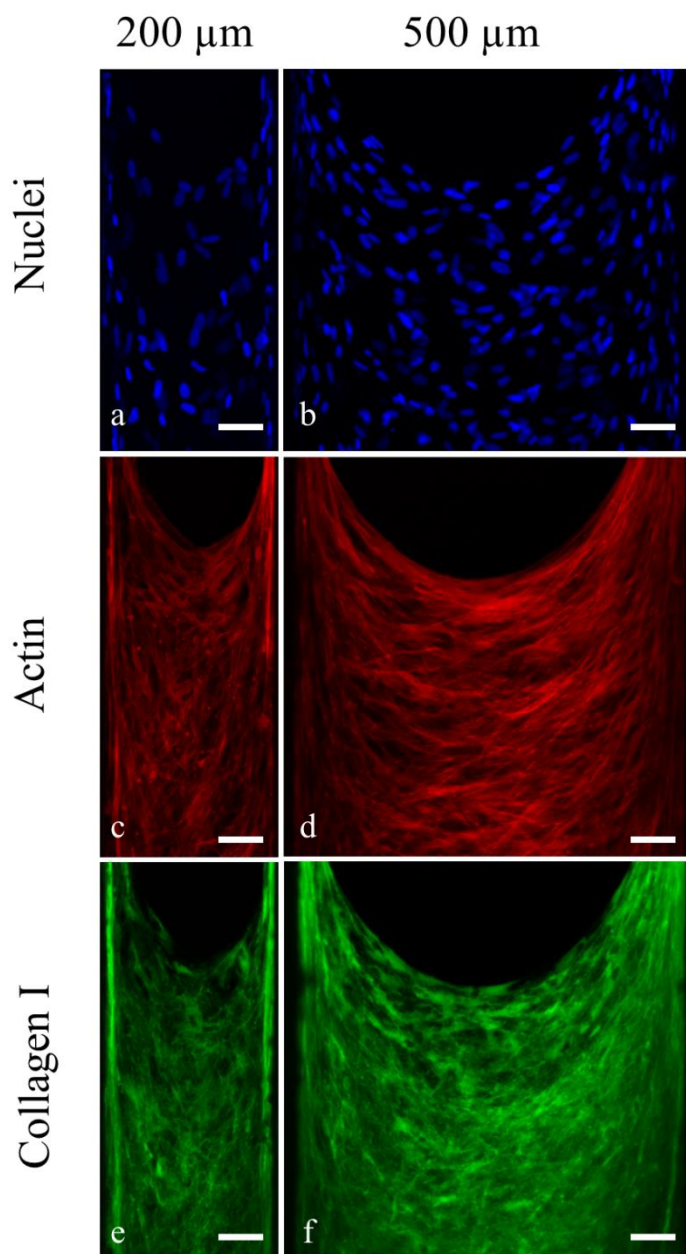


Fig. 4-10 Confocal microscopy images of the tissue components. (a, b) Cell nuclei stained with Hoescht dye in 200  $\mu\text{m}$  pore (a) and 500  $\mu\text{m}$  pore (b). (c, d) Actin cytoskeleton stained with Alexa Fluor 568-Phalloidin in 200  $\mu\text{m}$  pore (c) and 500  $\mu\text{m}$  pores (d). (e, f) Collagen I matrix stained with primary antibody anti-Collagen from rabbit and Alexa Fluor 488 anti-Rabbit in 200  $\mu\text{m}$  pore (e) and 500  $\mu\text{m}$  pore (f). Primary antibody was omitted for negative control. (Scale bar = 50  $\mu\text{m}$ )

### 4.2.6 Cell Orientation Distribution

The cell orientation data obtained displayed striking differences between the two pore widths (Fig. 4-11). For the 200  $\mu\text{m}$  pore, patterns at the front and within the bulk are similar. More than 50% of the cells have an orientation relative to the longitudinal pore axis lower than  $18^\circ$ , then around 20% of the cells have an orientation angle between  $18^\circ$  and  $36^\circ$  and 20% have an angle higher than  $36^\circ$ . On the other hand, for the 500  $\mu\text{m}$  pore, the pattern is different from that for 200  $\mu\text{m}$ . The majority, i.e. 50% of the cells have an orientation angle higher than  $36^\circ$ , around 20% of the cells have an orientation angle between  $18^\circ$  and  $36^\circ$  and only 20% of the cells have an orientation lower than  $18^\circ$ .

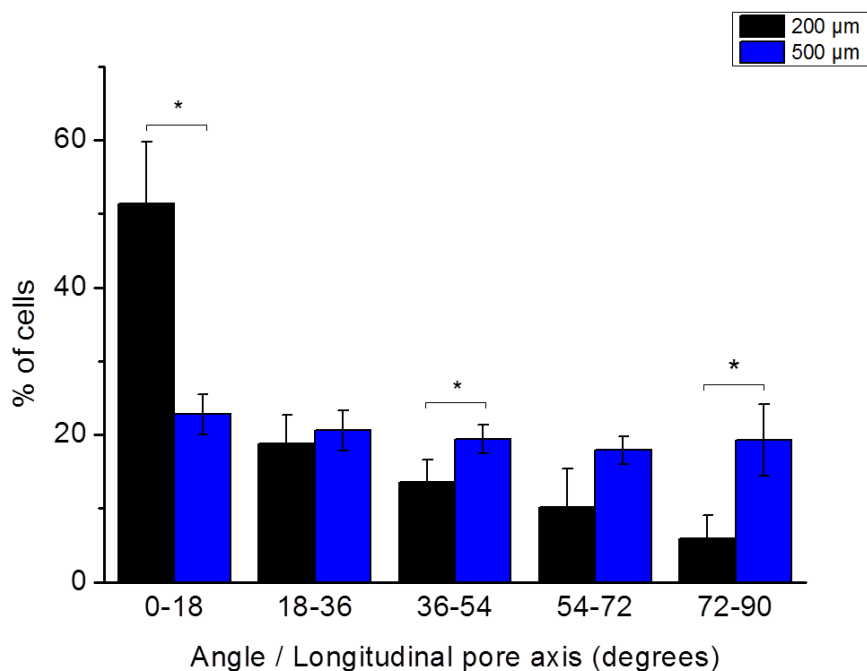


Fig. 4-11 Cell orientation distribution in 200  $\mu\text{m}$  pore and 500  $\mu\text{m}$  pore. (n=6 per conditions)

### 4.2.7 Spatial Tissue Organisation

Orientation measurements of cell nuclei (Fig. 4-12), actin cytoskeleton (Fig. 4-13) and collagen fibres (Fig. 4-14) revealed relatively similar patterns for identical conditions. Generally, for both pore widths, the alignment with the longitudinal axis decreased when moving from the pore wall towards the centre. However, comparing the orientation between the two pore widths in each zone, the alignment was systematically and significantly higher in the 200  $\mu\text{m}$  pore (i.e. corresponding to lower angles, more parallel with the longitudinal pore axis, Fig. 4-3). Therefore, this showed that overall tissue alignment, in the 200  $\mu\text{m}$  pore was higher than in the 500  $\mu\text{m}$  pore. The highest differences between the two pore widths were observed in the central zone (zone 3). Tissue was oriented almost perpendicular to the pore axis in the 500  $\mu\text{m}$  case. Cell, actin cytoskeleton and collagen fibres had an orientation of  $68\pm 5^\circ$ ,  $81\pm 1^\circ$  and  $76\pm 10^\circ$  relative to the pore axis respectively, whereas in the 200  $\mu\text{m}$  pore the corresponding values were  $29\pm 7^\circ$ ,  $24\pm 18^\circ$  and  $19\pm 10^\circ$  (Fig. 4-12, Fig. 4-13, Fig. 4-14). Measurements for cells, actin cytoskeleton and collagen fibres orientation revealed relatively similar patterns for identical conditions.

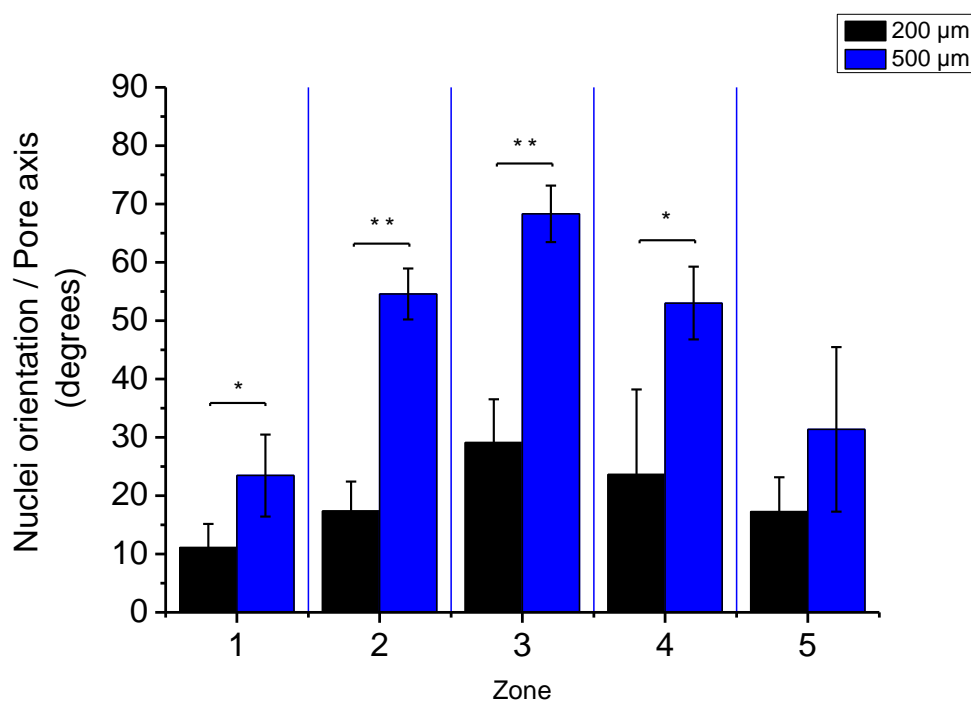


Fig. 4-12 Measurements of average nuclei orientation in the 5 zones across the pore width in (black) 200  $\mu\text{m}$  pore and (blue) 500  $\mu\text{m}$  pore (n=6).

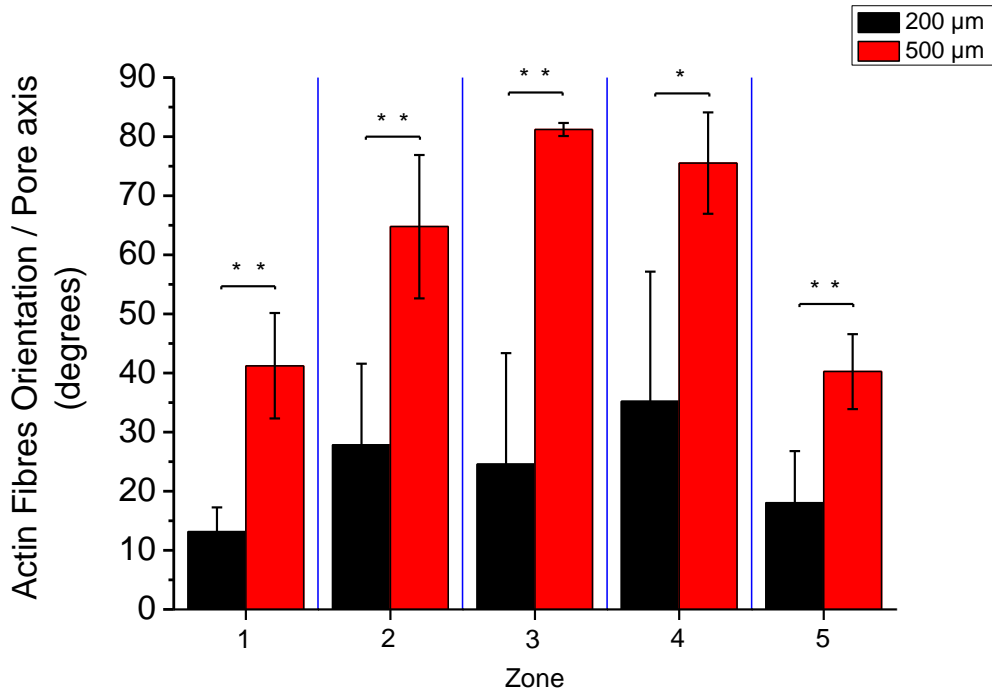


Fig. 4-13 Measurements of average actin fibre orientation in the 5 zones across the pore width in (a) 200 μm pore and (b) 500 μm pore (n=5).

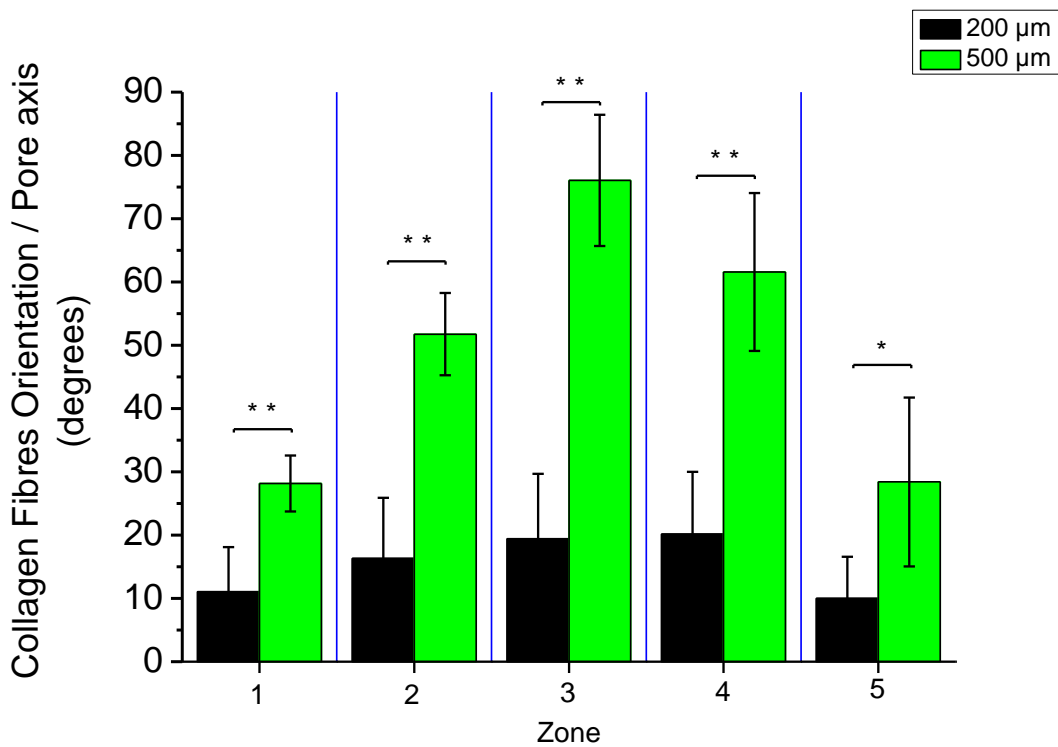


Fig. 4-14 Measurements of average collagen fibre orientation in the 5 zones across the pore width in (a) 200 μm pore and (b) 500 μm pore (n=5)

#### 4.2.8 Cell division orientation

Cells producing DNA were stained with EdU, showing that cell cycle is in process, and several cells are dividing (Fig. 4-15). On the micrograph, it appeared that generally cell division occurs more aligned with the longitudinal in the 200  $\mu\text{m}$  pore. This is supported by the detailed quantification provided in Fig. 4-16.

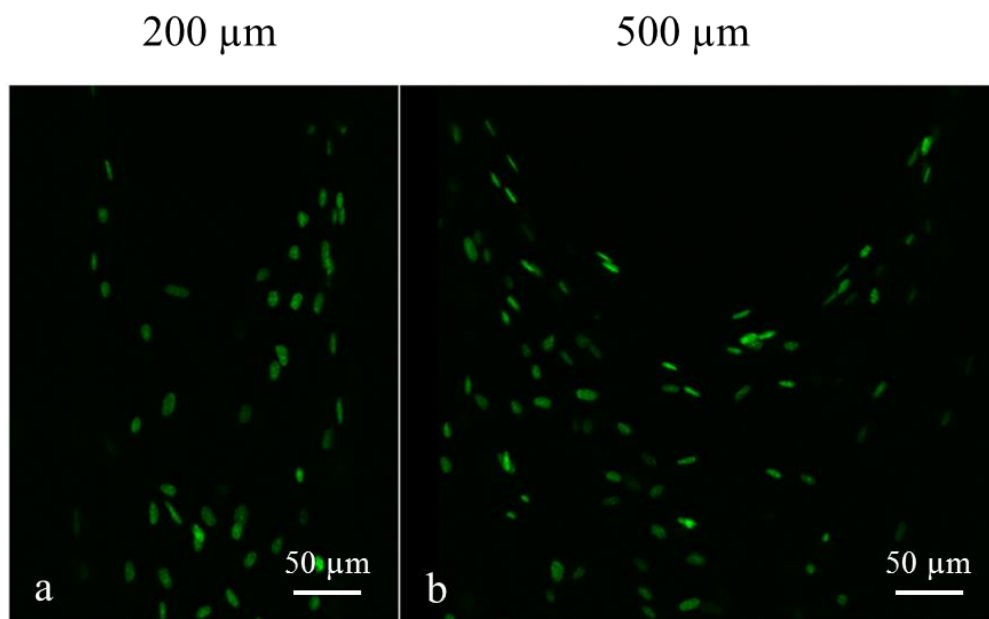


Fig. 4-15 EdU labelled cells reflecting DNA production in 200  $\mu\text{m}$  pore (a) and 500  $\mu\text{m}$  pore (b)

The orientation of dividing cells displayed striking differences between the two pore widths (Fig. 4-16). For the 200  $\mu\text{m}$  pore more than 60% of the dividing cells have an orientation relative to the longitudinal pore axis lower than  $18^\circ$ , then around 20% of the cells have an orientation angle between  $18^\circ$  and  $36^\circ$  and less than 20% have an angle higher than  $36^\circ$ . On the other hand, for the 500  $\mu\text{m}$  pore, the pattern is different from that for 200  $\mu\text{m}$ . More than 60% of the dividing cells have an orientation angle higher than  $36^\circ$ , around 25% of the cells have an orientation angle between  $18^\circ$  and  $36^\circ$  and only 15% of the cells have an orientation lower than  $18^\circ$ .

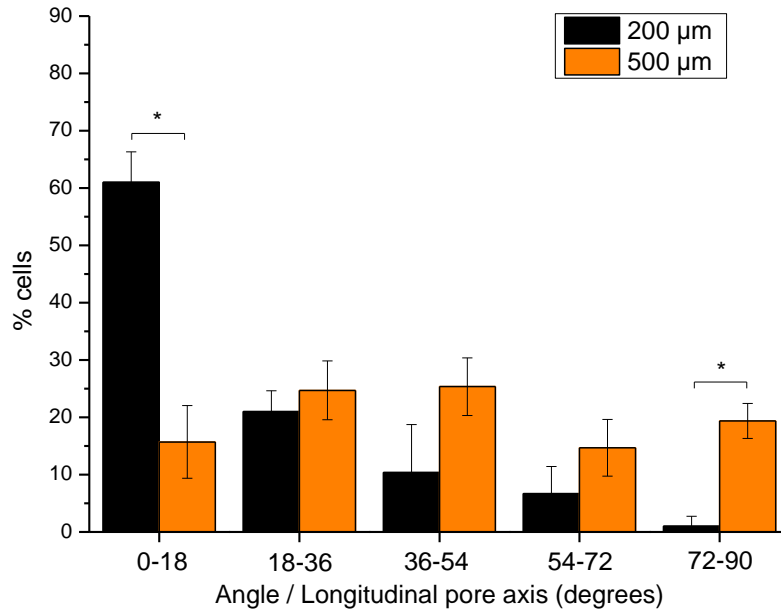


Fig. 4-16 Dividing cells orientation distribution in 200 μm pore and 500 μm pore (n=3 per condition).

The comparison of the orientation of the dividing cells between the two pore widths in each zone revealed a similar pattern to the cell orientation results (Fig. 4-17, Fig. 4-18). The alignment was systematically higher in the 200 μm pore. Therefore, this showed that overall, cell division occurs with a higher alignment relative to the longitudinal axis in the 200 μm pore compared to the 500 μm pore. Similarly to cells, actin and collagen, the highest differences between two pore widths were observed in the central zone (zone 3). Cell division was oriented almost perpendicular to the pore axis in the 500 μm pore. Cell division had an orientation of  $59 \pm 8^\circ$  relative to the pore axis, whereas in the 200 μm pore the corresponding value was  $25 \pm 19^\circ$ .

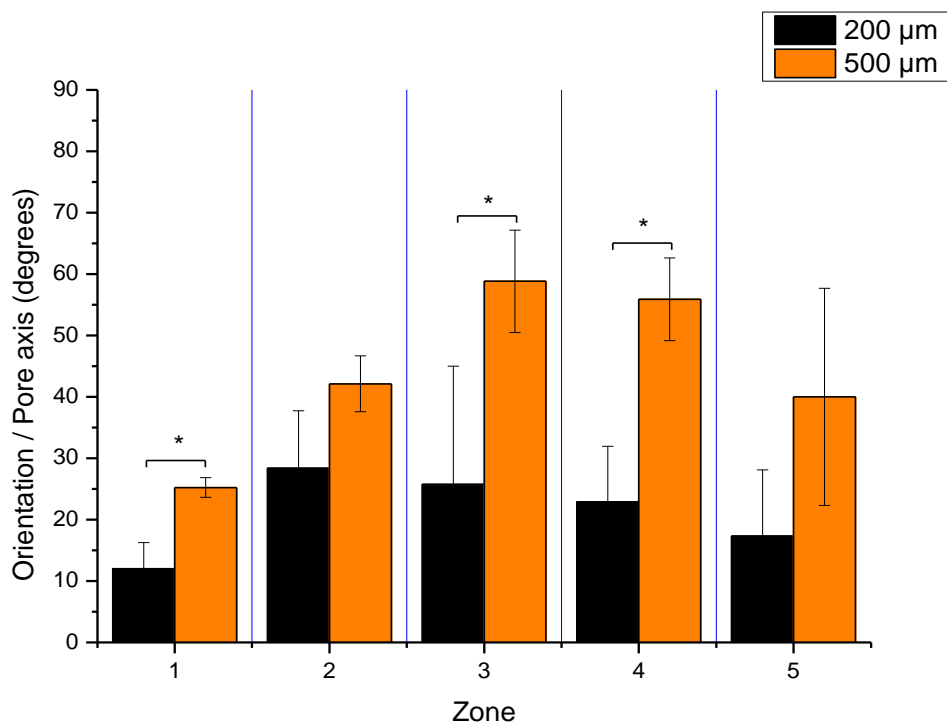


Fig. 4-17 Measurements of Nuclei orientation of dividing cells after 30 days in the 5 zones across the pore width in (black) 200 μm pore and (orange) 500 μm pore (n=3) .

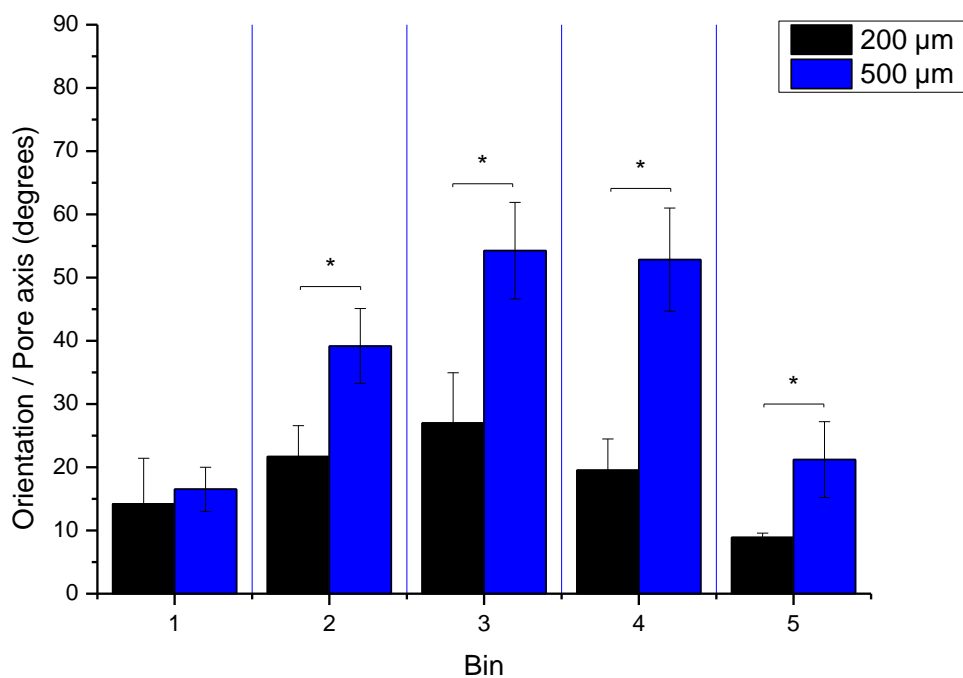


Fig. 4-18 Measurements of cell nuclei orientation after 30 days in the 5 zones across the pore width in (black) 200 μm pore and (blue) 500 μm pore (n=3) .

### 4.2.9 Osteogenic Lineage Commitment

Samples stained positively for ALP expression confirming osteogenic commitment after 28 days (Fig. 4-19). Differentiation of the tissue could be observed in both 200 and 500  $\mu\text{m}$  pores. Therefore, pore width did not influence osteogenic tissue formation potential. It was seen that the staining gradually became stronger when moving away from the front towards the end of the pore

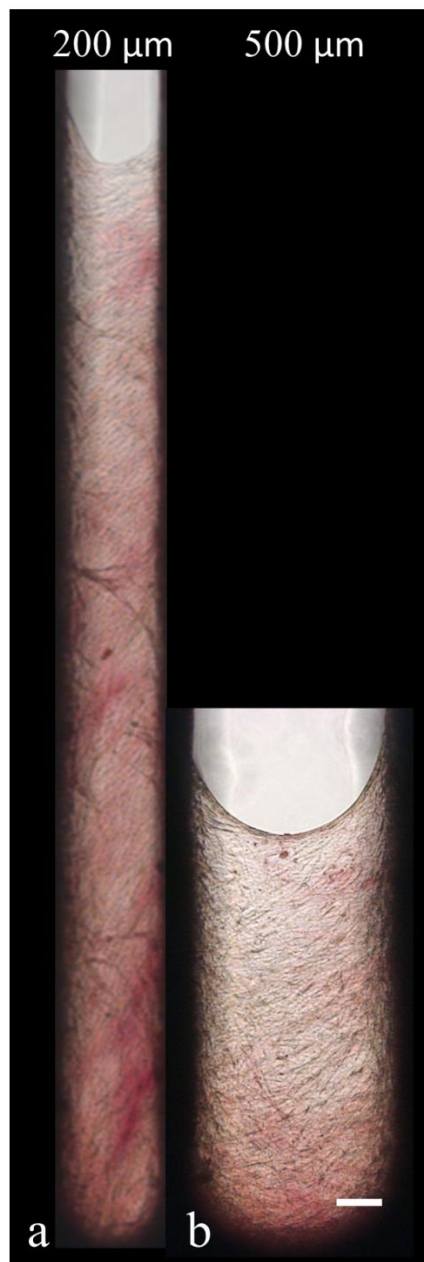


Fig. 4-19 Alkaline Phosphatase (ALP) staining in 200  $\mu\text{m}$  (a) and 500  $\mu\text{m}$  (b) pores at day 28. Pink colour shows positive staining for ALP reflecting osteogenic lineage commitment

## 4.3 Discussion

Pore architecture has been known to affect the capacity of tissue to fill a 3D space as well its organisation. Therefore, the research was focused on determining whether a specific tissue conformation, induced by particular pore architecture, is more favourable than others for tissue formation, and whether this could provide crucial guidance for scaffold design. Thus, in this study it was investigated how precisely defined structures could modulate tissue organisation and whether this could impact on neo-tissue formation. We showed that pore geometry influenced tissue orientation at the subcellular scale as well as cellular level. These differences in tissue orientation were associated with tissue formation capacity potentially due to cell division orientation. Tissue more oriented in the direction of ingrowth corresponded to greater pore colonization. Additionally, the neo-tissue formed produced a dense collagenous matrix and showed commitment to the osteogenic lineage in both pore geometries.

### 4.3.1 Tissue quantification

The results found here are in line with our previous findings (Chapter 3) showing that faster ingrowth occurred in narrower pores (Knychala et al. 2013). Furthermore, differences in tissue growth were maintained for 14 and up to 30 days. Additionally, the number of cells found was 3 times higher in 200  $\mu\text{m}$  pores compared to the number of cells found in the 500  $\mu\text{m}$  pores after 30 days. Therefore, this result confirms the projected tissue area suggested that a higher amount of tissue is formed within the narrower pore. Tissue colonized the narrow pore  $\sim 3.6$  times faster. This would imply that for the same pore space to fill, 200  $\mu\text{m}$  pores allow more rapid colonization than 500  $\mu\text{m}$  pores. For example, 5 pores of 200  $\mu\text{m}$  which represent the same pore space as 2 pores of 500  $\mu\text{m}$  will be filled  $\sim 3.6$  times quicker. However, for practical scaffold design, increasing the number of small pore channels may imply a lower overall porosity, depending on wall thickness, which has to be balanced against the significantly faster invasion rate demonstrated here. Interestingly, the estimated tissue volume was found to be equivalent in both pore sizes, but PTA and more importantly, the number of cells is higher for the narrow pore. However, the volume estimation result needs to be taken in account moderately. Indeed, this measurement is only based on the thickness of a stack acquired by imaging cell nuclei. Furthermore, the measurement

does not account for the 3D shape observed in Fig. 3-13. Additionally, accurate tissue volume measurements should take in account the amount of extracellular matrix which has not been investigated in this study. Therefore, the method is not fully accurate and only provides an interesting approximation to be confirmed in future studies.

### **4.3.2 Tissue Constraints & Actin Patterns**

In our configuration, the tissue consists of cells directly attached to the pore walls and neighbouring cells confined in the tissue among others cells. All cells are connected together via cell-cell adhesions and their actin cytoskeleton (Fig. 4-10c, d). By exerting tension, cells generate a tensile stress which is propagated throughout the whole tissue and maintains the tissue constrained between the pore walls. Thus, the actin cytoskeleton configuration is dependent on the geometric constraints provided by the pore walls and it has been found previously that cells rearrange themselves in order to experience maximum effective stiffness (Bischofs et al. 2003). At the front of migration this is reflected by the formation of a strong band of aligned actin along the free surface, of which curvature changes depending on pore width as previously shown (Knychala et al. 2013). Once established, the shape of the curved front could then serve as an initial template that guides further spreading of cells on the surface, which then straighten out by contraction, as in the proposed “chord” model for tissue growth on curved surfaces (Bidan et al. 2012). Additionally, this curved front also guides tissue rearrangement behind the front as our results suggested. Indeed, curvature is still distinguishable as the central zones 2, 3 and 4 (zones not contacting the walls) are less aligned with the pore axis compared to zone 1 and 5 (zones contacting the walls) in both 200 and 500  $\mu\text{m}$  (Fig. 4-13). Furthermore, local actin orientation is the net result of the tension cells exert on the wall and the resistance provided by neighbouring cells pulling back. This is how the local changes observed in the orientation of the different zones arise. However, looking at the prevalent actin organisation throughout the whole tissue, tissue is constrained predominantly parallel the to the pore axis in the 200  $\mu\text{m}$  pore, whereas in 500  $\mu\text{m}$  the constraintment is close to perpendicular. Several studies showed that constraints are important in determining tissue organisation, and that this organisation is dependent on the actin cytoskeleton. For example, the direction of constraintment reflected by the actin network has been shown to determine cell and collagen orientation (Kanda et al. 1994; Eastwood et al. 1998; Seliktar et al. 2000; Henshaw et al. 2006;

Boerboom et al. 2008; Rubbens et al. 2009; Gauvin et al. 2011). This is confirmed by our results, which show that actin cytoskeleton, cell nuclei and collagen fibres all displayed a similar pattern in terms of orientation.

### **4.3.3 Actin organisation and tension on cell number**

During tissue development, cell generated forces mediated by the actin cytoskeleton play a critical role. Cell number, size and shape are modulated by intracellular forces. The estimation of tissue volume, the numbers of cells, the percentage of dividing cells and the distinct actin organisations between the two pore widths strongly suggest that actin remodelling occurs differently. Upon new cell apparition within the tissue, the tensile equilibrium established by neighbouring cells is modified (Fig. 4-20). Furthermore, cells undergo different net stresses according to pore size as previously discussed in paragraph 3.3.4. Therefore, actin remodelling during cell division should occur differently depending on pore widths. Consequently, the differences in the amount of cells found between two pore widths could be linked with actin organisation and tensile state affecting cell division. The entrance in mitosis (Phase M), the ultimate phase leading to the appearance of a new cell is partly controlled by mechanical intracellular clues. Indeed, actin remodelling modulates signalling pathways regulating gene expression of proteins triggering mitosis (Hardie et al. 1995; Mammoto et al. 2012). Moreover, actin remodelling might occur differently during mitosis in 200  $\mu\text{m}$  or 500  $\mu\text{m}$  pore as suggested by the results. Therefore, higher amount of cells in the narrow pores could emanate from differences in actin remodelling between the two pore widths. Furthermore, higher percentage of EdU positive cells in 500  $\mu\text{m}$  pores and higher cell number in 200  $\mu\text{m}$  could be interpreted as contradictory. However, the results presented here consist of EdU assays. A positive staining only reflects the fact that DNA synthesis occurs in cells i.e. entrance the division cycle (Fig. 4-15), more precisely in the S phase (Fig. 4-21). Therefore, the progression of cells from S phase to M phase could vary due to different actin remodelling i.e. delayed in 500  $\mu\text{m}$  pores in the case presented here. This is supported by findings from Nelson et al., which reported that cells located in zones under high tension undergo higher proliferation (Nelson et al. 2005).

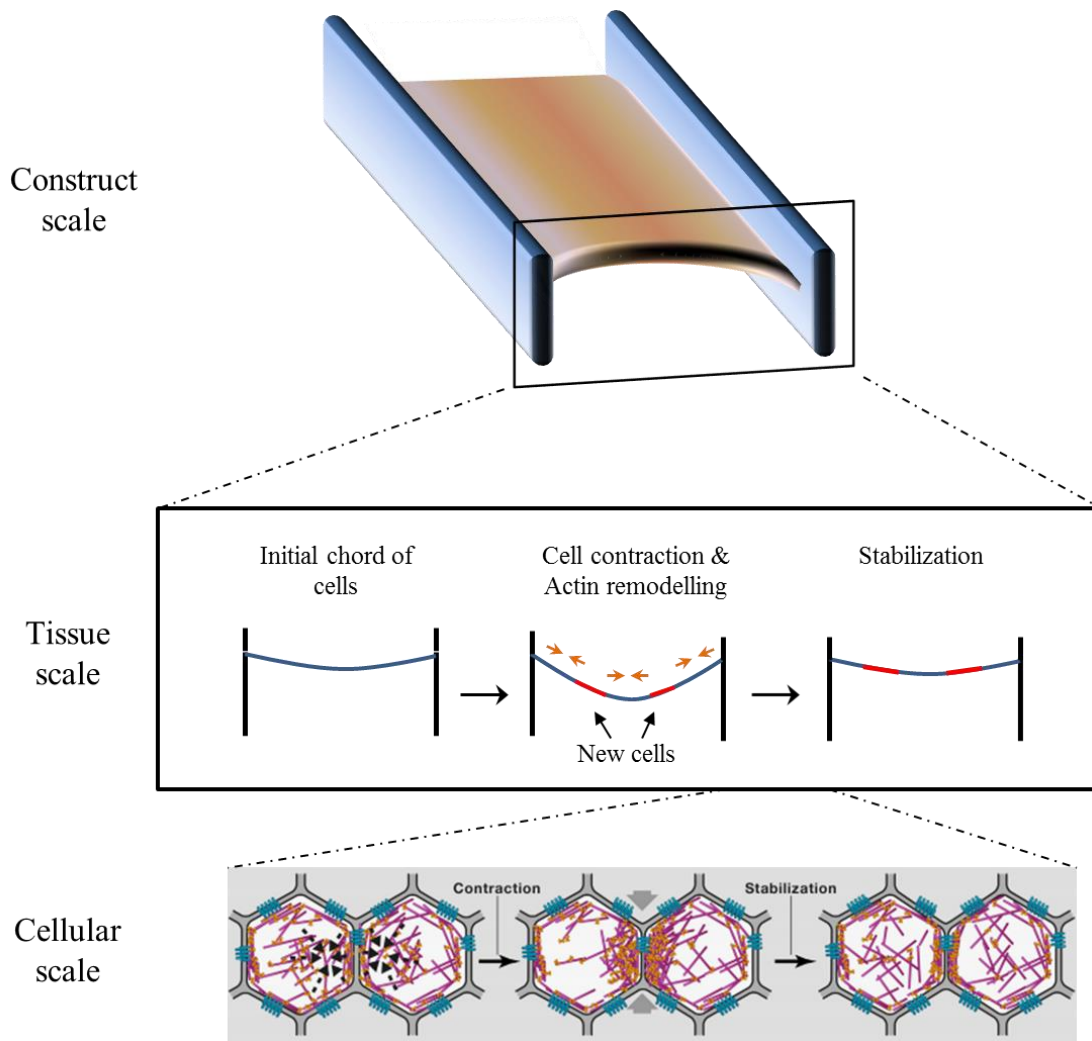


Fig. 4-20 Actin remodelling during tissue formation. Tissue scale: Illustration of tension changes and mechanical equilibrium recovery via actin remodelling during new cell apparition (Red parts). Cellular Scale: Illustration of actin remodelling around cellular boundaries during cell contraction. Subsequently, actin distribution is evened after stabilization. Drawing from (Heisenberg et al. 2013)

The volume estimation provides further indications regarding differences in tensile state in the tissue depending on pore width. The results would imply that tissue is denser in the 200  $\mu\text{m}$  pore. Therefore, to occupy similar volume with a lower amount of cells, cells could presumably be more stretched in the 500  $\mu\text{m}$ . Therefore, this would support the fact that tissue undergoes a different tensile state according to pore width. During cell cycle, cell volume increases constantly (Mitchison 2003). Therefore, the volume of the tissue is affected by the amount of cells having entered the cell cycle. Thus, as more cells have entered in the division cycle in 500  $\mu\text{m}$ , a higher volume would be occupied with same amount of cells in 500  $\mu\text{m}$  pores compared to the 200  $\mu\text{m}$  pore. This could explain a higher volume in 500  $\mu\text{m}$  pore compared to the number of cells.

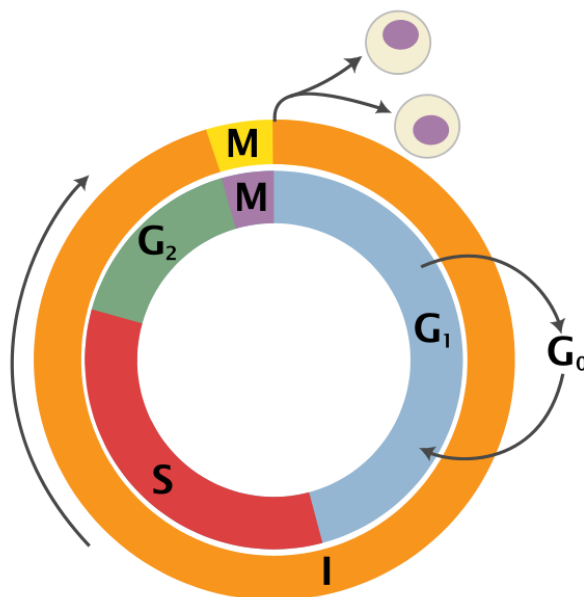


Fig. 4-21 Cell division cycle phases. G<sub>1</sub> phase ensures that DNA synthesis can take place. During S Phase, DNA replication occurs. G<sub>2</sub> phase ensures that mitosis can take place. During phase M, two daughter cells appear

#### 4.3.4 Extracellular Matrix Orientation

Guiding matrix anisotropy is suggested to strongly depend on the ability to control cytoskeletal and cellular orientation. In our results, the two different structures readily modulated cell and actin stress-fibres orientation which were seen to match Collagen I fibre orientation in both conditions (Fig. 4-10c-f, Fig. 4-13, Fig. 4-14). In a study using MC3T3-E1 osteoblasts, cells seeded on 2D micro-grooved surfaces oriented themselves along the directions of the micro-grooves within hours after seeding. Subsequently, the Collagen I matrix produced by the cells was highly oriented in the direction of the micro-grooves (Wang et al. 2003). Furthermore, previous results showed that collagen is aligned parallel to the actin stress-fibres of cells (Engelmayr et al. 2006; Lakshman et al. 2007). Therefore, Collagen I fibre orientation is suggested to be the consequence of cell and actin stress orientation. This is confirmed by the fact that destruction of the stress fibres results in partial re-organisation of the collagen (Sawhney et al. 2002). Thus, these findings suggest that initial collagen organisation is strongly dependent on actin orientation. In our case, matrix production is a subsequent step to cell settlement, thus actin orientation serves as an initial template for subsequent matrix formation and orientation. Furthermore, matrix deposition has been shown to be oriented via cell traction which translates and aligns individual collagen fibres (Harris et al. 1981; Stopak

et al. 1982) through a process involving lamellipodia extension and retraction (Meshel et al. 2005). However, also contact guidance has been shown to guide cell orientation and to be dominant over external mechanical stimulation (Foolen et al. 2012). Therefore, initially, actin-cell orientation might dictate matrix orientation but once tissue is formed, contact guidance provided by established matrix might be the ruling cue for subsequent tissue rearrangement. Nonetheless, the most important implication of these results is that matrix anisotropy can be controlled by modulating pore geometry.

### **4.3.5 Cell Division Orientation**

Actin fibres, which reflect tissue orientation, are hypothesised to influence tissue expansion by guiding the orientation of cell division. During mitosis, cells separate in two distinct daughter cells of which positions are determined by the cell division axis. The cell division axis is determined by spindle orientation during mitosis. Cell shape anisotropy and polarity have been shown to be involved in spindle orientation. It has been shown that the spindle orients along the long cell axis in epithelial NRK cells. Therefore, a mechanism by which spindle orientation was driven solely by the anisotropy of cell geometry has been proposed (O'Connell et al. 2000). Nevertheless, not only cell shape governs spindle orientation, it is also influenced by some cortical cues. Membrane associated filamentous actin is necessary to guide spindle orientation (Théry et al. 2005) and promote its lengthening (Woolner et al. 2008) through interactions with astral microtubules (Wühr et al. 2008) leading to chromosomes separation during anaphase. Astral microtubules are directly attached to the centrosome which are attached themselves to the other microtubules (Polar and Kinetochore microtubules) responsible for chromosome segregation (Sandquist et al. 2011). Therefore, actin fibres pulling on the astral microtubules indirectly induce spindle orientation and separation hence on a larger scale guide cell division orientation. Furthermore, this is supported by the fact that actin stress fibres orientation has been shown to be the main parameter determining mitosis orientation. Although actin fibres orientation itself can be modulated by exogenous factors such as drugs or mechanical stretching, mitosis orientation is always directly correlated with stress fibres orientation when their integrity is preserved (Zhao et al. 2011). Thus, cell division orientation is directed by actin orientation. In our configuration, cells and more importantly actin orientation, are nearly parallel in a 200  $\mu\text{m}$  pore, therefore, cell division occurs

predominantly more aligned with the pore axis than in a 500  $\mu\text{m}$  pore (Fig. 4-16 & Fig. 4-17). This is also clearly supported by our observation of cell division during time lapse microscopy (Fig. 4-22).

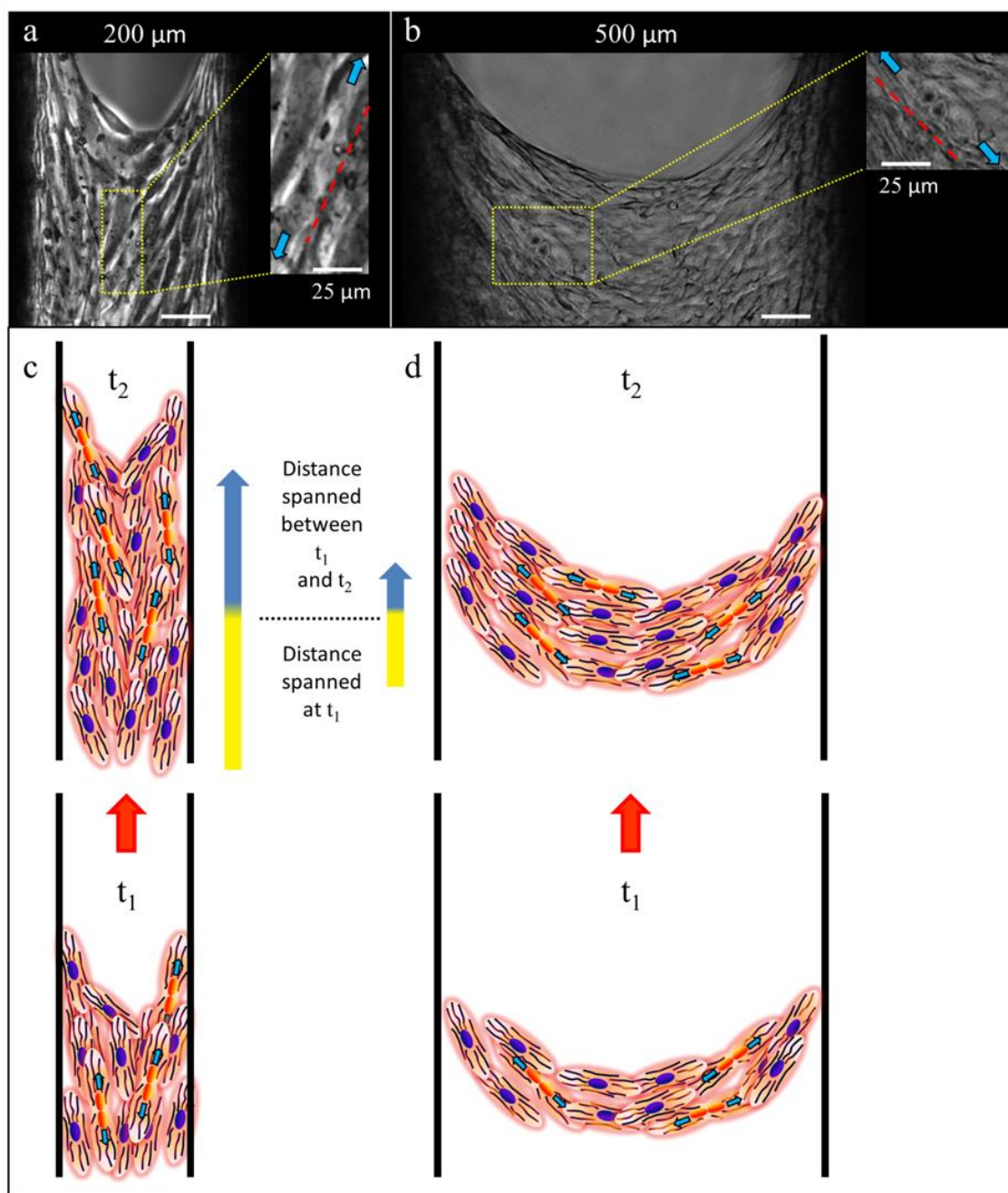


Fig. 4-22 (a, b) Cell division within the zone investigated for tissue orientation. Time Lapse results showing cells dividing along longitudinal axis in 200  $\mu\text{m}$  pore (a) and 500  $\mu\text{m}$  pore (b). Schematic for proposed mechanism of the contribution of the orientation of cell division in tissue growth in 200  $\mu\text{m}$  pore (c) and 500  $\mu\text{m}$  pore (d). Cell division orientation in the same direction as the one imposed by the confinement of the structure enhances tissue ingrowth (Scale bar = 50  $\mu\text{m}$  unless indicated otherwise)

The pore confinement imposes a direction of growth along its longitudinal axis, independent of tissue arrangement. However, when cell division is directed along the long pore via actin orientation, tissue elongation is facilitated and growth is enhanced in a narrow pore (Fig. 4-22c, d). Similarly, *in vivo*, organ shape in *Drosophila* model is regulated by specifically oriented cell division i.e., organ elongation occurs in the direction in which cell division is oriented (Baena-Lopez et al. 2005). Furthermore, the situation we are describing here can be closely related to a wound healing process, in which it has already been seen that actin fibres achieve an orientation nearly parallel to the long axis of the wound (Petroll et al. 1993). Therefore, cell division orientation which is the downstream results of actin orientation, influences the capacity of formation of the tissue.

### 4.4 Summary

In this study we showed that solely by modulating pore geometry, it is possible to control tissue organisation, specifically with respect to actin cytoskeleton, collagen matrix and cell orientation, therefore, cell orientation division. The results strongly suggested that actin is the primary element guiding tissue organisation i.e. cellular orientation and matrix anisotropy. Furthermore, it was shown that tissue organisation appeared to have a major impact on its capacity for growth. Indeed, a narrow structure permits the tissue to orient itself along the direction of growth, a more favourable configuration facilitating tissue formation. This was supported by the fact that the tissue regenerated within the narrower pore contained an amount of cells 3 times superior to that in 500  $\mu\text{m}$  pores. Furthermore, guided by pore geometry, the actin cytoskeleton appeared to be governing the orientation of cell division. Oriented cell division could contribute to enhanced tissue formation when aligned with the overall direction of growth. Therefore, by guiding actin, which guides cell division and matrix anisotropy, we showed that tissue organisation could strongly impact on its ability to expand and that this can be controlled solely by modulating pore geometry.

## **Chapter 5**

### **Tissue Differentiation**

In this chapter, the aim was to characterise tissue differentiation within structures previously used. Although most of the findings of this thesis concern the initial formation of cellular neo-tissues, the ultimate aim is to regenerate bone-like tissue. In the previous chapter the presence of Collagen I, an early marker of osteogenic lineage commitment, was already shown. However, collagen I is expressed in a variety of tissues hence is not specific enough to conclude for bone like tissue formation. Therefore, in this chapter the presence of intermediate and late osteogenic markers was investigated in order to assess the stage of differentiation. Comparison between the two conditions i.e. pore size, was done using different semi-quantitative methods.

#### **5.1 Material and Methods**

##### **5.1.1 Cell isolation, Scaffold fabrication & Tissue growth kinetics**

The same methods were used as in Chapter 4 for cell isolation, scaffold fabrication and tissue culture in the constructs. The results presented in this study were obtained from experiments carried out in  $\alpha$ -MEM media supplemented with 10% FBS on patient F63<sub>1</sub>.

##### **5.1.2 Alkaline Phosphatase Assay**

Tissue was rinsed twice with PBS and fixed for 15 min in 95 % ethanol. Subsequently, the fixed tissue was incubated in the dark at 37 °C for 45 min in reaction solution. The solution consists of Naphtol AS-MX Phosphate Alkaline Solution (Sigma) diluted in dH<sub>2</sub>O (4 %) in which Fast Violet Salt (Sigma) was added (0.002 %) just prior incubation with the samples. The reaction was stopped by rinsing samples with dH<sub>2</sub>O

### 5.1.3 Laser confocal Microscopy

Prior to staining, all samples were washed 3 times in PBS and fixed in paraformaldehyde-PBS 4 % (w/v) for 20 min at room temperature. Next, samples were washed 3 times in PBS, incubated 20 min in PBS-Triton 0.5 % (v/v) for permeabilization and then incubated in 1 % BSA (Sigma)-PBS (w/v) for 30 min to block unspecific binding, followed by labelling for the different tissue components. For Osteopontin staining, samples were rinsed 3 times in PBS, incubated 30 min in PBS-BSA 1 % and incubated with a primary antibody anti-Osteopontin raised in rabbit (Abcam, 1/200) overnight at 4 °C. Secondly, samples were rinsed 3 times in PBS and 3 times in PBS-BSA 1 % and incubated overnight at 4 °C with secondary antibody Alexa 564 anti-rabbit. Negative control was done following the same procedure with the primary antibody (Anti-Osteopontin) omitted. Cell Nuclei were labelled using Hoescht stain for 30 min (1/1000 dilution (v/v) in PBS, Molecular probes, Invitrogen). Eventually, after labelling samples were rinsed 3 times in PBS and imaged either immediately or within 1-3 days. Samples were imaged using a laser confocal microscope (Leica TCS SP2, Germany). Z-axis image acquisition was performed using a 20× water-dipping objective (Leica, HCX APO L 20×/0.50 W U-V-I). Individual images planes were acquired in bi-directional scanning mode at 1 μm z-axis intervals with a resolution of 512×512.

### 5.1.4 Semi quantitative assessment of ALP intermediate bone marker expression

Images acquired for samples stained for ALP expression assay were used to assess ALP staining intensity as well as expression over time. In brief, each individual colour image consisting of the three RGB (red, green, blue) channels was converted into three grey-scale images ( $I_R$ ,  $I_G$ ,  $I_B$ ) which contained one single channel of the original image (Fig. 5-1). ALP images consisted of higher red channel values, resulting in a brighter  $I_R$  image. However, the colour white consists of high values for each of the three RGB channels, therefore  $I_R$  alone cannot be used to identify visually red areas. To eliminate any white or grey areas and enhance colour specificity, i.e. to extract desired red areas,  $I_{RS} = I_R - I_G$  and  $I_{RS} = I_R - I_B$  were used. Either the  $I_G$  or  $I_B$  channel was subtracted from the  $I_R$  channel, the result of which was stored in the red staining intensity  $I_{RS}$ . The

resulting image therefore contained only the grey-scale pixels (value = 0-255) representing the desired red channel (Fig. 5-1b), wherein intense red areas were represented by white pixels, light red areas were represented by grey pixels and the rest of the image were represented by black pixels.

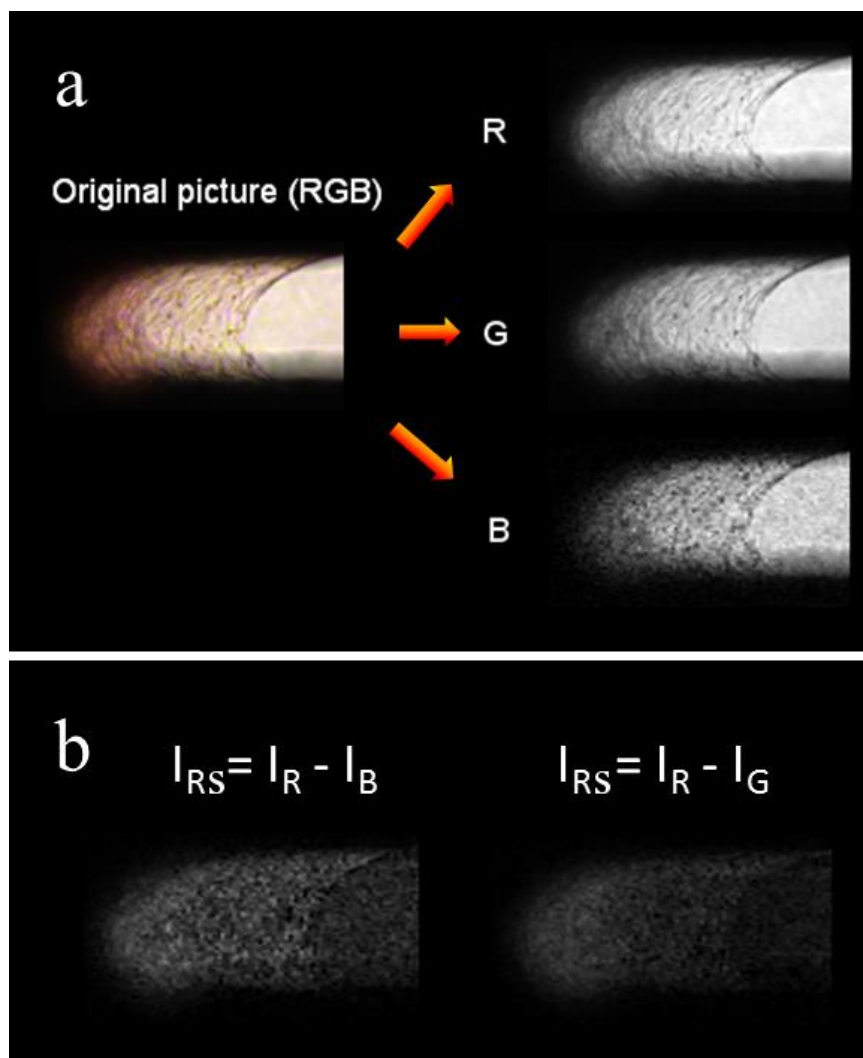


Fig. 5-1 An example of image reconstruction using ImageJ. (a) The original picture (RGB) is split in three colours: Red (R), Green (G) and Blue (B). (b) Isolation of the colour of interest, different ALP red stain intensity measures  $I_{RS}$ , as represented by grey-scale pixels, Red - Blue (left) and Red - Green (right)

Subsequently, the pictures were cropped to obtain only the region of interest i.e. the neo- tissue formed in the pore. In order to obtain stain intensity as a function of location along the longitudinal pore axis, the pixel value of each vertical line across the pore width was averaged as described in Fig. 5-2.

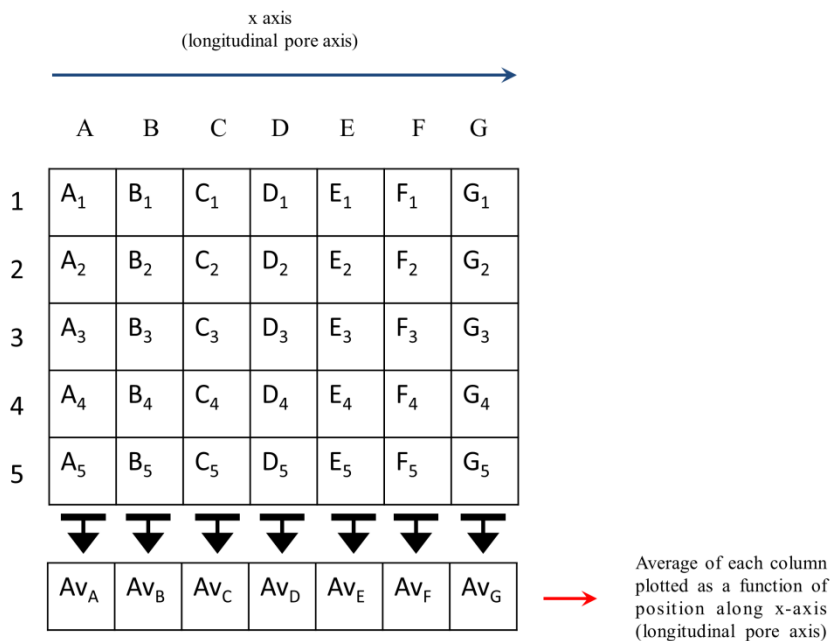


Fig. 5-2 Schematic explaining how the grey scale values representing red intensity along longitudinal axis of pore are obtained. Subsequently, these values were plotted as a function of their location on the longitudinal axis in section 5.2.3.1.

### 5.1.5 Semi quantitative assessment of Osteopontin late bone marker expression

For this purpose, ImageJ software was used (Fig. 5-3). Starting from the original picture (1), the blue colour was removed using the colour balance function (2). Next the picture is converted to 8 bits (3) in order to proceed to the thresholding. Finally, a mask is created (4) and the percentage of the total area occupied by the mask is calculated.

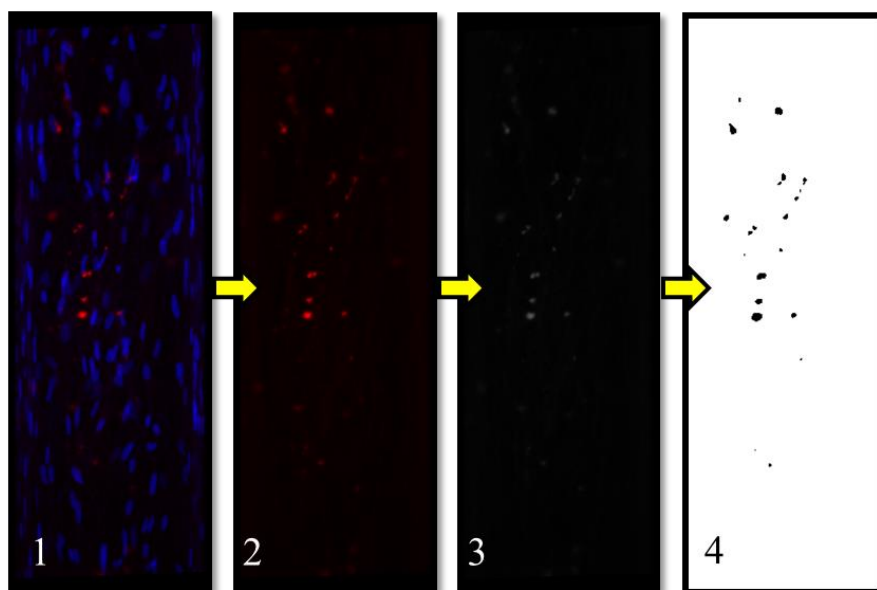


Fig. 5-3 Osteopontin (red) area analysis using thresholding & masking method

## 5.2 Results

### 5.2.1 Kinetics

The results presented in this part of the results show the tissue invasion kinetics in the two different pore width over 30 days for the 3 individual replicates of F63<sub>1</sub>.

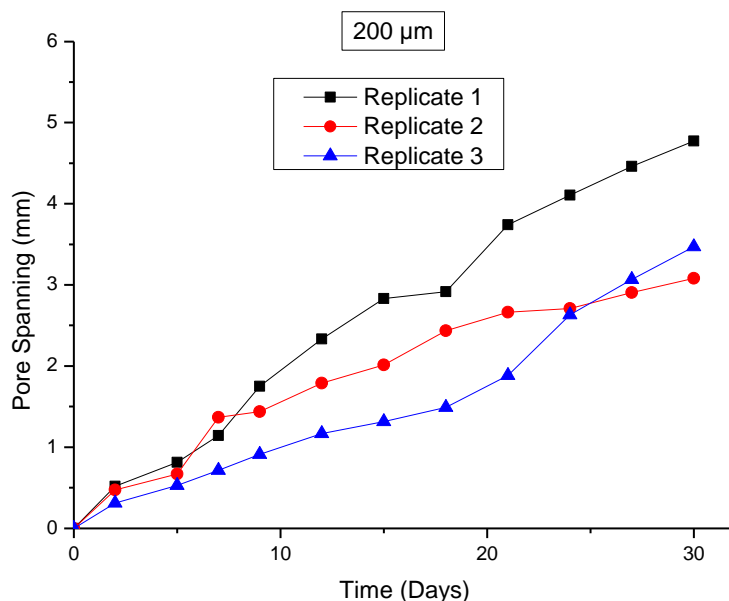


Fig. 5-4 Tissue growth kinetics monitored over 30 days on 3 different replicates in a 200 µm pore for F63<sub>1</sub>

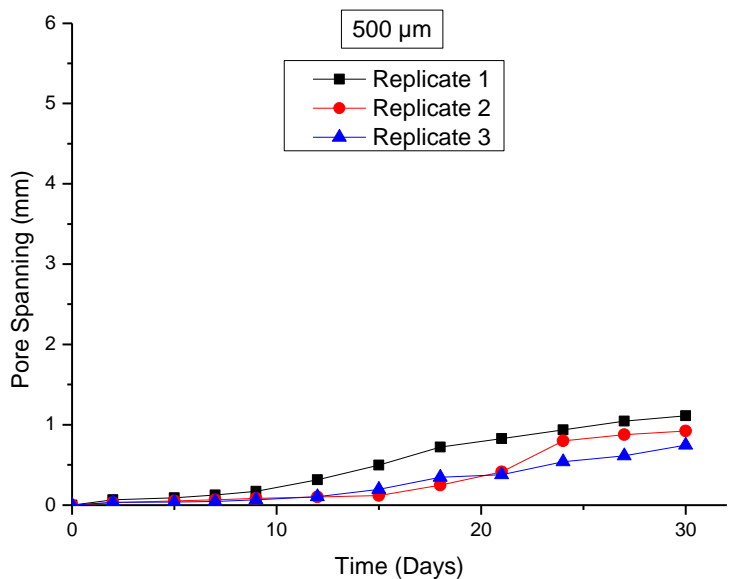


Fig. 5-5 Tissue growth kinetics monitored over 30 days on 3 different replicates in a 500 µm pore for F63<sub>1</sub>

---

## 5.2.2 Tissue Imaging – Intermediate & Late Markers Staining

The tissue was processed to verify the commitment into osteogenic lineage. Two markers were investigated, ALP and Osteopontin.

### 5.2.2.1 Alkaline Phosphatase

Positive ALP stain consists of a Pink/Red colour. ALP staining showed a positive reaction in all the samples stained in both conditions i.e. 200 & 500  $\mu\text{m}$  pores. (Fig. 5-7a, Fig. 5-8a, Fig. 5-9a, Fig. 5-10a, Fig. 5-11a, Fig. 5-11a). A general staining pattern can be observed, where the colour intensity of the stain increased progressively towards the end of the pore extremity from where the tissue started to grow. Only replicate 2, in 500  $\mu\text{m}$  pore did not display this pattern (Fig. 5-10a). This replicate displayed a uniform stain across the whole tissue formed.

### 5.2.2.2 Osteopontin

The presence of Osteopontin in the tissue was revealed by red fluorescent staining. Osteopontin was seen to be present in all the samples processed (Fig. 5-7b, Fig. 5-8b, Fig. 5-9b, Fig. 5-10b, Fig. 5-11b, Fig. 5-11b). In general, only a small amount of Osteopontin was apparent within the tissue. However, within the replicates, significant variability can be observed as it appears that some samples contain more Osteopontin than others, regardless of the pore size. Indeed, for both pore sizes, the replicates n°1 appear to have less Osteopontin (Fig. 5-6b, Fig. 5-9b). It is noticed that these replicates produced a higher amount of tissue than others. On the other hand, conversely to ALP staining, there is not any pattern noticeable concerning the Osteopontin distribution throughout the tissue. Osteopontin is present both right at the front where the tissue is “young” as well as at the back where the tissue is “aged”.

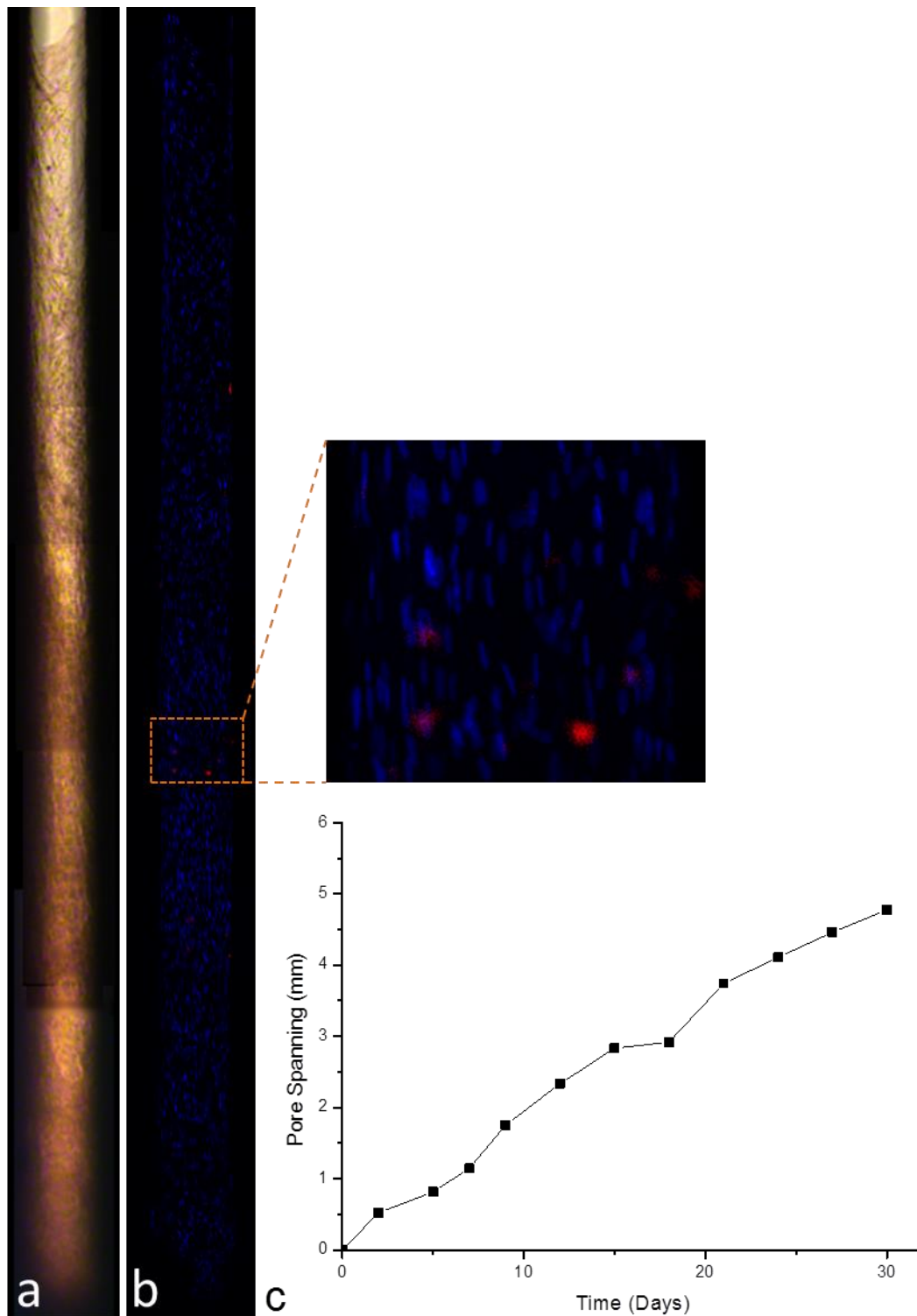


Fig. 5-6 Tissue in 200  $\mu\text{m}$  pore, replicate 1. (a) ALP staining at day 30. (b) Nuclei stained with Hoescht (blue) & Osteopontin stained with Alexa Fluor 564 at day 30. (c) Kinetics over 30 days for replicate 1

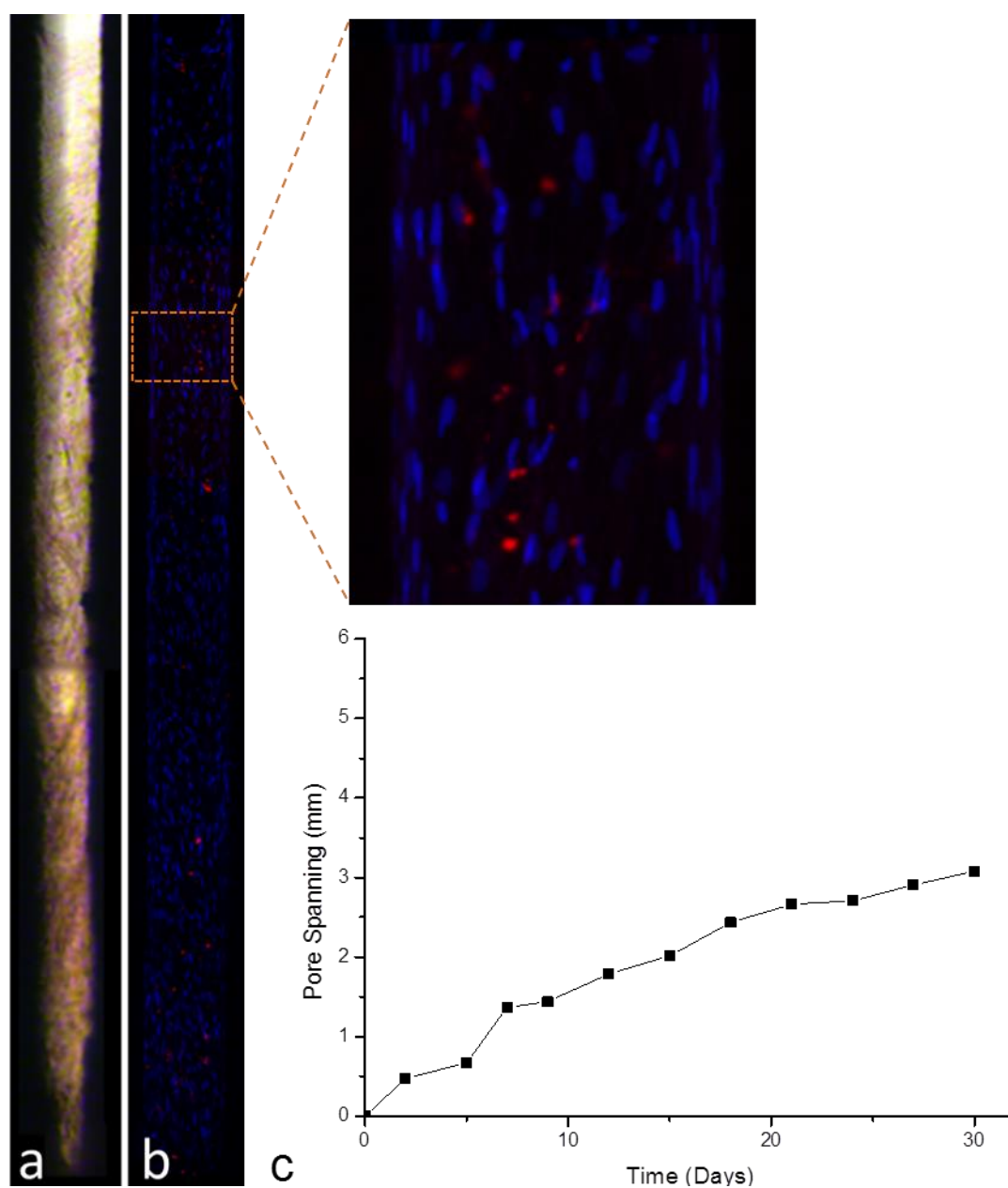


Fig. 5-7 Tissue in 200  $\mu\text{m}$  pore, replicate 2. (a) ALP staining at day 30. (b) Nuclei stained with Hoescht (blue) & Osteopontin stained with Alexa Fluor 564 at day 30. (c) Kinetics over 30 days for replicate 2

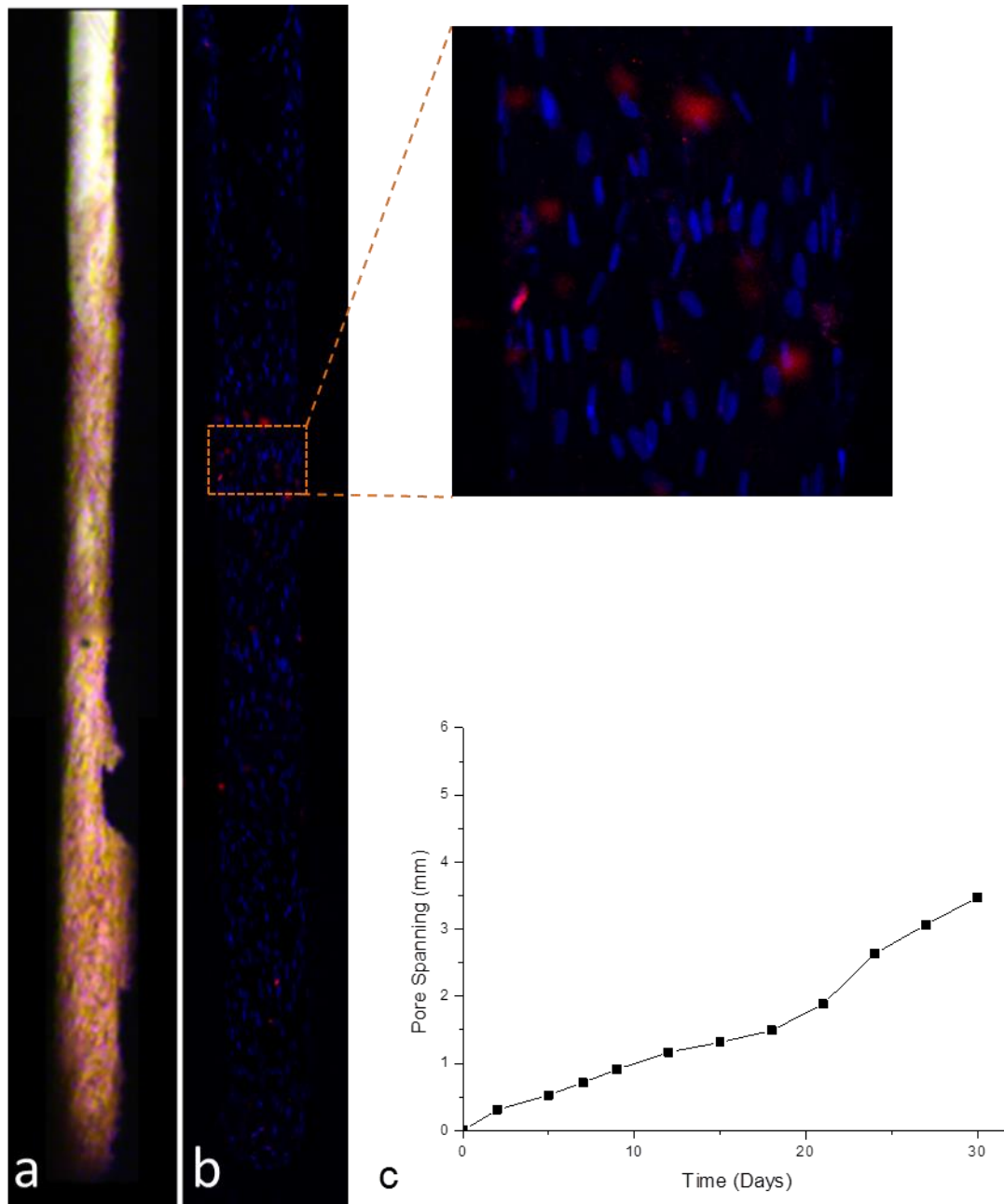


Fig. 5-8 Tissue in 200  $\mu\text{m}$  pore, replicate 3. (a) ALP staining at day 30. (b) Nuclei stained with Hoescht (blue) & Osteopontin stained with Alexa Fluor 564 at day 30. (c) Kinetics over 30 days for replicate 3

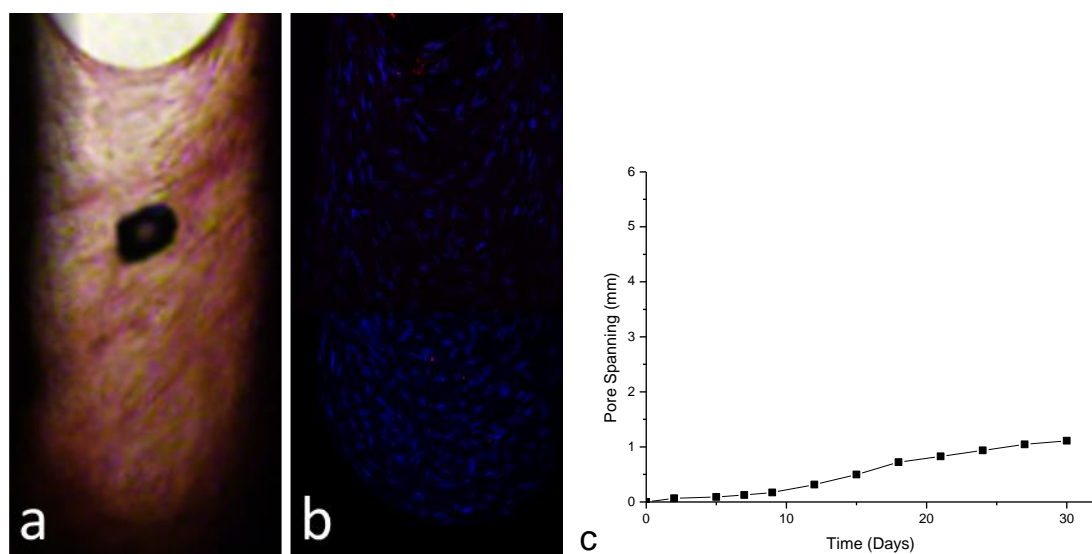


Fig. 5-9 Tissue in 500 μm pore, Replicate 1. (a) ALP staining at day 30. (b) Nuclei stained with Hoescht (blue) & Osteopontin stained with Alexa Fluor 564 at day 30. (c) Kinetics over 30 days for replicate 1

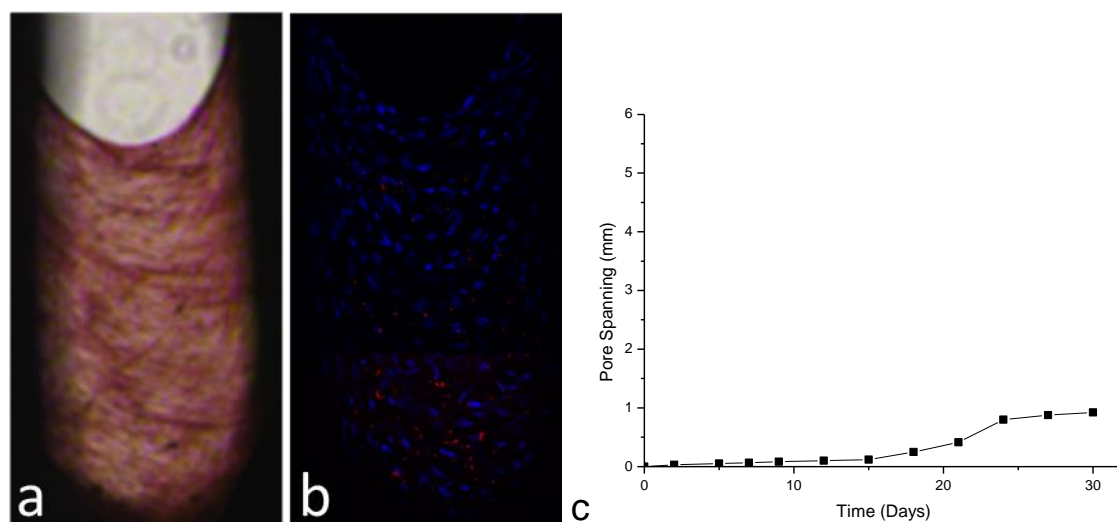


Fig. 5-10 Tissue in 500 μm pore, Replicate 2. (a) ALP staining at day 30. (b) Nuclei stained with Hoescht (blue) & Osteopontin stained with Alexa Fluor 564 at day 30. (c) Kinetics over 30 days for replicate 2

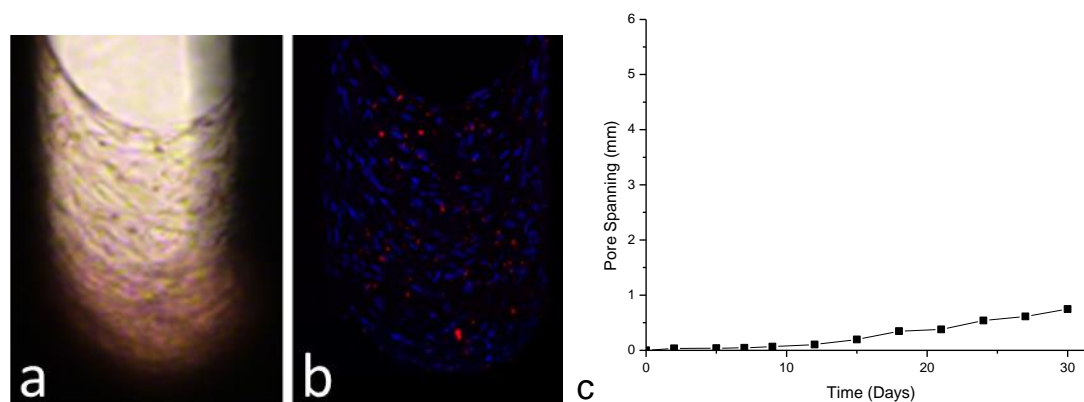


Fig. 5-11 Tissue in 500  $\mu\text{m}$  pore, replicate 3. (a) ALP staining at day 30. (b) Nuclei stained with Hoescht (blue) & Osteopontin stained with Alexa Fluor 564 at day 30. (c) Kinetics over 30 days for replicate 3

### 5.2.3 Osteogenic Lineage Commitment Assessment

In this section, ALP and Osteopontin expression were aimed to be semi-quantified in the two pore sizes conditions.

#### 5.2.3.1 Differentiation over time – ALP

The results presented in the following section aimed to assess ALP expression over time by measuring the red colour intensity across the neo-tissue formed (Fig. 5-13, Fig. 5-14, Fig. 5-15, Fig. 5-16, Fig. 5-17, Fig. 5-17). On the bottom x axis, positions along the longitudinal axis of the pore are displayed. The labels on the top x axis correspond to the day at which tissue spanned the distance corresponding to the bottom x-axis. The y-axis displays the pixel values on the grey scale (0-255) representing red staining intensity, which are assumed to correspond to ALP.

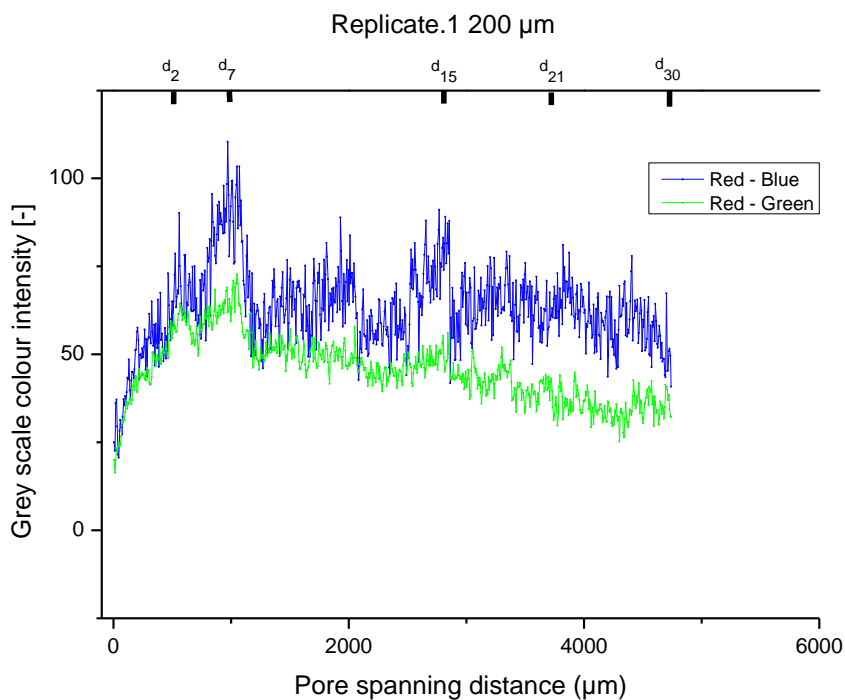


Fig. 5-12 Replicate.1, 200  $\mu\text{m}$ . Red intensity as a function of tissue location along longitudinal pore axis. Red – Blue (Blue) & Red – Green (Green) curves are plotted in order to isolate the signal on a grey scale. The labels on the top x axis correspond to the day at which tissue spanned the distance corresponding to the bottom x-axis

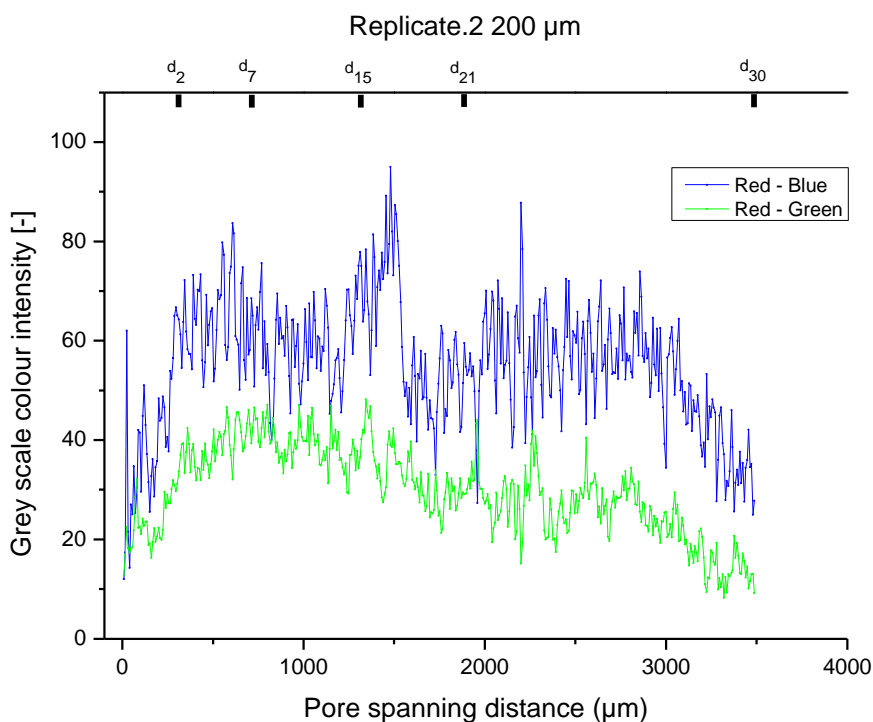


Fig. 5-13 Replicate.2, 200  $\mu\text{m}$ . Red intensity as a function of tissue location along longitudinal pore axis. Red – Blue (Blue) & Red – Green (Green) curves are plotted in order to isolate the signal on a grey scale. The labels on the top x axis correspond to the day at which tissue spanned the distance corresponding to the bottom x-axis

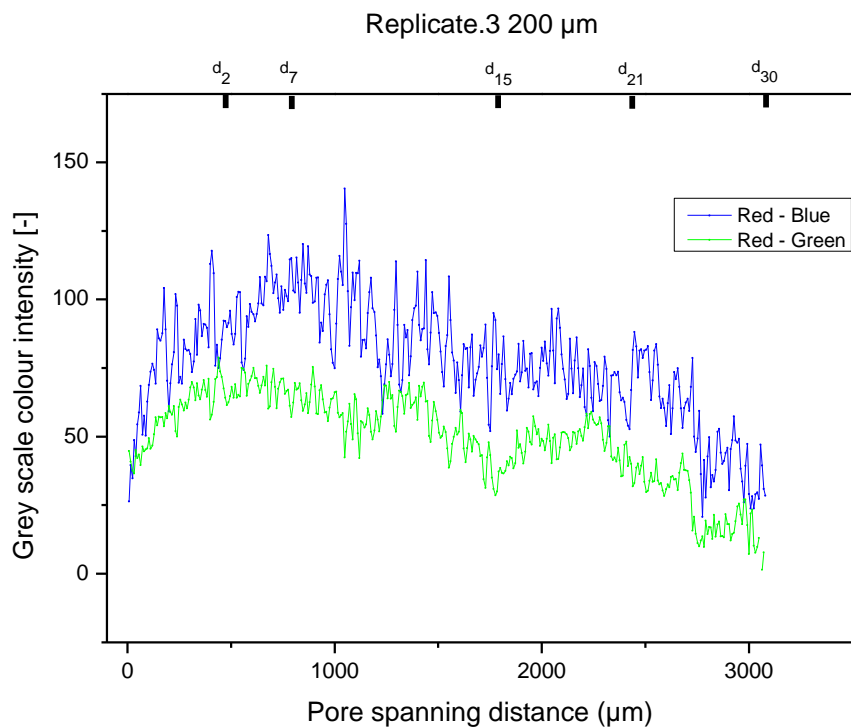


Fig. 5-14 Replicate.3, 200  $\mu\text{m}$ . Red intensity as a function of tissue location along longitudinal pore axis. Red – Blue (Blue) & Red – Green (Green) curves are plotted in order to isolate the signal on a grey scale. The labels on the top x axis correspond to the day at which tissue spanned the distance corresponding to the bottom x-axis.

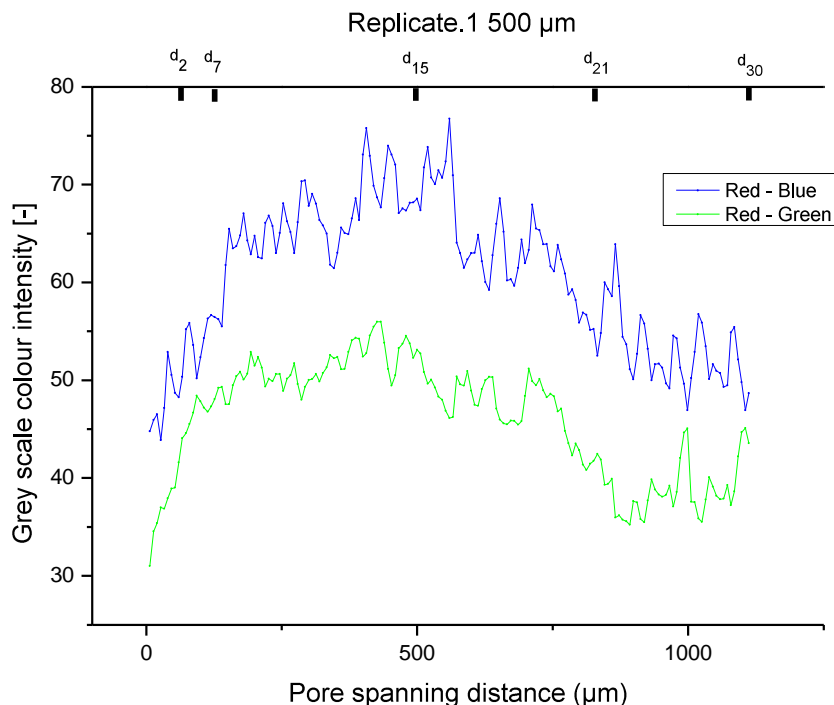


Fig. 5-15 Replicate.1, 500  $\mu\text{m}$ . Red intensity as a function of tissue location along longitudinal pore axis. Red – Blue (Blue) & Red – Green (Green) curves are plotted in order to isolate the signal on a grey scale. The labels on the top x axis correspond to the day at which tissue spanned the distance corresponding to the bottom x-axis

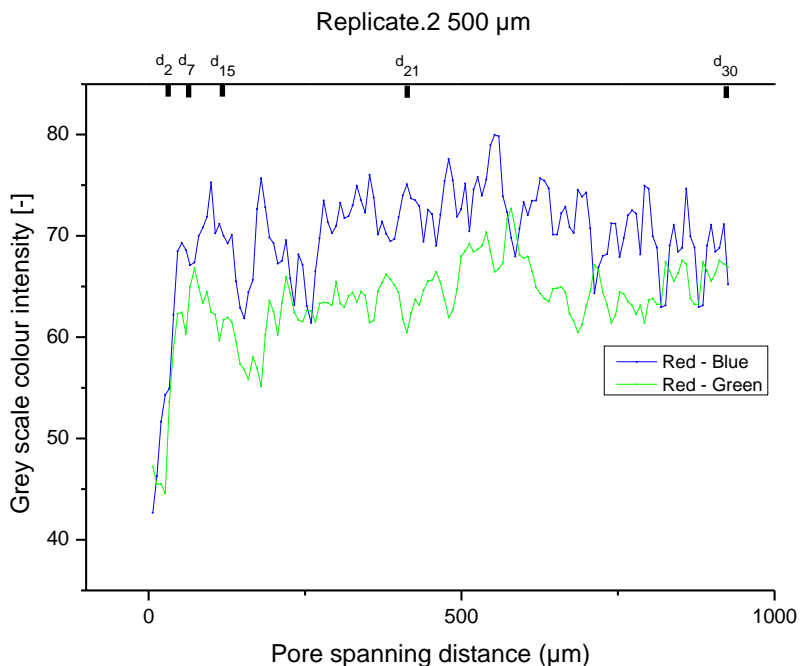


Fig. 5-16 Replicate.2, 500  $\mu\text{m}$ . Red intensity as a function of tissue location along longitudinal pore axis. Red – Blue (Blue) & Red – Green (Green) curves are plotted in order to isolate the signal on a grey scale. The labels on the top x axis correspond to the day at which tissue spanned the distance corresponding to the bottom x-axis

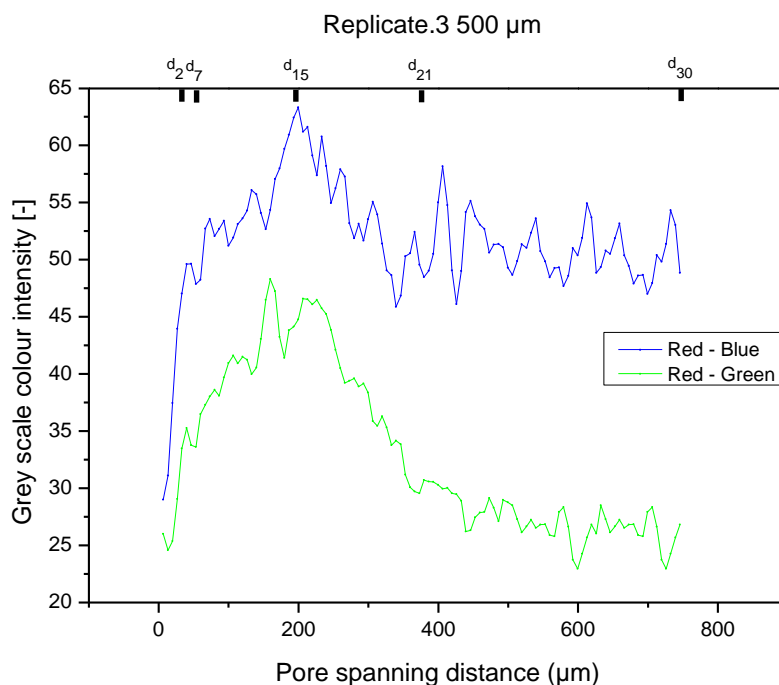


Fig. 5-17 Replicate.3, 500  $\mu\text{m}$ . Red intensity as a function of tissue location along longitudinal pore axis. Red – Blue (Blue) & Red – Green (Green) curves are plotted in order to isolate the signal on a grey scale. The labels on the top x axis correspond to the day at which tissue spanned the distance corresponding to the bottom x-axis

As a first order assessment, assuming that the expression of ALP would occur gradually and linearly, a straight line was fitted to the intensity figures. For 200  $\mu\text{m}$  replicates, all the slopes of the linear fit had negative values for both curves i.e. Red – Blue & Red – Green (Table 5-1). These results correspond to the observations from the pictures of the stained tissue where the intensity is seen to increase towards the starting point of tissue growth. For the 500  $\mu\text{m}$  pores, the same trend is observed except for replicate 2 where the slope is actually positive (Table 5-2). This observation for the replicate 2 corresponds to the observation made from the pictures, as the stain appeared to be uniform throughout the tissue. Therefore the methods we used here to assess ALP stain intensity seem to provide results reflecting the observations from the pictures. The initial low values up to  $d_2$  can attributed to the shadow caused by the pore walls, circular pore shape and picture quality. These issues will be discussed further in the next section.

Table 5-1 Slope values of linear fit of Red staining intensity curves in 200  $\mu\text{m}$  pores

<b>Linear Fitting Slope (200 <math>\mu\text{m}</math>)</b>			
	Replicate 1	Replicate 2	Replicate 3
Red – Blue	- 0.0002	- 0.0022	- 0.0139
Red – Green	- 0.0041	- 0.0051	- 0.0141

Table 5-2 Slope values of linear fit of Red staining intensity curves in 500  $\mu\text{m}$  pores

<b>Linear Fitting Slope (500 <math>\mu\text{m}</math>)</b>			
	Replicate 1	Replicate 2	Replicate 3
Red – Blue	- 0.0068	0.0059	- 0.0018
Red – Green	- 0.0087	0.0083	- 0.0239

### 5.2.3.2 Semi-quantitative analysis – Osteopontin

To evaluate Osteopontin production within the regenerated tissue, the area occupied by Osteopontin was measured (Fig. 5-18). 3 replicates for each condition were investigated. Results for individual replicate were presented considering the variability observed. Indeed, the averaged values show that the amount of Osteopontin is doubled in 500  $\mu\text{m}$  pores. However, the values are not significantly different due to a high variability among the 3 replicates for each condition. For the 200  $\mu\text{m}$  pore, values range from 0.09% to 0.56% and from 0.11% to 0.96%. Nevertheless, these results provide an order of magnitude of Osteopontin/Tissue ratio.

Table 5-3 Percentage of the total area occupied by Osteopontin for each replicates

% of Total Area Covered by OP			
	Replicate 1	Replicate 2	Replicate 3
<b>200 <math>\mu\text{m}</math></b>	0.09 %	0.56 %	0.27 %
<b>500 <math>\mu\text{m}</math></b>	0.11 %	0.65 %	0.96 %

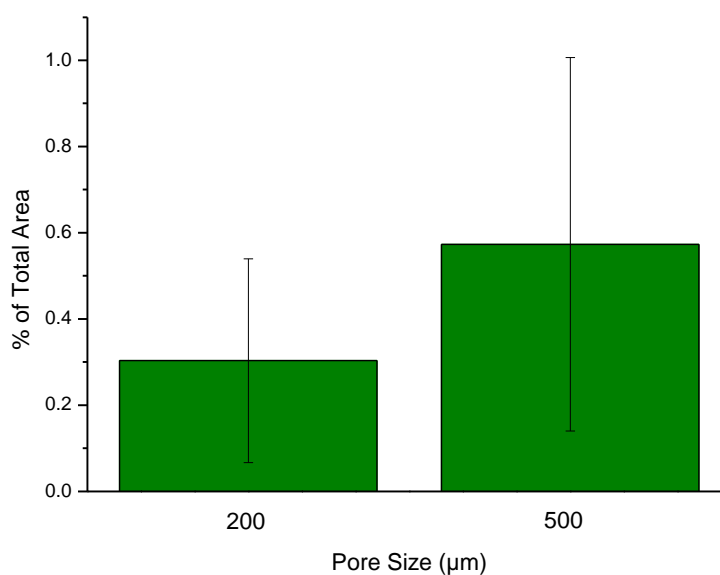


Fig. 5-18 Measurement of the percentage of total tissue area covered by Osteopontin stain.

## 5.3 Discussion

The goal of this study was to assess osteogenic tissue differentiation towards bone. For this purpose, two bone markers were investigated, an intermediate and a late one, namely Alkaline Phosphatase (ALP) and Osteopontin (OPN). Comparison of differentiation between the two pore sizes was attempted. However, this was hampered by the large variability in the results for different replicates. Secondly, it was aimed to obtain temporal-spatial distributions of markers for bone differentiation. ALP stain provided expected results by appearing gradually according to tissue “age”. However, Osteopontin appeared to be randomly distributed throughout the tissue.

### 5.3.1 Alkaline Phosphatase

ALP is present in all tissue throughout the entire body. Four isozymes of ALP have been found in humans. The one produced by osteoblasts is the non-specific liver/bone/kidney ALP isoform. ALP is a metallo-enzyme bound at the membrane of undifferentiated pluripotent cells and osteoblasts. Therefore, the stain is collocated with the cells producing ALP. In other words, the stain appears where cells undergo differentiation. The progressive increase in ALP expression relative to tissue “age” is observed in most of the samples. Tissue produces ALP according to its age. For instance, only in one replicate out of six, ALP has been produced right at the front suggesting that differentiation was triggered right after tissue was formed. For all the other samples, ALP appeared as tissue age increased.

The results obtained by pixel colour analysis needs to be discussed to be interpreted correctly. Due to the shadow produced at the pore extremity from which tissue started to grow, ALP stain appeared darker. On the image, this resulted in pixels of darker colour, therefore lower intensity values. Additionally, the local area of tissue at the pore extremity is decreased due to its concave shape, which was not accounted for in the averaging over pore width. Therefore, the average pixel value at the extremity is lower than it would be in the middle of the pore. Consequently, the curve peaks from  $d_0$  and  $d_2$  which corresponds to the first measurement of pore spanning. However, it can be observed that pixel values at  $d_2$  were higher than at  $d_{30}$  and between these two points the general trend tends to decrease. This is supported by the linear fitting performed on the curves, which indeed displayed negative values for the slope (fits were done between  $d_0$

---

and  $d_{30}$ , i.e. including the initial rise between  $d_0$  and  $d_2$ , therefore underestimating downwards slope). Therefore, these results confirm that ALP stain is increasing as tissue becomes “older”. However, a quantitative comparison between the two pore width conditions cannot be performed due to the poor image quality. For composite images, camera lighting appeared inhomogeneous, leading to jumps in the intensity profile. This in contrast to proof of concept results using the earlier high quality ALP images from Chapter 4, Fig. 4-19 (1 replicate only), see appendix 2.

The results obtained in this study and from previous findings (Chapter 3) showing the existence of finite zone where cell proliferation was taking place suggest that beyond this zone, tissue differentiation takes place increasingly. This pattern has already been seen in a study where researchers noticed weak ALP expression within a proliferative zone and higher expression in a maturing zone in tibial and vertebral growth plates in rats (Miao et al. 2002).

The pattern seen in the present case displaying the gradual apparition of different zones could also be related to the pattern observed in endochondral ossification (noting the difference in cell type and *in vitro* vs. *in vivo*) (Fig. 5-19), which also occurs during natural healing of bone fractures (Brighton et al. 1986). Tissue appeared to be polarized, ageing from one extremity to another. At one extremity tissue is “younger”, in a proliferative zone in which it develops by expanding in length (along the longitudinal pore axis) by constant cell division. At the other extremity, tissue is “older” and differentiates into bone by producing proteins involved in tissue mineralization. Between these two zones, an intermediate zone would exist where some cells would proliferate and start to produce collagen, some others would secrete vesicles and initiate tissue mineralization. Therefore, the concept of spatial partitioning of function is characteristic of the results presented. It is important to precise that the analogy with endochondral ossification account only for the fact that different zones seem to be present along the tissue and that a higher differentiation is noticed at one extremity of the tissue. Here, presence of chondrocytes has not been shown, therefore the situation described in the present case cannot be completely matched with endochondral ossification.

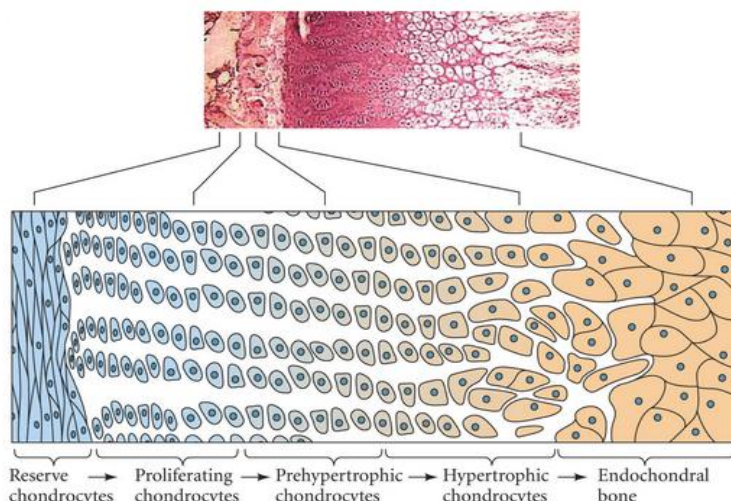


Fig. 5-19 Schematic of endochondral ossification process showing the different zones and progressive differentiation along the bone long axis.

Furthermore, this would also suggest that cell motility within the tissue would be limited i.e. a regenerated cell remains where it appeared within the tissue. Nevertheless, highly motile cells at the front were seen in results presented in Chapter 3. Therefore, cell motility might be reduced due to entrapment in denser collagenic extra cellular matrix in the bulk of the tissue. The presence of ALP suggests that the concentration in inorganic phosphate ions is locally increased (Lorch 1949). Thus, the local environment becomes favourable for calcium phosphate crystal formation which would eventually lead to tissue mineralization. Therefore, ALP expression suggests that the tissue regenerated was committing to the osteogenic lineage.

### 5.3.2 Osteopontin

#### *Osteopontin area*

Although the results obtained are not from quantitative methods, the values found do not seem to be out of range. For instance, in human and bovine bone, Osteopontin has been found to represent approximately 0.15% of the matrix (Poundarik et al. 2012). The results of this study provide values in the same order of magnitude. Indeed, the percentage of total area occupied by Osteopontin ranged from 0.09% to 0.56% for 200  $\mu\text{m}$  pore and 0.11% to 0.96% for 500  $\mu\text{m}$ . Nonetheless, comparing the results between the two pores size did not show any statistically significant difference due to high variability among the replicates.

---

*Osteopontin distribution & potential role of ALP*

OPN expression is increased in response to increasing phosphate concentrations in soft tissues (Beck et al. 2000). Thus, the expression of OPN is hypothesised to be partly triggered by ALP phosphatase activity. ALP can be active at values near neutrality, depending on the substrate concentration (Ross et al. 1951). Therefore, when expressed by the cells, ALP enzymatic activity causes an increase of the soluble inorganic phosphate (Pi) concentration within the media. Thus, as a free diffusing ion throughout the media, Pi can potentially interact with cells that are not located at the site of Pi production and stimulate OPN secretion. This could partially explain the unexpected random distribution of Osteopontin throughout the tissue. Furthermore, Osteopontin is released in a soluble form by osteoblasts (Giachelli et al. 2000). Therefore, once released in the extracellular media, OPN molecules can also diffuse throughout the media and create bounds with cells surfaces by bounding to integrins (Liaw et al. 1995). These details provide indications for another possible explanation of the spatially random distribution of OPN throughout the tissue formed. Furthermore, the fact that a highly heterogeneous population of cells (Pevsner-Fischer et al. 2011), with large variation in differentiation potential (Sengers et al. 2010) was used can be an alternative explanation to the random osteopontin distribution.

*Potential Osteopontin activation by ALP for mineralization initiation*

The results show that the regenerated tissue expressed Osteopontin, which is known to be involved in mineralization. However, in its phosphorylated form, Osteopontin inhibits bone mineralization *in vitro* (Hunter et al. 1994). Whether OPN is phosphorylated or not has not been investigated. However, ALP could potentially also activate OPN as ALP activity is preserved in its soluble form (Pizauro et al. 1995) and is present in the vesicles secreted by osteoblasts (Stagni et al. 1983). Furthermore, ALP has already been used to dephosphorylate OPN *in vitro* (Boskey et al. 1993) proving that OPN can serve as a substrate for ALP. Thus, the hypothesis that after stimulating OPN expression by increasing Pi, ALP would also directly activate OPN by dephosphorylating it, could be envisaged. However, it has been shown in calcified bone tissue that ALP does dephosphorylate only less than 10 % of the OPN present, whereas Osteoclastic Tartrate-resistant Acid phosphatase dephosphorylates 43% of the OPN (Ek-Rylander et al. 1994). Therefore, the presence of osteoclasts should be investigated

to avoid further speculation. The important point here is that Osteopontin is expressed and according to literature, is involved in mineralization process in its dephosphorylated form. ALP contribution to Osteopontin activation is suggested, therefore, the presence of both of these markers suggest that tissue is likely to undergo mineralization. Nevertheless, mineralization would need to be confirmed in further studies.

### **5.3.3 Potential implications of internal tension**

In Chapter 4, paragraph 4.3.3, it was discussed that different actin remodelling and tensile state could affect tissue formation and particularly the cell cycle. The same reasons i.e. tensile state and actin remodelling could modulate differentiation as discussed in paragraph 2.5.7.2. However, differences regarding differentiation could not be established with the methods used in the present study.

### **5.3.4 Summary**

The main results of this study concern the expression of intermediate and late markers by the regenerated tissue. ALP and Osteopontin were seen to be expressed demonstrating the ability of the new tissue formed to differentiate into bone and reach a state where all the components required for tissue mineralization are present. This was observed regardless of the pore size the tissue was growing in. However, it was not possible to state whether one condition was more osteogenic than another. This was due to the methods used, which were only semi-quantitative. The two markers displayed differences on their spatial distribution. ALP appeared increasingly according to tissue “age”. On the other hand, Osteopontin distribution did not display a regular pattern, and was observed to be randomly deposited throughout the tissue. Regarding the ALP pattern, an analogy with osteochondral ossification process was suggested due to fact that different zones seemed to appear across the tissue. At one extremity, i.e. the rear of the pore, where the tissue is “aged”, there is a zone where cell division would be only sporadic and differentiation would be the major phenomena taking place. At the other extremity, i.e. the front, as highlighted in previous chapters, cell division, potentially modulated by cell mechanics, is taking place in order to fill the pore interstice. This confirms the suggestions arising from previous chapter that differentiation and proliferation would have different locations.

# Chapter 6

## Discussion and Conclusion

The present chapter summarises the outcomes of this study, the limitations and the issues which remain to be answered in the future.

### 6.1 Summary of the thesis outcomes

The aim of this study was to improve the understanding of tissue formation within porous structures using an original experimental device.

We showed that solely as a function of pore width, different pore structures can modulate pore colonization by newly formed tissue as well as the amount of tissue formed i.e. invasion rate, projected tissue area, cell number and approximation of tissue volume. In other words, the amount of neo-tissue that can be regenerated can be different according to the 3D environment provided. In the case of the structures investigated in this study, the tissue has been seen to form at a constant rate over periods up to 30 days. This indicates the regeneration potential despite elderly cell donors. Eventually, the most important finding was that a narrower long open pore resulted in an enhanced tissue invasion rate.

Results also showed that this phenomenon occurred independent of the donor variability (age & gender). HBMSC were used as they are one of the most relevant cell types for skeletal repair and regeneration strategies. The cells were extracted from bone marrow taken from patients undergoing hip replacement surgery. Therefore, usually the cells are obtained predominantly from elderly patients. However, elderly patients represent the relevant clinical target group.

Results showed that there are two zones participating in tissue formation. First, the role of the interface between the tissue and the empty pore space was emphasised. Second, the underlying tissue located “behind” the front of migration was further characterised. In the first zone described, it was showed that mechanical forces generated by cells themselves (as apparent from cell contraction) and cell division take place, separately or simultaneously. Also, a shape parameter has been noticed. The shape at the front, namely the degree of curvature, was proposed to be a factor affecting tissue growth. The level of curvature would determine the local force distribution applied to the underlying tissue. Locally, in other words, right at the interface between leading cells and the void to be colonized, , it was argued that due to a higher curvature the forces leading to tissue expansion would be higher, based on the concept of the “purse string”. Regarding the forces applied to the tissue located “behind” the front of migration, a higher curvature would result in a higher net stress applied to the underlying tissue. Therefore, the forces “dragging” the tissue towards the interstice would be higher and result in an enhanced tissue expansion. However, it has to be borne in mind that this was based on observations of actin organisation and time lapse of cell contraction and that it is actually difficult to measure forces directly within the setup. Thus, the interface between tissue and the interstice was one of the principal focus points of this work. Interestingly, it was seen that the zone “behind” the front of migration was also active, conversely to previous studies claiming that tissue growth was occurring solely at the interface between tissue and the interstice. Indeed, during time lapse experiments, a large amount of cell motion was noticed and most importantly, that cell division was taking place also within a certain finite zone behind the immediate front of migration.

It has been found that tissue organises itself in a different manner according to the 3D environment provided. Cells, actin cytoskeleton and collagenic matrix displayed a distinct organisation depending on pore width. Moreover, the organisations of the main tissue components appeared to be linked. Indeed, all the elements investigated displayed a similar pattern for the same pore width. Additionally, the results connected to the literature review strongly suggested that actin is the component guiding the orientations of the other elements (Cells & Matrix). In the narrower pore, the tissue organisation was shown to be oriented predominantly parallel to the longitudinal pore axis, which is also the direction of migration. On the other hand, in the larger pore, tissue was oriented

---

almost perpendicular to the pore axis. Furthermore, tissue orientation was seen to correspond to cell division orientation. Therefore, a mechanism was proposed in which cell division, guided by tissue orientation, would be a determinant factor for the ability of the tissue to expand. The main concept of this mechanism is based on the fact that cell division orientated along the direction of migration would result in enhanced tissue formation. Additionally, cell density within the tissue was estimated to be 3 times higher in narrow pores. Cell density associated with the different actin organisation could reflect different tensile states within the tissue according to pore width.

Tissue differentiation has been investigated. Early, intermediate and late bone markers were seen to be expressed. Indeed, production of Collagen I, expression of Alkaline Phosphate and production of Osteopontin were observed. It has been attempted to assess tissue differentiation over time as the tissue formed provides an overview of the development history, containing both young and old tissue. Cells produced Collagen I right at the front of the tissue as seen in Chapter 4 (Fig. 4-10e, f). Therefore, it was assumed that Collagen I started appearing as soon as the tissue formed i.e. instantaneously. ALP was seen to appear gradually over time. However, Osteopontin appeared to be spread irregularly over time/space. Furthermore, the form in which the device has been used during the study did not allow proceeding of tissue differentiation quantification using methods such as qPCR.

Overall, the results provided interesting insights in tissue formation within porous structures *in vitro*

Table 6-1). The primary findings concern the effect of pore size on tissue formation. The results demonstrated the implications of several phenomena in 3D tissue formation which can be modulated by pore geometry. In the first place, the potential contribution of cell generated forces to tissue development, cytoskeletal & collagenic matrix rearrangement and their effect on tissue formation. Furthermore, cell division, as mediated by cytoskeletal rearrangement is an important factor. Differences found in cellular density suggested differences in tensile state dependent on pore size. Variations in tensile state were suggested to impact on proliferation rate, which was found to be different between the two pore sizes. Tissue differentiation assessment revealed that tissue is regenerated following a mechanism in which a progressive switch from proliferation to differentiation over time and space is observed (Fig. 6-1). These

observations display similarities with endochondral ossification where a transition from proliferation to differentiation occurs over space. However, endochondral ossification begins with chondrocytes which proliferate, become hypertrophic and eventually differentiate into bone cells. This is not observed in the study presented here as the presence of chondrocytes has not been investigated.

Eventually, with respect to 3D scaffold design, a compromise may have to be found between different aspects, e.g. using concave features with high curvature to promote tissue formation, while preserving porosity. In addition, narrow aligned channels could be used to guide rapid tissue colonization, while allowing a sufficient pore size for osteon formation and vascularisation *in vivo*. For example, the findings from the present study could inform inter fibre spacing in lattice type scaffolds created using 3D printing fibre deposition techniques.

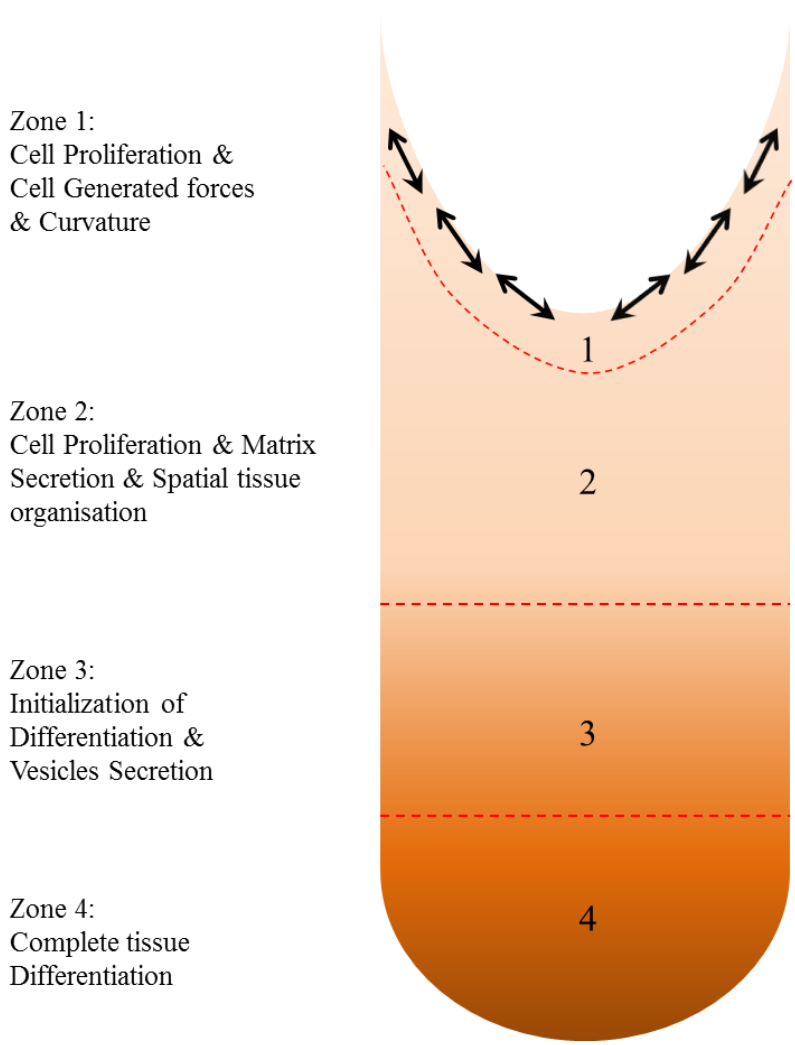


Fig. 6-1 Proposed zones with allocated behaviour throughout the tissue

Table 6-1: Outcomes

**Pore Geometry Regulates Human Bone Marrow Cells Tissue Formation**

Quantification of tissue expansion was accomplished:

- Pore width affects tissue capacity to expand in terms of projected tissue area
- Pore width affects cytoskeleton organisation
- Mechanical forces generated by internal cellular stress occur during tissue expansion in 3D
- Cell proliferation during tissue expansion occurs in a finite zone

**Ingrowth enhancement due to pore-induced tissue orientation**

Tissue orientation was quantified:

- Pore width affects Cell Orientation & Matrix orientation
- Pore width affects Cell division orientation
- Pore width affects the number of cells present
- Tissue orientation affects tissue capacity to expand via cell division orientation.

**Tissue differentiation**

Tissue differentiation was assessed:

- Tissue produces early, intermediate and late stage differentiation bone markers
- Transition from proliferation to differentiation over space.
- System not suitable for differentiation quantification using conventional bulk methods

## 6.2 Experimental Limitations and Optimisation

As with every study a number of limitations exist and this is also the case for this thesis.

### 6.2.1 Limitations

- Several layers of tissue forming in different planes of focus complicating (non-confocal) microscopic analysis
- The cells seeded in slots of different size are cultured in a single well. Therefore, paracrine signalling from cells growing in one pore size could affect the growth of cells in a different pore size
- No possibility for molecular biology experiments (gene expression measurement by real time PCR): Cells occupy the surface of the structure outside the pore, therefore not only tissue within the gaps would be harvested. Furthermore, harvesting the tissue using other means than reagents de-attaching/lysing the tissue (Proteases, Trypsin, and Calcium Chelatant) would be inaccurate as the same amount of tissue may not be harvested in each case (e.g. when using simple scraping). Secondly, due to the fragility of the samples, a high risk of breaking the sample is encountered.
- During seeding, some issues have been encountered.
  - Low density seeding: Pore spanning delayed up to 4 weeks until 2D confluence is reached on the inside surface of the pore.
  - High density seeding: Cells form clumps within the gaps. Therefore, monitoring pore spanning is disrupted.
- In order to address some of the issues described, it would be advantageous to redesign the device in such way that the surface available for 2D growth on the outer surface of the construct beside the pore slot would be minimized.

- Using a device similar to the one represented on the sketch below, would facilitate tissue harvesting, simply by using trypsin to detach cells from the construct.

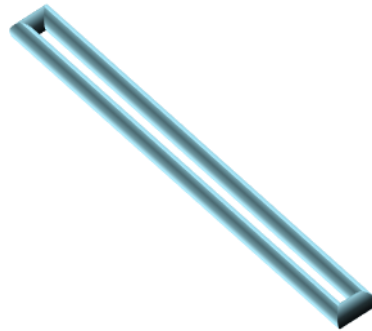


Fig. 6-2 Schematic of an optimized device with less surface available for 2D growth

- The material used for this study is calcium phosphate cement. This type of material is highly rigid and brittle, therefore external strain cannot be readily applied to the device
- The device does not allow for direct internal tension measurements. This is also due to the mechanical properties of the material for construct fabrication. Using such device made of compliant polymers containing fluorescent beads could permit internal tension assessment. For example, this could be achieved by measuring beads displacement while tissue is developing.
- The device is fabricated by mould casting. The cement is spread over a silicon mould as a paste form. The cement is then left for hardening on the silicone mould. However, during the removal of the mould, there is a high risk of breaking the sample. Using micro-milling tools could result in a higher number of unbroken samples as the features are created while the cements is already set and hardened. Alternatively 3D printing could be used.

### 6.2.2 Advantages

- The main advantage of the open pore device is the ease of tissue monitoring. Indeed, tissue expansion can be monitored using all sorts of microscopy, which are non-invasive means. Furthermore, the tissue can be monitored on a very wide time scale, ranging from minutes to weeks.
- 3D Environment provided for tissue formation and minimized nutrient supply restrictions.
- The type of experimental system developed here could serve as a platform to accurately quantify growth in different culture conditions, as well as to assess the impact of biomaterial, surface modification and biochemical factors on tissue growth.

### 6.3 Open questions and future work

In this section some of the questions which have arisen as a result of this thesis and remain to be answered in the future will be discussed. From this perspective potential future research steps will be proposed.

The results clearly showed the effect of pore geometry on tissue growth and the potential role of cell mechanics. Nevertheless, cell mechanics is highly complex and is not the only factor governing tissue growth, thus the degree of the contribution of each cellular process needs to be assessed more precisely. In addition, the composition of the extracellular matrix needs to be investigated to determine the relationships between growth and differentiation. In a further part, cell ingrowth and angiogenesis should be investigated as it is a crucial parameter for implant acceptance. Additionally, if an optimal structure for tissue formation in static conditions has been established, then mechanical loading could be a supplementary method to enhance the quality of the tissue formed *in vitro*.

### 6.3.1 Tissue formation in different media conditions

Preliminary results showed that pore spanning was not affected by addition of Vitamin-D in the culture media during 12 days (Fig. 6-3). The question whether cells should be treated with other chemicals than the ones required for basal growth to modulate tissue formation has been raised previously. Researchers investigated the effect of dexamethasone treatment on MSCs prior to subcutaneous implantation in rats. The results showed an enhanced osteogenic response after implantation, demonstrating that using tissue culture technology presents advantages for bone tissue regeneration (Yoshikawa et al. 1996). Nowadays, dexamethasone is commonly used in order to induce osteogenic differentiation *in vitro*. However, it is still unknown whether the use of such chemical affects tissue formation capacity in 3D. Thus, future work should be carried out to investigate the effect of osteogenic inductors on tissue development. Preliminary results demonstrated that a known osteogenic inductor i.e. vitamin D, did not affect the amount of tissue formed compared to basal conditions. Therefore, osteogenic factors in culture media have no adverse effect on tissue growth and enhance differentiation. Therefore, it confirmed the benefits of adding osteogenic factors to regenerate tissue *ex vivo*.

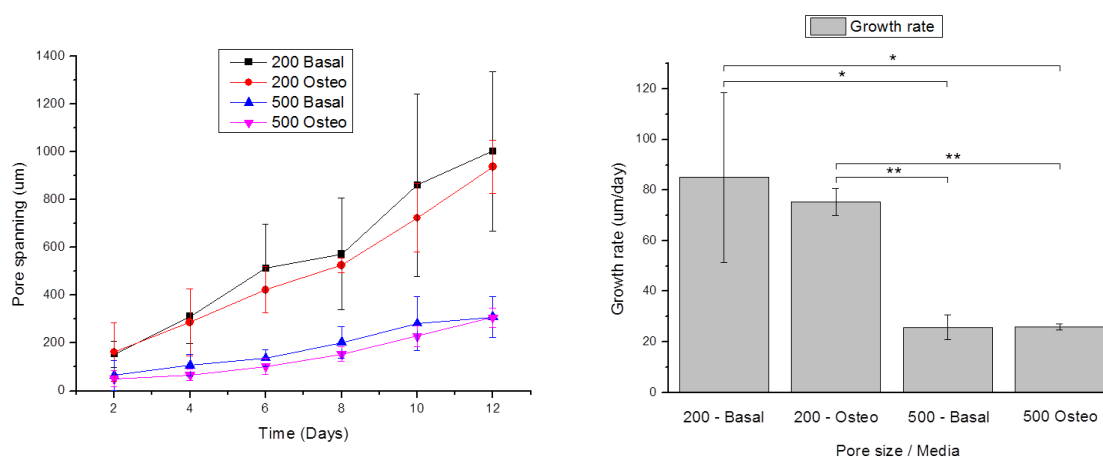


Fig. 6-3 Tissue growth monitoring over 12 days in basal and osteogenic media. (Left) Pore spanning monitored over 12 days. (Right) Tissue growth velocity in each conditions obtained by linear fitting.

### 6.3.2 Internal tension and cell division modulation with drugs

Several drugs can modulate internal tension generated via the actin network. Commonly used drugs to decrease internal tension are Cytochalasin, a myosin II inhibitor and Blebbistatin which is an actin fibre formation inhibitor. On the other hand, to increase internal tension, Lysophosphatidic acid (LPA) is widely used to raise internal tension by stimulating the Rho a pathway. A pilot study was carried out using ROCK pathway inhibitor (Y 27632), which prevent RhoA-induced formation of stress fibres, to investigate whether this could affect tissue invasion rate.

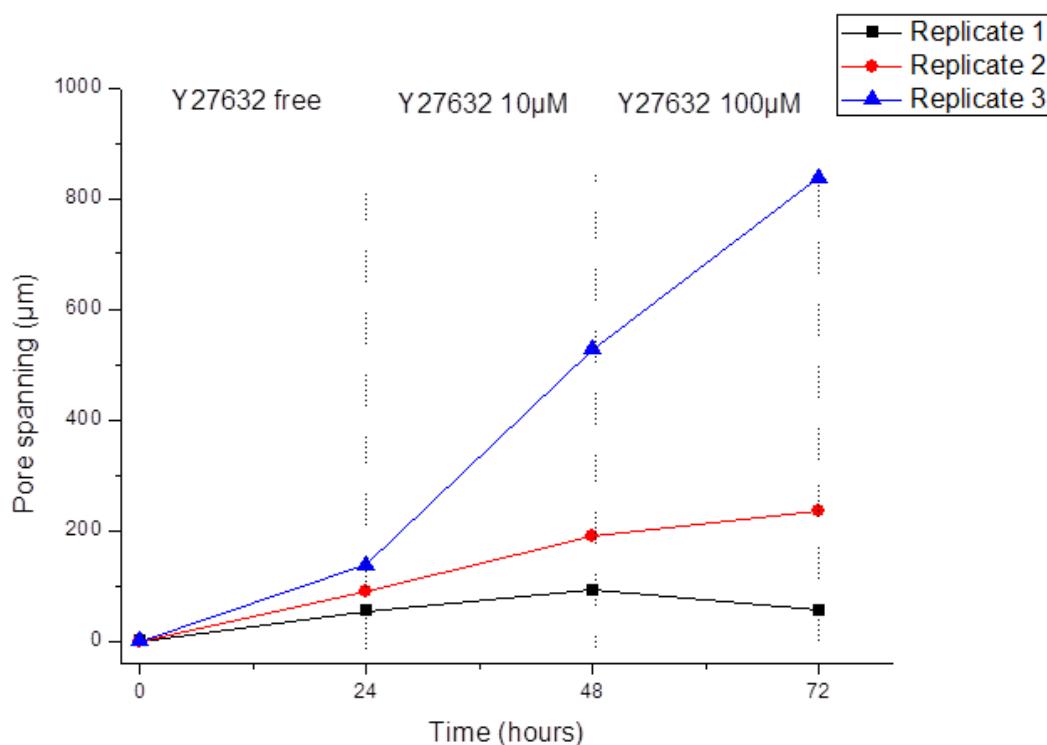


Fig. 6-4 Pore spanning rate under the influence of actin fibres formation inhibitor. From 0 to 24h, the media was Y27632 free. From 24h-48h, the media was containing 10 µM Y27632. From 48h-72h, the media was containing 100 µM Y27632.

However, results obtained during this set of experiments were inconclusive. For the replicate 1 and 2, it can be seen that 10 µM of Y27632 did not have any effect on tissue growth. Furthermore, tissue formation in the replicate 2 slightly decreased in the presence of Y27632 at 100 µM. However, this could also be a pattern of growth expected in absence of Y 27632 considering the low effect observed and the short duration of monitoring. Thus, no effect of 100 µM Y27632 can be observed on replicate 2. Nevertheless, on replicate 1, the expected effect could be noticed as the tissue

---

formation was prevented. Indeed, the front of migration went backwards, opposite the direction of migration. On the other hand, Y27632 seemed to have enhanced tissue formation in replicate 3 at both concentration 10  $\mu\text{M}$  and 100  $\mu\text{M}$ . Generally, these results are highly heterogeneous, thus no definite effect of Y27632 can be concluded from these experiments. Such experiments might provide clearer results after serum starvation of the cells. In order to maintain itself suspended between the pore walls, the level of tension within the tissue is likely to be high. Therefore, it can be envisioned that the effect of Y27632 was negligible compared to the actual tensile state. These results were completely unexpected. Consequently, part of the future work should comprise studies involving the use of such drugs to measure the contribution of cell mechanics in the overall process of tissue formation *in vitro* by comparing growth rates under influence of tension modulator compared to control conditions. This would also provide information about which structure induces the highest level of mechanical stimuli.

As it has already been discussed, tissue formation *in vitro* is a process involving several cellular processes such as cell division and cell migration. The involvement of each process could be determined by running the same type of experiment of growth monitoring in our structures under the effect of a cell division inhibitor such as mytomycin C compared to control conditions.

The results will provide relative involvement of cell migration, division and cell generated forces. Therefore, by having an estimate of the relative contribution of each process, the relevance of different scaffold aspects and treatment could be assessed. Indeed, if a cell migration effect is dominant the importance of scaffold treatment with a protein enhancing migration via haptotaxis for example would be highlighted. On the other hand, if cell division is seen to have a major impact, the importance of growth factors would be emphasized. Finally, if it would be found that cell mechanics are mostly involved, the necessity to account for such fact in micro-architecture design would be confirmed.

Direct investigation of cell mechanics would be a challenging part of the future work. Indeed, the ability to measure tension within different region of the regenerated tissue would provide results of great interest. Such data would clarify the role of internal tension in tissue growth in 3D. For example, whether there is a threshold of tension triggering cell division, protein expression or tissue differentiation. Recently,

researchers developed a molecular tool permitting internal tension using FRET microscopy (Grashoff et al. 2010). By using this method, researchers were able to sense internal tension with pico-newton sensitivity (pN). This tool consists of a modified Vinculin molecule with a tension sensor module with two fluorophores tethered to each extremity between the two domains of the protein. The tension is evaluated by FRET, as this method is sensitive to the distance between the fluorophores, FRET intensity should decrease when a tension is applied to the device (Grashoff et al. 2010).

Therefore, reproducing the experiments done in this work using FRET and such vinculin transfected bone marrow cells would be a valuable option in order to elucidate the role of internal tension in 3D tissue formation. Other tools such as AFM Nano-indentation could be used to investigate the level of internal tension present. By probing the tissue with an AFM cantilever, the local stiffness of the tissue could be assessed and possibly reflect the tensile state of a particular region. However, differences could also be attributed to matrix production or even mineralization.

### **6.3.3 Molecular biology**

The methods used in this work to determine the amount of tissue formation provided accurate results (i.e. cell count and PTA measurements). However, techniques are available in order to characterise the type of tissue regenerated more precisely. For instance, the usage of real-time PCR and ELISA assays to quantify cell expression. Indeed, such experiments would provide further quantitative insights into bone markers expression, protein composition and their proportions. As these are intrinsically bulk measures, for this purpose, the use of an improved device with allowance for tissue collection and minimized surface area for cell growth outside the pore of interest would be required as a viable alternative.

### **6.3.4 Tissue behaviour under mechanical loading**

After the composition of the extracellular matrix has been determined, and once the mechanism of tissue formation and the involvement of internal actin related forces has been fully characterized, the effect of external mechanical loading on tissue development will need to be investigated. In the group, a loading device has been designed in order to apply a pure mechanical strain on a structure. This device can either

apply compression or tension on the construct. Both compression and tension are relevant modes of deformation to investigate as they occur *in vivo* during motion.

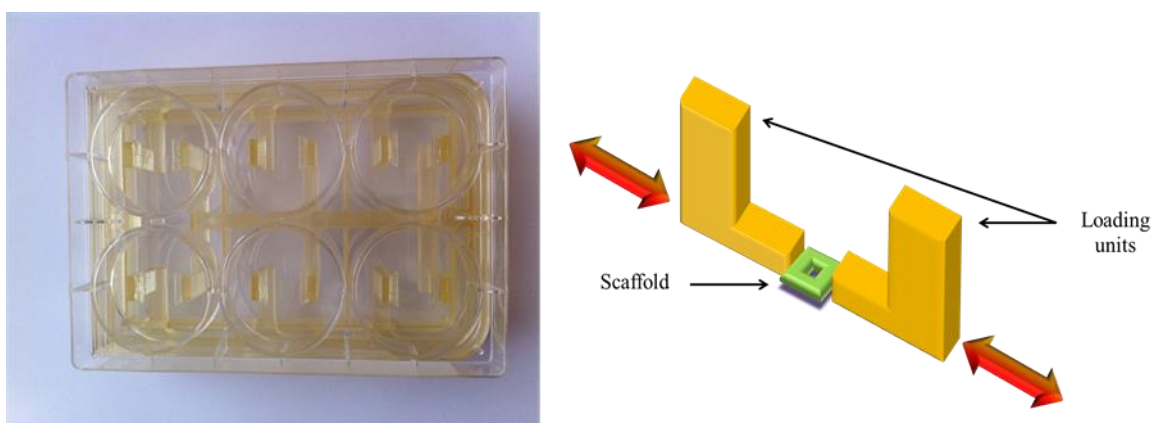


Fig. 6-5 Mechanical loading device fitting on top of a 6 well culture plate (left). Schematic picture of a scaffold mechanically loaded by two loading units (right).

The device has been designed to fit on top of a 6 well culture plate and will not be affecting any nutrient or oxygen supply (Fig. 6-5). The construct for this part of the work should be a compliant gel with appropriate surface modification for cell adhesion. Similar experimental methods as the ones employed in this work would be used i.e. seeding cells on the structure and applying mechanical strains on the device whilst the tissue grows in the pore slots.

### 6.3.5 Computational Modelling

The ability to predict cell growth with a simple curvature based model using only a single parameter has been achieved. However, From a tissue engineering perspective, further work is needed to precisely characterize 3D tissue geometry and fibre organisation, and translate these results in more complex mechanistic computational models accounting for cytoskeletal dynamics, force generation and fibre reorientation, indicating directions for future research (Deshpande et al. 2007; Biton et al. 2009; Sanz-Herrera et al. 2009).

### 6.3.6 Summary of future work

The proposed future work will provide a large quantity of data on tissue formation *in vitro*, as well as insights in how tissue develops in porous structure in a 3D configuration using cell generated forces. The level of involvement of different cellular

processes will be established, hence guiding further research on specific means to accelerate tissue formation in porous scaffolds for bone tissue engineering purposes. The final achievement of tissue engineering is to generate fully differentiated tissue and this work will provide clear answers about what kind of treatment is best for bone tissue regeneration. Furthermore, the effect of mechanical loading *in vitro* to reproduce more closely *in vivo* conditions will be revealed. Indeed, the device developed allows a way of loading tissue with conditions close to those displayed *in vivo*. The device allows changing the frequency of loading and its magnitude by simple computer control. Furthermore, the orientation of the tissue is easily changeable. Therefore, the effect of a wide variety of possible loading conditions (strains) that bone can be exposed to *in vivo* will be established and the relevance of these mechanical parameters for tissue engineering *in vitro* will be established.

### 6.3.7 Open questions

- Is there a certain level of tension representing a critical threshold for triggering different cellular processes?
- How precisely tension affects cell proliferation?
- How the level of tension is affected by matrix production and vice versa
- Is there a geometric configuration more favourable for tissue differentiation?
- What is the relative impact of each cellular process including cell division, cell migration, and cell generated forces?
- How the process of mineralization would take place? i.e. forming a gradient similar to ALP, or according to a more random spatial distribution co-located with non-collagenous proteins (NCPs).

## 6.4 Epilogue

The concept of tissue engineering has been applied practically for the first time in 1668. The Dutch surgeon Job van Meekeren filled a bone defect in a soldier's cranium with a

piece of skull from a dog. Removal of the graft was requested by the soldier after two years in order to be allowed back in his church, not because of pain. Further progress in tissue engineering has been reported in the early part of the 20<sup>th</sup> century, achieved by Dr. Fred Albee. He was the pioneer of autologous bone graft transplantation before the World War I, when he made several successful operations such as using patients own bone for alleviating hip pain in case of rheumatism. Furthermore, he introduced the replacement of metal by bone for spinal fusion procedures. Later in the century, the use of allografts and autografts became a common procedure to treat bone defects. However, several issues regularly evocated were associated with these practices such as immune rejection, donor site morbidity, availability and most importantly patient pain consequent to biopsy. Therefore, researchers oriented their research towards alternative solutions. The most promising concept is the application of bone substitutes combining engineered materials with cells.

The impact of 3D environment on tissue regeneration was the central focus of this thesis as well as the elucidation of the underlying tissue formation mechanisms. Interesting data emanated from this work showing that 3D surroundings can influence the amount of tissue regenerated, its organisation and the way it expands. Consequently, this emphasizes the importance of scaffold 3D architecture design for bone engineering purposes. However, the intrinsic structure of porous implants is a component among many others governing tissue regeneration in bone graft substitutes. Indeed, tissue engineering is a multi-disciplinary topic involving the latest technology from several fields including biology, chemistry, engineering and computational modelling. Therefore, the path to achieve the ultimate goal of bone engineering, which is creating functionalized implants with minimized inflammation and optimized osteointegration as well as vascularisation, essentially requires a pluridisciplinary research approach



# Appendices

# Appendix 1 – Supplementary materials

Electronic material is accompanying this thesis. Specifically:

- Video 1 (Tissue Kinetics): Time-lapse video showing tissue formation within a 200  $\mu\text{m}$  pore over 48h.
- Video 2: (Tissue Kinetics) Time-lapse video showing tissue formation within a 500  $\mu\text{m}$  pore over 48h.
- Video 3: (Tissue Stress) Time-lapse video showing cell contraction due to cell generated forces occurring during tissue formation within 200  $\mu\text{m}$  pore over 10h
- Video 4: (Tissue Stress) Time-lapse video showing cell contraction due to cell generated forces occurring during tissue formation within 500  $\mu\text{m}$  pore over 10h

## Appendix 2 – ALP staining analysis: Proof of concept

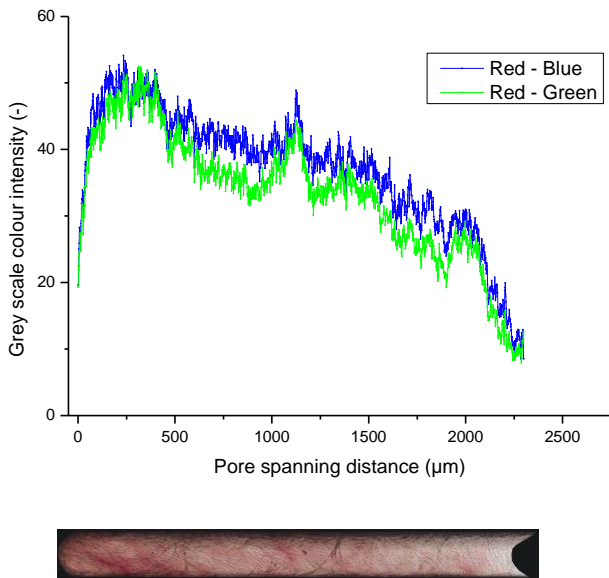


Fig. A.1: Analysis of ALP over space/time using the methods described in 5.1.4 on high quality pictures in a 200 µm pore. (Top) ALP intensity calculated by grey scale intensity as function of position along longitudinal pore axis. A progressive gradient reflecting ALP staining on the picture (Bottom) is obtained

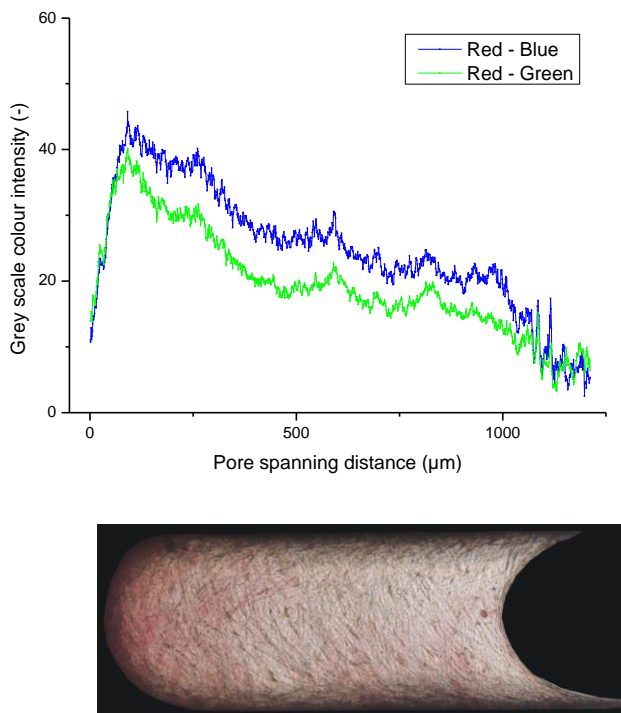


Fig. A.2: Analysis of ALP over space/time using methods described in 5.1.4 on high quality pictures in a 500 µm pore. (Top) ALP intensity calculated by grey scale intensity as function of position along longitudinal pore axis. A progressive gradient reflecting ALP staining on the picture (Bottom) is obtained .

## Appendix 3 – Publications

### Refereed Articles

1. **J Knychala**, N Bouropoulos, C J Catt, O L Katsamenis, C P Please, B G Sengers, **2013** " *Pore Geometry Regulates Early Stage Human Bone Marrow Cell Tissue Formation and Organisation*". Annals of Biomedical Engineering. vol 41, issue 5, 2013

Cited by: P Joly et al. "*Geometry-Driven Cell Organization Determines Tissue Growths in Scaffold Pores: Consequences for Fibronectin Organization*". PLOSOne, 2013

2. **J Knychala**, N Bouropoulos, O L Katsamenis, B G Sengers, **2013** "*Ingrowth enhancement by pore geometry-induced tissue orientation*". (Resubmission in preparation)

### Conference Abstracts and Proceedings

1. **J. Knychala**, N.Bouropoulos, M.Taylor, B.G.Sengers "*Interactions between cell mechanics, pore geometry and tissue growth*", Annual Meeting of the Scandinavian Society for Biomaterials Annual, May 2012, Uppsala, Sweden and published as an extended abstract in the European Journal of Cells & Materials (eCM), vol 23, supplement 5, 2012
2. **J. Knychala**, N.Bouropoulos, B.G.Sengers , "*Interactions between cell mechanics, pore geometry, tissue growth and orientation*", Tissue Engineering & Regenerative Medicine International Society (TERMIS) World Congress, September 2012 Vienna, Austria,

## List of References / Bibliography

- Adams, C. L. and W. J. Nelson (1998). "Cytomechanics of cadherin-mediated cell-cell adhesion." Current opinion in cell biology **10**(5): 572-577.
- Akay, G., M. A. Birch and M. A. Bokhari (2004). "Microcellular polyHIPE polymer supports osteoblast growth and bone formation in vitro." Biomaterials **25**(18): 3991-4000.
- Andriotis, O., O. Katsamenis, D. Mouzakis and N. Bouropoulos (2010). "Preparation and characterization of bioceramics produced from calcium phosphate cements." Crystal Research and Technology **45**(3): 239-243.
- Aratyn-Schaus, Y., P. W. Oakes and M. L. Gardel (2010). "Dynamic and structural signatures of lamellar actomyosin force generation." Mol Biol Cell **22**(8): 1330-1339.
- Aubin, J. E. (2001). "Regulation of osteoblast formation and function." Rev Endocr Metab Disord **2**(1): 81-94.
- Ayers, R. A., S. J. Simske, T. A. Bateman, A. Petkus, R. L. Sachdeva and V. E. Gyunter (1999). "Effect of nitinol implant porosity on cranial bone ingrowth and apposition after 6 weeks." J Biomed Mater Res **45**(1): 42-47.
- Baena-Lopez, L. A., A. Baonza and A. Garcia-Bellido (2005). "The orientation of cell divisions determines the shape of Drosophila organs." Curr Biol **15**(18): 1640-1644.
- Balaban, N. Q., U. S. Schwarz, D. Riveline, P. Goichberg, G. Tzur, I. Sabanay, D. Mahalu, S. Safran, A. Bershadsky, L. Addadi and B. Geiger (2001). "Force and focal adhesion assembly: a close relationship studied using elastic micropatterned substrates." Nature Cell Biology **3**(5): 466-472.
- Ballestrem, C., B. Hinz, B. A. Imhof and B. Wehrle-Haller (2001). "Marching at the front and dragging behind differential  $\alpha\beta3$ -integrin turnover regulates focal adhesion behavior." The Journal of cell biology **155**(7): 1319-1332.
- Beck, G. R., Jr., B. Zerler and E. Moran (2000). "Phosphate is a specific signal for induction of osteopontin gene expression." Proc Natl Acad Sci U S A **97**(15): 8352-8357.
- Bergsma, E. J., F. R. Rozema, R. R. Bos and W. C. D. Bruijn (1993). "Foreign body reactions to resorbable poly (L-lactide) bone plates and screws used for the fixation of unstable zygomatic fractures." Journal of Oral and Maxillofacial surgery **51**(6): 666-670.
- Bershadsky, A. D., N. Q. Balaban and B. Geiger (2003). "Adhesion-dependent cell mechanosensitivity." Annual Review of Cell and Developmental Biology **19**: 677-695.
- Bertet, C., L. Sulak and T. Lecuit (2004). "Myosin-dependent junction remodelling controls planar cell intercalation and axis elongation." Nature **429**(6992): 667-671.
- Best, S., A. Porter, E. Thian and J. Huang (2008). "Bioceramics: past, present and for the future." Journal of the European Ceramic Society **28**(7): 1319-1327.
- Bidan, C. M., K. P. Kommareddy, M. Rumpler, P. Kollmannsberger, Y. J. M. Brechet, P. Fratzl and J. W. C. Dunlop (2012). "How Linear Tension Converts to Curvature: Geometric Control of Bone Tissue Growth." Plos One **7**(5).
- Bischofs, I. B. and U. S. Schwarz (2003). "Cell organization in soft media due to active mechanosensing." Proceedings of the National Academy of Sciences **100**(16): 9274-9279.
- Biton, Y. Y. and S. A. Safran (2009). "The cellular response to curvature-induced stress." Phys Biol **6**(4): 046010.

- Boerboom, R. A., M. P. Rubbens, N. J. B. Driessen, C. V. C. Bouten and F. P. T. Baaijens (2008). "Effect of strain magnitude on the tissue properties of engineered cardiovascular constructs." Annals of biomedical engineering **36**(2): 244-253.
- Borisy, G. G. and T. M. Svitkina (2000). "Actin machinery: pushing the envelope." Current opinion in cell biology **12**(1): 104-112.
- Boskey, A. L., M. Maresca, W. Ullrich, S. B. Doty, W. T. Butler and C. W. Prince (1993). "Osteopontin-hydroxyapatite interactions in vitro: inhibition of hydroxyapatite formation and growth in a gelatin-gel." Bone Miner **22**(2): 147-159.
- Bowers, K. T., J. C. Keller, B. A. Randolph, D. G. Wick and C. M. Michaels (1992). "Optimization of surface micromorphology for enhanced osteoblast responses in vitro." Int J Oral Maxillofac Implants **7**(3): 302-310.
- Brakebusch, C. and R. Fässler (2003). "The integrin-actin connection, an eternal love affair." The EMBO journal **22**(10): 2324-2333.
- Bruder, S. P., K. H. Kraus, V. M. Goldberg and S. Kadiyala (1998). "The Effect of Implants Loaded with Autologous Mesenchymal Stem Cells on the Healing of Canine Segmental Bone Defects\*." The Journal of Bone & Joint Surgery **80**(7): 985-996.
- Bruder, S. P., A. A. Kurth, M. Shea, W. C. Hayes, N. Jaiswal and S. Kadiyala (1998). "Bone regeneration by implantation of purified, culture-expanded human mesenchymal stem cells." J Orthop Res **16**(2): 155-162.
- Buxboim, A., I. L. Ivanovska and D. E. Discher (2010). "Matrix elasticity, cytoskeletal forces and physics of the nucleus: how deeply do cells 'feel' outside and in?" J Cell Sci **123**(Pt 3): 297-308.
- Cai, D., R. Marty-Roix, H. P. Hsu and M. Spector (2001). "Lapine and canine bone marrow stromal cells contain smooth muscle actin and contract a collagen-glycosaminoglycan matrix." Tissue engineering **7**(6): 829-841.
- Cao, W. and L. L. Hench (1996). "Bioactive materials." Ceramics international **22**(6): 493-507.
- Carotenuto, G., G. Spagnuolo, L. Ambrosio and L. Nicolais (1999). "Macroporous hydroxyapatite as alloplastic material for dental applications." Journal of Materials Science: Materials in Medicine **10**(10-11): 671-676.
- Chen, Q., P. Xiao, J. N. Chen, J. Y. Cai, X. F. Cai, H. Ding and Y. L. Pan (2010). "AFM studies of cellular mechanics during osteogenic differentiation of human amniotic fluid-derived stem cells." Anal Sci **26**(10): 1033-1037.
- Choquet, D., D. P. Felsenfeld and M. P. Sheetz (1997). "Extracellular matrix rigidity causes strengthening of integrin-cytoskeleton linkages." Cell **88**(1): 39-48.
- Chu, Y.-S., O. Eder, W. A. Thomas, I. Simcha, F. Pincet, A. Ben-Ze'ev, E. Perez, J. P. Thiery and S. Dufour (2006). "Prototypical type I E-cadherin and type II cadherin-7 mediate very distinct adhesiveness through their extracellular domains." Journal of Biological Chemistry **281**(5): 2901-2910.
- Chu, Y.-S., W. A. Thomas, O. Eder, F. Pincet, E. Perez, J. P. Thiery and S. Dufour (2004). "Force measurements in E-cadherin-mediated cell doublets reveal rapid adhesion strengthened by actin cytoskeleton remodeling through Rac and Cdc42." The Journal of cell biology **167**(6): 1183-1194.
- Connolly, J. F. and R. Shindell (1986). "Percutaneous marrow injection for an ununited tibia." Nebr Med J **71**(4): 105-107.
- Crotty, T. P. (1999). "Contraction in the smooth muscle cell." Med Hypotheses **53**(5): 432-446.
- Dalby, M. J., N. Gadegaard, R. Tare, A. Andar, M. O. Riehle, P. Herzyk, C. D. Wilkinson and R. O. Oreffo (2007). "The control of human mesenchymal cell differentiation using nanoscale symmetry and disorder." Nat Mater **6**(12): 997-1003.
- Davis, M. J., J. A. Donovan and J. D. Hood (1992). "Stretch-Activated Single-Channel and Whole Cell Currents in Vascular Smooth-Muscle Cells." American Journal of Physiology **262**(4): C1083-C1088.

- Dawson, J. I. and R. O. Oreffo (2008). "Bridging the regeneration gap: stem cells, biomaterials and clinical translation in bone tissue engineering." Arch Biochem Biophys **473**(2): 124-131.
- Dean, D. D., Z. Schwartz, L. Bonewald, O. E. Muniz, S. Morales, R. Gomez, B. P. Brooks, M. Qiao, D. S. Howell and B. D. Boyan (1994). "Matrix vesicles produced by osteoblast-like cells in culture become significantly enriched in proteoglycan-degrading metalloproteinases after addition of beta-glycerophosphate and ascorbic acid." Calcif Tissue Int **54**(5): 399-408.
- Deligianni, D., N. Katsala, S. Ladas, D. Sotiropoulou, J. Amedee and Y. Missirlis (2001). "Effect of surface roughness of the titanium alloy Ti-6Al-4V on human bone marrow cell response and on protein adsorption." Biomaterials **22**(11): 1241-1251.
- Dennis, J. E., J.-P. Carbillet, A. Caplan and P. Charbord (2001). "The STRO-1+ marrow cell population is multipotential." Cells Tissues Organs **170**(2-3): 73-82.
- Deshpande, V. S., R. M. McMeeking and A. G. Evans (2007). "A model for the contractility of the cytoskeleton including the effects of stress-fibre formation and dissociation." Proceedings of the Royal Society A: Mathematical, Physical and Engineering Science **463**(2079): 787-815.
- Dorozhkin, S. V. (2007). "Calcium orthophosphates." Journal of materials science **42**(4): 1061-1095.
- Dorozhkin, S. V. (2009). "Calcium orthophosphate-based biocomposites and hybrid biomaterials." Journal of materials science **44**(9): 2343-2387.
- Dorozhkin, S. V. (2010). "Bioceramics of calcium orthophosphates." Biomaterials **31**(7): 1465-1485.
- Ducheyne, P. and Q. Qiu (1999). "Bioactive ceramics: the effect of surface reactivity on bone formation and bone cell function." Biomaterials **20**(23): 2287-2303.
- Eastwood, M., V. Mudera, D. McGrouther and R. Brown (1998). "Effect of precise mechanical loading on fibroblast populated collagen lattices: morphological changes." Cell motility and the cytoskeleton **40**(1): 13-21.
- Ek-Rylander, B., M. Flores, M. Wendel, D. Heinegard and G. Andersson (1994). "Dephosphorylation of osteopontin and bone sialoprotein by osteoclastic tartrate-resistant acid phosphatase. Modulation of osteoclast adhesion in vitro." J Biol Chem **269**(21): 14853-14856.
- Engelmayr, G. C., Jr., G. D. Papworth, S. C. Watkins, J. E. Mayer, Jr. and M. S. Sacks (2006). "Guidance of engineered tissue collagen orientation by large-scale scaffold microstructures." J Biomech **39**(10): 1819-1831.
- Engler, A. J., S. Sen, H. L. Sweeney and D. E. Discher (2006). "Matrix elasticity directs stem cell lineage specification." Cell **126**(4): 677-689.
- Foolen, J., V. S. Deshpande, F. M. Kanters and F. P. Baaijens (2012). "The influence of matrix integrity on stress-fiber remodeling in 3D." Biomaterials **33**(30): 7508-7518.
- Frosch, K. H., F. Barvencik, C. H. Lohmann, V. Viereck, H. Siggelkow, J. Breme, K. Dresing and K. M. Sturmer (2002). "Migration, matrix production and lamellar bone formation of human osteoblast-like cells in porous titanium implants." Cells Tissues Organs **170**(4): 214-227.
- Frosch, K. H., F. Barvencik, V. Viereck, C. H. Lohmann, K. Dresing, J. Breme, E. Brunner and K. M. Sturmer (2004). "Growth behavior, matrix production, and gene expression of human osteoblasts in defined cylindrical titanium channels." J Biomed Mater Res A **68**(2): 325-334.
- Gabbiani, G. (1998). "Evolution and clinical implications of the myofibroblast concept." Cardiovasc Res **38**(3): 545-548.
- Gabbiani, G., G. B. Ryan and G. Majne (1971). "Presence of modified fibroblasts in granulation tissue and their possible role in wound contraction." Experientia **27**(5): 549-550.

- Galbraith, C. G. and M. P. Sheetz (1997). "A micromachined device provides a new bend on fibroblast traction forces." Proc Natl Acad Sci U S A **94**(17): 9114-9118.
- Garg, N. K., S. Gaur and S. Sharma (1993). "Percutaneous autogenous bone marrow grafting in 20 cases of ununited fracture." Acta Orthop Scand **64**(6): 671-672.
- Gauthier, O., J. M. Bouler, P. Weiss, J. Bosco, G. Daculsi and E. Aguado (1999). "Kinetic study of bone ingrowth and ceramic resorption associated with the implantation of different injectable calcium-phosphate bone substitutes." Journal of biomedical materials research **47**(1): 28-35.
- Gauvin, R., R. Parenteau-Bareil, D. Larouche, H. Marcoux, F. Bisson, A. Bonnet, F. A. Auger, S. Bolduc and L. Germain (2011). "Dynamic mechanical stimulations induce anisotropy and improve the tensile properties of engineered tissues produced without exogenous scaffolding." Acta Biomaterialia **7**(9): 3294-3301.
- Gavard, J., M. Lambert, I. Grosheva, V. Marthiens, T. Irinopoulou, J. F. Riou, A. Bershadsky and R. M. Månge (2004). "Lamellipodium extension and cadherin adhesion: two cell responses to cadherin activation relying on distinct signalling pathways." Journal of cell science **117**(2): 257.
- Giachelli, C. M. and S. Steitz (2000). "Osteopontin: a versatile regulator of inflammation and biomineralization." Matrix Biol **19**(7): 615-622.
- Giannoudis, P. V., H. Dinopoulos and E. Tsiridis (2005). "Bone substitutes: an update." Injury **36 Suppl 3**: S20-27.
- Goffin, J. M., P. Pittet, G. Csucs, J. W. Lussi, J. J. Meister and B. Hinz (2006). "Focal adhesion size controls tension-dependent recruitment of alpha-smooth muscle actin to stress fibers." J Cell Biol **172**(2): 259-268.
- Gothard, D., R. S. Tare, P. D. Mitchell, J. I. Dawson and R. O. Oreffo (2011). "In search of the skeletal stem cell: isolation and separation strategies at the macro/micro scale for skeletal regeneration." Lab on a Chip **11**(7): 1206-1220.
- Grashoff, C., B. D. Hoffman, M. D. Brenner, R. B. Zhou, M. Parsons, M. T. Yang, M. A. McLean, S. G. Sligar, C. S. Chen, T. Ha and M. A. Schwartz (2010). "Measuring mechanical tension across vinculin reveals regulation of focal adhesion dynamics." Nature **466**(7303): 263-U143.
- Gugala, Z. and S. Gogolewski (1999). "Regeneration of segmental diaphyseal defects in sheep tibiae using resorbable polymeric membranes: a preliminary study." Journal of orthopaedic trauma **13**(3): 187-195.
- Gunnam, R. (2011). "Bone Graft Substitutes - Global Pipeline Analysis, Competitive Landscape and Market Forecast to 2017." from <http://www.onlineprnews.com/news/152417-1309935300-bone-graft-substitutes-global-pipeline-analysis-competitive-landscape-and-market-forecast-to-2017.html>.
- Han, S. J. and N. J. Sniadecki (2011). "Simulations of the contractile cycle in cell migration using a bio-chemical-mechanical model." Comput Methods Biomech Biomed Engin **14**(5): 459-468.
- Hardie, D. G. and S. Hanks (1995). Protein kinase factsbook, Academic Pr.
- Harris, A. K., D. Stopak and P. Wild (1981). "Fibroblast traction as a mechanism for collagen morphogenesis."
- Healey, J. H., P. A. Zimmerman, J. M. McDonnell and J. M. Lane (1990). "Percutaneous bone marrow grafting of delayed union and nonunion in cancer patients." Clin Orthop Relat Res(256): 280-285.
- Heisenberg, C.-P. and Y. Bellaïche (2013). "Forces in Tissue Morphogenesis and Patterning." Cell **153**(5): 948-962.
- Hench, L. L. (1991). "Bioceramics: from concept to clinic." Journal of the American Ceramic Society **74**(7): 1487-1510.
- Henshaw, D. R., E. Attia, M. Bhargava and J. A. Hannafin (2006). "Canine ACL fibroblast integrin expression and cell alignment in response to cyclic tensile

- strain in three-dimensional collagen gels." Journal of orthopaedic research **24**(3): 481-490.
- Herman, I. M. (1993). "Actin isoforms." Curr Opin Cell Biol **5**(1): 48-55.
- Hing, K., S. Best and W. Bonfield (1999). "Characterization of porous hydroxyapatite." Journal of Materials Science: Materials in Medicine **10**(3): 135-145.
- Hollinger, J. O. (2004). Bone tissue engineering, CRC Press.
- Hollinger, J. O., T. A. Einhorn, B. Doll and C. Sfeir (2004). Bone tissue engineering, CRC Press.
- Hollister, S. J., R. D. Maddox and J. M. Taboas (2002). "Optimal design and fabrication of scaffolds to mimic tissue properties and satisfy biological constraints." Biomaterials **23**(20): 4095-4103.
- Huang, G., L. Wang, S. Wang, Y. Han, J. Wu, Q. Zhang, F. Xu and T. J. Lu (2012). "Engineering three-dimensional cell mechanical microenvironment with hydrogels." Biofabrication **4**(4): 042001.
- Hulbert, S. F., F. A. Young, R. S. Mathews, J. J. Klawitter, C. D. Talbert and F. H. Stelling (1970). "Potential of ceramic materials as permanently implantable skeletal prostheses." J Biomed Mater Res **4**(3): 433-456.
- Hunter, G. K., C. L. Kyle and H. A. Goldberg (1994). "Modulation of crystal formation by bone phosphoproteins: structural specificity of the osteopontin-mediated inhibition of hydroxyapatite formation." Biochem J **300 ( Pt 3)**: 723-728.
- Ishaug-Riley, S. L., G. M. Crane-Kruger, M. J. Yaszemski and A. G. Mikos (1998). "Three-dimensional culture of rat calvarial osteoblasts in porous biodegradable polymers." Biomaterials **19**(15): 1405-1412.
- Isogai, N., W. Landis, T. H. Kim, L. C. Gerstenfeld, J. Upton and J. P. Vacanti (1999). "Formation of Phalanges and Small Joints by Tissue-Engineering\*†." The Journal of Bone & Joint Surgery **81**(3): 306-316.
- Itoh, M., A. Shimazu, I. Hirata, Y. Yoshida, H. Shintani and M. Okazaki (2004). "Characterization of CO<sub>3</sub>-Ap-collagen sponges using X-ray high-resolution microtomography." Biomaterials **25**(13): 2577-2583.
- Jones, A. C., C. H. Arns, D. W. Hutmacher, B. K. Milthorpe, A. P. Sheppard and M. A. Knackstedt (2009). "The correlation of pore morphology, interconnectivity and physical properties of 3D ceramic scaffolds with bone ingrowth." Biomaterials **30**(7): 1440-1451.
- Jones, A. C., C. H. Arns, A. P. Sheppard, D. W. Hutmacher, B. K. Milthorpe and M. A. Knackstedt (2007). "Assessment of bone ingrowth into porous biomaterials using MICRO-CT." Biomaterials **28**(15): 2491-2504.
- Kanda, K. and T. Matsuda (1994). "Mechanical stress-induced orientation and ultrastructural change of smooth muscle cells cultured in three-dimensional collagen lattices." Cell transplantation **3**(6): 481.
- Karageorgiou, V. and D. Kaplan (2005). "Porosity of 3D biomaterial scaffolds and osteogenesis." Biomaterials **26**(27): 5474-5491.
- Karsdal, M. A., L. Larsen, M. T. Engsig, H. Lou, M. Ferreras, A. Lochter, J. M. Delaisse and N. T. Foged (2002). "Matrix metalloproteinase-dependent activation of latent transforming growth factor-beta controls the conversion of osteoblasts into osteocytes by blocking osteoblast apoptosis." J Biol Chem **277**(46): 44061-44067.
- Keogh, M. B., F. J. O'Brien and J. S. Daly (2010). "Substrate stiffness and contractile behaviour modulate the functional maturation of osteoblasts on a collagen-GAG scaffold." Acta Biomater **6**(11): 4305-4313.
- Kiener, H. P., C. S. Stipp, P. G. Allen, J. M. Higgins and M. B. Brenner (2006). "The cadherin-11 cytoplasmic juxtamembrane domain promotes  $\alpha$ -catenin turnover at adherens junctions and intercellular motility." Molecular biology of the cell **17**(5): 2366-2376.
- Knust, E. and O. Bossinger (2002). "Composition and formation of intercellular junctions in epithelial cells." Science **298**(5600): 1955-1959.

- Knychala, J., N. Bouropoulos, C. J. Catt, O. L. Katsamenis, C. P. Please and B. G. Sengers (2013). "Pore Geometry Regulates Early Stage Human Bone Marrow Cell Tissue Formation and Organisation." Ann Biomed Eng.
- Kong, H. J., T. R. Polte, E. Alsberg and D. J. Mooney (2005). "FRET measurements of cell-traction forces and nano-scale clustering of adhesion ligands varied by substrate stiffness." Proceedings of the National Academy of Sciences of the United States of America **102**(12): 4300-4305.
- Kose, G. T., S. Ber, F. Korkusuz and V. Hasirci (2003). "Poly(3-hydroxybutyric acid-co-3-hydroxyvaleric acid) based tissue engineering matrices." J Mater Sci Mater Med **14**(2): 121-126.
- Kuboki, Y., Q. Jin and H. Takita (2001). "Geometry of carriers controlling phenotypic expression in BMP-induced osteogenesis and chondrogenesis." J Bone Joint Surg Am **83-A Suppl 1**(Pt 2): S105-115.
- Laffargue, P., H. F. Hildebrand, M. Rtaimate, P. Frayssinet, J. P. Amoureux and X. Marchandise (1999). "Evaluation of human recombinant bone morphogenetic protein-2-loaded tricalcium phosphate implants in rabbits' bone defects." Bone **25**(2 Suppl): 55S-58S.
- Lakshman, N., A. Kim, K. Bayless, G. Davis and W. Petroll (2007). "Rho plays a central role in regulating local cell-matrix mechanical interactions in 3D culture." Cell motility and the cytoskeleton **64**(6): 434-445.
- Lamolle, S. F., M. Monjo, M. Rubert, H. J. Haugen, S. P. Lyngstadaas and J. E. Ellingsen (2009). "The effect of hydrofluoric acid treatment of titanium surface on nanostructural and chemical changes and the growth of MC3T3-E1 cells." Biomaterials **30**(5): 736-742.
- Landsverk, M. L. and H. F. Epstein (2005). "Genetic analysis of myosin II assembly and organization in model organisms." Cell Mol Life Sci **62**(19-20): 2270-2282.
- Laukaitis, C. M., D. J. Webb, K. Donais and A. F. Horwitz (2001). "Differential dynamics of  $\alpha 5$  integrin, paxillin, and  $\alpha$ -actinin during formation and disassembly of adhesions in migrating cells." The Journal of cell biology **153**(7): 1427-1440.
- Leckband, D. and A. Prakash (2006). "Mechanism and dynamics of cadherin adhesion." Annu. Rev. Biomed. Eng. **8**: 259-287.
- Lecuit, T. and L. Le Goff (2007). "Orchestrating size and shape during morphogenesis." Nature **450**(7167): 189-192.
- Lecuit, T. and E. Wieschaus (2002). "Junctions as organizing centers in epithelial cells? A fly perspective." Traffic **3**(2): 92-97.
- Legant, W. R., A. Pathak, M. T. Yang, V. S. Deshpande, R. M. McMeeking and C. S. Chen (2009). "Microfabricated tissue gauges to measure and manipulate forces from 3D microtissues." Proc Natl Acad Sci U S A **106**(25): 10097-10102.
- Legeros, R. Z. and R. G. Craig (1993). "Strategies to affect bone remodeling: osteointegration." Journal of Bone and Mineral Research **8**(S2): S583-S596.
- Li, B., F. Li, K. M. Puskar and J. H. Wang (2009). "Spatial patterning of cell proliferation and differentiation depends on mechanical stress magnitude." J Biomech **42**(11): 1622-1627.
- Li, X. and R. B. Nicklas (1995). "Mitotic forces control a cell-cycle checkpoint." Nature **373**(6515): 630-632.
- Lian, J. B., G. S. Stein, J. L. Stein and A. J. van Wijnen (1998). "Transcriptional control of osteoblast differentiation." Biochem Soc Trans **26**(1): 14-21.
- Liaw, L., M. P. Skinner, E. W. Raines, R. Ross, D. A. Cheresch, S. M. Schwartz and C. M. Giachelli (1995). "The adhesive and migratory effects of osteopontin are mediated via distinct cell surface integrins. Role of  $\alpha v \beta 3$  in smooth muscle cell migration to osteopontin in vitro." J Clin Invest **95**(2): 713-724.
- Lincks, J., B. D. Boyan, C. R. Blanchard, C. H. Lohmann, Y. Liu, D. L. Cochran, D. D. Dean and Z. Schwartz (1998). "Response of MG63 osteoblast-like cells to

- titanium and titanium alloy is dependent on surface roughness and composition." Biomaterials **19**(23): 2219-2232.
- Lohmann, C. H., L. F. Bonewald, M. A. Sisk, V. L. Sylvia, D. L. Cochran, D. D. Dean, B. D. Boyan and Z. Schwartz (2000). "Maturation state determines the response of osteogenic cells to surface roughness and 1,25-dihydroxyvitamin D3." J Bone Miner Res **15**(6): 1169-1180.
- Lorch, I. J. (1949). "Alkaline phosphatase and the mechanism of ossification." J Bone Joint Surg Br **31B**(1): 94-99.
- Lossdörfer, S., Z. Schwartz, L. Wang, C. Lohmann, J. Turner, M. Wieland, D. Cochran and B. Boyan (2004). "Microrough implant surface topographies increase osteogenesis by reducing osteoclast formation and activity." Journal of Biomedical Materials Research Part A **70**(3): 361-369.
- Lowenstam, H. A. and S. Weiner (1989). On biomineralization, Oxford University Press.
- Lu, J., B. Flautre, K. Anselme, P. Hardouin, A. Gallur, M. Descamps and B. Thierry (1999). "Role of interconnections in porous bioceramics on bone recolonization in vitro and in vivo." Journal of Materials Science: Materials in Medicine **10**(2): 111-120.
- Lu, J. X., B. Flautre, K. Anselme, P. Hardouin, A. Gallur, M. Descamps and B. Thierry (1999). "Role of interconnections in porous bioceramics on bone recolonization in vitro and in vivo." J Mater Sci Mater Med **10**(2): 111-120.
- Mammoto, A., T. Mammoto and D. E. Ingber (2012). "Mechanosensitive mechanisms in transcriptional regulation." Journal of cell science **125**(13): 3061-3073.
- Maniotis, A. J., C. S. Chen and D. E. Ingber (1997). "Demonstration of mechanical connections between integrins, cytoskeletal filaments, and nucleoplasm that stabilize nuclear structure." Proc Natl Acad Sci U S A **94**(3): 849-854.
- Marieb, H. (2010). Human anatomy & Physiology.
- Martin, C., H. Winet and J. Bao (1996). "Acidity near eroding polylactide-polyglycolide in vitro and in vivo in rabbit tibial bone chambers." Biomaterials **17**(24): 2373-2380.
- Martys, N. S., S. Torquato and D. P. Bentz (1994). "Universal scaling of fluid permeability for sphere packings." Phys Rev E Stat Phys Plasmas Fluids Relat Interdiscip Topics **50**(1): 403-408.
- Mathur, A., S. W. Moore, M. P. Sheetz and J. Hone (2012). "The role of feature curvature in contact guidance." Acta Biomater **8**(7): 2595-2601.
- McBeath, R., D. M. Pirone, C. M. Nelson, K. Bhadriraju and C. S. Chen (2004). "Cell shape, cytoskeletal tension, and RhoA regulate stem cell lineage commitment." Dev Cell **6**(4): 483-495.
- Mege, R. M., J. Gavard and M. Lambert (2006). "Regulation of cell-cell junctions by the cytoskeleton." Curr Opin Cell Biol **18**(5): 541-548.
- Meinig, R. P., B. Rahn, S. M. Perren and S. Gogolewski (1996). "Bone regeneration with resorbable polymeric membranes: treatment of diaphyseal bone defects in the rabbit radius with poly (L-lactide) membrane. A pilot study." Journal of orthopaedic trauma **10**(3): 178-190.
- Melchels, F. P., A. M. Barradas, C. A. van Blitterswijk, J. de Boer, J. Feijen and D. W. Grijpma (2010). "Effects of the architecture of tissue engineering scaffolds on cell seeding and culturing." Acta Biomater **6**(11): 4208-4217.
- Melchels, F. P. W., A. Barradas, C. A. Van Blitterswijk, J. De Boer, J. Feijen and D. W. Grijpma (2010). "Effects of the architecture of tissue engineering scaffolds on cell seeding and culturing." Acta Biomaterialia **6**(11): 4208-4217.
- Menard, C., S. Mitchell and M. Spector (2000). "Contractile behavior of smooth muscle actin-containing osteoblasts in collagen-GAG matrices in vitro: implant-related cell contractions." Biomaterials **21**(18): 1867-1877.

- Meshel, A. S., Q. Wei, R. S. Adelstein and M. P. Sheetz (2005). "Basic mechanism of three-dimensional collagen fibre transport by fibroblasts." Nature cell biology **7**(2): 157-164.
- Miao, D. and A. Scutt (2002). "Histochemical localization of alkaline phosphatase activity in decalcified bone and cartilage." J Histochem Cytochem **50**(3): 333-340.
- Mitchison, J. (2003). "Growth during the cell cycle." International review of cytology **226**: 165-258.
- Mitra, S. K., D. A. Hanson and D. D. Schlaepfer (2005). "Focal adhesion kinase: in command and control of cell motility." Nature Reviews Molecular Cell Biology **6**(1): 56-68.
- Moore, M. J., E. Jabbari, E. L. Ritman, L. Lu, B. L. Currier, A. J. Windebank and M. J. Yaszemski (2004). "Quantitative analysis of interconnectivity of porous biodegradable scaffolds with micro-computed tomography." J Biomed Mater Res A **71**(2): 258-267.
- Moroni, L., J. R. de Wijn and C. A. van Blitterswijk (2006). "3D fiber-deposited scaffolds for tissue engineering: influence of pores geometry and architecture on dynamic mechanical properties." Biomaterials **27**(7): 974-985.
- Murray, J. D. (2003). Spatial models and biomedical applications. Mathematical biology.
- Nathan, A. S., B. M. Baker, N. L. Nerurkar and R. L. Mauck (2011). "Mechanotopographic modulation of stem cell nuclear shape on nanofibrous scaffolds." Acta Biomater **7**(1): 57-66.
- Nelson, C. M. (2009). "Geometric control of tissue morphogenesis." Biochim Biophys Acta **1793**(5): 903-910.
- Nelson, C. M., R. P. Jean, J. L. Tan, W. F. Liu, N. J. Sniadecki, A. A. Spector and C. S. Chen (2005). "Emergent patterns of growth controlled by multicellular form and mechanics." Proc Natl Acad Sci U S A **102**(33): 11594-11599.
- Nelson, W. J. (2003). "Adaptation of core mechanisms to generate cell polarity." Nature **422**(6933): 766-774.
- O'Connell, C. B. and Y. L. Wang (2000). "Mammalian spindle orientation and position respond to changes in cell shape in a dynein-dependent fashion." Mol Biol Cell **11**(5): 1765-1774.
- Ong, J. L. and D. C. Chan (2000). "Hydroxyapatite and their use as coatings in dental implants: a review." Critical Reviews™ in Biomedical Engineering **28**(5&6).
- Oreffo, R. and J. Triffitt (1999). "Future potentials for using osteogenic stem cells and biomaterials in orthopedics." Bone **25**(2): 5S-9S.
- Otsuki, B., M. Takemoto, S. Fujibayashi, M. Neo, T. Kokubo and T. Nakamura (2006). "Pore throat size and connectivity determine bone and tissue ingrowth into porous implants: three-dimensional micro-CT based structural analyses of porous bioactive titanium implants." Biomaterials **27**(35): 5892-5900.
- Pamula, E., L. Bacakova, E. Filova, J. Buczynska, P. Dobrzynski, L. Noskova and L. Grausova (2008). "The influence of pore size on colonization of poly(L-lactide-glycolide) scaffolds with human osteoblast-like MG 63 cells in vitro." J Mater Sci Mater Med **19**(1): 425-435.
- Parfitt, A. M. (1977). "The cellular basis of bone turnover and bone loss: a rebuttal of the osteocytic resorption--bone flow theory." Clin Orthop Relat Res(127): 236-247.
- Pathak, A. and S. Kumar (2012). "Independent regulation of tumor cell migration by matrix stiffness and confinement." Proceedings of the National Academy of Sciences **109**(26): 10334-10339.
- Pek, Y. S., A. C. Wan and J. Y. Ying (2010). "The effect of matrix stiffness on mesenchymal stem cell differentiation in a 3D thixotropic gel." Biomaterials **31**(3): 385-391.

- Petite, H., V. Viateau, W. Bensaid, A. Meunier, C. de Pollak, M. Bourguignon, K. Oudina, L. Sedel and G. Guillemain (2000). "Tissue-engineered bone regeneration." Nat Biotechnol **18**(9): 959-963.
- Petroll, W. M., H. D. Cavanagh, P. Barry, P. Andrews and J. V. Jester (1993). "Quantitative analysis of stress fiber orientation during corneal wound contraction." J Cell Sci **104 ( Pt 2)**: 353-363.
- Pevsner-Fischer, M., S. Levin and D. Zipori (2011). "The origins of mesenchymal stromal cell heterogeneity." Stem Cell Reviews and Reports **7**(3): 560-568.
- Peyton, S. R., C. M. Ghajar, C. B. Khatiwala and A. J. Putnam (2007). "The emergence of ECM mechanics and cytoskeletal tension as important regulators of cell function." Cell Biochem Biophys **47**(2): 300-320.
- Pittenger, M. F., A. M. Mackay, S. C. Beck, R. K. Jaiswal, R. Douglas, J. D. Mosca, M. A. Moorman, D. W. Simonetti, S. Craig and D. R. Marshak (1999). "Multilineage potential of adult human mesenchymal stem cells." science **284**(5411): 143-147.
- Pizauro, J. M., P. Ciancaglini and F. A. Leone (1995). "Characterization of the phosphatidylinositol-specific phospholipase C-released form of rat osseous plate alkaline phosphatase and its possible significance on endochondral ossification." Mol Cell Biochem **152**(2): 121-129.
- Poundarik, A. A., T. Diab, G. E. Sroga, A. Ural, A. L. Boskey, C. M. Gundberg and D. Vashishth (2012). "Dilatational band formation in bone." Proceedings of the National Academy of Sciences **109**(47): 19178-19183.
- Puelacher, W., J. Vacanti, N. Ferraro, B. Schloo and C. Vacanti (1996). "Femoral shaft reconstruction using tissue-engineered growth of bone." International journal of oral and maxillofacial surgery **25**(3): 223-228.
- Quarto, R., M. Mastrogiacomo, R. Cancedda, S. M. Kutevov, V. Mukhachev, A. Lavroukov, E. Kon and M. Marcacci (2001). "Repair of large bone defects with the use of autologous bone marrow stromal cells." New England Journal of Medicine **344**(5): 385-386.
- Raisz, L. G. (1999). "Physiology and pathophysiology of bone remodeling." Clin Chem **45**(8 Pt 2): 1353-1358.
- Rauzi, M., P. Verant, T. Lecuit and P. F. Lenne (2008). "Nature and anisotropy of cortical forces orienting Drosophila tissue morphogenesis." Nature cell biology **10**(12): 1401-1410.
- Reilly, G. C. and A. J. Engler (2010). "Intrinsic extracellular matrix properties regulate stem cell differentiation." J Biomech **43**(1): 55-62.
- Rezakhaniha, R., A. Agianniotis, J. T. C. Schrauwen, A. Griffa, D. Sage, C. V. C. Bouten, F. van de Vosse, M. Unser and N. Stergiopoulos (2012). "Experimental investigation of collagen waviness and orientation in the arterial adventitia using confocal laser scanning microscopy." Biomechanics and modeling in mechanobiology **11**(3): 461-473.
- Rezwan, K., Q. Z. Chen, J. J. Blaker and A. R. Boccaccini (2006). "Biodegradable and bioactive porous polymer/inorganic composite scaffolds for bone tissue engineering." Biomaterials **27**(18): 3413-3431.
- Rose, F. R., L. A. Cyster, D. M. Grant, C. A. Scotchford, S. M. Howdle and K. M. Shakesheff (2004). "In vitro assessment of cell penetration into porous hydroxyapatite scaffolds with a central aligned channel." Biomaterials **25**(24): 5507-5514.
- Rubbens, M. P., A. Driessen-Mol, R. A. Boerboom, M. M. J. Koppert, H. C. Van Assen, B. M. TerHaar Romeny, F. P. T. Baaijens and C. V. C. Bouten (2009). "Quantification of the temporal evolution of collagen orientation in mechanically conditioned engineered cardiovascular tissues." Annals of biomedical engineering **37**(7): 1263-1272.
- Ruiz, S. A. and C. S. Chen (2008). "Emergence of patterned stem cell differentiation within multicellular structures." Stem Cells **26**(11): 2921-2927.

- Rumpler, M., A. Woesz, J. W. Dunlop, J. T. van Dongen and P. Fratzl (2008). "The effect of geometry on three-dimensional tissue growth." J R Soc Interface **5**(27): 1173-1180.
- Rumpler, M., A. Woesz, F. Varga, I. Manjubala, K. Klaushofer and P. Fratzl (2007). "Three-dimensional growth behavior of osteoblasts on biomimetic hydroxylapatite scaffolds." J Biomed Mater Res A **81**(1): 40-50.
- Sabtrasekh, R., H. Tiainen, J. Reseland, J. Will, J. Ellingsen, S. Lyngstadaas and H. Haugen (2010). "Impact of trace elements on biocompatibility of titanium scaffolds." Biomedical Materials **5**(1): 015003.
- Sandquist, J. C., A. M. Kita and W. M. Bement (2011). "And the dead shall rise: Actin and myosin return to the spindle." Developmental cell **21**(3): 410-419.
- Sanz-Herrera, J. A., P. Moreo, J. M. Garcia-Aznar and M. Doblare (2009). "On the effect of substrate curvature on cell mechanics." Biomaterials **30**(34): 6674-6686.
- Sawhney, R. K. and J. Howard (2002). "Slow local movements of collagen fibers by fibroblasts drive the rapid global self-organization of collagen gels." The Journal of cell biology **157**(6): 1083-1092.
- Seliktar, D., R. A. Black, R. P. Vito and R. M. Nerem (2000). "Dynamic mechanical conditioning of collagen-gel blood vessel constructs induces remodeling in vitro." Annals of biomedical engineering **28**(4): 351-362.
- Sengers, B. G., J. I. Dawson and R. O. Oreffo (2010). "Characterisation of human bone marrow stromal cell heterogeneity for skeletal regeneration strategies using a two-stage colony assay and computational modelling." Bone **46**(2): 496-503.
- Stagni, N., F. Vittur and B. De Bernard (1983). "Solubility properties of alkaline phosphatase from matrix vesicles." Biochim Biophys Acta **761**(3): 246-251.
- Stopak, D. and A. K. Harris (1982). "Connective tissue morphogenesis by fibroblast traction. I. Tissue culture observations." Dev Biol **90**(2): 383-398.
- Sundelacruz, S. and D. L. Kaplan (2009). "Stem cell- and scaffold-based tissue engineering approaches to osteochondral regenerative medicine." Semin Cell Dev Biol **20**(6): 646-655.
- Tambe, D. T., C. Corey Hardin, T. E. Angelini, K. Rajendran, C. Y. Park, X. Serra-Picamal, E. H. Zhou, M. H. Zaman, J. P. Butler, D. A. Weitz, J. J. Fredberg and X. Trepat "Collective cell guidance by cooperative intercellular forces." Nat Mater.
- Tan, J. L., J. Tien, D. M. Pirone, D. S. Gray, K. Bhadriraju and C. S. Chen (2003). "Cells lying on a bed of microneedles: an approach to isolate mechanical force." Proc Natl Acad Sci U S A **100**(4): 1484-1489.
- Tan, J. L., J. Tien, D. M. Pirone, D. S. Gray, K. Bhadriraju and C. S. Chen (2003). "Cells lying on a bed of microneedles: An approach to isolate mechanical force." Proceedings of the National Academy of Sciences of the United States of America **100**(4): 1484-1489.
- Tare, R. S., J. C. Babister, J. Kanczler and R. O. Oreffo (2008). "Skeletal stem cells: phenotype, biology and environmental niches informing tissue regeneration." Mol Cell Endocrinol **288**(1-2): 11-21.
- Tare, R. S., P. D. Mitchell, J. Kanczler and R. O. Oreffo (2012). Isolation, differentiation, and characterisation of skeletal stem cells from human bone marrow in vitro and in vivo. Bone Research Protocols, Springer: 83-99.
- Théry, M., V. Racine, A. Pépin, M. Piel, Y. Chen, J. B. Sibarita and M. Bornens (2005). "The extracellular matrix guides the orientation of the cell division axis." Nature cell biology **7**(10): 947-953.
- Thoumine, O., M. Lambert, R.-M. Mège and D. Choquet (2006). "Regulation of N-cadherin dynamics at neuronal contacts by ligand binding and cytoskeletal coupling." Molecular biology of the cell **17**(2): 862-875.
- Tsuruga, E., H. Takita, H. Itoh, Y. Wakisaka and Y. Kuboki (1997). "Pore size of porous hydroxyapatite as the cell-substratum controls BMP-induced osteogenesis." J Biochem **121**(2): 317-324.

- Wang, H., J. Pieper, F. Peters, C. A. van Blitterswijk and E. N. Lammé (2005). "Synthetic scaffold morphology controls human dermal connective tissue formation." Journal of Biomedical Materials Research Part A **74**(4): 523-532.
- Wang, H. and C. A. van Blitterswijk (2010). "The role of three-dimensional polymeric scaffold configuration on the uniformity of connective tissue formation by adipose stromal cells." Biomaterials **31**(15): 4322-4329.
- Wang, J. H., F. Jia, T. W. Gilbert and S. L. Woo (2003). "Cell orientation determines the alignment of cell-produced collagenous matrix." J Biomech **36**(1): 97-102.
- Wang, J. H. C., F. Jia, T. W. Gilbert and S. L. Y. Woo (2003). "Cell orientation determines the alignment of cell-produced collagenous matrix." Journal of biomechanics **36**(1): 97-102.
- Wehrle-Haller, B. and B. A. Imhof (2003). "Actin, microtubules and focal adhesion dynamics during cell migration." The international journal of biochemistry & cell biology **35**(1): 39-50.
- Weiner, S. and H. D. Wagner (1998). "The material bone: structure-mechanical function relations." Annual Review of Materials Science **28**(1): 271-298.
- Werntz, J. R., J. M. Lane, A. H. Burstein, R. Justin, R. Klein and E. Tomin (1996). "Qualitative and quantitative analysis of orthotopic bone regeneration by marrow." J Orthop Res **14**(1): 85-93.
- Woolner, S., L. L. O'Brien, C. Wiese and W. M. Bement (2008). "Myosin-10 and actin filaments are essential for mitotic spindle function." The Journal of cell biology **182**(1): 77-88.
- Wühr, M., T. J. Mitchison and C. M. Field (2008). "Mitosis: new roles for myosin-X and actin at the spindle." Current Biology **18**(19): R912-R914.
- Yang, S., H. Yang, X. Chi, J. R. Evans, I. Thompson, R. J. Cook and P. Robinson (2008). "Rapid prototyping of ceramic lattices for hard tissue scaffolds." Materials & Design **29**(9): 1802-1809.
- Yang, S. F., H. Y. Yang, X. P. Chi, J. R. G. Evans, I. Thompson, R. J. Cook and P. Robinson (2008). "Rapid prototyping of ceramic lattices for hard tissue scaffolds." Materials & Design **29**(9): 1802-1809.
- Yoshikawa, T., H. Ohgushi and S. Tamai (1996). "Immediate bone forming capability of prefabricated osteogenic hydroxyapatite." Journal of biomedical materials research **32**(3): 481-492.
- Zaleskas, J. M., B. Kinner, T. M. Freyman, I. V. Yannas, L. J. Gibson and M. Spector (2004). "Contractile forces generated by articular chondrocytes in collagen-glycosaminoglycan matrices." Biomaterials **25**(7-8): 1299-1308.
- Zeltinger, J., J. K. Sherwood, D. A. Graham, R. Mueller and L. G. Griffith (2001). "Effect of pore size and void fraction on cellular adhesion, proliferation, and matrix deposition." Tissue Eng **7**(5): 557-572.
- Zhao, L., C. Sang, C. Yang and F. Zhuang (2011). "Effects of stress fiber contractility on uniaxial stretch guiding mitosis orientation and stress fiber alignment." J Biomech **44**(13): 2388-2394.
- Zhu, B. and S. K. Murthy (2012). "Stem cell separation technologies." Current opinion in chemical engineering.

# Notes









